On the Inextensional Theory of Deformation of a Right Circular Cylindrical Shell[1]

By R. M. HERMES,[2] SANTA CLARA, CALIF.

The inextensional theory of bending of shells is considered. By the method of superposition the known solution is extended to include two cases which can easily be investigated experimentally. The experimental results are compared with the theoretical solution, indicating the degree of approximation involved in the use of the inextensional theory.

Introduction

IN even the simplest cases the application of the general theory of bending of cylindrical shells under static loads is onerous, if not impossible. Many attempts have been made to avoid these difficulties through the postulation of simplifying assumptions, the more prominent of which are the membrane theory of shells, and the theory of the inextensional deformation of shells, i.e., that the middle surface undergoes no strain. It is the purpose of this paper to report observations made on a cylinder, the loading being of a type which calls for the direct application of the latter theory and to compare those observations with the results predicted by that theory.

The theory of the inextensional deformation of shells was developed by Lord Rayleigh (1, 2)[3] and appears in his Theory of Sound (3). Although Love questioned the theory (4), he devotes a chapter of his Theory of Elasticity (5) to its development. Both Rayleigh (3) and Timoshenko (6) consider the circular cylinder loaded by concentrated loads applied at opposite ends of a diameter (see Fig. 1), Rayleigh with the caveat "... although it is true that so highly localized a force hardly comes within the scope of the investigation," while Timoshenko states, "the shortening

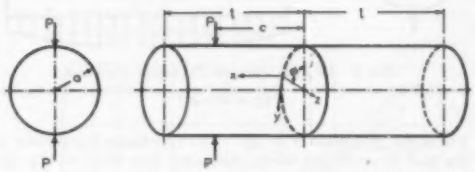

FIG. 1 CLASSICAL PROBLEM IN THEORY OF INEXTENSIONAL BENDING OF THIN-WALL CYLINDERS

of the diameter along which the forces act can be found with good accuracy (by this method)." Yuan considered the same problem (7) without using the simplifying assumption of inextensionality and concluded, "the results obtained in the case of inextensional deformations correspond only to a first approximation to the results (obtained by the more general method)."

From the foregoing it appears desirable from an engineering point of view to report experimental results which will indicate something concerning the accuracy of the inextensional solution. To this end we first use the solution given by Rayleigh (3) and Timoshenko (6), together with the well-known theory of superposition to obtain solutions for cases which are more easily investigated experimentally than is the case shown in Fig. 1.

Using Timoshenko's notation,[4] the solution for the displacements in the right circular cylinder shown in Fig. 1 is as follows: If u is the displacement in the x-direction, v that in the y-direction, and w that in the z-direction, their values are

$$u = \frac{Pa^2}{\pi Dl} \sum_{n=2,4,6,\cdots} \frac{ac \cos n\phi}{(n^2-1)^2[\frac{1}{2}n^2l^2 + 2(1-\nu)a^2]}$$

$$v = \frac{Pa^2}{\pi Dl} \sum_{n=2,4,6,\cdots} \left\{ \frac{1}{(n^2-1)^2 n} + \frac{nc x}{(n^2-1)^2[\frac{1}{2}n^2l^2 + 2(1-\nu)a^2]} \right\} \sin n\phi \qquad \ldots [1]$$

$$w = \frac{Pa^2}{\pi Dl} \sum_{n=2,4,6,\cdots} \left\{ \frac{1}{(n^2-1)^2} + \frac{n^2 c x}{(n^2-1)^2[\frac{1}{2}n^2l^2 + 2(1-\nu)a^2]} \right\} \cos n\phi$$

where

ν = Poisson's ratio

D = flexural rigidity of cylinder and is given by

$$D = E h^3/12(1-\nu^2)$$

E = Young's modulus

h = wall thickness

n = parameter of summation.

Other quantities are defined as in Fig. 1.

By the method of superposition, this solution can be extended to yield the displacements in cylinders under other types of load.

[1] The experimental data included herein are taken from a thesis for the Bachelor's degree by M. Butler, J. Pearce, and E. Texiera, who investigated a related problem.

[2] Research Professor, University of Santa Clara. Mem. ASME.

[3] Numbers in parentheses refer to the Bibliography at the end of the paper.

Presented at the West Coast National Conference of the Applied Mechanics Division, Stanford, Calif., June 22–23, 1951, of THE AMERICAN SOCIETY OF MECHANICAL ENGINEERS.

Discussion of this paper should be addressed to the Secretary, ASME, 29 West 39th Street, New York, N. Y., and will be accepted until January 10, 1952, for publication at a later date. Discussion received after the closing date will be returned.

NOTE: Statements and opinions advanced in papers are to be understood as individual expressions of their authors and not those of the Society. Manuscript received by ASME Applied Mechanics Division, January 30, 1951. Paper No. 51—APM-2

[4] Reference (6), p. 432.

Of considerable interest is a load which is symmetrical about a plane normal to and bisecting the elements of the cylinder, as shown in Fig. 2. Let the magnitude of the load at the distance

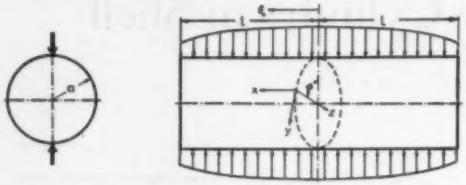

FIG. 2 AN EXTENSION OF CLASSICAL PROBLEM
(Load W [ξ] assumed to be symmetrical about mid-plane of cylinder, i.e., $W[\xi] = W[-\xi]$.)

ξ from this mid-plane be $W(\xi)$. The hypothesis of symmetry of the load is equivalent to the statement that $W(\xi) = W(-\xi)$. The displacements u, v, and w at any point whose abscissa is x are from Equations [1]

$$\left.\begin{aligned} u &= \int_{-l}^{l} \frac{W(\xi)\, a^3 d\xi}{\pi D l} \sum_{n=2,4,6,\cdots} \frac{a\xi \cos n\phi}{(n^2-1)^2 \left[\frac{1}{3} n^2 l^2 + 2(1-\nu)a^2\right]} \\ v &= \int_{-l}^{l} \frac{W(\xi)\, a^3 d\xi}{\pi D l} \sum_{n=2,4,6,\cdots} \left\{ \frac{1}{n(n^2-1)^2} + \frac{n\xi x}{(n^2-1)^2 \left[\frac{1}{3} n^2 l^2 + 2(1-\nu)a^2\right]} \right\} \sin n\phi \\ w &= \int_{-l}^{l} \frac{W(\xi)\, a^3 d\xi}{\pi D l} \sum_{n=2,4,6,\cdots} \left\{ \frac{1}{(n^2-1)^2} + \frac{n^2 \xi x}{(n^2-1)^2 \left[\frac{1}{3} n^2 l^2 + 2(1-\nu)a^2\right]} \right\} \cos n\phi \end{aligned}\right\} \quad \ldots [2]$$

In carrying out the integrations in Equations [2] we can rearrange the equations so that we have

$$\left.\begin{aligned} u &= \left\{ \frac{a^3}{\pi D l} \sum_{n=2,4,6,\cdots} \frac{a \cos n\phi}{(n^2-1)^2 \left[\frac{1}{3} n^2 l^2 + 2(1-\nu)a^2\right]} \right\} \int_{-l}^{l} W(\xi)\xi d\xi \\ v &= \left\{ \frac{a^3}{\pi D l} \sum_{n=2,4,6,\cdots} \frac{\sin n\phi}{n(n^2-1)^2} \right\} \int_{-l}^{l} W(\xi) d\xi + \left\{ \frac{a^3}{\pi D l} \sum_{n=2,4,6,\cdots} \frac{n x \sin n\phi}{(n^2-1)^2 \left[\frac{1}{3} n^2 l^2 + 2(1-\nu)a^2\right]} \right\} \int_{-l}^{l} W(\xi)\xi d\xi \end{aligned}\right\} \quad \ldots [3]$$

and for w an expression similar to that for v. Since $W(\xi)$ is an even function of ξ, $\int_{-l}^{l} W(\xi) d\xi$ is equal to the total load applied to the upper element of the cylinder while $\int_{-l}^{l} W(\xi)\xi d\xi$ vanishes. With the notation $L = \int_{-l}^{l} W(\xi) d\xi$, Equations [3] become

$$\left.\begin{aligned} u &= 0 \\ v &= \frac{La^3}{\pi D l} \sum_{n=2,4,6,\cdots} \frac{\sin n\phi}{n(n^2-1)^2} \\ w &= \frac{La^3}{\pi D l} \sum_{n=2,4,6,\cdots} \frac{\cos n\phi}{(n^2-1)^2} \end{aligned}\right\} \quad \ldots\ldots\ldots [4]$$

The following implications of Equations [4] should be noted:

1 The x-co-ordinate has vanished. Hence the displacements u, v, and w are independent of position along the axis of the cylinder.

2 The shape of the load curve has no effect on the displacements so long as it is symmetrical about the mid-plane of the cylinder. The only property of a symmetrical load which influences the displacements is its total magnitude. Thus a total load of P lb should produce the same displacements whether it is uniformly distributed along the entire length of the upper element or only along, say, the middle third of this element, the support on the lower element being identical with the load on the upper element.

These implications warrant comparison with observation. A 3-ft length of cold-rolled, seamless tubing, 8 in. OD, and 1/4 in. wall thickness was loaded first as shown in Fig. 3, and subsequently as shown in Fig. 4. Electric-resistance strain gages were mounted on the tube as shown in Fig. 5. Strains developed in the tube under load were recorded by means of a multichannel oscillograph with attendant static-load strain-gage control equipment.

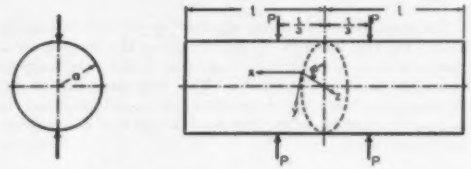

FIG. 3 TWO-POINT LOADING ON THIN-WALL CYLINDER
(This is the first case investigated experimentally and reported in this paper.)

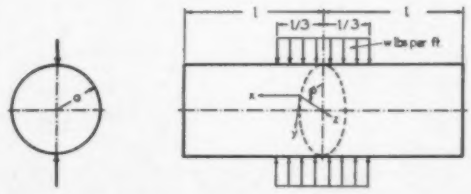

FIG. 4 DISTRIBUTED LOADING ON THIN-WALL CYLINDER
(This is the second case investigated experimentally and reported in this paper.)

The observed strains are plotted as dependent variable versus total applied load as independent variable in Figs. 6 to 9, inclusive. In Fig. 10 are plotted circumferential strains developed at the

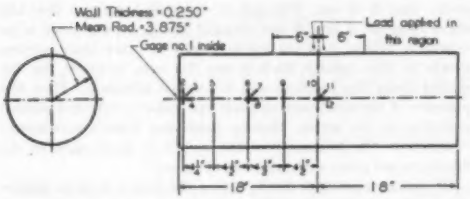

FIG. 5 LOCATION OF STRAIN GAGES FOR EXPERIMENTAL INVESTIGATION
(Gages 2, 3, and 4; 6, 7, and 8; 10, 11, and 12 are SR-4 type AR-1 rosettes, while gages 1, 5, and 9 are SR-4 type A-1.)

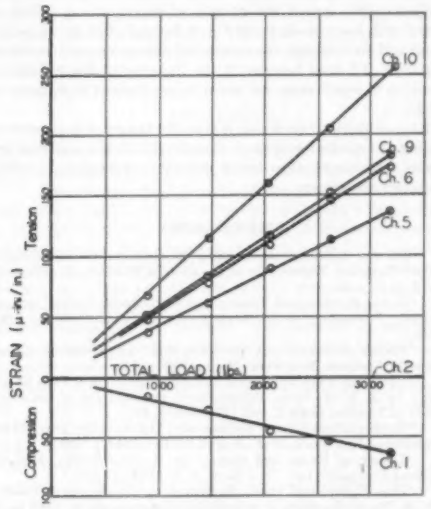

FIG. 6 VARIATION OF CIRCUMFERENTIAL STRAIN AS A FUNCTION OF TOTAL LOAD FOR TWO-POINT LOADING

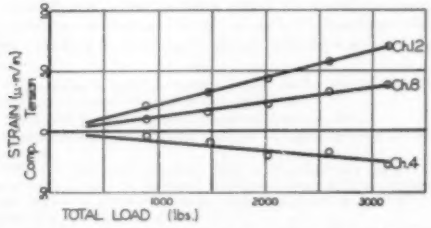

FIG. 7 VARIATION OF AXIAL STRAIN AS A FUNCTION OF THE TOTAL LOAD FOR TWO-POINT LOADING

largest test load as functions of distance along the axis of the tube.

There is also plotted in Fig. 10 the value of the circumferential strain computed from Equations [4]. For the computation we need the equations[6]

[6] Reference (6), pp. 439 and 354.

$$\left.\begin{aligned} \chi_x &= \frac{\partial^2 w}{\partial x^2} \\ \chi_y &= \frac{1}{a^2}\left(\frac{\partial v}{\partial \phi} + \frac{\partial^2 w}{\partial \phi^2}\right) \\ \epsilon_x &= \epsilon_1 - z\chi_x \\ \epsilon_y &= \epsilon_2 - z\chi_y \end{aligned}\right\} \qquad [5]$$

where

z = distance from middle surface
χ_x, χ_y = changes of curvature
ϵ_1, ϵ_2 = strains in middle surface.

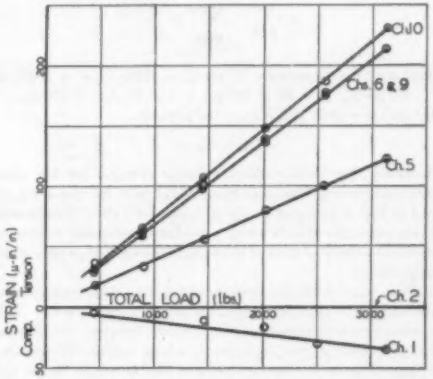

FIG. 8 VARIATION OF CIRCUMFERENTIAL STRAIN AS A FUNCTION OF TOTAL LOAD FOR DISTRIBUTED LOAD

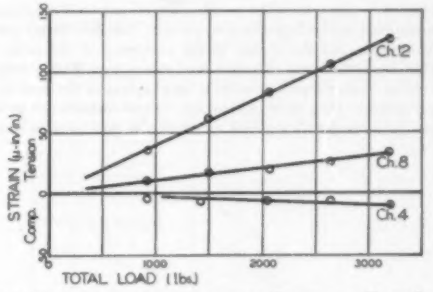

FIG. 9 VARIATION OF AXIAL STRAIN AS A FUNCTION OF TOTAL LOAD FOR DISTRIBUTED LOAD

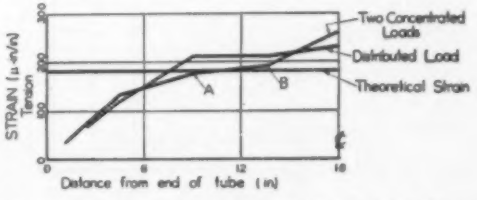

FIG. 10 VARIATION OF CIRCUMFERENTIAL STRAIN ALONG LENGTH OF CYLINDER

ϵ_x, ϵ_y denote strains in axial and circumferential directions at distance z from middle surface.

Due to the hypothesis that the bending is inextensional, we have at once that $\epsilon_1 = \epsilon_2 = 0$. Moreover, from Equations [4] $\chi_x = 0$ and

$$\chi_y = -\frac{La}{\pi Dl} \sum_{n=2,4,6,\ldots} \frac{\cos n\phi}{n^2 - 1} \quad \ldots\ldots [6]$$

Hence the strains in the axial and circumferential directions are given by

$$\left.\begin{aligned} \epsilon_x &= 0 \\ \epsilon_y &= \frac{Laz}{\pi Dl} \sum_{n=2,4,6,\ldots} \frac{\cos n\,\phi}{n^2 - 1} \end{aligned}\right\} \quad \ldots\ldots [7]$$

Evaluation of Equations [7] for $L = 3200$ lb, $a = 3.875$ in., $z = -0.125$ in., $E = 30 \times 10^6$ psi, $\nu = 0.28$, $h = 0.250$ in., $l = 18$ in., and $\phi = \pi/2$, yields $\epsilon_y = 184$ μ-in./in.

Discussion

Generally, the data yielded a linear relation for the strain versus load curves, Figs. 6 to 9, although in some cases, e.g., for gage 4 of Fig. 7, and gage 1 of Fig. 8, the data show some scatter. In these cases the strains which were being measured were of the order of sensitivity of the recording equipment so that this scatter is insignificant.

In Figs. 6 and 8 the circumferential strain on the outer surface at the end of the cylinder (gage 2) is shown as being zero. Actually, some strain was developed in this direction but was too small to be measured by the equipment, whose sensitivity was ± 10 μ-in./in. The same situation obtains for the strain in the axial direction at the same point for the distributed load (gage 4, Fig. 8).

In Fig. 10 it will be noted that the observed strain for the two-point load agrees with that predicted by theory. This appears in essence to agree with the results pointed out by Timoshenko as mentioned in the Introduction, namely, that the theory gives reliable values for the change in the diameters at the point of application of the load. The observed strains were 90 deg around the circumference from the point of application of the load so it seems unlikely that there existed any violent disturbance in the strain between the two points at which the strains were measured; that is to say, although we have no assurance that the curve between A and B is a straight line as drawn, there is no reason to believe that the curve should be other than varying slowly in this region. Such is not the case, however, for the strains along the topmost and lowermost elements. Here the presence of the concentrated loads can cause a wide and sudden variation in the strain, thereby justifying Yuan's statement,[6] "stresses in the proximity of the points of application of the forces are not given with sufficient accuracy."

Of greater interest is the fact that the theory fails to predict the maximum circumferential strain developed in the cylinder, the error being 46 per cent and 37 per cent of the predicted value for the two-point load and the distributed load, respectively.

It should be pointed out that the discrepancy between the theoretical values and the observed values can in no way be ascribed to the use of the method of superposition. Had we started with loads as shown in Fig. 2, instead of as shown in Fig. 1, and had we followed the method of derivation used to obtain Equations [1], then because of the linearity of the differential equations of equilibrium we would have obtained Equations [4] directly.

The conclusion to be drawn is that the theory of inextensional bending of cylinders is open to considerable doubt and that any solution based upon this theory warrants experimental verification before acceptance.

BIBLIOGRAPHY

1 "On the Infinitesimal Bending of Surfaces of Revolution," by Lord Rayleigh, Proceedings of the London Mathematical Society, vol. 13, 1881, p. 4.

2 "On the Bending and Vibration of Thin Elastic Shells," by Lord Rayleigh, Proceedings of the Royal Society of London, vol. 45, 1888, p. 105.

3 "Theory of Sound," by Lord Rayleigh, 1st American edition, Dover Publications, New York, N. Y., 1945, p. 412.

4 "The Small Free Vibrations and Deformation of a Thin Elastic Shell," by A. E. H. Love, Philosophical Transactions of the Royal Society of London, series A, vol. 179, 1888, p. 491.

5 "Mathematical Theory of Elasticity," by A. E. H. Love, Dover Publications, New York, N. Y., fourth edition, 1944, p. 499.

6 "Theory of Plates and Shells," by S. Timoshenko, McGraw Hill Book Company, Inc., New York, N. Y., 1940, p. 427.

7 "Thin Cylindrical Shells Subjected to Concentrated Loads," by S. W. Yuan, *Quarterly of Applied Mathematics*, vol. 4, 1946, p. 13.

[6] Reference (7), p. 13.

The Behavior of Graphite Under Alternating Stress[1]

By LEON GREEN, JR.,[2] DOWNEY, CALIF.

The fatigue properties of grade AUF[4] extruded polycrystalline graphite were investigated at ambient and elevated temperatures. Specimens cut parallel to the axis of extrusion were stressed in reversed bending at room temperature and at 3550 F. The endurance limit of this graphite was found to increase from 2500 psi at room temperature to about 4400 psi at 3550 F. The increase in endurance limit is correlative with the increase in short-time tensile strength with temperature observed in earlier studies of graphite.

Introduction

EXPERIMENTAL studies of the mechanical properties of graphite (1)[3] made in order to evaluate the suitability of the material for high-temperature structural applications have shown graphite to exhibit unique refractory characteristics in that its short-time tensile strength and unrelaxed Young's modulus increase with temperature in the range from room temperature to about 4500 F. The favorable high-temperature strength properties and the low density possessed by graphite make it appear attractive as a possible structural material for gas-turbine application, for example. For purpose of comparison of the strength properties of graphite with those of some other materials proposed for turbine use, tensile data for grade ECA graphite[4] (cut parallel to the axis of extrusion) are presented in Fig. 1, together with corresponding data for several ceramic oxides and a good high-temperature alloy, as reported by Norton (2) in terms of the short-time tensile strength divided by the nominal specific gravity of the material. It is apparent that graphite can be used at temperatures much higher than those permissible with the other materials. In Fig. 2 the temperature dependence of the Young's modulus of center-cut AUF graphite (3) is contrasted with that reported for several ceramic oxides by Ryschkewitsch (4).

Graphite also exhibits marked superiority to ceramic materials in resistance to thermal shock. Analysis (5) has shown that for high resistance to cracking by thermal stresses, a material should have a high value of the parameter $ks/\alpha E$ where

k = thermal conductivity
s = tensile strength
α = coefficient of thermal expansion
E = modulus of elasticity

Values of this thermal-shock parameter calculated by Gangler (6) and the summarized results of his experiments with several

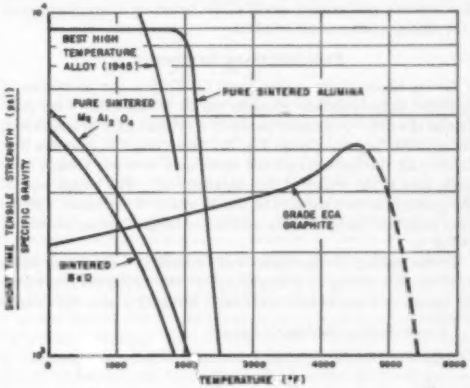
BEST HIGH TEMPERATURE ALLOY (1945)
PURE SINTERED ALUMINA
PURE SINTERED $Mg Al_2 O_4$
GRADE ECA GRAPHITE
SINTERED BeO
SHORT TIME TENSILE STRENGTH (psi) / SPECIFIC GRAVITY
TEMPERATURE (°F)

FIG. 1 STRENGTH-TO-WEIGHT RATIO FOR SEVERAL MATERIALS AS A FUNCTION OF TEMPERATURE

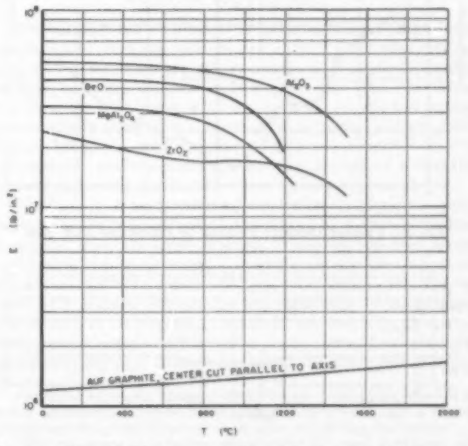

FIG. 2 YOUNG'S MODULUS OF SOME REFRACTORY MATERIALS VERSUS TEMPERATURE

---

[1] This paper is based on studies conducted for the Atomic Energy Commission under Contract AT-11-1-GEN-8.

[2] Research Engineer, North American Aviation, Inc.

[3] Numbers in parentheses refer to the Bibliography at end of the paper.

[4] ECA is the term originally used by the National Carbon Company to designate an extruded polycrystalline graphite possessing a high degree of grain orientation and graphitized at 3000 C. This material is now designated as AUF.

Presented at the West Coast National Conference of the Applied Mechanics Division, Stanford, Calif., June 22-23, 1951, of THE AMERICAN SOCIETY OF MECHANICAL ENGINEERS.

Discussion of this paper should be addressed to the Secretary, ASME, 29 West 39th Street, New York, N. Y., and will be accepted until January 10, 1952, for publication at a later date. Discussion received after the closing date will be returned.

NOTE: Statements and opinions advanced in papers are to be understood as individual expressions of their authors and not those of the Society.

Manuscript received at ASME Headquarters, February 6, 1951. Paper No. 51—APM-3.

TABLE 1 CORRELATION OF MATERIAL PROPERTIES WITH RESISTANCE TO FRACTURE BY THERMAL SHOCK[a]

Order of merit of materials evaluated in thermal shock	Thermal shock[b] (cycles before failure) 1800 F	2000 F	2200 F	2400 F	Coefficient of thermal expansion, α (10^{-6}/deg F)	Thermal conductivity k, Btu/hr (ft² deg F/in)	Elastic modulus E, at 1800 F, (10^6 psi)	Tensile strength s, at 1800 F, (psi)	$\frac{k\,s}{(\alpha\,E)}$
Graphite	[c]	[c]	[c]	[c]	1.2	1040	0.12	4200	3,030000
Titanium carbide	25	25	25	21	4.12	240[d]	5.5[d]	17200	18200
Beryllium oxide	25	3			5.28	233	4.28	6200	6390
Zircon	1				2.24	14.5	2.4	8700	2345
Magnesium oxide	1/2				6.94	17.7–40.8	1.24	3100	641–1840
Stabilized zirconia	0				4.95	6.4	2.5	6750	345

[a] Ceramic data from Gangler (6).
[b] Shock: hot specimen was quenched in a stream of room-temperature air.
[c] Graphite specimens at about 3000 F have been quenched in water without damage. Spalling has been obtained, however, by quenching in liquid sodium.
[d] Data for cemented carbide (0.80 TiC, 0.20 Co). Thermal-shock parameter for pure carbide would probably be lower than foregoing value.

ceramics are presented in Table 1. Corresponding approximate values for graphite included for comparison indicate its relative superiority in this respect.

Although graphite thus appeared promising on the basis of its strength and thermal-shock properties, an evaluation of its usefulness for structures subjected to conditions of repeated or periodic loading required knowledge of its fatigue properties. For this reason a preliminary study of the behavior of graphite under alternating stress was undertaken.

Procedure and Equipment

It was known from earlier work (1, 3) that the properties of extruded polycrystalline graphite varied considerably with position in the rod. A density profile of a typical AUF graphite rod, for example, is presented in Fig. 3. In an effort to promote uniformity of the material all the specimens were cut from a 4-in-diam core at the center of the extruded rod. The length axes of the specimens were parallel to the direction of extrusion. Pertinent details of the specimens used in the fatigue testing are shown in Fig. 4.

In the testing, the specimen was stressed as a cantilever beam in reversed bending at a frequency of 1900 cycles per min (cpm) by means of a mechanical oscillator[4] utilizing a cam with variable eccentricity to effect positive constant-amplitude displacement of the specimen. As is shown in Fig. 5, a 6-in. length of $^1/_{16}$-in-diam steel wire served as a flexible linkage connecting the specimen and the oscillator. Failure of the specimen allowed the linkage (pivoted at the crosshead) to open a microswitch controlling the oscillator, thus stopping the test automatically.

[4] Krouse Testing Machine Company.

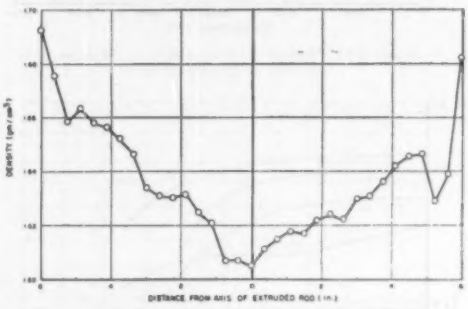

Fig. 3 Typical Density Profile of Extruded AUF Rod

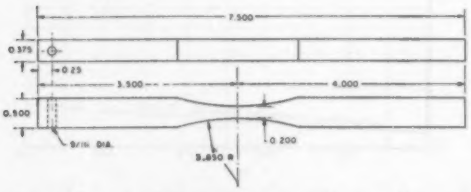

Fig. 4 Details of Specimens Used in Fatigue Testing

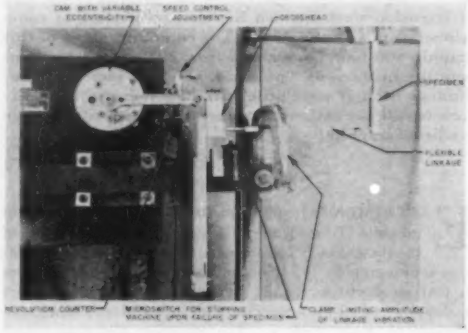

Fig. 5 View of Oscillator, Flexible Linkage, and Graphite Specimen

Stresses in the specimens were calculated by calibrating each specimen individually, that is, the deflection of each specimen loaded under the cantilever conditions of the test was determined as a function of load. The deflections were measured with the use of a cathetometer. A typical load-deflection curve is shown in Fig. 6. The lack of the linearity (which might be expected on the basis of the simple-beam-theory expression (7) for the end deflection δ of a cantilever beam with load P applied at the end

$$\delta = \frac{P}{E}\left(\frac{l^3}{3\,I}\right)_{eq} \qquad [1]$$

where

$\left(\frac{l^3}{3\,I}\right)_{eq}$ = constant of proportionality, a length parameter defining the dimensions of an equivalent uniform beam)

is attributed to the nonlinear elasticity of graphite and does not represent any permanent deformation of the material. Knowledge of the amplitude of vibration (determined as a function of the cam eccentric setting) thus permitted calculation of the nominal maximum fiber stress S in the specimen by means of the simple beam theory

$$S = \frac{M\,c}{I} \qquad [2]$$

where

M = applied moment at point in question

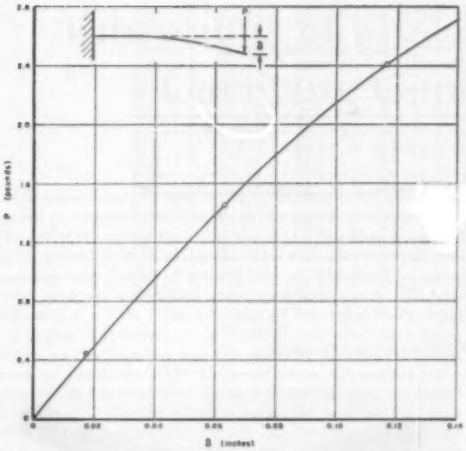

FIG. 6 TYPICAL LOAD-DEFLECTION CURVE FOR A FATIGUE SPECIMEN OF AUF GRAPHITE

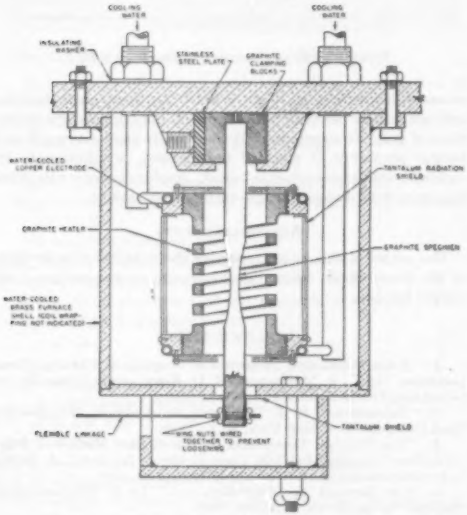

FIG. 7 SCHEMATIC VIEW OF FURNACE USED IN HIGH-TEMPERATURE TESTING

I = cross-sectional moment of inertia at point in question
c = distance of extreme fiber from central axis of beam

The furnace used in the high-temperature testing is shown diagrammatically in Fig. 7. The specimen was heated by radiation from a surrounding graphite helix carrying a direct current. Temperatures at the central region of the specimen were determined by optical-pyrometer measurements made through quartz windows. An inert atmosphere was maintained by a 16-cfh flow of helium entering at the top of the furnace and leaving through the linkage slot at the bottom.

It seemed conceivable that an error in the high-temperature tests might arise as a result of the possible presence of residual moisture in the porous structure of the graphite. Any oxidation of the material when the specimen was heated to high temperatures could easily give rise to serious errors in the experimental results. In order to mitigate this difficulty all specimens used in the high-temperature tests were dried at 300 F for 2 hr, cooled in a vacuum desiccator, and stored in the desiccator until used.

Calculation of the stresses in the high-temperature work was complicated by the change in Young's modulus of the material with temperature. Due to the increased dynamic modulus observed in graphite at elevated temperatures (1, 3), any calculation based only upon the room-temperature load-deflection calibration of the specimens would necessarily underestimate the true stresses obtaining. As a first approximation, therefore, it was assumed on the basis of Equations [1] and [2] that, for a given deflection, the true stress at a given temperature would be in the same ratio to the nominal room-temperature stress as would be the corresponding Young's moduli at the two temperatures concerned

$$\frac{S}{S_0} = \frac{E}{E_0} = f(T) \qquad [3]$$

This ratio as a function of temperature is known from Young's modulus data for center-cut AUF graphite presented in Fig. 2.

In view of the nonlinear elasticity exhibited by graphite, the foregoing assumption is of course valid only as a first approximation. In addition, another approximation was involved in considering the test temperature to be that observed at the middle of the specimen, the point of fracture. Since the great part of the deflection was due to strain concentrated in the narrow central region, however, and because of the slight thermal dependence of the elastic modulus of graphite, this approximation also appears reasonable. In view of the statistical and rather crude nature of a fatigue test, it was decided that more elaborate refinements in the stress calculation[6] and control of the temperature distribution would not be justified for the present preliminary study. It should be emphasized that the foregoing technique could not be used in the testing of metals because of the pronounced thermal dependence of their elastic properties.

RESULTS AND DISCUSSION

The results of the two series of fatigue tests using AUF graphite specimens at room temperature and at 3550 F are presented in Fig. 8 in terms of the nominal maximum fiber stress versus the number of cycles to failure. It may be seen that the room-temperature curve is somewhat similar in form to the S-N curves obtained with many metals, but that the horizontal portion of the curve (defining an endurance limit of 2500 psi) is reached after a considerably smaller number of cycles than is required in the case of most metals (8), and that the "knee" is not pronounced.

Fatigue tests on metals have indicated a definite proportionality between the endurance limit of a metal and its short-time tensile strength. Since the tensile strength of graphite had been found to increase with temperature, it was believed that the endurance limit would exhibit a similar increase. The data in Fig. 8 show that AUF graphite possesses an endurance limit of about 4400 psi at 3550 F, an increase of about 75 per cent over its room-temperature value. Another effect of the elevated temperature revealed by Fig. 9 is that an apparently increased brittleness[7] of the

[6] Thermal expansion of the flexible linkage presumably effected a small nonzero mean stress in the fatigue cycle even though a rough compensation for this effect was made when connecting the linkage.

[7] The resistance to long-time deformation by creep is reduced at high temperatures (1). The thermal dependence of the impact strength of graphite has not yet been determined.

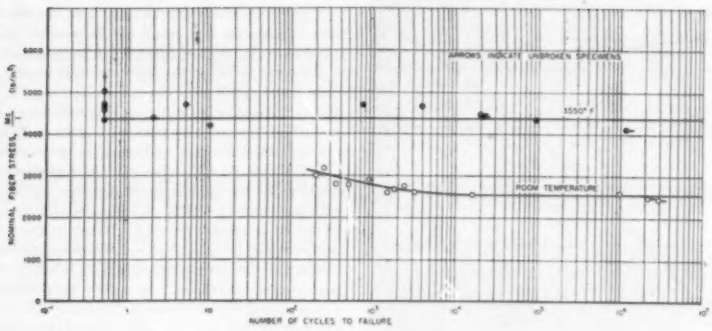

FIG. 8 FATIGUE BEHAVIOR OF CENTER-CUT AUF GRAPHITE

graphite tended to eliminate the inclined portion of the S-N curve (which was poorly defined even at room temperature). Despite the scatter of the points (probably due to the unavoidable nonuniformity of the specimens), the data indicate that raising the temperature increases the tendency for the material to fail on the first half-cycle of any stress greater than the endurance limit. At high temperatures, accordingly, the high-frequency, creep-independent endurance limit should approach the short-time tensile strength. Preliminary tensile data on AUF graphite[8] appear to verify this prediction.

All the surfaces revealed by failure of the specimens at both high and low temperature were characteristic of brittle fracture, as had been all the fracture surfaces obtained in the earlier tensile testing (1). A typical specimen broken at 3550 F is shown in Fig. 9. No evidence of the fatigue-crack propagation encountered in metals was noted in any of the failures, which appeared to take place abruptly during a single stress peak.

The tendency of fatigue failures of graphite at elevated temperatures to occur as "all-or-none" processes suggests that graphite behavior cannot be interpreted in terms of the theory of the fatigue of metals proposed by Orowan (9), which associates fatigue failure with the work-hardening of plastic inhomogeneities within the specimen. During the early tensile testing of graphite specimens (1), moreover, no evidence of work-hardening as a result of plastic slip could be detected, and the permanent elongations realized are tentatively attributed to deformation by creep, which may be considered to be a diffusion mechanism involving no storage of strain energy. Although they cannot be regarded as completely conclusive, the graphite data encourage consideration of the contention of Freudenthal (10) that plastic slip and strain-hardening are not inseparable features of fatigue failure, and that the fatigue process may possibly be considered as "an essentially statistical effect of happenings on a submicroscopic scale."

CONCLUSIONS

The fatigue behavior of AUF graphite specimens cut parallel to the axis of extrusion was investigated at room temperature and at 3550 F. Well-defined endurance limits were found in both cases, indicating the suitability of graphite for structural applications under conditions of alternating stress. Since the endurance limit (like the short-time tensile strength) was found to increase with temperature, it is concluded that creep characteristics and not fatigue behavior will determine the temperature limitations of graphite structures. Because of its unique strength and fatigue properties at elevated temperature, in addition to its excellent resistance to thermal shock, graphite appears attractive as a refractory material for gas-turbine applications.

[8] Although grades ECA and AUF are nominally identical, the variations in the properties of commercial graphite within a given grade, batch, or piece are great enough to invalidate comparison of data unless careful control of the specimen material (usually on the basis of density) is maintained.

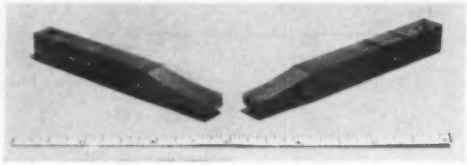

FIG. 9 TYPICAL SPECIMEN BROKEN AT 3550 F

ACKNOWLEDGMENTS

The author wishes to acknowledge the valuable contributions of Mr. Harry Strahl during the construction and operation of the fatigue furnace.

BIBLIOGRAPHY

1 "Some Mechanical Properties of Graphite at Elevated Temperatures," by C. R. Malmstrom, R. D. Keen, and L. Green, Jr., to be published in the *Journal of Applied Physics*.

2 "Refractories," by F. H. Norton, third edition, McGraw-Hill Book Company, Inc., New York, N. Y., 1949.

3 "The Thermal Dependence of the Elastic Moduli of Polycrystalline Graphite," by F. E. Faris, L. Green, Jr., and C. A. Smith, to be communicated to the *Journal of Applied Physics*.

4 "Oxydkeramik der Einstoffsysteme," by R. Ryschkewitsch, Springer Verlag, Berlin, Germany, 1948.

5 "Correlation of Physical Properties of Ceramic Materials With Resistance to Fracture by Thermal Shock," by W. G. Lindman and A. R. Bobrowsky, NACA Technical Note No. 1918, 1949.

6 "Some Physical Properties of Eight Refractory Oxides and Carbides," by J. J. Gangler, *Journal of the American Ceramic Society*, vol. 33, 1950, p. 367.

7 "Elements of Strength of Materials," by S. Timoshenko and G. H. MacCullough, D. Van Nostrand Company, Inc., New York, N. Y., 1940.

8 "Prevention of the Failure of Metals Under Repeated Stress," Battelle Memorial Institute, John Wiley & Sons, Inc., New York N. Y., 1941.

9 "Theory of the Fatigue of Metals," by E. Orowan, Proceedings of the Royal Society of London, vol. 171, 1939, p. 79.

10 "The Statistical Aspect of Fatigue of Materials," by A. M. Freudenthal, Proceedings of the Royal Society of London, vol. 187, 1946, p. 416.

Vibrations of a Clamped Circular Plate Carrying Concentrated Mass

By R. E. ROBERSON,[1] WASHINGTON, D. C.

The vibrations of a circular plate clamped at its edge and carrying a concentrated mass at its center are considered. The plate is excited by a motion of the framing, assumed rigid, to which it is clamped. The first four natural frequencies are displayed graphically as functions of mass ratio, and are calculated more precisely for $\mu = 0$, $\mu = 0.05$, and $\mu = 0.10$. The motions of two subsystems with one degree of freedom are compared, one subsystem being driven by the framing and the other by the concentrated mass on the plate. The plate-mounted subsystem has a response in excess of the response of the framing-mounted subsystem if the framing is suddenly put into motion with constant velocity. Except in the neighborhood of their peaks, whose locations depend upon mass ratio, the subsystem resonance curves are depressed in height by increasing the mass ratio.

Nomenclature

The following nomenclature is used in this paper:

$A_n = A_n(q_n)$ nth normal mode component of deflection of plate center
a = plate radius
$D = 2Eh^3/3(1 - \nu^2)$ = flexural rigidity
E = Young's modulus
$f(t)$ = driving displacement of plate edge, with $f(0) = 0$
$G(q)$ = combination of Bessel functions defined by Equation [7]
h = half-thickness of plate
I_n, J_n, K_n, Y_n = Bessel functions of order n
m = magnitude of concentrated mass
$p(\tau) = f(t)/a$, dimensionless driving displacement
$P(s)$ = Laplace transform of $p(\tau)$
$q = \sqrt{is}$
q_n $(n = 1, 2, \ldots)$ = real zeros of $G(q)$
r = radial co-ordinate
s = transform variable
t = real time
$u(r, t)$ = transverse deflection of plate
$w(\xi, \tau) = u(r, t)/a$, dimensionless plate deflection
$W(\xi, s)$ = Laplace transform of $w(\xi, \tau)$
$x(\tau)$ = relative position of a subsystem driven by motion of concentrated mass
$y(\tau)$ = relative position of a subsystem driven by motion of framing
$z(\tau) = x(\tau) - y(\tau)$
δ = an impulse or "δ-function"
η = "unit step function"
$\mu = m/2\pi h\rho_0 a^2$ = mass ratio
ν = Poisson ratio
$\xi = r/a$ = dimensionless plate radius
ρ_0 = intrinsic density of plate material
$\sigma(\tau)$ = inverse transform of Σ
$\Sigma(s)$ = system function defined by Equation [11]
$\tau = t\sqrt{D/2h\rho_0 a^4}$ = dimensionless time
φ_i $(i = 1, 2, 3)$ = combinations of Bessel functions defined by Equations [6]
$\omega_n = q_n^2$ = natural frequencies of plate
Ω = frequency of vibration of plate edge (i.e., framing)
Ω^* = natural frequency of subsystem with one degree of freedom

$$\nabla_v^2 = \frac{\partial}{\partial v^2} + \frac{1}{v}\frac{\partial}{\partial v}, \; v \text{ being any variable}$$

Subscripts r, t, ξ, τ denote partial derivatives with respect to the indicated variable. Primes denote differentiation with respect to the argument.

Introduction

This paper is motivated by the following physical problem: Consider a complex structure of plates and framing, which is put into motion by a shock or periodic excitation. Suppose that a piece of equipment is mounted on one of the component plates. An important question which may be asked about the motion of this system concerns the forces which act on the equipment as a result of the excitation to the structure. In effect, what is the filtering action of the plate on the excitation forces?

The motion of such a general structure does not seem to be amenable to theoretical analysis. However, some insight into the problem may be obtained by considering a model system, suitably idealized to permit quantitative treatment. Toward this end, we shall discuss the behavior of a single circular plate which carries a concentrated mass at its center. We may imagine that it is carried in a rigid frame which is in a prescribed state of motion. Although the edge conditions which most realistically correspond to the physical situation are unknown, we suppose that the edges are clamped in the frame.[2]

The procedure follows that of a previous paper,[3] in which the concentrated mass is replaced by a density impulse at the appropriate position. After listing the assumptions and formulating the problem symbolically, the method of the Laplace transform is used to solve the vibration equations. The first few natural frequencies are found as functions of the mass ratio (concentrated mass/plate mass). The complete motion of the plate is not in

---

[1] Mechanics Division, Naval Research Laboratory. Jun. ASME.

Presented at the West Coast Conference of the Applied Mechanics Division, Stanford, Calif., June 22–23, 1951, of The American Society of Mechanical Engineers.

Discussion of this paper should be addressed to the Secretary, ASME, 29 West 39th Street, New York, N. Y., and will be accepted until January 10, 1952, for publication at a later date. Discussion received after the closing date will be returned.

Note: Statements and opinions advanced in papers are to be understood as individual expressions of their authors and not those of the Society. Manuscript received by ASME Applied Mechanics Division, April 26, 1951. Paper No. 51—APM-5.

[2] The results obtained under this assumption are not entirely unrealistic. This may be a bounding case, in the sense that the natural frequencies lie above those for the case of a spring-constrained edge.

[3] "Transverse Vibrations of a Free Circular Plate Carrying Concentrated Mass," by R. E. Roberson, ASME paper No. 50—A-24. Equation [5] of this paper, which we desire to use here, contains an error. Before the $W(0, s)$ should stand a factor s^2.

question, so an explicit expression is written only for the motion of the concentrated mass.

As a further step, the response is found of a subsystem with one degree of freedom attached to the concentrated mass. The amount by which this response exceeds that of an identical system attached directly to the frame is determined and graphed for the case where the frame is suddenly put into motion with constant velocity.

The System

The assumptions which suffice to describe the system are as follows:

1 The plate is circular.
2 Circular symmetry is maintained during vibration.
3 An auxiliary mass m is concentrated at the center of the plate and exerts no effect upon the flexibility of the plate.
4 The edges of the plate are clamped.
5 The clamped edge of the initially plane and quiescent plate is given a displacement $f(t)$ normal to the undisturbed plate face, with $f(0) = 0$.
6 There are no body forces acting on the plate.
7 The usual linear thin-plate small-bending theory holds. No shear corrections are made.

In view of these assumptions, the system of equations to be solved is

$$\left.\begin{aligned} D\nabla_r^4 u(r,t) &= -2h[\rho_0 + m\delta(r)/4\pi r h]u_{tt}(r,t) \\ u(r,0) &= u_t(r,0) = 0 \\ u_r(a,t) &= 0 \\ u(a,t) &= f(t) \quad (t>0) \end{aligned}\right\} \ldots [1]$$

Here, all variables and parameters have the definitions which are given in the first section of the paper. The deflection $u(r, t)$ is measured from the position of the undeflected plate surface. In terms of previously defined dimensionless variables, the equations to be treated are

$$\left.\begin{aligned} \nabla_\xi^4 w(\xi,\tau) &= -[1+\mu\delta(\xi)/2\xi]w_{\tau\tau}(\xi,\tau) \\ w(\xi,0) &= w_\tau(\xi,0) = 0 \\ w_\xi(1,\tau) &= 0 \\ w(1,\tau) &= p(\tau) \quad (\tau>0) \end{aligned}\right\} \ldots [2]$$

The Solution

Taking the Laplace transform of Equations [2], we obtain

$$\left.\begin{aligned} (\nabla_\xi^4 - q^4)W(\xi,s) &= -\mu s^2 W(0,s)\delta(\xi)/2\xi \\ W_\xi(1,s) &= 0 \\ W(1,s) &= P(s) \end{aligned}\right\} \ldots [3]$$

where we have observed that $W(\xi, s)\delta(\xi) = W(0, s)\delta(\xi)$ because of the properties of the δ-function. By analogy with Equation [5] of the reference[3] Equation [3a] has the solution

$$W(\xi,s) = B_1 J_0(q\xi) + B_2 I_0(q\xi) + [\mu s^2 W(0,s)/4q^2]\left[\frac{\pi}{2}\,Y_0(q\xi) + K_0(q\xi)\right] \ldots [4]$$

in terms of constants B_1 and B_2, not yet determined. The continuity relation $\lim_{\xi\to 0} W(\xi, s) = W(0, s)$ implies $W(0, s) = B_1 + B_2$, so Equation [4] becomes

$$W(\xi,s) = B_1\left\{J_0(q\xi) - \frac{\mu q^2}{4}\left[\frac{\pi}{2}Y_0(q\xi) + K_0(q\xi)\right]\right\} + B_2\left\{I_0(q\xi) - \frac{\mu q^2}{4}\left[\frac{\pi}{2}\,Y_0(q\xi) + K_0(q\xi)\right]\right\} \ldots [5]$$

The constants B_1 and B_2 can be evaluated immediately by Equations [3b] and [3c]. It is convenient to introduce the combinations[4]

$$\left.\begin{aligned} \varphi_1 &= \frac{\pi}{2}(I_1 Y_0 + I_0 Y_1) + 1/q \\ \varphi_2 &= (J_1 K_0 - J_0 K_1) + 1/q \\ \varphi_3 &= I_0 J_1 + I_1 J_0 \end{aligned}\right\} \ldots [6]$$

In these terms, the characteristic equation is

$$G(q) = \varphi_3 - \frac{\mu q^2}{4}(\varphi_1 + \varphi_2) = 0 \ldots [7]$$

Its form depends, of course, only upon the boundary conditions, and in particular is independent of the manner of excitation of the plate. For the case $\mu = 0$, the characteristic equation reduces to the well-known form for a uniform clamped plate.[5] The constants B_1 and B_2 have the values

$$\left.\begin{aligned} B_1 &= \frac{P(s)}{G(q)}\left[I_1 + \frac{\mu q^2}{4}\left(\frac{\pi}{2}\,Y_1 + K_1\right)\right] \\ B_2 &= \frac{P(s)}{G(q)}\left[J_1 - \frac{\mu q^2}{4}\left(\frac{\pi}{2}\,Y_1 + K_1\right)\right] \end{aligned}\right\} \ldots [8]$$

so that

$$W(\xi,s) = \frac{P(s)}{G(q)}\left\{J_0(q\xi)\left[I_1 + \frac{\mu q^2}{4}\left(\frac{\pi}{2}\,Y_1 + K_1\right)\right] + I_0(q\xi)\left[J_1 - \frac{\mu q^2}{4}\left(\frac{\pi}{2}\,Y_1 + K_1\right)\right] - \frac{\mu q^2}{4}(I_1 + J_1)\left[\frac{\pi}{2}\,Y_0(q\xi) + K_0(q\xi)\right]\right\} \ldots [9]$$

Equation [9] can be inverted formally to give $w(\xi, \tau)$. However, we are not really interested in the deflection everywhere on the plate surface. From the point of view of the motivating physical problem, the quantity of immediate interest to us is the motion of the concentrated mass at the center of the plate. From Equation [9]

$$W(0,s) = P(s)\left[\frac{I_1 + J_1}{G(q)}\right] \ldots [10]$$

Define a system function

$$\Sigma(s) = \frac{I_1 + J_1}{sG(q)} \ldots [11]$$

whose singularities are simple poles at $s = 0$ and $s_n = \pm i\omega_n$ (where ω_n are the squares of the real zeros of G). This system function inverts to

$$\sigma(\tau) = \left[1 + \sum_{n=1}^{\infty} A_n \cos\omega_n\tau\right]\eta(\tau) \ldots [12]$$

where $\eta(\tau)$ is a unit step function

$$\eta(\tau) = \begin{cases} 0 & \tau < 0 \\ 1 & \tau > 0 \end{cases} \ldots [13]$$

and

[4] When a functional argument is unspecified, it is to be understood to be q.

[5] "Partial Differential Equations of Mathematical Physics," by A. G. Webster, second edition; Stechert, New York, N. Y., 1933, p. 355.

$$A_n = \frac{2}{q_n}\left[\frac{I_1(q_n) + J_1(q_n)}{{}^1/_2\, G'(q_n)}\right] \quad \ldots\ldots\ldots\ldots [14]$$

The explicit expression for G' is

$$^1/_2\, G'(q_n) = I_0(q_n)J_0(q_n) - \frac{1}{q_n}\varphi_1(q_n) - \frac{\mu q_n^2}{4}\left[\frac{\pi}{2} I_0(q_n)Y_0(q_n) + J_0(q_n)K_0(q_n)\right] \quad \ldots\ldots\ldots [15]$$

One can express $w(0, \tau)$ in terms of $p(\tau)$ and $\sigma(\tau)$ by applying the Laplace convolution theorem. The result is

$$w(0, \tau) = p(\tau) + \sum_{n=1}^{\infty} A_n \int_0^{\tau} p'(\lambda) \cos \omega_n (\tau - \lambda) d\lambda \ldots [16]$$

Since the first term in Equation [16] is just the displacement of the plate edge, the series represents the excess of the displacement of the concentrated mass at the plate center over that of the plate edge.

The two cases which may be of greatest physical interest are those for which $p(\tau)$ has the form

$$\text{Case I} \quad p(\tau) = \tau\eta(\tau)$$

$$\text{Case II} \quad p(\tau) = \eta(\tau) \sin \Omega\tau$$

The first of these is the case when the framing to which the plate is attached is suddenly put into motion with a constant unit velocity. It corresponds to a shock excitation of the structure.[6] The second is the case of sinusoidal motion, and, if damping were present in the structures, would lead to the steady-state vibration. Only Case I will be considered in detail. In this case

$$w_1(0, \tau) = \left[\tau + \sum_{n=1}^{\infty} \frac{A_n}{\omega_n} \sin \omega_n \tau\right] \eta(\tau) \ldots\ldots [17]$$

The Response of a Subsystem

The first four natural frequencies $\omega_n = q_n^2$ are shown as functions of mass ratio μ in Fig. 1. Table 1 gives more precise values of ω_n ($n = 1, 2, 3, 4$) for $\mu = 0$, 0.05, 0.10, and the values of A_n corresponding to these cases.[7] It should be noted that for the clamped plate, the natural frequencies are independent of the value of the Poisson ratio for the plate.

The results of Equation [17] for $w_1(0, \tau)$ can be given a physical setting in the following way: Suppose that a small linear conservative subsystem with one degree of freedom is attached to the concentrated mass. Suppose further that its own mass is so small compared to m that it exerts an entirely negligible reaction on the plate system. As shown in Fig. 2, it can be visualized as a simple mass-spring system, driven by a displacement $w_1(0, \tau)$ applied to the free end of its spring. Denote by $x(\tau)$ the deflection of the subsystem (relative to the base upon which it is mounted) under the excitation w_1. The equation of motion of the subsystem is

$$x''(\tau) + \Omega^{*2} x(\tau) = -w_1''(0, \tau) \ldots\ldots [18]$$

[6] Strictly speaking, only the first portion of a shock excitation may appear as a velocity step, or perhaps not even this. It is common practice, however, to attempt to simulate shock excitation on laboratory testing machines with velocities which are nearly steps.

[7] Compare the $\mu = 0$ values with those given in "Vibration Problems in Engineering," by S. Timoshenko, second edition, D. Van Nostrand Company, Inc., New York, N. Y., 1937, p. 430.

TABLE 1

n (mode)	$\mu = 0$ ω_n	$\mu = 0$ A_n	$\mu = 0.05$ ω_n	$\mu = 0.05$ A_n	$\mu = 0.10$ ω_n	$\mu = 0.10$ A_n
1	10.214	−1.0251	9.0120	−0.80444	8.1111	−0.74473
2	39.766	0.70290	32.833	0.52626	29.681	0.40677
3	89.114	−0.57651	72.012	−0.31087	67.733	−0.20782
4	158.18	0.49955	129.39	0.17819	125.69	0.11479

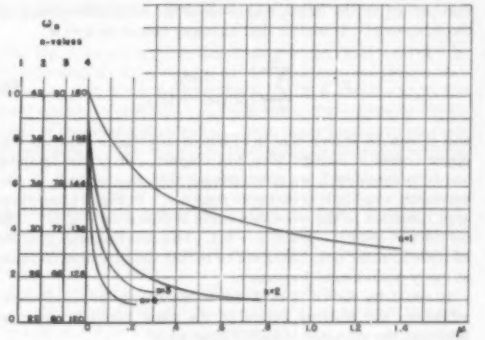

Fig. 1 Natural Frequency ω_n Versus Mass Ratio μ for Several Values of n

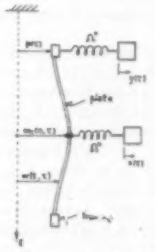

Fig. 2 Subsystem With Natural Dimensionless Frequency Ω^* Carried by the Concentrated Mass

It is easy to see that if the natural frequency Ω^* of the subsystem does not coincide with any plate natural frequency

$$x(\tau) = -\frac{1}{\Omega^*} \sin \Omega^* \tau + \sum_{n=1}^{\infty} \frac{A_n \omega_n}{(\omega_n^2 - \Omega^{*2})}\left[\frac{\omega_n}{\Omega^*} \sin \Omega^* \tau - \sin \omega_n \tau\right], \ (\tau > 0) \ldots\ldots [19]$$

On the other hand, a response

$$y(\tau) = -\frac{1}{\Omega^*} \sin \Omega^* \tau \ldots\ldots\ldots\ldots [20]$$

would have been obtained if the same subsystem had been attached to the frame at the plate edge rather than at the center of the plate, and if the frame had been put into motion in the same way. The difference $z(\tau) = x(\tau) - y(\tau)$ may be called the "excessive response" of the plate-mounted subsystem. It is a measure of the filterlike behavior of the plate. Equations [19] and [20] imply that if $\Omega^* = \omega_n$

$$z(\tau) = \sum_{n=1}^{\infty} \frac{A_n \omega_n}{(\omega_n^2 - \Omega^{*2})} \left[\frac{\omega_n}{\Omega^*} \sin \Omega^* \tau - \sin \omega_n \tau \right] \quad [21]$$

Equation [21] shows that when the excitation of the frame is a velocity step, the subsystem carried by the concentrated mass on the plate has a greater amplitude of relative vibration than that carried by the frame, regardless of the natural frequency of the subsystem. It is clear that an upper bound on $z(\tau)$ is

$$Z_{max} = \sum_{n=1}^{\infty} \left| \frac{A_n \omega_n}{\Omega^* (\omega_n - \Omega^*)} \right| \quad [22]$$

and it can be shown that $z(\tau)$ comes arbitrarily close to this upper bound if enough time has elapsed. Since no damping has been considered, we must assume that z_{max} actually is the maximum amplitude of excessive response. In Fig. 3 a four-term approximation to the resonance curve is shown for $0 < \Omega^* < 60$ for the two cases $\mu = 0$ and $\mu = 0.1$. One sees from this that the increase in mass ratio has acted to reduce the excessive response at every nonresonant frequency.

It could be shown that if the framing were in steady-state vibration, the filtering action of the plate might be used to minimize the vibration of such a subsystem.

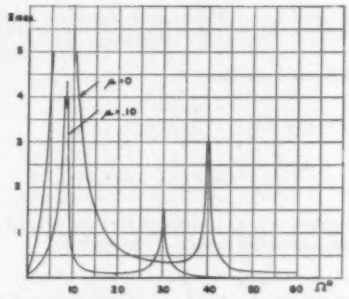

FIG. 3 MAXIMUM "EXCESSIVE RESPONSE" OF A SUBSYSTEM OF NATURAL FREQUENCY Ω^*

Although the case which has actually been considered is a specialized one, the results which have been obtained may have implications in the question of choosing locations (within structures) for equipments. These possibilities will not be developed in the present paper, pending the investigation of more general cases.

A General Method of Calculating the $M\epsilon_{max}$ Diagram in Plastic Bending of Beams[1]

By ARIS PHILLIPS,[2] STANFORD UNIVERSITY, CALIF.

In this paper we give a new method for finding the $M\epsilon_{max}$ curve in the case of symmetrical pure bending of bars in plasticity. This method is both accurate and comparatively easy to use. At the end of the paper we show how it is possible to express any σ-ϵ curve as the sum of a number of elastic plastic-stress strain lines.

Introduction

THE problem of finding the relationship between bending moment M and maximum strain ϵ_{max} in the case of symmetrical pure bending of bars in plasticity has been discussed repeatedly in the literature.[3] This paper presents a new method of calculation of the $M\epsilon_{max}$ curve, which seems to the writer to be more satisfactory than any one of the methods proposed up to now. This is especially so when the cross section has only one axis of symmetry.

This new method is based upon approximating the σ-ϵ curves for tension and compression by means of polygonal lines as shown in Fig. 1. By increasing the number of sides of these polygonal lines we can approximate the σ-ϵ curves with any desired degree of approximation. As the use of the two polygonal lines instead of the σ-ϵ curves is the only approximation entered in the method, we shall be able to find the $M\epsilon_{max}$ curve with as high accuracy as is desired.

The analytical expression for the polygonal σ-ϵ line is

$$\left.\begin{aligned}
&\sigma = E\epsilon \ldots\ldots\ldots\ldots, 0 \leqq \epsilon \leqq \epsilon_1\\
&\sigma = \sigma_1 + E_1\epsilon \ldots\ldots\ldots, \epsilon_1 \leqq \epsilon \leqq \epsilon_2\\
&\sigma = \sigma_2 + E_2\epsilon \ldots\ldots\ldots, \epsilon_2 \leqq \epsilon \leqq \epsilon_3\\
&\qquad\ldots\ldots\ldots\ldots\ldots\ldots\ldots\ldots\\
&\sigma = \sigma_n + E_n\epsilon \ldots\ldots\ldots, \epsilon_n \leqq \epsilon \leqq \epsilon_{n+1}\\
&\qquad\ldots\ldots\ldots\ldots\ldots\ldots\ldots\ldots\\
&\sigma = \sigma_k + E_k\epsilon \ldots\ldots\ldots, \epsilon_k \leqq \epsilon
\end{aligned}\right\} \text{Tension} \ldots\ldots [1]$$

$$\left.\begin{aligned}
&\sigma = E'\epsilon \ldots\ldots\ldots\ldots\ldots, 0 \leqq \epsilon \leqq \epsilon_1'\\
&\sigma = \sigma_1' + E_1'\epsilon \ldots\ldots\ldots, \epsilon_1' \leqq \epsilon \leqq \epsilon_2'\\
&\sigma = \sigma_2' + E_2'\epsilon \ldots\ldots\ldots, \epsilon_2' \leqq \epsilon \leqq \epsilon_3'\\
&\qquad\ldots\ldots\ldots\ldots\ldots\ldots\ldots\ldots\\
&\sigma = \sigma_m' + E_m'\epsilon \ldots\ldots\ldots, \epsilon_m' \leqq \epsilon \leqq \epsilon_{m+1}'\\
&\qquad\ldots\ldots\ldots\ldots\ldots\ldots\ldots\ldots\\
&\sigma = \sigma_l' + E_l'\epsilon \ldots\ldots\ldots, \epsilon_l' \leqq \epsilon
\end{aligned}\right\} \text{Compression} \ldots\ldots [2]$$

We remark that σ and ϵ are positive for both tension and compression.

In Fig. 2 we see a strain distribution in the cross section. In order to simplify the presentation of the method, we assume that the upper part of the cross section is loaded in tension while the lower part is compressed. ϵ_{max} represents the maximum tensile strain in the cross section and ϵ_{max}' represents the maximum compressive strain. For the strain distribution in this figure we have

$$\epsilon_3 < \epsilon_{max} < \epsilon_4, \quad \epsilon_3' < \epsilon'_{max} < \epsilon_2'$$

The corresponding stress distribution is shown in Fig. 2(a), while in Fig. 2(b), we see the regions in the cross section where the strain lies between o and ϵ_1 (region 0011), between ϵ_1 and ϵ_2 (region 1122), and so on.

Let us introduce next the following notations:

A_i and A_i' represent the cross-sectional areas between the neutral axis oo and lines ii and $i'i'$, respectively.

$\bar{A}_i$ and $\bar{A}_i'$ represent the cross-sectional areas between line ii and the upper boundary RR, and between line $i'i'$ and the lower boundary $R'R'$, respectively.

A and A' represent the cross-sectional areas between the neutral axis oo and upper and lower boundaries RR and $R'R'$, respectively.

$S_i, \bar{S}_i, S_i', \bar{S}_i', S, S'$ represent the statical moments, with respect to the neutral axis oo, of $A_i, \bar{A}_i, A_i', \bar{A}_i', A, A'$, respectively.

I_i, I_i' represent the moments of inertia, with respect to the neutral axis oo, of areas A_i, A_i', respectively.

$\omega_i, \omega_i', h, h'$, represent the distances between the neutral axis oo and ii, $i'i'$, RR, $R'R'$, respectively.

k_i, k_i' represent $S_i + \omega_i \bar{A}_i$ and $S_i' + \omega_i' \bar{A}_i'$, respectively.

l_i, l_i' represent $I_i + \omega_i \bar{S}_i$ and $I_i' + \omega_i' \bar{S}_i'$, respectively.

In the Appendix it will be shown that the first equation of equilibrium for the strain line in Fig. 2 is

$$\sigma_4 \frac{k_1}{\omega_1} + (\sigma_2 - \sigma_1)\frac{k_2}{\omega_2} + (\sigma_3 - \sigma_2)\frac{k_3}{\omega_3} + E_3\,\epsilon_{max}\frac{S}{h} = \sigma_3'\frac{k_1'}{\omega_1'} + E_1'\epsilon_{max}'\frac{S'}{h'} \ldots\ldots [3]$$

We shall find also that the second equation of equilibrium for the strain line in Fig. 2 is

$$M = \sigma_1\frac{l_1}{\omega_1} + (\sigma_2 - \sigma_1)\frac{l_2}{\omega_2} + (\sigma_3 - \sigma_2)\frac{l_3}{\omega_3} + E_3\,\epsilon_{max}\frac{I}{h} + \sigma_1'\frac{l_1'}{\omega_1'} + E_1'\epsilon_{max}'\frac{I'}{h'} \ldots\ldots [4]$$

If we had had $\epsilon_n \leqq \epsilon_{max} \leqq \epsilon_{n+1}$ and $\epsilon_m' \leqq \epsilon_{max}' \leqq \epsilon_{m+1}'$, then Equations [3] and [4] would have the forms

$$\left.\begin{aligned}
&\sigma_1\frac{k_1}{\omega_1} + (\sigma_2 - \sigma_1)\frac{k_2}{\omega_2} + \ldots + (\sigma_n - \sigma_{n-1})\frac{k_n}{\omega_n}\\
&+ E_n\,\epsilon_{max}\frac{S}{h}
\end{aligned}\right\} \ldots [3a]$$

[1] The results presented in this paper were obtained in the course of research conducted under a contract sponsored by the Office of Naval Research.

[2] Acting Assistant Professor, Mechanical Engineering Department, Stanford University.

[3] References are given in the Bibliography at the end of the paper.

Presented at the West Coast National Conference of the Applied Mechanics Division, Stanford, Calif., June 22-23, 1951, of The American Society of Mechanical Engineers.

Discussion of this paper should be addressed to the Secretary, ASME, 29 West 39th Street, New York, N. Y., and will be accepted until January 10, 1952, for publication at a later date. Discussion received after the closing date will be returned. Paper No. 51—APM-6.

Notes Statements and opinions advanced in papers are to be understood as individual expressions of their authors and not those of the Society. Manuscript received at ASME Applied Mechanics Division, February 12, 1951.

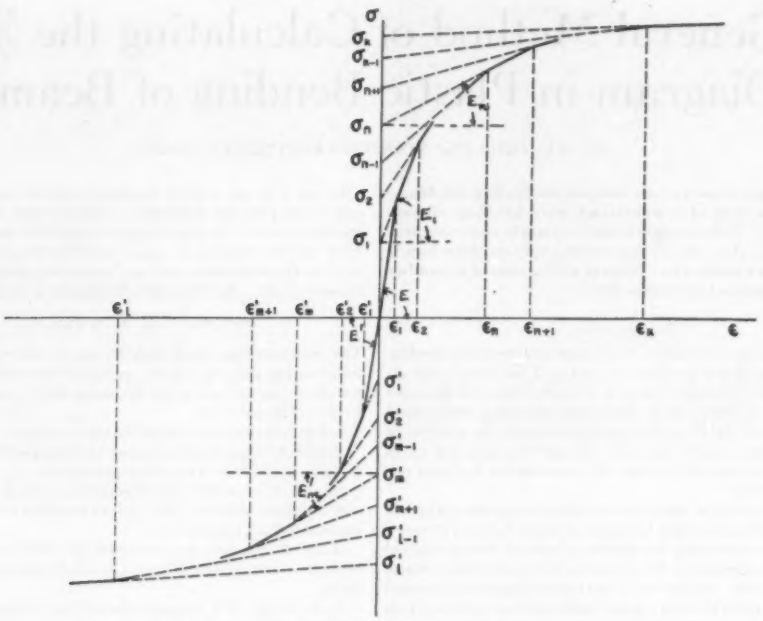

FIG. 1

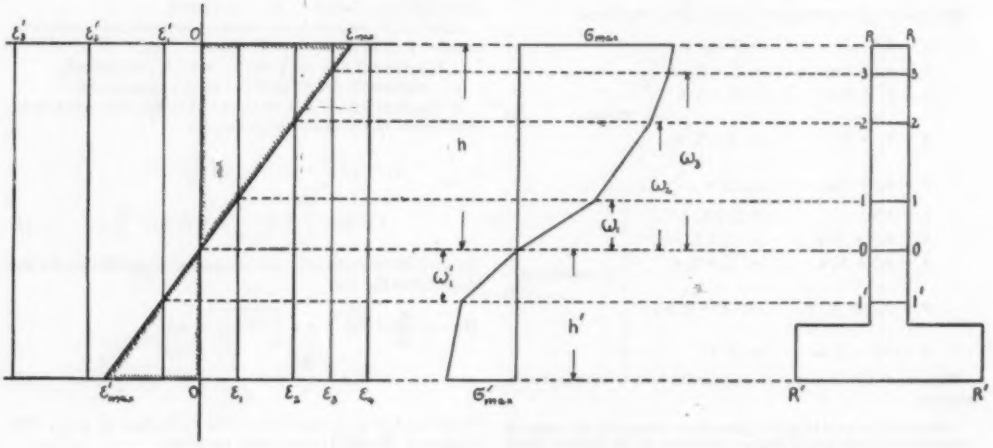

FIG. 2

FIG. 2(a)

FIG. 2(b)

$$= \sigma_1' \frac{k_1'}{\omega_1'} + (\sigma_2' - \sigma_1') \frac{k_2'}{\omega_2'} + \ldots + (\sigma_m' - \sigma_{m-1}') \frac{k_m'}{\omega_m'} + E_m' \epsilon_{max}' \frac{S'}{h'} \quad \ldots [3a]$$

and

$$M = \sigma_1 \frac{l_1}{\omega_1} + (\sigma_2 - \sigma_1) \frac{l_2}{\omega_2} + \ldots + (\sigma_n - \sigma_{n-1}) \frac{l_n}{\omega_n} + E_n \epsilon_{max} \frac{I}{h} + \sigma_1' \frac{l_1'}{\omega_1'} + (\sigma_2' - \sigma_1') \frac{l_2'}{\omega_2'} + \ldots + (\sigma_m' - \sigma_{m-1}') \frac{l_m'}{\omega_m'} + E_m' \epsilon_{max}' \frac{I'}{h'} \quad \ldots [4a]$$

Equation [3] or [3a] will be used for determining the position of the neutral axis for a given ϵ_{max} while Equation [4] or [4a] will be used for determining the value of the bending moment M corresponding to the selected ϵ_{max} and position of the neutral axis.

A Graphical Construction

We shall give a simple graphical construction facilitating the use of these two equations. By means of this construction we shall be able to find the values of the quantities entering into Equations [3] and [4], or [3a] and [4a]. In Fig. 3 we see the cross section of a beam, while in Fig. 3(*a*) the line bp'–area line–is drawn in such a manner that beginning from the top of the cross section any area (*RRii*) will be represented by means of the length cc'. Hence, if *oo* is the neutral axis and *ii* is the line where the strain is equal to $\epsilon_i (i = 1, 2, \ldots)$ then

$$cc' = \overline{A}_i, dd' = A, ed' = A_i, ol = \omega_i, bd = h$$

We remark also that the slope of curve bp' at point c', with respect to bp, is equal to the width *ii* of the cross section.

The statical moment of any element dA of the cross section in Fig. 3, with respect to *oo*, will be dAy = shaded trapezoidal area in Fig. 3(*a*). Therefore the statical moment of the area (*iioo*), with respect to *oo*, is equal to area ($c'ed'$); while the statical moment of area (*RRii*), with respect to *oo*, is equal to area ($bc'edb$). We remark also that the statical moment of area (*RRii*), with respect to *ii*, is equal to area (bcc'). Therefore

$$S_i = (c'd'e), \overline{S}_i = (bc'edb), S = (bd'd)$$

In Fig. 3(*b*) the line BP'—statical moment line—is drawn in such a manner that beginning from the top of the cross section any area ($bc'c$) in Fig. 3(*a*) will be represented by means of the length CC'. Hence the slope of curve BP' at point C', with respect to BP, is equal to the width cc'. Therefore area ($bc'c$) = CC'

$$S = DD', S_i = FD', \overline{S}_i = DF$$

where $C'F$ is the tangent to the curve BP' at C'.

The moment of inertia of the element dA, with respect to *oo*, is equal to $dAy^2 = (dAy)y$ = [shaded trapezoidal area in Fig. 3(*a*)] $\times y = LMy = 2 \times$ [shaded area in Fig. 3(*b*)]. Hence the moment of inertia of the area (*iioo*), with respect to *oo* is equal to $2 \times$ area ($C'FD'$)

In Fig. 3(*c*) the line $\beta\omega'$—moment-of-inertia line—is drawn in such a manner that beginning from the top of the cross section any area (BCC') in Fig. 3(*b*) will be represented by means of the length $\gamma\gamma'$.

We see now that $k_i = S_i + \omega_i\overline{A}_i$ is equal to area ($cc'd'd$) = area (bdd') — area (bcc') = $DD' - CC' = C'G$. We have also $S = DD' = BC$. Furthermore, we find that

$$\begin{aligned} l_i &= I_i + \omega_i\overline{S}_i = 2(C'FD') + (DF)(CD) \\ &= 2(C'FD') + 2(DC'F) = 2(DC'D') \\ &= 2(BDD') - 2(BC'C) - 2(CC'D) \\ &= 2\,\delta\delta' - 2\gamma\gamma' - CD \times CC' = 2\,\epsilon\delta' - \epsilon\eta \end{aligned}$$

where $\gamma'\eta$ is the tangent to curve $\beta\omega'$ at γ'. Hence

$$l_i = 2\left(\epsilon\delta' - \frac{\epsilon\eta}{2}\right) = 2\,\Theta\sigma'$$

where Θ is the middle of $\epsilon\eta$. We have also $I = 2\,\delta\delta'$.

For finding the values k_i', l_i' and generally all quantities with a prime, we construct similar diagrams beginning from the bottom of the cross section. In Figs. 4 to 4(*c*) we give a complete picture of the construction.

When $\epsilon_{max} \leqq \epsilon_1$ and $\epsilon'_{max} \leqq \epsilon_1'$—elastic case—then the first equation of equilibrium becomes

$$E\epsilon_{max}\frac{S}{h} = E'\epsilon'_{max}\frac{S'}{h'}$$

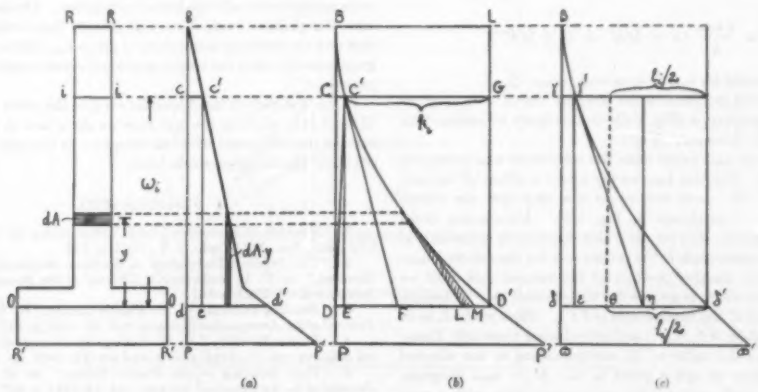

FIG. 3

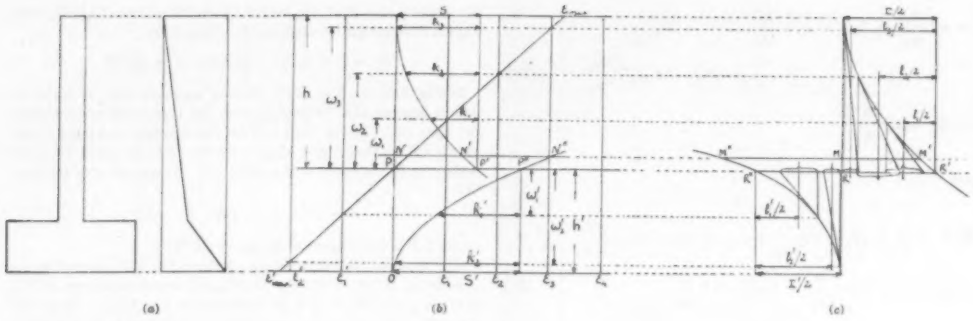

FIG. 4

But we have

$$\epsilon_{max}/h = \epsilon'_{max}/h'$$

Hence

$$E'/E = S/S'$$

Thus in this case the neutral axis coincides with the line NN' for which $NN'/NN'' = E'/E$, Fig. 4(*b*); the position of the neutral axis is constant for $\epsilon_{max} \leqq \epsilon_1$ and $\epsilon_{max}' \leqq \epsilon_1'$. The corresponding bending moment is

$$M = E\,\epsilon_{max}\frac{I}{h} + E'\epsilon'_{max}\frac{I'}{h'} = \frac{\epsilon_{max}}{h}(EI + E'I') \quad \ldots [5]$$

We have $I = 2\,MM'$ and $I' = 2\,MM''$, Fig. 4(*c*).

On the basis of what we have said up to now we can find the $M - \epsilon_{max}$ curve by means of the following procedure, Fig. 4:

1 We select the polygonal line $\sigma - \epsilon$, Fig. 1.

2 We make a drawing of the cross section, Fig. 4, and of the following lines: 1 area lines, Fig. 4(*a*), 2 statical moment lines Fig. 4(*b*), and 3 moment-of-inertia lines, Fig. 4(*c*). We remark that the statical moment lines have been superimposed upon the network . . $\epsilon_2'\epsilon_3'\epsilon_1'0\epsilon_1\epsilon_2\epsilon_3 \ldots$.

3 We find the elastic position of the neutral axis NN'', using formula $(NN')/(NN'') = E'/E$.

4 We find MM' and MM'' from Fig. 4(*c*), and we use equation

$$M = \frac{2\,\epsilon_{max}}{h}(E \times MM' + E \times MM'')$$

This formula is valid for $\epsilon_{max} \leqq \epsilon_1$ as long as $\epsilon_{max}' \leqq \epsilon_1'$.

5 We represent graphically the straight line $M - \epsilon_{max}$ given by the foregoing equation [Fig. 4(*d*)—in this figure we assume that when $\epsilon_{max} = \epsilon_1$ we have $\epsilon_{max}' \leqq \epsilon_1'$].

6 We select an ϵ_{max} larger than the maximum ϵ_{max} permitted in Equation [5]. For this ϵ_{max} we try a new position of the neutral axis PP''. We draw the strain line and find the values ω_1, ω_2, k_1, k_2, . . . as shown in Fig. 4(*b*). Introducing these values into Equation [3*a*] we see if this equation is satisfied. If it is, then this neutral axis is the proper one for the selected ϵ_{max}. Otherwise, we try another position of the neutral axis until we find the position which is proper for the selected ϵ_{max}. Assume that this position of the neutral axis is PP''. Then we find, as in Fig. 4(*c*), the values of l_1, l_2, . . . and introducing them into Equation [4*a*], we get the value of M, corresponding to the selected ϵ_{max}. In this way we get a point in the $M - \epsilon_{max}$ diagram. After finding enough such points, we connect them with a continuous curve, thus getting the $M - \epsilon_{max}$ curve, Fig. 4(*d*).

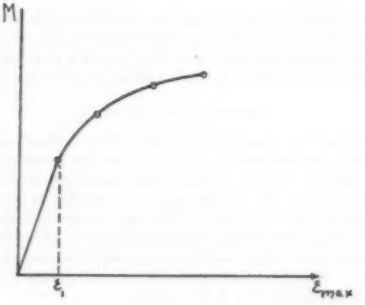

FIG. 4(*d*)

CONCLUSION

After having explained this method we can now give the reasons why we consider this method more satisfactory than any one of the methods proposed up to now. From the point of view of accuracy this method is as good as the most exact method devised up to now, that is, the method described by Timoshenko.[4] However, Timoshenko's method is very involved when used for a cross section with only one axis of symmetry. On the other hand, with the present method we are able to find both the neutral axis and the bending moment for a given ϵ_{max} with comparatively great ease by using the simple graphical construction given in this paper.

In the first part of the Appendix we give the proof of Equations [3] and [4]; while in the last part we show how it is possible to express the polygonal stress-strain curve as the sum of a number of elastic-plastic stress-strain lines.

BIBLIOGRAPHY

1 "Strength of Materials," by S. Timoshenko, D. Van Nostrand Company, Inc., New York, N. Y., 1941, p. 362.

2 "The Stresses Developed in Sections Subjected to Bending Moment," by T. L. Beilschmidt, *Journal of the Royal Aeronautical Society*, vol. 46, 1942, p. 161.

3 "Bending Strength in the Plastic Range," by F. P. Cossone, *Journal of the Aeronautical Sciences*, vol. 10, 1943, p. 137.

4 "Plastic Bending," by W. R. Osgood, *Journal of the Aeronautical Sciences*, vol. 11, 1944, p. 213, and vol. 12, 1945, pp. 253 and 408.

5 "Pure Bending in the Plastic Range," by H. A. Williams, *Journal of the Aeronautical Sciences*, vol. 14, 1947, p. 457.

[4] Reference (1) in the Bibliography

6 "Elastic and Plastic Bending of Beams," by Tsun Kuei Wang, *Journal of the Aeronautical Sciences*, vol. 14, 1947, p. 422.

7 "Theory of Inelastic Bending With Reference to Limit Design," by A. Hrennikoff, Trans. ASCE, vol. 113, 1948, p. 213.

8 "Theory of Plasticity—Elements of Simple Theory," by J. W. Roderick, *Philosophical Magazine*, series 7, vol. 39, 1948, p. 529.

9 "Carrying Capacity of Simply Supported Mild Steel Beams," by J. W. Roderick and I. H. Phillips, *Engineering Structures*, Butterworth's Scientific Publications, London, England, 1949, p. 9.

10 "Theory of Flow and Fracture of Solids," by A. Nadai, McGraw-Hill Book Company, Inc., New York, N. Y., 1950, p. 353.

11 "On Symmetrical Pure Bending of Beams," by Aris Phillips, Navy Contract N6-ONR-251, Task Order XI, Technical Report no. 4, Stanford University, Stanford, Calif., 1949.

12 "On Symmetrical Pure Bending of Beams, Part 2," by Aris Phillips, Navy Contract N6-ONR-251 Task Order XI, Technical Report no. 5, Stanford University, Stanford, Calif., 1949.

13 "Symmetrical Pure Bending of Beams in Plasticity. A General Solution," by Aris Phillips, Navy Contract N6-ONR-251 Task Order XI, Technical Report No. 7, 1950.

Appendix

Proof for Equations [3] and [4]

The first equation of equilibrium is

$$\Sigma \sigma \, dA = 0 \ldots\ldots\ldots\ldots\ldots\ldots [6]$$

Using Equations [1] and [2] and the known formula $\epsilon = y/\rho$ of the elementary bending theory, we have, according to Figs. 2 to 2(*b*), a new expression for Equation [6]

$$\int_0^{\omega_1} E \frac{y}{\rho} b(y)\,dy + \int_{\omega_1}^{\omega_2} \sigma_1 b(y)\,dy + \int_{\omega_1}^{\omega_2} E_1 \frac{y}{\rho} b(y)dy + \int_{\omega_2}^{\omega_3} \sigma_2 b(y)dy + \int_{\omega_2}^{\omega_3} E_2 \frac{y}{\rho} b(y)dy + \int_{\omega_3}^{h} \sigma_3 b(y)dy + \int_{\omega_3}^{h} E_3 \frac{y}{\rho} b(y)dy = \int_0^{\omega_1'} E' \frac{y}{\rho} b(y)dy + \int_{\omega_1'}^{\omega_2'} \sigma_1' b(y)dy + \int_{\omega_1'}^{h'} E_1' \frac{y}{\rho} b(y)\,dy$$

This equation can also be written in the form

$$\frac{E}{\rho} S_1 + \sigma_1 (\bar{A}_1 - \bar{A}_2) + \frac{E_1}{\rho} (S_2 - S_3) + \sigma_2(\bar{A}_2 - \bar{A}_3) + \frac{E_2}{\rho} (S_3 - S_3) + \sigma_3\bar{A}_3 + \frac{E_3}{\rho} (S - S_3) = \frac{E'}{\rho} \bar{S}_1' + \sigma_1'\bar{A}_1' + \frac{E_1'}{\rho} (\bar{S}' - \bar{S}_1')$$

Remarking that

$$\frac{1}{\rho} = \frac{\epsilon_{max}}{h} = \frac{\epsilon_{max}'}{h'} = \frac{\epsilon_1}{\omega_1} = \frac{\epsilon_2}{\omega_2} = \frac{\epsilon_3}{\omega_2} = \frac{\epsilon_1'}{\omega_1'}$$

and

$$(E - E_1)\epsilon_1 = \sigma_1, \; (E_1 - E_2)\epsilon_2 = \sigma_2 - \sigma_1, \; (E_2 - E_3)\epsilon_3 = \sigma_3 - \sigma_2$$
$$(E' - E_1')\epsilon_1' = \sigma_1'$$

we find finally Equation [3], the generalization of which is Equation [3*a*].

In the same way we prove that the second equation of equilibrium

$$\Sigma \sigma y \, dA = M$$

has the form given in Equation [4] or [4*a*].

Expression of Polygonal Stress-Strain Curve as Sum of a Number of Elastic-Plastic Stress-Strain Lines

Equations [1] may be written in the form

$$\sigma = (E - E_1)\epsilon + (E_1 - E_2)\epsilon + \ldots + (E_{n-1} - E_n)\epsilon + \ldots + (E_{k-1} - E_k)\epsilon + E_k\epsilon, \; 0 \leqq \epsilon \leqq \epsilon_1$$
$$\sigma = \sigma_1 + (E_1 - E_2)\epsilon + \ldots + (E_{n-1} - E_n)\epsilon + \ldots + (E_{k-1} - E_k)\epsilon + E_k\epsilon, \; \epsilon_1 \leqq \epsilon \leqq \epsilon_2$$
$$\sigma = \sigma_1 + (\sigma_2 - \sigma_1) + \ldots + (E_{n-1} - E_n)\epsilon + \ldots + (E_{k-1} - E_k)\epsilon + E_k\epsilon, \; \epsilon_2 \leqq \epsilon \leqq \epsilon_3$$
$$\ldots\ldots\ldots\ldots\ldots\ldots\ldots\ldots\ldots\ldots\ldots\ldots\ldots\ldots\ldots\ldots$$

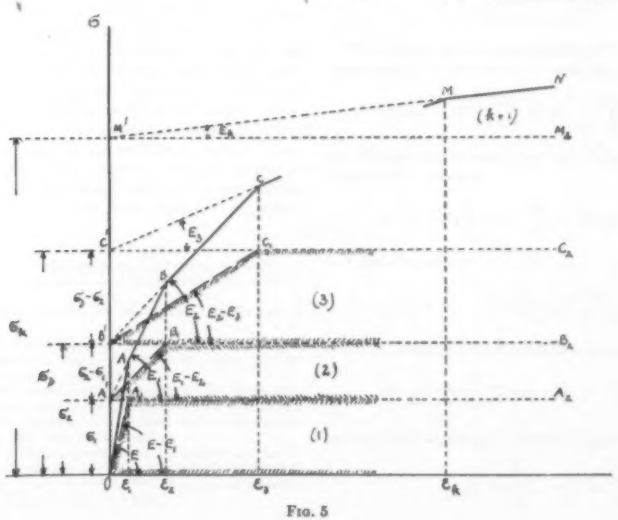

FIG. 5

$$\sigma = \sigma_1 + (\sigma_2 - \sigma_1) + \ldots + (\sigma_n - \sigma_{n-1}) + \ldots + (E_{k-1} - E_k)\epsilon + E_k\epsilon, \ \epsilon_n \leqq \epsilon \leqq \epsilon_{n+1}$$

$$\sigma = \sigma_1 + (\sigma_2 - \sigma_1) + \ldots + (\sigma_n - \sigma_{n-1}) + \ldots + (\sigma_k - \sigma_{k-1}) + E_k\epsilon, \ \epsilon_k \leqq \epsilon$$

Hence we may represent the line defined by Equations [1] as the sum of k elastic-plastic stress-strain lines

$$\left.\begin{aligned} \sigma &= (E - E_1)\epsilon \ldots\ldots 0 \leqq \epsilon \leqq \epsilon_1 \\ \sigma &= \sigma_1 \qquad\quad \ldots\ldots \epsilon_1 \leqq \epsilon \end{aligned}\right\} \ldots\ldots\ldots (1)$$

$$\left.\begin{aligned} \sigma &= (E_1 - E_2)\epsilon \ldots 0 \leqq \epsilon \leqq \epsilon_2 \\ \sigma &= \sigma_2 - \sigma_1 \ldots\ldots \epsilon_2 \leqq \epsilon \end{aligned}\right\} \ldots\ldots\ldots (2)$$

$$\left.\begin{aligned} \sigma &= (E_2 - E_3)\epsilon \ldots 0 \leqq \epsilon \leqq \epsilon_3 \\ \sigma &= \sigma_3 - \sigma_2 \ldots\ldots \epsilon_3 \leqq \epsilon \end{aligned}\right\} \ldots\ldots\ldots (3)$$

$$\ldots\ldots$$

$$\ldots\ldots$$

$$\left.\begin{aligned} \sigma &= (E_{n-1} - E_n)\epsilon \ldots 0 \leqq \epsilon \leqq \epsilon_n \\ \sigma &= \sigma_n - \sigma_{n-1} \ldots\ldots \epsilon_n \leqq \epsilon \end{aligned}\right\} \ldots\ldots\ldots (n)$$

$$\left.\begin{aligned} \sigma &= (E_{k-1} - E_k)\epsilon \ldots 0 \leqq \epsilon \leqq \epsilon_k \\ \sigma &= \sigma_k - \sigma_{k-1} \ldots\ldots \epsilon_k \leqq \epsilon \end{aligned}\right\} \ldots\ldots\ldots (k)$$

and of one elastic stress-strain line

$$\sigma = E_1\epsilon \ldots 0 \leqq \epsilon \ldots\ldots\ldots\ldots\ldots\ldots\ldots\ldots (k+1)$$

In Fig. 5 we give the graphical analysis of line 1 into its component lines. The original $\sigma - \epsilon$ line is the polygonal line $OABC \ldots MN$. The elastic-plastic materials are represented by

$$OA_1A_2,\ A_2A'B_1B_2,\ B_2B'C_1C_2 \ldots$$

while the elastic material is represented by $M_2M'M$. A similar analysis is valid for the stress-strain line expressed by Equations [2].

Bending of Thin Ring-Sector Plates

By L. I. DEVERALL[1] and C. J. THORNE,[2] SALT LAKE CITY, UTAH

General expressions for the deflection of plates whose planform is a sector of a circular ring are given for cases in which the straight edges have arbitrary but given deflection and bending moment. The solutions are given for all combinations of physically important edge conditions on the two circular edges. Sectors of circular plates are included as special cases. Solutions are given for a general load which is a continuous function of r, and a sectionally continuous function of θ, where r and θ are the usual polar co-ordinates with the pole at the center of the ring. Several specific examples are given.

Introduction

SOME problems for plates in the form of a sector have been solved by Nadai. In particular, the solution for a uniformly loaded sector of a circular plate with the straight edges simply supported (as well as a reference to Nadai's work) may be found in Timoshenko (1).[3] Kuhn (2) has tabulated the deflections, moments, shearing forces, and reactions for a simply supported semicircular plate with a uniform load. The problem of finding the bending moments in a uniformly loaded clamped plate whose planform is a sector of a circle has been investigated by Carrier (3).

Finite integral operators have been used by Tolotti (4, 5), to investigate the stress distribution in rectangular parallelopipeds and plates whose planform is a sector of a circular ring. By defining the deflection in terms of an integral operator (transform) the integrand of which depends upon r (radius vector in polar co-ordinates) and a parameter λ, and applying this transform to the partial differential equation of bending of the plate, a new ordinary differential equation is obtained. Since this new differential equation involves the values of the deflection and its normal derivatives at the edges of the plate, Tolotti's method of solution would require solving an integro-differential equation. He completes no specific example by this method.

In this paper the finite Fourier sine transform is used to find the deflection of a thin homogeneous isotropic plate whose planform is a sector of a circular ring, and which has arbitrary but given deflection and bending moments along its straight edges, and any physically important edge conditions along its curved edges. The method was used by the authors to obtain similar results for rectangular plates (6). Values of the constants (in terms of a general load function) which appear in the expression for the deflection are given for the three physically important combinations of edge conditions at the two curved edges. Several specific examples are carried out in detail.

The Problem

The deflection $w(r, \theta)$ of a thin homogeneous plate must satisfy

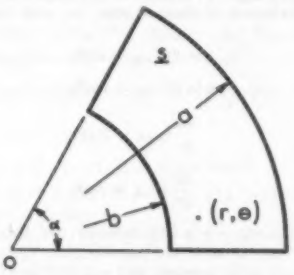

Fig. 1 The Plate

the following differential equation over the region S bounded by the plate (7)

$$\nabla^2\nabla^2 w(r, \theta) = q(r, \theta)/D \quad \ldots\ldots [1]$$

where

$$\nabla^2 = \left[\frac{\partial^2}{\partial r^2} + (1/r)\frac{\partial}{\partial r} + (1/r^2)\frac{\partial^2}{\partial \theta^2}\right]$$

$q(r, \theta)$ = load function
$D = Eh^3/12(1 - \nu^2)$, flexural rigidity
E = Young's modulus
h = thickness of plate
ν = Poisson's ratio

The bending moment per unit length M_r (in polar co-ordinates perpendicular to direction r = const) is equal to

$$M_r = -D\left[\frac{\partial^2 w}{\partial r^2} + \nu\left(\frac{1}{r}\frac{\partial w}{\partial r} + \frac{1}{r^2}\frac{\partial^2 w}{\partial \theta^2}\right)\right] \quad \ldots [2]$$

and the bending moment per unit length M_t (perpendicular to direction θ = const) is

$$M_t = -D\left[(1/r)\frac{\partial w}{\partial r} + (1/r^2)\frac{\partial^2 w}{\partial \theta^2} + \nu\frac{\partial^2 w}{\partial r^2}\right] \quad \ldots [3]$$

and cross moment

$$M_{rt} = (1 - \nu)D\left[(1/r)\frac{\partial^2 w}{\partial r\,\partial \theta} - (1/r^2)\frac{\partial w}{\partial \theta}\right] \quad \ldots\ldots [4]$$

The expression for the shearing force is

$$Q_r = -D\frac{\partial}{\partial r}(\nabla^2 w), \quad Q_t = -D(1/r)\frac{\partial}{\partial \theta}(\nabla^2 w) \quad \ldots\ldots [5]$$

and the reaction along the circular edge is

$$V_r = \left[Q_r - (1/r)\frac{\partial M_{rt}}{\partial \theta}\right] \quad \ldots\ldots [6]$$

---

[1] Instructor, Department of Mathematics, University of Utah.

[2] Associate Professor, Department of Mathematics, University of Utah.

[3] Numbers in parentheses refer to the Bibliography at the end of the paper.

Presented at the West Coast National Conference of the Applied Mechanics Division, Stanford, Calif., June 22–23, 1951, of The American Society of Mechanical Engineers.

Discussion of this paper should be addressed to the Secretary, ASME, 29 West 39th Street, New York, N. Y., and will be accepted until January 10, 1952, for publication at a later date. Discussion received after the closing date will be returned.

Note: Statements and opinions advanced in papers are to be understood as individual expressions of their authors and not those of the Society. Manuscript received by ASME Applied Mechanics Division, July 21, 1950. Paper No. 51—APM-1.

We shall take on the edges $\theta = 0$, and $\theta = \alpha$

$$w(r, \theta)\,|_{\theta=0} = w_1(r) \quad [7]$$

$$w(r, \theta)\,|_{\theta=\alpha} = w_2(r) \quad [8]$$

$$M_t\,|_{\theta=0} = M_1(r) \quad [9]$$

$$M_t\,|_{\theta=\alpha} = M_2(r) \quad [10]$$

The edge conditions for the edges $r = a$, and $r = b$ ($a > b$, $b \neq 0$) are as follows:

Case 1 The edges $r = a$, and $r = b$, with deflection and slope given (generalization of clamped edge, i.e., with deflection and slope zero)

$$w(r, \theta)|_{r=a} = w_3(\theta) \quad [11]$$

$$w(r, \theta)|_{r=b} = w_4(\theta) \quad [12]$$

$$\frac{\partial w}{\partial r}\,|_{r=a} = S_1(\theta) \quad [13]$$

$$\frac{\partial w}{\partial r}\,|_{r=b} = S_2(\theta) \quad [14]$$

Case 2 The edge $r = a$ with deflection and slope given; the edge $r = b$ with moment and reaction given (generalization of free edge, i.e., with moment and reaction zero). Equations [11] and [13] together with

$$M_r\,|_{r=b} = M_4(\theta) \quad [15]$$

$$V_r\,|_{r=b} = V_1(\theta) \quad [16]$$

Case 3 The edges $r = a$, and $r = b$, both with moment and reaction given. Equations [15] and [16] together with

$$M_r\,|_{r=a} = M_3(\theta) \quad [17]$$

$$V_r\,|_{r=a} = V_2(\theta) \quad [18]$$

The case of the sector of the circle (i.e., with $b = 0$) will be treated later. There exist other mathematically possible combinations of edge conditions, and the problems corresponding to these sets of edge conditions can be worked out by the method to be presented. The three cases given seem to be of most practical importance.

The Sine Transform

Let $y(\theta)$ be a function which is equal to its Fourier sine series for $0 < \theta < \alpha$. The "finite Fourier sine transform" of $y(\theta)$ is the function $y_s(\beta)$ obtained by the linear integral operation defined as follows

$$y_s(\beta) \equiv S[y(\theta)] = \int_0^{\alpha} y(\theta) \sin \beta\theta \, d\theta \quad [19]$$

where

$$\beta = (n\pi/\alpha),\ (0 < \theta < \alpha,\ n = 1, 2, \ldots)$$

since

$$y(\theta) = \sum_{n=1}^{\infty} b_n \sin \beta\theta, \quad (0 < \theta < \alpha) \quad [20]$$

where

$$b_n = (2/\alpha) \int_0^{\alpha} y(\theta) \sin \beta\theta \, d\theta = (2/\alpha)\, y_s(\beta) \quad [21]$$

we have

$$y(\theta) = (2/\alpha) \sum_{n=1}^{\infty} y_s(\beta) \sin \beta\theta, \quad (0 < \theta < \alpha) \quad [22]$$

This Expression [22] for $y(\theta)$ is the "inverse sine transform" of $y_s(\beta)$.

Repeated integration by parts yields the following formulas for the transforms of second and fourth derivatives

$$S\left[\frac{d^2y}{d\theta^2}\right] = -\beta^2 y_s(\beta) - \beta[(-1)^n\, y(\alpha) - y(0)] \quad [23]$$

$$S\left[\frac{d^4y}{d\theta^4}\right] = \beta^4 y_s(\beta) - \beta[(-1)^n y''(\alpha) - y''(0)] + \beta^2[(-1)^n\, y(\alpha) - y(0)] \quad [24]$$

When writing the sine transform (or inverse transform) of any function, we shall assume that the function has properties necessary for that transform or inverse transform to exist (8). Also, we assume continuity of all derivatives.

Solution of the Problem

By expanding the left-hand member of Equation [1], and then taking the sine transform with respect to θ, the following differential equation involving the sine-transformed deflection $w_s(r, \beta)$ is obtained

$$\left.\begin{aligned} &w_s^{(4)}(r, \beta) + (2/r)w_s^{(3)}(r, \beta) - (1/r^2)(1 + 2\beta^2)w_s^{(2)}(r, \beta) \\ &+ (1/r^3)(1 + 2\beta^2)w_s'(r, \beta) + [\beta^2(\beta^2 - 4)/r^4]w_s(r, \beta) \\ &= q_s(r, \beta)/D + (2\beta/r^3)[(-1)^n w^{(2)}(r, \alpha) - w^{(2)}(r, 0)] \\ &- (2\beta/r^3)[(-1)^n w'(r, \alpha) - w'(r, 0)] \\ &+ [(4\beta - \beta^3)/r^4][(-1)^n w(r, \alpha) - w(r, 0)] \\ &+ (\beta/r^4)\left[(-1)^n \frac{\partial^2 w(r, \alpha)}{\partial\theta^2} - \frac{\partial^2 w(r, 0)}{\partial\theta^2}\right] \end{aligned}\right\} \quad [25]$$

where $w_s^{(4)}(r, \beta)$ denotes the fourth derivative of $w_s(r, \beta)$ with respect to r. From edge conditions, Equations [7], [8], [9], [10], Equation [25] becomes

$$\left.\begin{aligned} &w_s^{(4)}(r, \beta) + (2/r)w_s^{(3)}(r, \beta) - (1/r^2)(1 + 2\beta^2)w_s^{(2)}(r, \beta) \\ &+ (1/r^3)(1 + 2\beta^2)w_s'(r, \beta) + [\beta^2(\beta^2 - 4)/r^4]w_s(r, \beta) \\ &= q_s(r, \beta)/D + (2\beta/r^3)[(-1)^n w_2^{(2)}(r) - w_1^{(2)}(r)] \\ &- (2\beta/r^3)[(-1)^n w_2'(r) - w_1'(r)] \\ &+ [(4\beta - \beta^3)/r^4][(-1)^n w_2(r) - w_1(r)] \\ &- (\beta/r^2)\{(-1)^n [M_2(r)/D + (1/r)w_2'(r) + \nu w_2^{(2)}(r)] \\ &- [M_1(r)/D + (1/r)w_1'(r) + \nu w_1^{(2)}(r)]\} \end{aligned}\right\} \quad [26]$$

The solution of this differential equation is

$$w_s(r, \beta) = C_1 r^{\beta} + C_2 r^{-\beta} + C_3 r^{\beta+2} + C_4 r^{-\beta+2} + G(r, \beta), \ (\beta \neq 1) \quad [27]$$

$$w_s(r, 1) = C_1 r + C_2 r^{-1} + C_3 r^3 + C_4 r \log r + G(r, 1) \quad [28]$$

where $G(r, \beta)$ is a particular solution corresponding to the nonhomogeneous part of Equation [26].

The inverse sine transform $w(r, \theta)$ of $w_s(r, \beta)$ is found from Equation [22]

$$w(r, \theta) = (2/\alpha) \sum_{n=1}^{\infty} w_s(r, \beta) \sin \beta\theta, \ (0 < \theta < \alpha) \quad [29]$$

Evaluation of the Constants

By taking the sine transform of edge conditions, Equations [11] to [18], inclusive, with the aid of Equations [3], [5], and [6], we can evaluate the arbitrary constants in Equations [27] and [28]. The values of these constants are as follows:

Case 1 For $\beta \neq 1$

$$2C_1D_1 = -a^{2\beta}b^2\,[G(a,\beta) - W_{1s}(\beta)]\,[(\beta+2)a^{2\beta+2} + (\beta^2-\beta-2)a^2b^{2\beta} - \beta^2b^{2\beta+2}] - a^{\beta+1}b^{\beta+1}[G'(a,\beta) - S_{1s}(\beta)]\,[(\beta+1)a^2b^{2\beta} - \beta b^{2\beta+2} - a^{2\beta+2}] - a^2b^\beta[G(b,\beta) - W_{1s}(\beta)]\,[\beta^2a^{2\beta+2} - (\beta^2-\beta-2)a^2b^2 + (\beta+2)b^{2\beta+2} - \beta^2a^{2\beta+2}] + a^\beta b^{\beta+1}\,[G'(b,\beta) - S_{1s}(\beta)]\,[\beta a^{2\beta+2} - (\beta+1)\,a^{2\beta}b^2 + b^{2\beta+2}] \quad [30a]$$

$$2C_2D_1 = -a^{\beta+2}b^{2\beta+2}[G(a,\beta) - W_{2s}(\beta)]\,[(\beta^2+\beta-2)a^{2\beta} - \beta^2a^{2\beta-2}b^2 - (\beta-2)b^{2\beta}] + a^{\beta+2}b^{2\beta+2}\,[G'(a,\beta) - S_{1s}(\beta)]\,[(\beta-1)a^{2\beta} - \beta a^{2\beta-2}b^2 + b^{2\beta}] + a^{2\beta+2}b^{\beta+2}[G(b,\beta) - W_{1s}(\beta)]\,[(\beta-2)a^{2\beta} + \beta^2a^2b^{2\beta-2} - (\beta^2+\beta-2)b^{2\beta}] + a^{2\beta+2}b^{\beta+2}\,[G'(b,\beta) - S_{2s}(\beta)]\,[a^{2\beta} - \beta a^2b^{2\beta-2} + (\beta-1)b^{2\beta}] \quad [30b]$$

$$2C_3D_1 = \beta a^\beta b^\beta[G(a,\beta) - W_{2s}(\beta)]\,[a^{2\beta} + (\beta-2)a^2b^{2\beta-2} - (\beta-1)b^{2\beta}] + a^{\beta+1}\,b^2[G'(a,\beta) - S_{1s}(\beta)]\,[\beta a^2b^{2\beta-2} - a^{2\beta} - (\beta-1)b^{2\beta}] + \beta a^2b^\beta\,[G(b,\beta) - W_{1s}(\beta)]\,[(\beta-2)a^{2\beta-2}b^2 - (\beta-1)a^{2\beta} + b^{2\beta}] + a^2b^{\beta+1}\,[G'(b,\beta) - S_{2s}(\beta)]\,[\beta a^{2\beta-2}b^2 - (\beta-1)\,a^{2\beta} - b^{2\beta}] \quad [30c]$$

$$2C_4D_1 = \beta a^\beta b^{2\beta}\,[G(a,\beta) - W_{1s}(\beta)]\,[(\beta+2)a^{2\beta+2} - (\beta+1)a^{2\beta}b^2 - b^{2\beta+2}] + a^{\beta+1}b^{2\beta}\,[G'(a,\beta) - S_{1s}(\beta)]\,[(\beta+1)a^2b^{2\beta} - \beta a^{2\beta+2} - b^{\beta+2}] + \beta a^{2\beta}b^\beta\,[G(b,\beta) - W_{1s}(\beta)]\,[(\beta+2)b^{2\beta+2} - (\beta+1)a^2b^{2\beta} - a^{2\beta+2}] + a^{2\beta}b^{\beta+1}\,[G'(b,\beta) - S_{2s}(\beta)]\,[(\beta+1)a^2b^{2\beta} - \beta b^{2\beta+2} - a^{2\beta+2}] \quad [30d]$$

where

$$D_1 = a^2b^2(a^{2\beta} - b^{2\beta})^2 - \beta^2a^{2\beta}b^{2\beta}(a^2-b^2)^2$$

For $\beta = 1$

$$4C_5(a^2-b^2)\,[(a^2-b^2) - (a^2+b^2)\log_e(a/b)] = [G(a,1) - W_{1s}(1)]\,[a^{-1}b^2 - a - 2a\log_e(a/b)] + [G'(a,1) - S_{1s}(1)]\,[(b^2-a^2) + 2a^2\log_e(a/b)] + [G(b,1) - W_{1s}(1)]\,[a^2b^{-1} - b + 2b\log_e(a/b)] + [G'(b,1) - S_{2s}(1)]\,[a^2 - \tfrac{1}{2}b^2 - 2b^2\log_e(a/b)] \quad [31a]$$

$$-2C_4\,[a^2-b^2-(a^2+b^2)\log_e(a/b)] = -[G(a,1) - W_{2s}(1)]\,(3a + a^{-1}b^2) + [G'(a,1) - S_{1s}(1)]\,(a^2-b^2) + [G(b,1) - W_{1s}(1)]\,[3b + b^{-1}a^2] + [G'(b,1) - S_{2s}(1)]\,(a^2-b^2) \quad [31b]$$

$$2C_2 = 2C_3a^4 + C_4a^2 - a\,[G(a,1) - W_{1s}(1)] + a^2\,[G'(a,1) - S_{1s}(1)] \quad [31c]$$

$$C_1 = C_2a^{-2} - 3C_3a^2 - (1+\log_e a)C_4 - [G'(a,1) - S_{1s}(1)] \quad [31d]$$

Case 2 For $\beta \neq 1$

$$C_6D_2 = \beta^2(\beta-1)(1-\nu)a^\beta b^{2\beta}\,[G(a,\beta) - W_{1s}(\beta)]\,[(\beta+2)(1-\nu)a^{2\beta+2} - (\beta+1)(1-\nu)a^{2\beta}b^2 + (3+\nu)\,b^{2\beta+2}] + \beta(\beta-1)(1-\nu)a^{\beta+1}\,b^{2\beta}\,[G'(a,\beta) - S_{1s}(\beta)]\,[(\beta+1)(1-\nu)\,a^{2\beta}\,b^2 - \beta(1-\nu)a^{2\beta+2} + (3+\nu)\,b^{2\beta+2}] + \beta a^{2\beta}b^\beta a^{\beta+2}A(b,\beta)\,[2(\beta+1)(1-\nu)a^{2\beta}b^2 - (2\beta+3)(1-\nu)a^{2\beta+2} + (\beta-1)(1-\nu)a^2b^{2\beta} - [\beta(1-\nu)+2(1+\nu)]\,b^{2\beta+2}] + a^{2\beta}b^{\beta+1}B(b,\beta)\,[(1-\nu)a^{2\beta+2} - (\beta-1)(1-\nu)a^2b^{2\beta} + [2(1+\nu) + \beta(1-\nu)]b^{2\beta+2}] \quad [32a]$$

$$(\beta+1)b^{\beta-2}C_3D_2 = -\beta^2(\beta^2-1)(1-\nu)a^\beta b^\beta\,[G(a,\beta) - W_{1s}(\beta)]\,[(3+\nu)a^{2\beta} - (\beta-2)(1-\nu)a^2b^{2\beta-2} + (1-\nu)(\beta-1)b^{2\beta}] + \beta(\beta^2-1)(1-\nu)a^{\beta+1}b^\beta\,[G'(a,\beta) - S_{1s}(\beta)]\,[(3+\nu)a^{2\beta} + \beta(1-\nu)a^2b^{2\beta-2} - (\beta-1)(1-\nu)b^{2\beta}] + \beta a^2b^\beta A(b,\beta)\,[2(\beta+1)(3+\nu)a^{2\beta-2} - (\beta+1)(\beta-3)(1-\nu)a^{2\beta}b^{2\beta-2} + (\beta-1)\,[\beta(1-\nu) - 2(1+\nu)]\,a^{2\beta-2}b^{2\beta} - (\beta-1)(1-\nu)b^{2\beta-2}] + (\beta-1)a^2b^{\beta+2}B(b,\beta)\,[(\beta+1)(1-\nu)a^{2\beta}b^{\beta-2} + (\beta-1)[-\beta(1-\nu) + 2(1+\nu)]\,a^{2\beta-2}b^{2\beta} + (1-\nu)b^{2\beta-2}] \quad [32b]$$

$$2\beta a^{\beta}b^{\beta}C_1 = -2(\beta+1)C_3a^{2\beta+2} - 2C_4a^2 - \beta a^\beta\,[G(a,\beta) - W_{2s}(\beta)] - a^{\beta+1}\,[G'(a,\beta) - S_{1s}(\beta)] \quad [32c]$$

$$a^{-\beta}C_2 = -C_1a^\beta - C_3a^{\beta+2} - C_4a^{-\beta+2} - [G(a,\beta) - W_{1s}(\beta)] \quad [32d]$$

where

$$D_2 = 2\beta(\beta-1)\,[2(\beta^2-1)(1-\nu)^2a^{2\beta+2}b^{2\beta+2} - (1-\nu)(3+\nu)a^2b^2(a^{4\beta}+b^{4\beta}) - \beta^2(1-\nu)^2a^2b^2b^{2\beta}(a^4+b^4) - 8(1+\nu)a^{2\beta}b^{2\beta+4}]$$

$$A(r,\beta) = G''(r,\beta) + (\nu/r)G'(r,\beta) - (\nu\beta^2/r^2)G(r,\beta) - (\nu\beta/r^2)\,[(-1)^nw(r,\beta) - w(r,0)] + S\,[M_r]/D$$

$$B(r,\beta) = \{G'''(r,B) + (1/r)G''(r,\beta) - (1/r^2)\,[1+\beta^2(2-\nu)]\,G'(r,\beta) + [\beta^2(3-\nu)/r^3]\,G(r,\beta) + [\beta(3-\nu)/r^3]\,[(-1)^nw(r,\beta) - w(r,0)] + [\beta(2-\nu)/r^2]\,[(-1)^nw'(r,\beta) - w'(r,0)]\} + S[V_r]/D$$

For $\beta = 1$

$$\nu[6(3+\nu)b^4 + 4(1-\nu)a^4]C_3 = (1-\nu)b(b^2+a^2)A(b,1) - b^2[(1+\nu)b^2 + (1-\nu)a^2]\,B(b,1) + 2\nu(1-\nu)a\,[G(a,1) - w_{2s}(1)] - 2\nu(1-\nu)a^2\,[G'(a,1) - S_{1s}(1)] \quad [33a]$$

$$4\nu[2(1-\nu)b^{-4} + 3(3+\nu)a^{-4}]C_3 = [2(1-\nu)b^{-3} - 3(3+\nu)a^{-2}]A(b,1) - [2(1+\nu)b^{-2} - 3(3+\nu)a^{-2}]\,B(b,1) - 6\nu(3+\nu)a^{-5}\,[G(a,1) - \tfrac{1}{3}W_{2s}(1)] + 6\nu(3+\nu)a^{-3}[G'(a,1) - S_{1s}(1)] \quad [33b]$$

$$2\nu C_4 = b^3B(b,1) - bA(b,1) \quad [33c]$$

$$aC_1 = -C_2a^{-1} - C_3a^2 - C_4a\log_e a - [G(a,1) - W_{1s}(1)] \quad [33d]$$

Case 3 For $b \neq 1$

$$(\beta+1)\,C_3D_3 = \beta a^\beta A(a,\beta)\,\{-(3+\nu)a^{2\beta} + [\beta(1-\nu) + 4]a^2b^{2\beta-2} - (\beta+1)(1-\nu)b^{2\beta}\} + \beta b^\beta A(b,\beta)\,\{-(\beta+1)(1-\nu)a^{2\beta} + [\beta(1-\nu)+4]a^{2\beta-2}b^2 - (3+\nu)b^{2\beta}\} + B(a,\beta)a^{\beta+1}\,\{-(3+\nu)a^{2\beta} + [-\beta(1-\nu) + 2(1+\nu)]\,a^2b^{2\beta-2} + (\beta+1)(1-\nu)b^{2\beta}\} + B(b,\beta)b^{\beta+1}\,\{(\beta+1)(1-\nu)a^{2\beta} - [\beta(1-\nu) - 2(1+\nu)]\,a^{2\beta-2}b^2 - (3+\nu)b^{2\beta}\} + B(a,\beta)a^{\beta+1}\,\{-(3+\nu)a^{2\beta} + [-\beta(1-\nu)+2(1+\nu)]a^2b^{2\beta-2} + (\beta+1)(1-\nu)b^{2\beta}\} + B(b,\beta)b^{\beta+1}\,\{[(\beta+1)(1-\nu)a^{2\beta} - [\beta(1-\nu) - 2(1+\nu)]\,a^{2\beta-2}b^2 - (3+\nu)b^{2\beta}\} \quad [34a]$$

$$(\beta-1)C_4D_3 = \beta a^{\beta}b^{2\beta-2}A(a,\beta)\{-[\beta(1-\nu) + 2(1+\nu)]a^{2\beta+2} - 2(\beta-1)(1-\nu)a^2b^{2\beta} + (\beta-1)(1-\nu)a^{2\beta}b^2 + [2\beta(1-\nu)+(1+3\nu)]b^{2\beta+2}\} + \beta a^{2\beta-2}b^{\beta}\{(3+\nu)a^{2\beta+2} + 3(\beta-1)(1-\nu)a^2b^{2\beta} - [3\beta(1-\nu)+4\nu]b^{2\beta+2}\} A(b,\beta) + a^{\beta+1}b^{2\beta-2}B(a,\beta)\{[4-\beta(1-\nu)]a^{2\beta+2} + 2(\beta-1)(1-\nu)a^2b^{2\beta} + (\beta-1)(1-\nu)a^{2\beta}b^2 - [2\beta(1-\nu)+(1+3\nu)]b^{2\beta+2}\} - a^{2\beta-2}b^{\beta+1}B(b,\beta)\{(3+\nu)a^{2\beta+2} + (\beta-1)(1-\nu)a^2b^{2\beta} - [\beta(1-\nu)-2(1+\nu)]b^{2\beta+2}\} \quad [34b]$$

$$2\beta^2(\beta-1)(1-\nu)C_1a^{2\beta} = -2\beta(\beta^2-1)(1-\nu)C_2a^{2\beta+2} + 2\beta(\beta-1)(3+\nu)C_4a^2 - \beta a^{\beta+2}A(a,\beta) + a^{\beta+2}B(a,\beta) \quad [34c]$$

$$2\beta^2(\beta+1)(1-\nu)C_3 = -2\beta(\beta+1)(3+\nu)C_2a^{2\beta+2} - 2\beta(\beta^2-1)(1-\nu)C_4a^2 - \beta a^{\beta+2}A(a,\beta) - a^{\beta+2}B(a,\beta) \quad [34d]$$

where

$$D_3 = 2\beta\{(3+\nu)^2a^{4\beta} + [\alpha^2(1-\nu)^2 - 2(5+2\nu+\nu^2)]a^{2\beta+2}b^{2\beta-2} + 2(1-\nu)[-\beta^2(1-\nu) + \beta(3+\nu) - 2(1+\nu)]a^{2\beta}b^{2\beta} + [\beta^2(1-\nu)^2 - 2\beta(3-2\nu-\nu^2) - 4(1+\nu)^2]a^{2\beta-2}b^{2\beta+2} - 2(\beta-1)(3+\nu)(1-\nu)a^2b^{4\beta-2} + (3+\nu)[2\beta(1-\nu) + (1+3\nu)]b^{4\beta}\}$$

For $\beta = 1$, in Case 3, the deflection in not uniquely determined.

Sector of a Circle

In case the plate has the planform of a sector of a circle, the solution to differential Equation [26] is

$$w_s(r,\beta) = C_1r^{\beta} + C_3r^{\beta+2} + G(r,\beta) \quad [35]$$

The conditions at the curved edge will be taken.

Case 4 The edge $r = a$ with deflection and slope given, Equations [11] and [13]

$$\left.\begin{aligned} 2a^{\beta}C_1 &= -(\beta+2)[G(a,\beta) - w_{1s}(\beta)] + a[G'(a,\beta) - S_{1s}(\beta)] \\ 2a^{\beta+2}C_3 &= \beta[G(a,\beta) - w_{1s}(\beta)] - a[G'(a,\beta) - S_{1s}(\beta)] \end{aligned}\right\} \quad [36]$$

Case 5 The edge $r = a$, with moment and reaction given, Equations [17] and [18]

$$\left.\begin{aligned} 2\beta^2(\beta^2-1)(1-\nu)(3+\nu)C_1 &= \beta A(a,\beta)[\beta^2(1-\nu) - \beta(3+\nu) - 4] + B(a,\beta)[\beta^2(1-\nu) + \beta(3+\nu) + 2(1+\nu)] \\ 2\beta(3+\nu)(\beta+1)C_3 &= -\beta A(a,\beta) - aB(a,\beta) \end{aligned}\right\} \quad [37]$$

Examples

We shall first take a sector of a circular plate whose angle is $\alpha = \pi/6$. Then $\beta = (n\pi/\alpha) = 6n$. We shall assume that the edges $\theta = 0$, and $\theta = \pi/6$ are simply supported (i.e., functions w_1, w_2, M_1, and M_2 equal to zero), and that the plate has a uniform load

$$q(r,\theta) = q_0 \qquad (q_0 = \text{const}) \quad [38]$$

then

$$q_s(r,\beta) = q_0[1-(-1)^n]/\beta \quad [39]$$

and

$$G(r,\beta) = q_0[1-(-1)^n]r^4/\beta\, D(\beta^4 - 20\beta^2 + 64) \quad [40]$$

Since $\beta = 6n$, $\beta^4 - 20\beta^2 + 64 \neq 0$, for any integer n.

We may take various edge conditions on the edge $r = a$. For example, if the edge $r = a$ is clamped (Case 4 with w_2 and S_1 equal to zero)

$$2a^{\beta}C_1 = q_0[1-(-1)^n](2-\beta)a^4/\beta D(\beta^4 - 20\beta^2 + 64) \quad [41]$$

$$2a^{\beta+2}C_3 = q_0[1-(-1)^n](\beta+4)a^4/\beta\, D(\beta^4 - 20\beta^2 + 64). \quad [42]$$

The deflection $w(r,\theta)$ is obtained by substituting in Equations [29] and [35].

It may be of interest to compare the deflections of a ring-sector plate and a rectangular plate, both subjected to a uniform load. Let us take the angle of the sector to be equal to $\pi/6$. For a uniform load, the load function is then given by Equation [38], and the function $G(r,\beta)$ by Equation [40]. We shall take the edges $r = a$ and $r = b$ clamped, and the edges $\theta = 0$, and $\theta = \pi/6$ simply supported. (Case 1 with M_1, M_2, w_1, and w_2 equal to zero.)

We shall compare the deflection at the center of the ring-sector plate [i.e., $r = (a+b)/2$, $\theta = \pi/12$] with the deflection at the center of a rectangular plate which has two opposite edges, simply supported and the remaining edges clamped. The length of the simply supported edges will be taken equal to c, and the length of the clamped edges equal to d. The values of the deflection for the rectangular plate are taken from Timoshenko (9).

By use of Equations [30], [27], [29], [38], and [40], we may find the deflection $w(r,\theta)$ for any given ratio of radii (a/b). We shall denote by S_1, the length of the central line arc $[r = (a+b)/2]$, and by S_2, the length of the straight edge of the ring-sector plate, Then for our example

$$\left.\begin{aligned} S_1 &= (a+b)\pi/12 \\ S_2 &= (a-b) \end{aligned}\right\} \quad [43]$$

Table 1 then gives the values of the constants C_1, C_2, C_3, and C_4

TABLE 1 VALUES OF CONSTANTS FOR $\alpha = (\pi/6)$, $\nu = 0.3$, AND UNIFORM LOAD q_0

	$\beta = 6$	$\beta = 18$
$\frac{S_1}{S_2} = 1$	$C_1b^2 = -0.0107658K_1$ $C_2/b^{10} = 0.0^3374426K_1$ $C_3b^4 = 0.0^3518607K_1$ $C_4/b^8 = -0.0^3145217K_1$	$C_1b^{14} = -0.0^4673920K_1$ $C_2/b^{22} = 0.0^6633144K_1$ $C_3b^{16} = 0.0^4926747K_1$ $C_4/b^{20} = -0.0^6208287K_1$
$\frac{S_1}{S_2} = 2$	$C_1b^2 = -0.0^3946555K_1$ $C_2/b^{10} = 0.0^3248465K_1$ $C_3b^4 = 0.0^3413770K_1$ $C_4/b^8 = -0.0^3608118K_1$	$C_1b^{14} = -0.0^4979360K_1$ $C_2/b^{22} = 0.0^6319971K_1$ $C_3b^{16} = 0.0^4104195K_1$ $C_4/b^{20} = -0.0^6570871K_1$
$\frac{S_1}{S_2} = \frac{1}{2}$	$C_1b^2 = -0.0113641K_1$ $C_2/b^{10} = 0.0^3154088K_1$ $C_3b^4 = 0.0^3567845K_1$ $C_4/b^8 = -0.0^3199418K_1$	$C_1b^{14} = -0.0^4984848K_1$ $C_2/b^{22} = 0.0^6960569K_1$ $C_3b^{16} = 0.0^4861742K_1$ $C_4/b^{20} = -0.0^6687737K_1$

for $\beta = 6$ and $\beta = 18$. The notation 0.0^4 means 0.0004, and the constant K_1 is defined by

$$K_1 = q_0/Eb^3 \quad [44]$$

Using the values of the constants in Table 1, the deflection $w[(a+b)/2, \pi/12]$ may be found for the ring-sector plate, Table 2.

As another example, let us consider a quarter-sector of circular-ring plate, with the edges $\theta = 0$, and $\theta = \pi/2$ simply supported (i.e., w_1, w_2, M_1, and M_2 equal to zero), and with load function

$$q(r,\theta) = q_0\theta r, \quad 0 < \theta < \pi/4$$

$$q(r,\theta) = q_0[(\pi/2) - \theta]r, \quad \pi/4 < \theta < \pi/2 \quad [45]$$

TABLE 2 CENTER DEFLECTIONS OF RING-SECTOR AND RECTANGULAR PLATES ($\nu = 0.3$)

Ring-sector plate $w[(a+b)/2, \pi/12]$		Rectangular plate $w(c/2, 0) = W_{max}$	
$\frac{S_1}{S_2} = 1$	$0.0235 q_0 S_2^4/Eh^3$	$\frac{d}{c} = 1$	$0.0209 q_0 d^4/Eh^3$
$\frac{S_1}{S_2} = 2$	$0.0260 q_0 S_2^4/Eh^3$	$\frac{d}{c} = 2$	$0.0284 q_0 c^4/Eh^3$
$\frac{S_1}{S_2} = \frac{1}{2}$	$0.0944 q_0 S_1^4/Eh^3$	$\frac{d}{c} = \frac{1}{2}$	$0.0987 q_0 d^4/Eh^3$

Then

$$q_e(r, \theta) = (2q_0 r/\beta^2) \sin(\pi\beta/4) \quad [46]$$

and

$$G(r, \beta) = \frac{2q_0 r^5 \sin(\pi\beta/4)}{\beta^2 D(\beta^4 - 34\beta^2 + 225)} \quad [47]$$

since $\beta = 2n$, $\beta^4 - 34\beta^2 + 225 \neq 0$, for any integer n.

As edge conditions, one may use any of the edge conditions in Cases 1 to 3, inclusive. Once the constants C_1, C_2, C_3, and C_4 are determined, the sine-transformed deflection may be obtained from Equation [27], and the deflection from Equation [29].

Many more examples could be worked out easily. The solution of problems is greatly facilitated if one has a table of sine transforms (6, 10).

It does happen for certain α's that two different particular solutions $G(r, \beta)$ must be determined. This occurs when the particular solution coincides with a term of the complementary solution for some integer value of n. This would have occurred in our first example for $\alpha = \pi/2$.

BIBLIOGRAPHY

1 "Theory of Plates and Shells," by S. Timoshenko, McGraw-Hill Book Company, Inc., New York, N. Y., and London, England, first edition, 1940, p. 272.

2 "Beitrag zur Berechnung der Halbkreisplatte," by R. Kuhn, *Ingenieur Archiv*, vol. 12, 1941, pp. 307–319.

3 "The Bending of the Clamped Sectorial Plate," by G. F. Carrier, Trans. ASME, vol. 66, 1944, pp. 134–139.

4 "Applicazione di un nuovo metodo di M. Picone all' integrazione delle equazione dell' elasticita in un parallelopipedo rettangolo," by C. Tolotti, Atti Accad. Italia, Rend. Cl. Sci. Fis. Mat. Nat., vol. 1, 1940, pp. 512–524.

5 "Sul calcolo della piastre elastiche a forme de settori anulari," by C. Tolotti, Atti Accad. Italia, Rend. Cl. Sci. Fis. Mat. Nat., vol. 2, 1940, pp. 517–525.

6 "Some Thin-Plate Problems by the Sine Transform," by L. I. Deverall and C. J. Thorne, JOURNAL OF APPLIED MECHANICS, Trans. ASME, vol. 73, 1951, pp. 152–156.

7 Reference (1), pp. 257–260.

8 "Modern Operational Mathematics in Engineering," by R. V. Churchill, McGraw-Hill Book Company, Inc., New York, N. Y., and London, England, first edition, 1944, pp. 267–278.

9 Reference (1), p. 206.

10 "A Generalisation of the Finite Fourier Sine Transform," by I. Roettinger, *Journal of Applied Mathematics*, vol. 5, July, 1947, pp. 298–319.

On the Stability of Plates Reinforced by Longitudinal Ribs

By J. M. KLITCHIEFF,[1] BELGRADE, YUGOSLAVIA

The stability of plates reinforced by any number of equal and equidistant longitudinal ribs has been considered. By transformation of the system of equations established by S. Timoshenko the general solution of it has been developed, giving directly the rigidity of ribs required to secure any given critical compressive force of the plate. Two numerical examples of stiffenings used in ship design have been discussed.

Nomenclature

The following nomenclature is used in the paper:

a = length of plate
b = width of plate
h = thickness of plate
E = Young's modulus
ν = Poisson's ratio
A = area of cross section of one rib
I = moment of inertia
$i - 1$ = number of ribs
N = critical compressive force per unit width
a_n = parameters

$$\beta = \frac{a}{b}$$

$$\delta = \frac{A}{bh}$$

$$\gamma = \frac{12\,(1 - \nu^2)\,I}{bh^3}$$

$$\lambda^2 = \frac{12\,(1 - \nu^2)}{\pi^2}\,\frac{Na^2}{Eh^3}$$

Critical Force and Rigidity of Ribs

S. Timoshenko[2] in 1915 established the system of equations, determining the critical compressive force of a plate stiffened by longitudinal ribs, Fig. 1. If the ribs are equal and equidistant, these equations become

$$a_n\,[(1 + n^2\beta^2)^2 - \lambda^2] + 2(\gamma - \delta\lambda^2) \sum_{i=1}^{i-1} \sin \frac{ni\pi}{j} \sum_{\rho=1}^{\infty} a_\rho \sin \frac{\rho i\pi}{j} = 0 \quad \ldots\ldots [1]$$

$$n = 1, 2, \ldots$$

By equating to zero the determinant of this system of homogeneous linear equations, an equation can be obtained for determining the critical compressive force corresponding to any given size of the ribs. S. Timoshenko solved it by approximations for the cases of one and of two ribs and tabulated the results.

In the ship and airplane structures the number of stiffeners is usually large, and the designer has to solve the inverse problem, i.e., to determine the size of ribs which could secure a given value to the critical force of the plate. Thus he is induced to solve the equation himself. He must repeat this tedious work several times, until he arrives by trials at the size of ribs required.

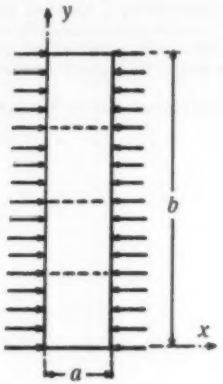

Fig. 1

As it was done in the case of transverse ribs, previously discussed by the author,[3] the dimensions of the ribs, corresponding to any given value of the critical force, can be determined directly, the form of the general solution, Equation [5], being simple. It takes the simplest form, Equation [8], in the usual case, when the designer endeavors to obtain the same value of the critical force, as if the ribs were absolutely rigid.

Details of Solution

It was shown in the previous paper[3] that

$$2\sum_{i=1}^{i-1} \sin \frac{ni\pi}{j} \sin \frac{\rho i\pi}{j} = \begin{cases} j \text{ if } \rho = n + 2mj \\ -j \text{ if } \rho = -n + 2mj \\ 0 \text{ for any other value of } \rho \end{cases}$$

Thus, for values of n being multiples of j, we obtain from Equation [1] a series of independent equations of the form

$$\lambda_n^2 = (1 + n^2\beta^2)^2 \quad \ldots\ldots [2]$$

For the values of n which are not multiples of j we obtain $j - 1$

---

[1] Belgrade University.

[2] "Theory of Elasticity," by S. Timoshenko, McGraw-Hill Book Company, Inc., New York, N. Y., 1936, pp. 371–378.

Contributed by the Applied Mechanics Division and presented at the Annual Meeting, New York, N. Y., November 26–December 1, 1950, of The American Society of Mechanical Engineers.

Discussion of this paper should be addressed to the Secretary, ASME, 29 West 39th Street, New York, N. Y., and will be accepted until January 10, 1952, for publication at a later date. Discussion received after the closing date will be returned.

Note: Statements and opinions advanced in papers are to be understood as individual expressions of their authors and not those of the Society. Manuscript received at ASME Headquarters, October 11, 1949. Paper No. 50—A-10.

[3] "On the Stability of Plates Reinforced by Ribs," by J. M. Klitchieff, Journal of Applied Mechanics, Trans. ASME, vol. 71, 1949, pp. 74–76.

independent systems of homogeneous linear equations of the form

$$\left.\begin{aligned} &a_n[(1+n^2\beta^2)^2-\lambda^2]+j(\gamma-\delta\lambda^2)S_n &&=0\\ &a_{2j-n}[[1+(2j-n)^2\beta^2]^2-\lambda^2]-j(\gamma-\delta\lambda^2)S_n &&=0\\ &a_{2j+n}[[1+(2j+n)^2\beta^2]^2-\lambda^2]+j(\gamma-\delta\lambda^2)S_n &&=0\\ &\cdots\cdots\cdots\cdots\cdots\cdots\cdots\cdots\cdots\cdots\cdots\cdots \end{aligned}\right\}\ldots[3]$$

where

$$S_n = a_n - a_{2j-n} + a_{2j+n} - a_{4j-n} + \ldots\ldots\ldots\ldots[4]$$

The equations of the form of Equation [2] give a series of values for the critical force corresponding to the buckling of the plate into j, $2j$, $3j$, ... half waves in the y-direction, when the ribs remain straight. The smallest of these values is the critical force, which can be reached practically at the plate with absolutely rigid ribs. By elimination of the parameters a_n from Equations [3], $j-1$ values of the critical force can be obtained, corresponding to the buckling into 1, 2, . . . $j-1$ half waves, which is possible with elastic ribs only.

Instead of equating to zero the determinant of Equations [3], as it was done in the previous paper,[3] another method can be adopted, leading directly to the final result. By elimination of S_n from the first pair of Equations [3] we obtain

$$a_{2j-n} = -\frac{\lambda^2-(1+n^2\beta^2)^2}{\lambda^2-[1+(2j-n)^2\beta^2]^2}\,a_n$$

Similarly, from the first and third equations

$$a_{2j+n} = \frac{\lambda^2-(1+n^2\beta^2)^2}{\lambda^2-[1+(2j+n)^2\beta^2]^2}\,a_n$$

and so on. Introducing these expressions into Equation [4], the first of the Equations [3] becomes

$$j(\gamma-\delta\lambda^2)\sum_{r=-\infty}^{r=+\infty}\frac{1}{\lambda^2-[1+(2rj+n)^2\beta^2]^2}=1\ldots.[5]$$

With $n=1, 2, \ldots j-1$ it represents $j-1$ equations, giving $j-1$ values of $(\gamma-\delta\lambda^2)$ for any imposed value of λ^2. The largest of them determines the size of the ribs required.

The Series [5] converges rapidly, but further simplification is still possible. The general term of the series can be written in the following form

$$\frac{\pi}{8j\beta\lambda\sqrt{\lambda-1}}\left\{\frac{1}{\frac{\sqrt{\lambda-1}+n\beta}{2j\beta}\pi+n\pi}+\frac{1}{\frac{\sqrt{\lambda-1}-n\beta}{2j\beta}\pi-n\pi}\right\}$$

$$+\frac{i\pi}{8j\beta\lambda\sqrt{\lambda+1}}\left\{\frac{1}{\frac{i\sqrt{\lambda+1}+n\beta}{2j\beta}\pi+n\pi}+\frac{1}{\frac{i\sqrt{\lambda+1}-n\beta}{2j\beta}\pi-n\pi}\right\}$$

where i denotes $\sqrt{-1}$. Then, using the known development

$$\cot\theta=\sum_{n=-\infty}^{n=+\infty}\frac{1}{\theta+n\pi}$$

we obtain

$$\sum_{r=-\infty}^{r=+\infty}\frac{1}{\lambda^2-[1+(2rj+n)^2\beta^2]^2}$$

$$=\frac{\pi}{4j\beta\lambda}\left\{-\frac{1}{\sqrt{\lambda-1}}\,\frac{\sin\frac{\sqrt{\lambda-1}}{j\beta}\pi}{\cos\frac{\sqrt{\lambda-1}}{j\beta}\pi-\cos\frac{n\pi}{j}}+\frac{1}{\sqrt{\lambda+1}}\,\frac{\sinh\frac{\sqrt{\lambda+1}}{j\beta}\pi}{\cosh\frac{\sqrt{\lambda+1}}{j\beta}\pi-\cos\frac{n\pi}{j}}\right\}$$

and Equation [5] becomes

$$\frac{\pi}{4}\,\frac{\gamma-\delta\lambda^2}{\beta\lambda}\left\{-\frac{1}{\sqrt{\lambda-1}}\,\frac{\sin\frac{\sqrt{\lambda-1}}{j\beta}\pi}{\cos\frac{\sqrt{\lambda-1}}{j\beta}\pi-\cos\frac{n\pi}{j}}+\frac{1}{\sqrt{\lambda+1}}\,\frac{\sinh\frac{\sqrt{\lambda+1}}{j\beta}\pi}{\cosh\frac{\sqrt{\lambda+1}}{j\beta}\pi-\cos\frac{n\pi}{j}}\right\}=1\ldots\ldots[6]$$

By introducing the stiffeners, the designer usually endeavors to obtain the maximal critical force possible, that is, the same value of it, as if the ribs were absolutely rigid. These values are given by the known expressions

$$\lambda^2=(1+j^2\beta^2)^2 \text{ if } j\beta<\sqrt{1.2}\ldots\ldots\ldots\ldots[7a]$$

$$\lambda^2=\left(2+\frac{1}{2}\,j^2\beta^2\right)^2 \text{ if } \sqrt{1.2}<j\beta<\sqrt{2.3}\ldots\ldots[7b]$$

and so on. The most usual case in practice is $j\beta<\sqrt{1.2}$. Introducing the corresponding value Equation [7a] in Equation [6], the first term in brackets vanishes. Neglecting $\cos n\pi/j$ and taking $\tanh\pi\sqrt{\lambda+1}/j\beta$ equal to 1, we get for all values of n

$$\sum_{r=-\infty}^{r=+\infty}\frac{1}{(1+j^2\beta^2)^2-[1+(2rj+n)^2\beta^2]^2}$$

$$=\frac{\pi}{4j\beta(1+j^2\beta^2)\sqrt{2+j^2\beta^2}}$$

Thus the whole computation left to the designer is reduced to the formula

$$\gamma-\delta(1+j^2\beta^2)^2=\frac{4}{\pi}\,\beta\,(1+j^2\beta^2)\,\sqrt{2+j^2\beta^2}\ldots.[8]$$

Examples

As a first example, let us consider the 12-ft 6-in-wide part of the deck plating of a cargo ship,[4] between the very rigid longitudinal girder and the shear strake. According to Lloyd's Rules the beam spacing is 28 in. and the deck plating is 0.46 in. thick.

The critical compressive stress of the plating would be 3.3 tons per sq in. Since the average value of the compressive stress in

[4] "The Design and Construction of Ships," by J. H. Biles, C. Griffin and Company, London, England, 1923.

the "sagging condition" is over 5.5 tons per sq in., the rigidity of the deck plating must be increased. It could be achieved by increasing its thickness (and its weight) by 20 per cent; or by sheathing the deck with 2-in-thick wood, it would increase the weight even more. Another solution is to weld three longitudinal angles, say, $1^1/_2$ in. $\times$ 3 in. $\times$ 0.32 in., to the deck plating and to reduce, at the same time, its thickness to 0.43 in.

With

$$\beta = \frac{28}{150} = 0.1867;\ j = 4;\ A = 1.34 \text{ sq in.};\ \nu = 0.3$$

$$\delta = \frac{1.34}{(150)\,0.43} = 0.021;\ j^2\beta^2 = 0.554$$

we have

$$\gamma = (1.554^2)\,0.021 + \left(\frac{4}{\pi}\,0.1867\right)\left(1.554\sqrt{2.554}\right) = 0.64$$

and

$$I = 0.64\,\frac{(150)\,0.43^3}{12(1-0.3^2)} = 0.70 \text{ in.}^4$$

The moment of inertia of the cross section of the angle, welded to the plating being much larger than that, the critical compressive stress of the deck plating is increased up to 6 tons per sq in., without any increase of its weight.

As a second example we shall take the deck plating of a river ship 0.236 in. thick, with 23.6 in. spacing of 70.8-in-long beams. It has been stiffened by welding four angles 1.18 in. $\times$ 1.77 in. $\times$ 0.197 in.

As in this case

$$\beta = \frac{23.6}{70.8} = \frac{1}{3};\ j = 5;\ j\beta = \frac{5}{3} > \sqrt{2}$$

Equation [8] cannot be used, and the general expressions, Equation [5] or [6], must be applied. With

$$\lambda = 2 + \frac{1}{2}\,\frac{25}{9} = \frac{61}{18};\ \frac{\sqrt{\lambda-1}}{j\beta}\,\pi = 2.92;\ \frac{\sqrt{\lambda+1}}{j\beta}\,\pi = 3.96$$

for $n = 1$, we have

$$\cos\frac{\pi}{5} = 0.81;\ \cosh 3.96 \approx \sinh 3.96 = 27.3$$

$$\sin 2.92 = 0.24;\ \cos 2.92 = -0.97$$

with $A = 0.543 \text{ in.}^2,\ \delta = \dfrac{0.543}{0.236 \times 70.8} = 0.032$

and we find, from Equation [6], $\gamma = 2.9$

Therefore

$$I = 2.9\,\frac{70.8\,(0.236)^3}{12\,(0.91)} = 0.247 \text{ in.}^4$$

On Symmetrical Strain in Solids of Revolution in Spherical Co-Ordinates

By CHIH-BING LING[1] and KUO-LIANG YANG,[2] TAIWAN, CHINA

This paper presents the expressions for the displacements and stresses in the spherical co-ordinates, in terms of a stress function, for a solid of revolution in the state of symmetrical strain. Such expressions are useful in dealing with solids of revolution, which consist of spherical boundaries. The expressions are applied, as an illustration, to find the stresses in a large tension member having a spherical cavity. The required stress function is constructed in terms of Legendre polynomials. It may be interesting to compare this solution with the known solutions.

Introduction

WHEN a solid of revolution is in the state of symmetrical strain, so that the displacement is the same in all planes through the axis of revolution, all the quantities that occur to describe the strained state of the solid, such as the displacements, strains, and stresses, may be expressed in terms of a single function. This function must be a biharmonic function and is usually called a stress function. The expressions for these quantities in the cylindrical co-ordinates have been well known (1).[3] It appears that from them the corresponding expressions in the spherical co-ordinates can be derived conveniently. Such expressions are useful in dealing with solids of revolution, which consist of spherical boundaries.

The aim of this paper is to present such expressions. As an illustration, the expressions will be applied to find the stresses in a large tension member having a spherical cavity.

The required stress function is constructed by means of the biharmonic functions referred to the spherical co-ordinates. The parametric coefficients involved are then determined from the boundary conditions on the surface of the cavity. It turns out that the resulting stress function is in a closed form.

This problem is also investigated by Leon (2) (1908), Southwell (3) (1926), Goodier (4) (1933), Neuber (5) (1937), and Ziemba (6) (1949). It may be interesting to compare the present solution with the known solutions.

Expressions in Cylindrical Co-Ordinates

Consider the following three systems of co-ordinates:

1 Rectangular co-ordinates (x, y, z).

2 Cylindrical co-ordinates (r, θ, z).

3 Spherical co-ordinates (ρ, ϕ, θ).

As shown in Fig. 1, these co-ordinate systems are connected with each other by

$$\left.\begin{aligned} x &= r\cos\theta, \qquad y = r\sin\theta \\ z &= \rho\cos\phi, \qquad r = \rho\sin\phi \end{aligned}\right\} \quad \ldots\ldots\ldots [1]$$

Note that the same symbol in different co-ordinate systems represents the same quantity.

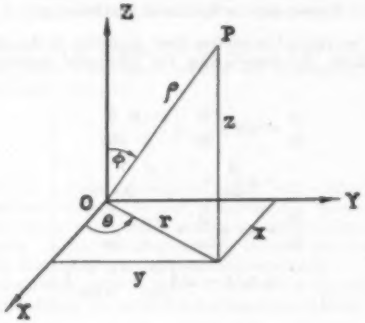

Fig. 1 Co-Ordinates of a Point P

Let the axis of revolution of the solid be coincident with the axis of z. When the solid is in the state of symmetrical strain about the axis of revolution, the displacement u_θ in the cylindrical co-ordinates vanishes identically throughout the solid; so also do the shear strains $\gamma_{r\theta}$, $\gamma_{z\theta}$ and the shear stresses $\tau_{r\theta}$, $\tau_{z\theta}$. The remaining nonvanishing displacements and stresses are known to be expressible in terms of a stress function χ as follows

$$\left.\begin{aligned} u_r &= -\frac{1+\nu}{E}\,\frac{\partial^2\chi}{\partial r\partial z} \\ u_z &= \frac{1+\nu}{E}\left\{2(1-\nu)\nabla^2\chi - \frac{\partial^2\chi}{\partial z^2}\right\} \end{aligned}\right\} \quad \ldots\ldots [2]$$

and

$$\left.\begin{aligned} \sigma_r &= \frac{\partial}{\partial z}\left(\nu\nabla^2\chi - \frac{\partial^2\chi}{\partial r^2}\right) \\ \sigma_\theta &= \frac{\partial}{\partial z}\left(\nu\nabla^2\chi - \frac{1}{r}\,\frac{\partial\chi}{\partial r}\right) \\ \sigma_z &= \frac{\partial}{\partial z}\left\{(2-\nu)\nabla^2\chi - \frac{\partial^2\chi}{\partial z^2}\right\} \\ \tau_{rz} &= \frac{\partial}{\partial r}\left\{(1-\nu)\nabla^2\chi - \frac{\partial^2\chi}{\partial z^2}\right\} \end{aligned}\right\} \quad \ldots\ldots [3]$$

where E and ν are modulus of elasticity and Poisson's ratio of the

---

[1] Senior Research Officer, Aeronautical Research Laboratory, Taiwan, China.

[2] Research Officer, Aeronautical Research Laboratory, Taiwan, China.

[3] Numbers in parentheses refer to the Bibliography at the end of the paper.

Contributed by the Applied Mechanics Division and presented at the Annual Meeting, Atlantic City, N. J., November 25–30, 1951, of The American Society of Mechanical Engineers.

Discussion of this paper should be addressed to the Secretary, ASME, 29 West 39th Street, New York, N. Y., and will be accepted until January 10, 1952, for publication at a later date. Discussion received after the closing date will be returned.

Note: Statements and opinions advanced in papers are to be understood as individual expressions of their authors and not those of the Society. Manuscript received by ASME Applied Mechanics Division on July 10, 1950. Paper No. 51—A-1.

material, respectively. As mentioned previously, χ must be a biharmonic function and so it satisfies the differential equation

$$\nabla^4\chi = 0 \quad \ldots\ldots [4]$$

where $\nabla^4 = \nabla^2\nabla^2$; ∇^2 being the Laplace operator. For symmetrical strain, the subjects of operation are independent of θ, and so this operator takes the following form in the cylindrical co-ordinates

$$\nabla^2 = \frac{\partial^2}{\partial r^2} + \frac{1}{r}\frac{\partial}{\partial r} + \frac{\partial^2}{\partial z^2} \quad \ldots\ldots [5]$$

The sum of the three normal stresses is equal to

$$\sigma_r + \sigma_\theta + \sigma_z = (1+\nu)\frac{\partial}{\partial z}\nabla^2\chi \quad \ldots\ldots [6]$$

For the sake of brevity, the corresponding expressions for the four nonvanishing strains will not be shown.

Expressions in Spherical Co-Ordinates

Now, we proceed to express these quantities in the spherical co-ordinates. By transforming the differential operators, we have

$$\left.\begin{aligned}\frac{\partial}{\partial z} &= \cos\phi\frac{\partial}{\partial\rho} - \frac{\sin\phi}{\rho}\frac{\partial}{\partial\phi}\\ &= \mu\frac{\partial}{\partial\rho} + \frac{1-\mu^2}{\rho}\frac{\partial}{\partial\mu}\\ \frac{\partial}{\partial r} &= \sin\phi\frac{\partial}{\partial\rho} + \frac{\cos\phi}{\rho}\frac{\partial}{\partial\phi}\\ &= \sqrt{1-\mu^2}\left(\frac{\partial}{\partial\rho} - \frac{\mu}{\rho}\frac{\partial}{\partial\mu}\right)\end{aligned}\right\} \quad \ldots\ldots [7]$$

where

$$\mu = \cos\phi, \qquad \sqrt{1-\mu^2} = \sin\phi \quad \ldots\ldots [8]$$

For convenience, the variable μ will henceforth be used instead of ϕ.

The Laplace operator in the spherical co-ordinates, when the subjects of operation are independent of θ, then becomes

$$\begin{aligned}\nabla^2 &= \frac{\partial^2}{\partial\rho^2} + \frac{2}{\rho}\frac{\partial}{\partial\rho} + \frac{1}{\rho^2\sin\phi}\frac{\partial}{\partial\phi}\left(\sin\phi\frac{\partial}{\partial\phi}\right)\\ &= \frac{1}{\rho^2}\frac{\partial}{\partial\rho}\left(\rho^2\frac{\partial}{\partial\rho}\right) + \frac{1}{\rho^2}\frac{\partial}{\partial\mu}\left\{(1-\mu^2)\frac{\partial}{\partial\mu}\right\} \quad \ldots\ldots [9]\end{aligned}$$

It is noted that the displacement u_θ is the same in both cylindrical and spherical co-ordinates. When the solid of revolution is in the state of symmetrical strain, it vanishes identically as stated before, and so also do the shear strains $\gamma_{\rho\theta}$, $\gamma_{\phi\theta}$ and the shear stresses $\tau_{\rho\theta}$, $\tau_{\phi\theta}$ in the spherical co-ordinates. The two remaining nonvanishing displacements in the spherical co-ordinates are connected to those in the cylindrical co-ordinates by

$$\left.\begin{aligned}u_\rho &= u_r\sin\phi + u_z\cos\phi\\ u_\phi &= u_r\cos\phi - u_z\sin\phi\end{aligned}\right\} \quad \ldots\ldots [10]$$

Consequently, by transforming the differential operators, the following expressions are obtained

$$\left.\begin{aligned}u_\rho &= \frac{2(1-\nu^2)}{E}\mu\nabla^2\chi - \frac{1+\nu}{E}\frac{\partial}{\partial\rho}\left(\mu\frac{\partial}{\partial\rho} + \frac{1-\mu^2}{\rho}\frac{\partial}{\partial\mu}\right)\chi\\ u_\phi &= \frac{1+\nu}{E}\sqrt{1-\mu^2}\left\{-2(1-\nu)\nabla^2\chi + \frac{1}{\rho}\frac{\partial}{\partial\mu}\left(\mu\frac{\partial}{\partial\rho} + \frac{1-\mu^2}{\rho}\frac{\partial}{\partial\mu}\right)\chi\right\}\end{aligned}\right\} \quad \ldots\ldots [11]$$

The four nonvanishing strains are connected to the displacements by

$$\left.\begin{aligned}\epsilon_{\rho\rho} &= \frac{\partial u_\rho}{\partial\rho}\\ \epsilon_{\phi\phi} &= \frac{u_\rho}{\rho} + \frac{1}{\rho}\frac{\partial u_\phi}{\partial\phi}\\ \epsilon_{\theta\theta} &= \frac{u_\rho}{\rho} + \frac{u_\phi}{\rho}\cot\phi\\ \gamma_{\rho\phi} &= \frac{\partial u_\phi}{\partial\rho} - \frac{u_\phi}{\rho} + \frac{1}{\rho}\frac{\partial u_\rho}{\partial\phi}\end{aligned}\right\} \quad \ldots\ldots [12]$$

With the aid of the well-known Hooke's law, the four nonvanishing stresses are thus found in terms of the stress function χ as follows

$$\left.\begin{aligned}\sigma_\rho &= \left\{(2-\nu)\mu\frac{\partial}{\partial\rho} + \frac{\nu(1-\mu^2)}{\rho}\frac{\partial}{\partial\mu}\right\}\nabla^2\chi\\ &\quad - \frac{\partial^2}{\partial\rho^2}\left(\mu\frac{\partial}{\partial\rho} + \frac{1-\mu^2}{\rho}\frac{\partial}{\partial\mu}\right)\chi\\ \sigma_\phi &= -(1-\nu)\left(\mu\frac{\partial}{\partial\rho} - \frac{1-\mu^2}{\rho}\frac{\partial}{\partial\mu}\right)\nabla^2\chi\\ &\quad + \frac{\partial^2}{\partial\rho^2}\left(\mu\frac{\partial}{\partial\rho} + \frac{1-\mu^2}{\rho}\frac{\partial}{\partial\mu}\right)\chi\\ &\quad + \left(\mu\frac{\partial}{\partial\rho} + \frac{1-\mu^2}{\rho}\frac{\partial}{\partial\mu}\right)\left(\frac{1}{\rho}\frac{\partial}{\partial\rho} - \frac{\mu}{\rho^2}\frac{\partial}{\partial\mu}\right)\chi\\ \sigma_\theta &= \nu\left(\mu\frac{\partial}{\partial\rho} + \frac{1-\mu^2}{\rho}\frac{\partial}{\partial\mu}\right)\nabla^2\chi\\ &\quad - \left(\mu\frac{\partial}{\partial\rho} + \frac{1-\mu^2}{\rho}\frac{\partial}{\partial\mu}\right)\left(\frac{1}{\rho}\frac{\partial}{\partial\rho} - \frac{\mu}{\rho^2}\frac{\partial}{\partial\mu}\right)\chi\\ \tau_{\rho\phi} &= \sqrt{1-\mu^2}\left\{-(1-\nu)\left(\frac{\partial}{\partial\rho} + \frac{\mu}{\rho}\frac{\partial}{\partial\mu}\right)\nabla^2\chi\right.\\ &\quad \left. + \frac{\partial}{\partial\rho}\left(\frac{1}{\rho}\frac{\partial}{\partial\mu}\right)\left(\mu\frac{\partial}{\partial\rho} + \frac{1-\mu^2}{\rho}\frac{\partial}{\partial\mu}\right)\chi\right\}\end{aligned}\right\} \quad \ldots\ldots [13]$$

The sum of the three normal stresses is equal to

$$\sigma_\rho + \sigma_\phi + \sigma_\theta = (1+\nu)\left(\mu\frac{\partial}{\partial\rho} + \frac{1-\mu^2}{\rho}\frac{\partial}{\partial\mu}\right)\nabla^2\chi \quad \ldots\ldots [14]$$

It may be shown readily that these expressions satisfy the following stress equations, provided that χ is a biharmonic function

$$\left.\begin{aligned}\rho\frac{\partial\sigma_\rho}{\partial\rho} + \frac{\partial\tau_{\rho\phi}}{\partial\phi} + 2\sigma_\rho - \sigma_\phi - \sigma_\theta + \tau_{\rho\phi}\cot\phi &= 0\\ \rho\frac{\partial\tau_{\rho\phi}}{\partial\rho} + \frac{\partial\sigma_\phi}{\partial\phi} + (\sigma_\phi - \sigma_\theta)\cot\phi + 3\tau_{\rho\phi} &= 0\end{aligned}\right\} \quad \ldots\ldots [15]$$

Note that the stress σ_θ is the same in both co-ordinate systems. The preceding expression for σ_θ may be obtained directly from the corresponding expression in the cylindrical co-ordinates by merely transforming the differential operators.

Stresses in a Large Tension Member Having a Spherical Cavity

As an illustration, the foregoing expressions will be applied to find the stresses in a large tension member having a "spherical" cavity. For convenience in calculation, the solid will be considered as of infinite extent. Suppose that the required stress function χ is composed of two parts as follows

$$\chi = \chi_0 + \chi_1 \quad [16]$$

where χ_0 is the "basic" stress function to produce a uniform tension T per unit area along the axis of z in an infinite solid without any cavity, while χ_1 is an "auxiliary" biharmonic function to be added to χ_0, such that the parametric coefficients involved can be adjusted to satisfy the boundary conditions on the surface of the cavity. χ_1 is thus tacitly supposed to produce no effect on the stresses at infinity.

The function χ_0 is given by the following biharmonic function

$$\chi_0 = \frac{T}{6(1+\nu)}\left\{3\nu r^2 z + (1-2\nu)z^3\right\} \quad [17]$$

which produces throughout the solid the only stress

$$\sigma_z = T \quad [18]$$

Next, consider a normal solution of the function χ_1 in the following form

$$\chi_1 = F(\rho)P_n(\mu) \quad [19]$$

where P_n is Legendre polynomial of degree n, which satisfies the Legendre equation

$$\frac{d}{d\mu}\left\{(1-\mu^2)\frac{dP_n}{d\mu}\right\} + n(n+1)P_n = 0 \quad [20]$$

and may be found from

$$P_n(\mu) = \frac{1}{2^n n!}\frac{d^n}{d\mu^n}(\mu^2-1)^n \quad [21]$$

In particular

$$\left.\begin{aligned} &P_0(\mu) = 1, && P_1(\mu) = \mu \\ &P_2(\mu) = \frac{1}{2}(3\mu^2-1), && P_3(\mu) = \frac{1}{2}(5\mu^3-3\mu) \end{aligned}\right\} \quad [22]$$

If χ_1 is a biharmonic function, the function $F(\rho)$ must satisfy the following differential equation

$$\rho^4\frac{d^4F}{d\rho^4} + 4\rho^3\frac{d^3F}{d\rho^3} - 2n(n+1)\rho^2\frac{d^2F}{d\rho^2} + (n-1)n(n+1) \times (n+2)F = 0 \quad [23]$$

The general solution of this equation is given by

$$F(\rho) = \frac{A}{\rho^{n+1}} + \frac{B}{\rho^{n-1}} + C\rho^n + D\rho^{n+2} \quad [24]$$

where A, B, C, D are constants of integration. This solution holds for any integral value of n, including zero.

Since $P_n(\mu)$ is even or odd in μ according as the degree n is even or odd, consequently a more general solution of χ_1 odd in μ is

$$\chi_1 = \sum_{n=0}^{\infty}\left(\frac{A_{2n+1}}{\rho^{2n+2}} + \frac{B_{2n+1}}{\rho^{2n}} + C_{2n+1}\rho^{2n+1} + D_{2n+1}\rho^{2n+3}\right) \times P_{2n+1}(\mu) \quad [25]$$

A similar solution but even in μ is

$$\chi_1 = \sum_{n=0}^{\infty}\left(\frac{A_{2n}}{\rho^{2n+1}} + \frac{B_{2n}}{\rho^{2n-1}} + C_{2n}\rho^{2n} + D_{2n}\rho^{2n+2}\right) P_{2n}(\mu). \quad [26]$$

In order to produce no effect on the stresses at infinity, the terms involving positive powers of ρ must be omitted from the general solution, except possibly those involving ρ and ρ^2 only. Besides, since the given solid has an additional symmetry about the plane $\phi = \pi/2$ or $\mu = 0$, the solution must be odd in μ. Thus we write

$$\chi_1 = T\sum_{n=0}^{\infty}\left(\frac{A_{2n+1}}{\rho^{2n+2}} + \frac{B_{2n+1}}{\rho^{2n}}\right) P_{2n+1}(\mu) \quad [27]$$

where the factor T is introduced merely for convenience in calculation. Here the terms involving ρ and ρ^2 are not included, for the former is trivial to the stresses and the latter is not odd in μ.

Furthermore, in dealing with an infinite solid containing a spherical cavity, it appears to be convenient to include also in the solution a term as follows

$$\chi_1 = TK\log\frac{1+\mu}{1-\mu} \quad [28]$$

where K is a parametric coefficient. This term is obviously biharmonic and odd in μ. In fact, it represents a "center of compression" at the origin, which produces no effect on the stresses at infinity. It may be interesting to compare this term with Legendre function of degree zero of the second kind.

By expressing χ_0 also in terms of Legendre polynomials of μ, we may thus write the required stress function as follows

$$\chi = \frac{T\rho^2}{30(1+\nu)}\left\{3P_1(\mu) + 2(1-5\nu)P_3(\mu)\right\} + TK\log\frac{1+\mu}{1-\mu} + T\sum_{n=0}^{\infty}\left(\frac{A_{2n+1}}{\rho^{2n+2}} + \frac{B_{2n+1}}{\rho^{2n}}\right) P_{2n+1}(\mu) \quad [29]$$

The boundary conditions to be satisfied are that on the surface of the cavity $\rho = \lambda$, say

$$\sigma_\rho = 0, \qquad \tau_{\rho\phi} = 0 \quad [30]$$

With the aid of the well-known recurrence formulas (7) for Legendre polynomials, we find from the preceding stress function the following stresses

$$\left.\begin{aligned} \frac{1}{T}\sigma_\rho = {} & \frac{1}{3} + \frac{2}{3}P_2(\mu) - \frac{4K}{\rho^2} + \frac{4(1-2\nu)B_1}{3\rho^3} \\ & + \sum_{n=1}^{\infty}\left\{2n(2n+1)(2n+2)A_{2n-1}\right. \\ & + \frac{4n(4n-3)(2n^2+3n-\nu)}{4n-1}\rho^3 B_{2n-1} \\ & + \frac{(2n+1)(4n+4)(6n-8n\nu+1-2\nu)}{4n+3} \\ & \left.\times B_{2n+1}\right\}\frac{P_{2n}(\mu)}{\rho^{2n+2}} \end{aligned}\right| \quad [31]$$

$$\left.\begin{aligned}\frac{1}{T\sqrt{1-\mu^2}}\,\tau_{\rho\phi} &= -\frac{1}{3}P_2'(\mu)\\ &+\sum_{n=1}^{\infty}\left\{2n(2n+2)A_{2n-1}\right.\\ &+\frac{2(4n-3)(2n^2+2n-3+\nu)}{4n-1}\rho^2B_{2n-1}\\ &\left.+\frac{(4n+4)(6n-8n\nu+1-2\nu)}{4n+3}B_{2n+1}\right\}\\ &\times\frac{P_{2n}'(\mu)}{\rho^{2n+2}}\end{aligned}\right\}\quad..[32]$$

where the accent on Legendre function denotes the derivative of the function with respect to μ.

Now, in order to satisfy the boundary conditions at $\rho = \lambda$, the coefficient of each term in these two expressions must vanish separately. This leads to the following set of equations

$$\left.\begin{aligned}&\frac{1}{3}-\frac{4}{\lambda^2}K+\frac{4(1-2\nu)}{3\lambda^2}B_1=0\\ &\frac{2}{3}+\left\{24A_1+\frac{4(5-\nu)}{3}B_1\lambda^2+\frac{24(7-10\nu)}{7}B_2\right\}\\ &\qquad\times\frac{1}{\lambda^2}=0\\ &-\frac{1}{3}+\left\{8A_1+\frac{2(1+\nu)}{3}B_1\lambda^2+\frac{8(7-10\nu)}{7}B_2\right\}\\ &\qquad\times\frac{1}{\lambda^2}=0\end{aligned}\right\}\quad..[33]$$

and for $n \geqslant 2$

$$\left.\begin{aligned}&2n(2n+1)(2n+2)A_{2n-1}\\ &+\frac{4n(4n-3)(2n^2+3n-\nu)}{4n-1}\lambda^2B_{2n-1}\\ &+\frac{(2n+1)(4n+4)(6n-8n\nu+1-2\nu)}{4n+3}\\ &\qquad\times B_{2n+1}=0\\ &2n(2n+2)A_{2n-1}\\ &+\frac{2(4n-3)(2n^2+2n-3+\nu)}{4n-1}\lambda^2B_{2n-1}\\ &+\frac{(4n+4)(6n-8n\nu+1-2\nu)}{4n+3}B_{2n+1}=0\end{aligned}\right\}\quad..[34]$$

The latter gives, for $n \geqslant 2$

$$A_{2n-1}=0,\qquad B_{2n-1}=0\quad.....[35]$$

Consequently, the former gives

$$\left.\begin{aligned}K&=-\frac{(1-5\nu)}{4(7-5\nu)}\lambda^2\\ A_1&=\frac{\lambda^2}{2(7-5\nu)}\\ B_1&=-\frac{5\lambda^2}{2(7-5\nu)}\end{aligned}\right\}\quad.....[36]$$

Therefore the required stress function turns out to be in the following closed form

$$\begin{aligned}\chi&=\frac{T\rho^2}{30(1+\nu)}\{3P_1(\mu)+2(1-5\nu)P_2(\mu)\}\\ &-\frac{T(1-5\nu)}{4(7-5\nu)}\lambda^2\log\frac{1+\mu}{1-\mu}-\frac{T\lambda^2}{2(7-5\nu)}\left(5-\frac{\lambda^2}{\rho^2}\right)P_1(\mu)\\ &=\frac{T\rho^2\mu}{6(1+\nu)}\{3\nu+(1-5\nu)\mu^2\}-\frac{T\lambda^2\mu}{2(7-5\nu)}\left(5-\frac{\lambda^2}{\rho^2}\right)\\ &\qquad-\frac{T(1-5\nu)}{4(7-5\nu)}\lambda^2\log\frac{1+\mu}{1-\mu}\quad.....[37]\end{aligned}$$

This function gives the following stresses

$$\left.\begin{aligned}\frac{1}{T}\sigma_\rho&=\frac{6\lambda^2}{(7-5\nu)\rho^2}\left(1-\frac{\lambda^2}{\rho^2}\right)\\ &\quad+\left\{1-\frac{5(5-\nu)\lambda^2}{(7-5\nu)\rho^2}+\frac{18\lambda^4}{(7-5\nu)\rho^4}\right\}\mu^2\\ \frac{1}{T}\sigma_\phi&=1+\frac{(4-5\nu)\lambda^2}{2(7-5\nu)\rho^2}+\frac{9\lambda^4}{2(7-5\nu)\rho^4}\\ &\quad-\left\{1-\frac{5(1-2\nu)\lambda^2}{2(7-5\nu)\rho^2}+\frac{21\lambda^4}{2(7-5\nu)\rho^4}\right\}\mu^2\\ \frac{1}{T}\sigma_\theta&=\frac{3\lambda^2}{2(7-5\nu)\rho^2}\left\{-2+5\nu+\frac{\lambda^2}{\rho^2}\right.\\ &\quad\left.+5\left(1-2\nu-\frac{\lambda^2}{\rho^2}\right)\mu^2\right\}\\ \frac{1}{T}\tau_{\rho\phi}&=-\mu\sqrt{1-\mu^2}\left\{1+\frac{5(1+\nu)\lambda^2}{(7-5\nu)\rho^2}\right.\\ &\quad\left.-\frac{12\lambda^4}{(7-5\nu)\rho^4}\right\}\end{aligned}\right\}\quad..[38]$$

which agree with the known results.

BIBLIOGRAPHY

1 "Mathematical Theory of Elasticity," by A. E. H. Love, Dover Publications, fourth edition 1944, pp. 274–277.

2 "Störungen der Spannungsverteilung (Disturbances of the Stress Distribution)," by A. Leon, Vienna, Austria, 1908. This reference is mentioned in Neuber's book, cited in reference (5).

3 "Concentration of Stress in the Neighborhood of a Small Spherical Flaw, etc.," by R. V. Southwell and H. J. Gough, *Philosophical Magazine*, vol. 1, 1926, pp. 71–97. The details of the solution are not given in this paper.

4 "Concentration of Stress Around Spherical and Cylindrical Inclusions and Flaws," by J. N. Goodier, Trans. ASME, vol. 55, 1933, pp. 39–44. A lucid description of the solution is also given in "Theory of Elasticity," by S. Timoshenko, McGraw-Hill Book Company, Inc., New York, N. Y., 1934, pp. 326–328. The solution is obtained by combining several special solutions.

5 "Theory of Notch Stresses," by H. Neuber, Edwards Bros. 1946, English translation, pp. 102–104. The original German edition was published by Julius Springer, in 1937 The solution is based on his three-function theory

6 "The Stress Function in Spherical Coordinates for Axisymmetric Stress and Strain Distributions," by S. Ziemba, *Archiwum Mechaniki Stosowanej*, vol. 1, 1949, pp. 311–338 This is a Polish journal. The paper itself is in French. The present writer is indebted to a referee for drawing his attention to this paper. The journal is unfortunately not available to him.

7 "Spherical Harmonics," by T. M. MacRobert, chapter 5. Methuen, 1927.

The Safety Factor of an Elastic-Plastic Body in Plane Strain[1]

By D. C. DRUCKER,[2] H. J. GREENBERG,[3] AND W. PRAGER[4]

Extremum principles are established for the safety factor of an elastic-plastic body made of a Prandtl-Reuss material and subjected to given surface tractions under conditions of plane strain. Since one of these principles establishes a maximum and the other a minimum property of the safety factor, it is possible to establish bounds for the safety factor by the joint use of these principles.

Introduction

THIS paper presents a practical method of estimating the safety factor of an elastic-plastic body under given surface tractions. For the sake of brevity it is assumed that the body is made of an incompressible material which obeys the stress-strain law of Prandtl (1)[5] and Reuss (2), and that it is deformed under conditions of plane strain. Neither of these conditions represents a restriction inherent in the method, but a fully general discussion of the method would far exceed the available space.

As an illustration of the type of problem to be discussed in the following, consider a hollow square prism of the cross section shown in Fig. 1, which is deformed under conditions of plane strain by gradually increasing internal pressure p. For sufficiently small values of p, the material is everywhere stressed elastically. Under increasing pressure, small plastic regions appear, presumably at the points marked 1 in Fig. 1; eventually, these plastic regions merge so that the hole is completely surrounded by a plastic region which, in turn, is enclosed by an elastic region. The dotted curve in Fig. 1 is meant to represent the elastic-plastic boundary at such a stage of the loading process. Of course, for the cross section considered here, this elastic-plastic boundary will not be circular.

As long as the plastic region remains enclosed by an elastic shell in this manner, the plastic strains must be of the order of magnitude of elastic strains. Moreover, an increase of plastic strain can be produced only by increasing the internal pressure p. Following W. Prager (3), this type of mechanical behavior of an elastic-plastic body will be termed "contained plastic deformation." The range of contained plastic deformation begins with

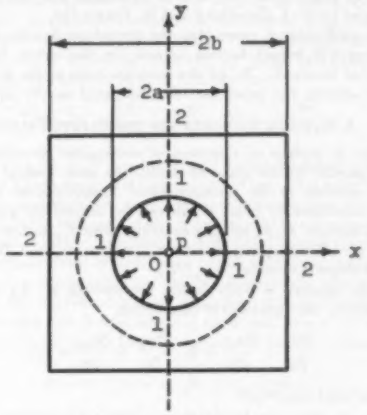

FIG. 1

the first appearance of plastic strains at the points marked 1 in Fig. 1, and ends when the elastic-plastic boundary reaches the exterior surface of the prism, presumably at the points marked 2 in Fig. 1. At this instant an increase of plastic strain under constant internal pressure becomes possible for the first time during the loading process. Obviously, the tube ceases to be useful as a pressure container at this instant of impending plastic flow. On the other hand, the mere presence of a plastic region does not interfere with the use of the tube as a pressure container as long as the plastic strains in this region are kept small by the surrounding elastic material. Therefore it seems appropriate to define the "safety factor" of the tube for a given internal pressure p as the number obtained by dividing p into the internal pressure for impending plastic flow.

In the following, the term safety factor will be used to denote the factor by which the given surface tractions must be multiplied before the elastic-plastic body reaches a state of impending plastic flow. Since the mechanical behavior in the plastic range depends on the history of loading, the concept of safety factor is meaningful only if the loading process is clearly defined. In the following it will be assumed that all surface tractions are increased so as to preserve their ratios (proportional loading). The state of impending plastic flow is reached when an increase of plastic strain under constant surface traction becomes possible for the first time during this loading process.

The stress-strain law of Prandtl-Reuss is an incremental law (4) which furnishes the increment of stress when the stress and the increment of strain are given. Since the state of impending plastic flow marks the end of the range of contained plastic deformation, it might appear at first glance that, to determine the pressure for impending plastic flow and hence the safety factor, one would have to follow the development of the elastic-plastic stress distribution from the end of the elastic range to the state of impending plastic flow. At present, this task could be ac-

[1] The results presented in this paper were obtained in the course of research conducted under Contract N7onr-35806 sponsored by the Office of Naval Research.

[2] Professor of Engineering, Brown University, Providence, R. I. Mem. ASME.

[3] Assistant Professor of Mathematics, Carnegie Institute of Technology, Pittsburgh, Pa.

[4] Professor of Applied Mechanics, Brown University, Providence, R. I. Mem. ASME.

[5] Numbers in parentheses refer to the Bibliography at the end of the paper.

Contributed by the Applied Mechanics Division and presented at the Annual Meeting, Atlantic City, N. J., November 25–30, 1951, of THE AMERICAN SOCIETY OF MECHANICAL ENGINEERS.

Discussion of this paper should be addressed to the Secretary, ASME, 29 West 39th Street, New York, N. Y., and will be accepted until January 10, 1952, for publication at a later date. Discussion received after the closing date will be returned.

NOTE: Statements and opinions advanced in papers are to be understood as individual expressions of their authors and not those of the Society. Manuscript received by ASME Applied Mechanics Division on July 5, 1950. Paper No. 51—A-3.

complished only in exceptional cases because no general analytical methods of treating problems of contained plastic flow have been developed to date. Under these circumstances, it seems worth while to draw attention to the fact that lower and upper bounds for the safety factor can be obtained without studying the development of the elastic-plastic stress distribution. To present a procedure by which this can be accomplished is the purpose of the present paper which extends to elastic-plastic bodies in plane strain methods of structural analysis recently developed by H. J. Greenberg and W. Prager (5).

The mathematical proof that the procedure described in the following will indeed furnish bounds for the safety factor is somewhat involved. To let the essential steps of the procedure appear clearly, the proof has been relegated to the Appendix.

A Maximum Principle for the Safety Factor

If the x, y-plane of a system of rectangular co-ordinates is taken parallel to the plane of strain, the most general field of stress possible in an incompressible Prandtl-Reuss material under conditions of plane strain can be defined by giving the normal stresses σ_x, σ_y and the shearing stress τ_{xy} as functions of x and y. (The shearing stresses τ_{xz}, τ_{yz} vanish, and the third normal stress is $\sigma_z = [\sigma_x + \sigma_y]/2$.)

In the absence of body forces, the stresses σ_x, σ_y, and τ_{xy} must satisfy the equations of equilibrium

$$\frac{\partial \sigma_x}{\partial x} + \frac{\partial \tau_{xy}}{\partial y} = 0, \quad \frac{\partial \sigma_y}{\partial y} + \frac{\partial \tau_{xy}}{\partial x} = 0 \quad \ldots\ldots [1]$$

and the yield condition[6]

$$(\sigma_x - \sigma_y)^2 + 4\tau_{xy}^2 \leq 4k^2 \quad \ldots\ldots [2]$$

where k denotes the yield stress in simple shear. The equality sign in Relation [2] holds only in the plastic region; in the elastic region the left-hand side of Relation [2] is smaller than the right-hand side.

At the cylindrical surface of the body under consideration, the stresses σ_x, σ_y, and τ_{xy} must be in equilibrium with the given surface tractions. If X and Y denote the components of the surface traction at a generic point P of the surface, Fig. 2, and if the exterior normal n of the surface at P makes the angle α with the positive x-direction, the stresses σ_x, σ_y, and τ_{xy} at P must satisfy the boundary conditions

$$\sigma_x \cos\alpha + \tau_{xy} \sin\alpha = X, \; \sigma_y \sin\alpha + \tau_{xy} \cos\alpha = Y \; . . [3]$$

Two new concepts will now be introduced which facilitate the statement of the maximum principle for the safety factor. A field of stress, i.e., a set of functions $\sigma_x(x, y)$, $\sigma_y(x, y)$ $\tau_{xy}(x, y)$, will be called statically admissible, if it satisfies the following:

(*a*) The equations of equilibrium [1] throughout the body with the possible exception of certain discontinuity surfaces which will be discussed later.

(*b*) The yield condition, Relation [2] throughout the body.

(*c*) The boundary conditions, Equation [3] over the entire surface.

If a statically admissible field of stress possesses a discontinuity surface (Fig. 3), and if the two sides of this surface are labeled 1 and 2, respectively, the traction transmitted across the discontinuity surface from the side 1 to the side 2 must be in equilibrium with the traction transmitted from 2 to 1. In the theory of perfectly plastic materials, discontinuity surfaces of this kind were first discussed by Prager (6) and studied further by Winzer and Carrier (7, 8), Lee (9), and Hodge (10).

If a statically admissible field of stress can be found for surface tractions which are obtained by multiplying all given surface tractions by the same factor $m_S \geq 1$, the number m_S will be called a "statically admissible multiplier." With this terminology the maximum principle for the safety factor can be stated as follows: *The safety factor of an elastic-plastic body under the action of given surface tractions is the largest statically admissible multiplier. It follows from this that any statically admissible multiplier is a lower bound for the safety factor.*

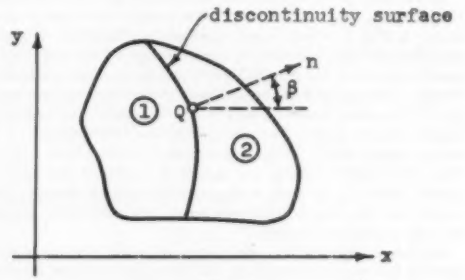

Fig. 3

A more familiar but not quite as general statement of this principle is as follows: An elastic-plastic body cannot reach a state of impending plastic flow under given surface tractions as long as there exists a field of stress which satisfies the equations of equilibrium in the interior and at the surface of the body (Equations [1] and [3] in the case of plane strain considered here), and for which the maximum shearing stress is everywhere smaller than the yield stress in simple shear. This form has sometimes been used as a heuristic basis of design. To the best of the authors' knowledge, however, the present paper contains the first complete proof of this principle; moreover, this proof includes discontinuous fields of stress. In many cases, a statically admissible field of stress is more readily constructed when discontinuities are admitted than when they are not.

The following discussion may serve as an illustration of the manner in which the maximum principle for the safety factor is applied. For the problem discussed in connection with Fig. 1, a statically admissible field of stress can be obtained as follows:

With reference to Fig. 4, consider a circular tube of interior radius a and exterior radius b made of a Prandtl-Reuss material which has the yield stress k in simple shear. Let p^* denote the

[6] Note that the expression "the stresses satisfy the yield condition" is here used in the sense "the maximum shearing stress does not exceed k" and not in the sense "the maximum shearing stress equals k." If the latter meaning is implied, the expression "the stresses satisfy the yield equation" will be used in the following.

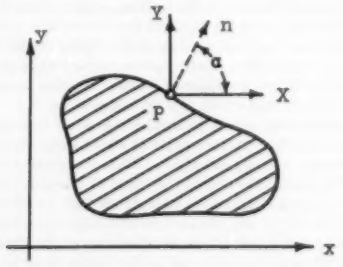

Fig. 2

internal pressure to which this tube must be subjected under conditions of plane strain to reach the state of impending plastic flow. Multiply the stresses of the well-known fully plastic stress distribution in this tube by p/p^*, where p is the given internal pressure to which the hollow square prism is subjected, and let

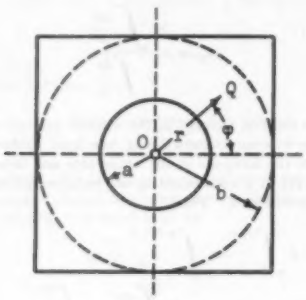

FIG. 4

the stresses in the region between the cylinder of radius b and the circumscribed square prism vanish identically. If $p \leq p^*$, the field of stress obtained in this manner is statically admissible. Indeed, the equations of equilibrium are satisfied anywhere in the hollow square prism except on the cylinder of radius b which is a discontinuity surface of the stress field. Since no traction is transmitted from either side of this discontinuity the equilibrium condition at the discontinuity surface is fulfilled. Furthermore, the maximum shearing stress τ has the value kp/p^* between the cylinders of the radii a and b and vanishes between the second cylinder and the circumscribed square prism. Since p/p^* is supposed to be smaller than unity, the yield condition is satisfied throughout the hollow square prism. Finally, the boundary conditions are satisfied at the interior as well as the exterior surfaces.

The multiplier associated with this statically admissible stress distribution equals p^*/p. Since[7] $p^* = 2k \log(b/a)$, the quantity

$$m_s = \frac{2k}{p} \log \frac{b}{a} \quad \ldots\ldots\ldots\ldots\ldots\ldots [4]$$

is a statically admissible multiplier and hence a lower bound for the safety factor of the hollow square prism subjected to the internal pressure p. This result is intuitively obvious, because the safety factor of the hollow square prism cannot be smaller than that of the circular tube of the radii a and b.

A Minimum Principle for the Safety Factor

Any field of plane plastic flow in an incompressible material can be defined by giving the velocity components v_x, v_y as functions of x and y so as to satisfy the condition of incompressibility

$$\frac{\partial v_x}{\partial x} + \frac{\partial v_y}{\partial y} = 0 \quad \ldots\ldots\ldots\ldots\ldots\ldots [5]$$

The strain rates of this field are

$$\epsilon_x = \frac{\partial v_x}{\partial x}, \quad \epsilon_y = \frac{\partial v_y}{\partial y} \; (= -\epsilon_x), \quad \gamma_{xy} = \frac{\partial v_y}{\partial x} + \frac{\partial v_x}{\partial y} \ldots [6]$$

[7] See, for instance (11), p. 188.

and the maximum shear rate is given by

$$\gamma = [(\epsilon_x - \epsilon_y)^2 + \gamma_{xy}^2]^{1/2} \quad \ldots\ldots\ldots\ldots\ldots [7]$$

Note that the square root in Equation [7] must always be taken with the positive sign.

The strain in an elastic-plastic material may be considered as the sum of the recoverable "elastic" strain and the permanent "plastic" strain. Similarly, the strain rate may be considered as the sum of the rates of change of the elastic and plastic strains. The elastic strain rate is related to the rate of change of the stress by Hooke's law and, in a Prandtl-Reuss material, the plastic strain rate is related to the stress by Mises' law (12). For plane strain this law can be written in the form

$$\frac{\sigma_x - \sigma_y}{2k} = \frac{\epsilon_x^{(p)} - \epsilon_y^{(p)}}{\gamma^{(p)}}, \quad \frac{\tau_{xy}}{k} = \frac{\gamma_{xy}^{(p)}}{\gamma^{(p)}} \quad \ldots\ldots\ldots [8]$$

where $\epsilon_x^{(p)}$, $\epsilon_y^{(p)}$, $\gamma_{xy}^{(p)}$ are the plastic strain rates and $\gamma^{(p)}$ the maximum plastic shear rate. Equations [8] state that the plastic strain rate and the stress have the same principal axes and that the plastic strain rate and the stress deviation have the same ratios of principal values.[8] Note that the right-hand sides of Equations [8] are homogeneous of order zero in the velocity components; if v_x and v_y are replaced by cv_x and cv_y, respectively, where c is a constant, the right-hand sides of Equations [8] are not affected. In other terms, the plastic material considered here is inviscid.

In plane plastic flow, the specific power of plastic deformation is

$$P = \sigma_x \epsilon_x^{(p)} + \sigma_y \epsilon_y^{(p)} + \tau_{xy} \gamma_{xy}^{(p)} \quad \ldots\ldots\ldots [9]$$

For the incompressible material considered here, $\epsilon_x^{(p)} = -\epsilon_y^{(p)}$. With the use of Equations [8] and [7], the expression, Equation [9], for the specific power of plastic deformation, therefore, can be transformed as follows

$$\begin{aligned} P &= (\sigma_x - \sigma_y)\epsilon_x^{(p)} + \tau_{xy}\gamma_{xy}^{(p)} \\ &= \frac{1}{2}(\sigma_x - \sigma_y)(\epsilon_x^{(p)} - \epsilon_y^{(p)}) + \tau_{xy}\gamma_{xy}^{(p)} \\ &= \frac{k}{\gamma^{(p)}} \left\{ [\epsilon_x^{(p)} - \epsilon_y^{(p)}]^2 + [\gamma_{xy}^{(p)}]^2 \right\} = k\gamma^{(p)} \quad \ldots\ldots [10] \end{aligned}$$

As will be proved in the second section of the Appendix, once the surface tractions have reached the intensity necessary for impending plastic flow, the "incipient plastic flow" takes place under constant stresses. Under these circumstances, the elastic strain rates vanish, and the plastic strain rates $\epsilon_x^{(p)}$, $\epsilon_y^{(p)}$, and $\gamma_{xy}^{(p)}$ can be identified with the total strain rates defined by Equations [6]. Also, $\gamma^{(p)}$ in Equation [10] can be identified with the maximum shear rate defined by Equation [7].

The incipient plastic flow can be treated as a quasi-static process. Accordingly, the total power of plastic deformation must equal the rate at which the surface tractions during the incipient plastic flow do work on the displacements of the points of the surface. If X, Y are the components along the co-ordinate axes of the given surface tractions, and S the factor of safety, the surface tractions during the incipient plastic flow have the components SX, SY. Therefore the equality of the power of these surface tractions and the total power of plastic deformation is expressed by the following equation

$$S \int (Xv_x + Yv_y) ds = k \int \gamma \, dA \quad \ldots\ldots\ldots [11]$$

In this equation, the integral on the right-hand side is extended over the area of a generic cross section of the body under con-

[8] For the general form of Mises' law see, for instance, reference (13).

sideration, and the integral on the left-hand side is extended over the contour of this cross section. If the velocity field of the incipient plastic flow were known, the safety factor could be found from Equation [11] as

$$S = \frac{k \int \gamma \, dA}{\int (Xv_x + Yv_y) ds} \quad \ldots\ldots [12]$$

Two new concepts will now be introduced which facilitate the statement of the minimum principle for the safety factor. A velocity field, i.e., a set of functions $v_x(x, y)$, $v_y(x, y)$, will be called "kinematically admissible" if it satisfies the following conditions:

(*a*) The velocity components v_x, v_y and their first derivatives with respect to x and y are continuous throughout the body with the possible exception of certain discontinuity surfaces which will be discussed later.

(*b*) The velocity components v_x, v_y fulfill the condition of incompressibility, Equation [5], in each of the regions bounded by the surface of the body and the discontinuity surfaces mentioned under (*a*).

(*c*) The signs of the velocity components have been chosen so that

$$\int (Xv_x + Yv_y) ds > 0 \quad \ldots\ldots [13]$$

where X, Y denote the components of the given surface tractions.

If a kinematically admissible velocity field possesses a discontinuity surface at all, only the velocity component v_T tangential to this surface is allowed to vary in a discontinuous manner; the normal velocity component v_N must be continuous.

The multiplier associated with the kinematically admissible field of velocity v_x, v_y will be defined as

$$m_K = \frac{k[\int \gamma \, dA + \int |v_T^{(1)} - v_T^{(2)}| \, ds']}{\int (Xv_x + Yv_y) ds} \quad \ldots\ldots [14]$$

where the second integral in the numerator is extended over the trace of the discontinuity surface in the cross-sectional plane.[9] The totality of the multipliers associated with all kinematically admissible velocity fields will be called the "kinematically admissible multipliers." With this terminology the minimum principle for the safety factor can be stated as follows: *The safety factor of an elastic-plastic body under the action of given surface tractions is the smallest kinematically admissible multiplier.* It follows from this that any kinematically admissible multiplier is an upper bound for the safety factor.

To illustrate the manner in which this principle can be applied, consider again the problem discussed in connection with Fig. 1. The field of a source at the origin O of the co-ordinates is a continuous velocity field which is kinematically admissible: the velocity at a generic point Q, Fig. 4, is directed along OQ and has the magnitude c/r, where c is a constant and r denotes the distance OQ. Accordingly, the velocity components v_x and v_y are given by

$$v_x = \frac{cx}{x^2 + y^2}, \quad v_y = \frac{cy}{x^2 + y^2} \quad \ldots\ldots [15]$$

and the strain rates by

$$\epsilon_x = \frac{c(y^2 - x^2)}{(x^2 + y^2)^2} = -\epsilon_y, \quad \gamma_{xy} = \frac{4cxy}{(x^2 + y^2)^2} \quad \ldots\ldots [16]$$

[9] Note that in the absence of discontinuity surfaces the right-hand sides of Equations [12] and [14] have the same form, the only difference being that v_x, v_y, γ refer to the actual velocity field of the incipient plastic flow in Equation [12] but to any kinematically admissible velocity field in Equation [14].

and the maximum rate of shear by

$$\gamma = \frac{2c}{x^2 + y^2} = \frac{2c}{r^2} \quad \ldots\ldots [17]$$

The multiplier associated with this field is

$$m_K = \frac{2k \int \frac{dA}{r^2}}{p \int \frac{ds}{a}} \quad \ldots\ldots [18]$$

where ds is the line element of the interior contour of the cross section, the exterior contour being free from surface tractions. To evaluate the integrals in the numerator and denominator of Equation [18], it is convenient to use polar co-ordinates r, with the origin at O, Fig. 4. Thus

$$\int \frac{dA}{r^2} = 8 \int_0^{\pi/4} d\varphi \int_a^{b \sec \varphi} \frac{dr}{r},$$

$$\text{and} \quad \int \frac{ds}{a} = \int_0^{2\pi} d\varphi \quad \ldots\ldots [19]$$

Evaluation of the definite integrals [19] yields

$$m_K = \frac{2k}{p}\left[\log \frac{b}{a} + \log 2 - \frac{2}{\pi} \times 0.9160\right]$$

$$= \frac{2k}{p}\left[\log \frac{b}{a} + 0.110\right] \quad \ldots\ldots [20]$$

Combination of the lower bound, Equation [4], and the upper bound, Equation [20], for the safety factor S yields

$$S = \frac{2k}{p}\left[\log \frac{b}{a} + 0.055 \pm 0.055\right] \quad \ldots\ldots [21]$$

For $b/a = 4$, for instance, Equation [21] gives the safety factor of the hollow square prism to within about ± 4 per cent. For $b/a = 1.5$, on the other hand, the bounds for S obtained from Equation [21] are $0.811\ k/p$ and $0.921\ k/p$. To improve these bounds, let us consider the discontinuous velocity field indicated in Fig. 5. The lines AB and ED are parallel to the diagonal OC and symmetrically situated with respect to this diagonal. The velocity field which is to be considered represents a translation of the portion $ABCDE$ in the direction of OC with the velocity v. Since this portion as well as the remainder of the body remains rigid, the first integral in the numerator of Equation [14] van-

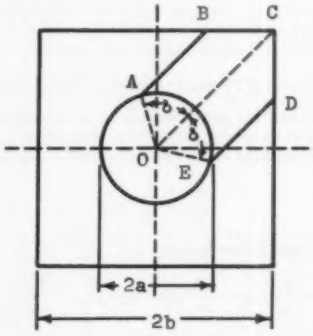

FIG. 5

ishes. The second integral equals the product of the length of the segment AB by $2v$, and the denominator integral equals the product of the length of the segment AE by pv. With the notations in Fig. 5

$$(AB) = b\sqrt{2} - a(\cos\delta + \sin\delta)$$

and

$$(AE) = 2a\sin\delta$$

Equation [14] therefore yields

$$m_K = \frac{k}{p}\,\frac{b\sqrt{2} - a(\cos\delta + \sin\delta)}{a\sin\delta} \qquad [22]$$

Since Equation [22] furnishes an upper bound for the safety factor, the angle δ should be chosen so as to minimize m_K. By elementary calculus it is found that for

$$\delta = \cos^{-1}\frac{a}{b\sqrt{2}} \qquad [23]$$

the kinematically admissible multiplier, Equation [22], assumes the minimum

$$\min m_K = \sqrt{2\,\frac{b^2}{a^2} - 1} - 1 \qquad [24]$$

For $b/a = 1.5$, for instance, this minimum value of m_K equals $0.871\ k/p$ and is assumed for $\delta = 69°15'$. Since Equation [21] furnishes the lower bound $0.811\ k/p$ in this case, the safety factor of the hollow square prism with $b/a = 1.5$ has been determined to within ± 3.6 per cent.

Relation to Saint Venant-Mises Theory

The preceding discussion throws welcome light on the relation between the Prandtl-Reuss theory and the older theory of Saint Venant (14) and Mises (12), a relation which has not been clearly understood in the past.

Whereas the Prandtl-Reuss theory takes account of the elastic as well as the plastic strains, the theory of Saint Venant and von Mises treats the elastic strains as negligible in comparison to the plastic strains. As a rule, adequate treatment of problems of contained plastic deformation therefore requires the use of the Prandtl-Reuss theory, and this fact is generally admitted. At the same time, the Saint Venant-Mises theory is generally accepted as an adequate tool for the treatment of problems of unrestricted plastic flow (as opposed to problems of contained plastic deformation). Since the range of unrestricted plastic flow develops from the range of contained plastic deformation, this rejection of the theory for the first range and its acceptance for the second might seem to be inconsistent in so far as the strain history plays an important role throughout the plastic range. The results presented in the foregoing sections make it possible to resolve this difficulty and to assess the precise value of the "solutions" furnished by the theory of Saint Venant and von Mises. Since this discussion would exceed the available space, however, it will be presented in a separate paper.

BIBLIOGRAPHY

1 "Spannungsverteilung in plastischen Körpern," by L. Prandtl, Proceedings of the First International Congress of Applied Mechanics, Delft, Holland, 1924, pp. 43–54.

2 "Berucksichtigung der elastischen Formaenderungen in der Plastizitaetstheorie," by E. Reuss, *Zeitschrift für angewandte Mathematik und Mechanik*, vol. 10, 1930, pp. 266–274.

3 "Plasticity for the Aerodynamicist," by W. Prager, *Journal of the Aeronautical Sciences*, vol. 15, 1948, pp. 253–262.

4 "Relation of Experiments to Mathematical Theory of Plasticity," by D. C. Drucker, Journal of Applied Mechanics, Trans. ASME, vol. 71, 1949, p. A-349.

5 "Limit Design of Beams and Frames," by H. J. Greenberg and W. Prager, to appear in Proceedings of the American Society of Civil Engineers; this paper is partly based on ideas presented by H. J. Greenberg under the title "The Principle of Limiting Stress for Structures," Second Symposium on Plasticity, Brown University, Providence, R. I., April, 1949.

6 "Discontinuous Solutions in the Theory of Plasticity," by W. Prager, Courant Anniversary Volume, Interscience Publishers, New York, N. Y., 1948, pp. 289–299.

7 "The Interaction of Discontinuity Surfaces in Plastic Fields of Stress," by A. Winzer and G. F. Carrier, Journal of Applied Mechanics, Trans. ASME, vol. 70, 1948, p. A-261.

8 "Discontinuities of Stress in Plane Plastic Flow," by A. Winzer and G. F. Carrier, Journal of Applied Mechanics, Trans. ASME, vol. 71, 1949, p. A-346.

9 "On Stress Discontinuities in Plane Plastic Flow," by E. H. Lee, to appear in Proceedings of the Third Symposium on Applied Mathematics, Ann Arbor, Mich., June 14–16, 1949; McGraw-Hill Book Company, Inc., New York, N. Y., 1950.

10 "Approximate Solutions of Problems in Plane Plastic Flow," by P. G. Hodge, Journal of Applied Mechanics, Trans. ASME, vol. 72, 1950, p. A-257.

11 "Plasticity, a Mechanics of the Plastic State of Matter," by A. Nadai, McGraw-Hill Book Company, Inc., New York, N. Y., 1931.

12 "Mechanik der festen Koerper im plastisch-deformablen Zustand," by R. von Mises, *Goettinger Nachrichten, mathematisch-physikalische Klasse*, 1913, pp. 582–592.

13 "The Stress-Strain Relations of the Mathematical Theory of Plasticity," by W. Prager, Journal of Applied Mechanics, Trans. ASME, vol. 70, 1948, p. A-226.

14 "Mémoire sur l'établissement des équations différentielles des mouvements intérieurs opérés dans les corps solides ductiles au delà des limites où l'élasticité pourrait les ramener à leur premier état," by B. de Saint Venant, Comptes Rendus, Paris, France, vol. 70, 1870, pp. 473–480.

Appendix

The extremum principles concerning the safety factor will be proved first in the special case where the stress and velocity fields under consideration do not exhibit the discontinuities discussed in the foregoing. Until further notice, σ_x, σ_y, τ_{xy}, v_x, and v_y, therefore, will be regarded as continuously differentiable functions.

Principle of Virtual Work

In the following, the principle of virtual work is used repeatedly. In the case of plane strain, this principle is expressed by the equation

$$\int(\sigma_x\epsilon_x + \sigma_y\epsilon_y + \tau_{xy}\gamma_{xy})dA = \int(Xv_x + Yv_y)ds \ldots [25]$$

where, on the left, the integration is extended over the cross section of the body under consideration and, on the right, along the contour of this cross section. The stresses σ_x, σ_y, τ_{xy} on the left-hand side of Equation [25] must satisfy the equations of equilibrium, Equations [1], throughout the cross section; the surface tractions X, Y on the right-hand side of Equation [25] are obtained from these stresses by means of Equations [3]. The velocities v_x, v_y on the right-hand side of Equation [25] will be assumed to satisfy the condition of incompressibility Equation [5], and the strain rates ϵ_x, ϵ_y, γ_{xy} on the left-hand side of Equation [25] are obtained from these velocities by means of Equations [6]. Note that the stresses and strain rates or the surface tractions and velocities are not related to each other as cause and effect; subject to the conditions just enumerated, the stress field and the velocity field Equation [25] can be chosen quite independently of each other. To prove Equation [25], express the strain rates in terms of the derivatives of the velocities in accordance with Equations [6], and use Green's formula to transform the area integral on the left-hand side into a contour inte-

gral using the fact that the stresses satisfy the equations of equilibrium, Equations [1]. Note that the principle of virtual work also can be applied to an equilibrium system of stress rates $\partial\sigma_x/\partial t$, $\partial\sigma_y/\partial t$, $\partial\tau_{xy}/\partial t$ and the rates of surface traction $\partial X/\partial t$, $\partial Y/\partial t$ obtained from these stress rates by equations similar to Equations [3]; thus

$$\int\left(\frac{\partial\sigma_x}{\partial t}\epsilon_x+\frac{\partial\sigma_y}{\partial t}\epsilon_y+\frac{\partial\tau_{xy}}{\partial t}\gamma_{xy}\right)dA = \int\left(\frac{\partial X}{\partial t}v_x+\frac{\partial Y}{\partial t}v_y\right)ds \quad [26]$$

Proof That Stresses Remain Constant During Incipient Plastic Flow

While Mises' law, Equations [8] allows for plastic flow under constant stress, by no means does it stipulate that the state of stress must remain constant during plastic flow. If the state of stress varies at all during plastic flow, the stress components and their rates of change must, at any instant, satisfy the equation

$$(\sigma_x-\sigma_y)\left(\frac{\partial\sigma_x}{\partial t}-\frac{\partial\sigma_y}{\partial t}\right)+4\tau_{xy}\frac{\partial\tau_{xy}}{\partial t}=0 \quad [27]$$

which is obtained by differentiating the yield equation with respect to time. Equation [27] expresses the fact that, for continued plastic flow, the change in stress must always be such that the new stress components continue to satisfy the yield equation.

If $\sigma_x-\sigma_y$ and τ_{xy} are substituted from Equations [8] into Equation [27], the following equation is obtained

$$\frac{1}{2}(\epsilon_x^{(p)}-\epsilon_y^{(p)})\left(\frac{\partial\sigma_x}{\partial t}-\frac{\partial\sigma_y}{\partial t}\right)+\gamma_{xy}^{(p)}\frac{\partial\tau_{xy}}{\partial t}=0 \quad [28]$$

As follows from its derivation, this equation is valid during any plastic flow; it also is valid, however, when no plastic flow occurs because the plastic strain rates vanish in this case.

To prove that the stresses remain constant during incipient plastic flow, assume that the stress rates do not vanish identically and show that this assumption leads to a contradiction. Let v_x, v_y be the actual velocities for incipient plastic flow, ϵ_x, ϵ_y, γ_{xy} the strain rates, and $\partial\sigma_x/\partial t$, $\partial\sigma_y/\partial t$, $\partial\tau_{xy}/\partial t$ the stress rates. By definition, incipient plastic flow takes place under constant surface tractions. Equation [26] shows, therefore, that

$$\int\left(\frac{\partial\sigma_x}{\partial t}\epsilon_x+\frac{\partial\sigma_y}{\partial t}\epsilon_y+\frac{\partial\tau_{xy}}{\partial t}\gamma_{xy}\right)dA=0 \quad [29]$$

For the incompressible material considered here, $\epsilon_z=-\epsilon_y$. Therefore Equation [29] can be written as follows

$$\int\left[\frac{1}{2}\left(\frac{\partial\sigma_x}{\partial t}-\frac{\partial\sigma_y}{\partial t}\right)(\epsilon_x-\epsilon_y)+\frac{\partial\tau_{xy}}{\partial t}\gamma_{xy}\right]dA=0 \quad [30]$$

The total strain rates $\epsilon_x,\ldots$ are now expressed as the sums of the elastic strain rates $\epsilon_x^{(e)},\ldots$ and the plastic strain rates $\epsilon_x^{(p)},\ldots$. On account of Equation [28], the term involving the plastic strain rates vanishes. Thus the total strain rates in Equation [30] can be replaced by the elastic strain rates. These, in turn, can be expressed in terms of the stress rates by means of Hooke's law. For the incompressible material considered here, this law has the form

$$\epsilon_x^{(e)}-\epsilon_y^{(e)}=\frac{1}{2G}\left(\frac{\partial\sigma_x}{\partial t}-\frac{\partial\sigma_y}{\partial t}\right),\ \gamma_{xy}^{(e)}=\frac{1}{G}\frac{\partial\tau_{xy}}{\partial t} \quad [31]$$

where G is the modulus of rigidity. Thus

$$\int\left[\left(\frac{\partial\sigma_x}{\partial t}-\frac{\partial\sigma_y}{\partial t}\right)^2+\left(\frac{\partial\tau_{xy}}{\partial t}\right)^2\right]dA=0 \quad [32]$$

For this equation to be satisfied, the following relations must hold throughout the body under consideration

$$\frac{\partial\sigma_x}{\partial t}=\frac{\partial\sigma_y}{\partial t},\ \frac{\partial\tau_{xy}}{\partial t}=0 \quad [33]$$

Now, the stress rates must satisfy the equations of equilibrium, Equations [1]. Together with Equations [33], these equations require that

$$\frac{\partial\sigma_x}{\partial t}=\frac{\partial\sigma_y}{\partial t}=\text{const},\ \frac{\partial\tau_{xy}}{\partial t}=0 \quad [34]$$

Since the rates of surface tractions $\partial X/\partial t$, $\partial Y/\partial t$ computed from the stress rates, [34] in accordance with Equations [3] must vanish by the definition of incipient plastic flow, the constant in the first of Equations [34] is seen to vanish. Thus the stress rates and hence the elastic strain rates vanish identically during incipient plastic flow.

Proof of Maximum Principle for Safety Factor

Let σ_x', σ_y', τ_{xy}' denote the stresses of a statically admissible field of stress for surface tractions, which are obtained by multiplying all given surface tractions by a statically admissible multiplier m_B, and let σ_x, σ_y, τ_{xy} and $\epsilon_x^{(p)}$, $\epsilon_y^{(p)}$, $\gamma_{xy}^{(p)}$ be the actual stresses and plastic strain rates during incipient plastic flow. In the proof of the maximum principle for the safety factor use will be made of the fact that, throughout the body under consideration

$$(\sigma_x-\sigma_x')\epsilon_x^{(p)}+(\sigma_y-\sigma_y')\epsilon_y^{(p)}+(\tau_{xy}-\tau_{xy}')\gamma_{xy}^{(p)}\geq 0 \quad [35]$$

This relation is obviously valid in those parts of the body where no plastic flow occurs because the plastic strain rates vanish there. On the other hand, wherever plastic flow occurs, the stresses σ_x, σ_y, τ_{xy} must satisfy the yield equation. To prove that Relation [35] is valid in these parts too, transform the left-hand side of this relation by means of the incompressibility condition $\epsilon_z^{(p)}=-\epsilon_y^{(p)}$ and the Mises law, Equations [8]. Thus Relation [35] is equivalent to

$$\frac{\gamma^{(p)}}{4k}\{[(\sigma_x-\sigma_x')-(\sigma_y-\sigma_y')](\sigma_x-\sigma_y)+4(\tau_{xy}-\tau_{xy}')\tau_{xy}\}\geq 0 \quad [36]$$

Here, the positive factor $\gamma^{(p)}/4k$ may be suppressed. Moreover, since the stresses σ_x, σ_y, τ_{xy} satisfy the yield equation, [36] is equivalent to

$$4k^2-[(\sigma_x-\sigma_y)(\sigma_x'-\sigma_y')+4\tau_{xy}\tau_{xy}']\geq 0 \quad [37]$$

By Schwarz's inequality[10] the expression in square brackets cannot be greater than

$$[(\sigma_x-\sigma_y)^2+4\tau_{xy}^2]^{1/2}[(\sigma_x'-\sigma_y')^2+4\tau_{xy}'^2]^{1/2}$$

Here, the first square root equals $2k$ because the stresses $\sigma_x,\ldots$ satisfy the yield equation, and the second square root can not exceed $2k$ because the stresses $\sigma_x',\ldots$ are admissible. Thus the Relation [37] and hence [35] from which it was derived are seen to be valid.

Consider now the integral

---

[10] In its simplest form, sufficient here, this inequality states that

$$a_1b_1+a_2b_2\leq(a_1^2+a_2^2)^{1/2}(b_1^2+b_2^2)^{1/2}$$

To apply this to [37], set $a_1=\sigma_x-\sigma_y$, $a_2=2\tau_{xy}$, $b_1=\sigma_x'-\sigma_y'$ $b_2=2\tau_{xy}'$.

$$\int [(\sigma_x - \sigma_x')\epsilon_x^{(p)} + (\sigma_y - \sigma_y')\epsilon_y^{(p)} + (\tau_{xy} - \tau_{xy}')\gamma_{xy}^{(p)}]\,dA \quad \ldots\ldots [38]$$

Since the elastic strain rates vanish during incipient plastic flow (see second section of the Appendix) the plastic strain rates $\epsilon_x^{(p)}, \ldots$ equal the total strain rates $\epsilon_x, \ldots$. After the superscripts (p) have thus been omitted in [38] this integral can be transformed in accordance with the principle of virtual work. Now, the actual stresses $\sigma_x, \ldots$ during incipient plastic flow are in equilibrium with the surface tractions SX, SY, where S is the safety factor; the admissible stresses $\sigma_x', \ldots$, on the other hand, were supposed to be in equilibrium with the surface tractions $m_S X$, $m_S Y$, where m_S is a statically admissible multiplier. The Integral [38] thus equals

$$(S - m_S)\int (Xv_x + Yv_y)ds \quad \ldots\ldots [39]$$

where v_x, v_y are the actual velocities during incipient plastic flow. According to [35], the Integral [38] and hence the Expression [39] cannot be negative. Moreover, S times the integral in [39] is the rate at which the actual surface tractions SX, SY do work during incipient plastic flow, and this is positive since energy is dissipated during plastic flow. Thus the factor in front of the integral in [39] cannot be negative. This establishes the maximum principle for the safety factor.

Proof of Minimum Principle for Safety Factor

Let v_x'', v_y'' denote kinematically admissible velocities, ϵ_x'', ϵ_y'', γ_{xy}'' the corresponding strain rates, γ'' the corresponding maximum shear rate, and σ_x, σ_y, τ_{xy} the actual stresses during incipient plastic flow. In the proof of the minimum principle for the safety factor use will be made of the fact that

$$\sigma_x\epsilon_x'' + \sigma_y\epsilon_y'' + \tau_{xy}\gamma_{xy}'' \leq k\gamma'' \quad \ldots\ldots [40]$$

throughout the body under consideration. To prove this, transform the left-hand side of [40] by means of the condition of incompressibility $\epsilon_z'' = -\epsilon_y''$. Thus [40] is equivalent to

$$\frac{1}{2}(\sigma_x - \sigma_y)(\epsilon_x'' - \epsilon_y'') + \tau_{xy}\gamma_{xy}'' \leq k\gamma'' \quad \ldots\ldots [41]$$

By Schwarz' inequality, the left-hand side of [41] cannot be greater than

$$[1/4\,(\sigma_x - \sigma_y)^2 + \tau_{xy}^2]^{1/2}\,[(\epsilon_x'' - \epsilon_y'')^2 + \gamma_{xy}''^2]^{1/2}$$

Here, the second square root equals γ'' by Equation [7], and the first square root cannot be greater than k because the stresses $\sigma_x, \ldots$ satisfy the yield condition, Relation [2]. Thus, the relation [41], and hence [40] from which it was derived are seen to be valid.

Consider now the integral

$$\int (\sigma_x\epsilon_x'' + \sigma_y\epsilon_y'' + \tau_{xy}\gamma_{xy}'')dA \quad \ldots\ldots [42]$$

The actual stresses $\sigma_x, \ldots$ during incipient plastic flow are in equilibrium with the surface tractions SX, SY, where S is the safety factor. According to the principle of virtual work, the Integral [42] therefore equals

$$S\int (Xv_x'' + Yv_y'')ds \quad \ldots\ldots [43]$$

On the other hand, [40] shows that the Integral [42] and hence the Expression [43] cannot be greater than

$$k\int \gamma''\,dA \quad \ldots\ldots [44]$$

On account of the Condition [13], the following relation must therefore hold

$$S \leq \frac{k\int \gamma''\,dA}{\int (Xv_x'' + Yv_y'')ds} \quad \ldots\ldots [45]$$

This establishes the minimum principle for the safety factor in the case of continuous velocity fields.

Discontinuous Stress Fields

To what extent must the proof of the third section of the Appendix be modified if the stress field $\sigma_x', \sigma_y', \tau_{xy}'$ has discontinuity surfaces of the type previously discussed? Obviously, the validity of the local Relations [35] to [37] is not impaired by the presence of such discontinuity surfaces. On the other hand, the continued validity of the principle of virtual work (used to establish the equality of [38] and [39]) cannot be accepted without careful investigation.

The traces of the discontinuity surfaces in the cross-sectional plane divide the cross section into a number of regions for each of which the principle of virtual work is valid. When the equations expressing this principle for each of these regions are added, the sum of the surface integrals is seen to equal the left-hand side of Equation [25]. The sum of the line integrals, on the other hand, contains not only the right-hand side of Equation [25], evaluated along the contour of the cross section, but also similar line integrals evaluated along the traces of the discontinuity surfaces in the cross-sectional plane. Now, each line element of such a trace appears as a portion of the boundary of the two adjacent regions, and the tractions which these regions transmit to each other across this line element have been stipulated to be equal in magnitude but opposite in direction. Thus the contributions which the considered line element makes toward the line integrals for the two adjacent regions will cancel each other. Therefore the presence of stress discontinuities of the type considered here does not impair the validity of the principle of virtual work.

Discontinuous Velocity Fields

The validity of the local Relations [40], [41] is not affected by the presence of discontinuity surfaces in the velocity field, but Equation [25] is no longer valid when such discontinuities are admitted, and [42] is hence no longer equal to [43]. In this case, the traces of the discontinuity surfaces in the cross-sectional plane again divide the cross section of the considered body in a number of regions for each of which the principle of virtual work is valid. When the equations expressing this principle for each of these regions are added, the sum of the surface integrals again equals the left-hand side of Equation [25]. The sum of the line integrals, however, contains not only the right-hand side of Equation [25], evaluated along the contour of the cross section, but also similar line integrals evaluated along the traces of the discontinuity surfaces. To discuss the contribution made by the line element ds' of such a trace, label the adjacent regions 1 and 2, as in Fig. 3, and choose positive directions along the normal and tangent of ds', for instance, the direction from 1 toward 2 as the positive direction along the normal, and the direction obtained from this by a counterclockwise rotation through 90 deg as the positive direction along the tangent. Denote by N and T the normal and tangential stresses which, during incipient plastic flow, are actually transmitted across ds' from the side 2 to the side 1. In the discontinuous, kinematically admissible velocity field under consideration, let v_N'' be the velocity component normal to ds' and $v_T''^{(1)}$, $v_T''^{(2)}$ the tangential velocity components on the sides 1 and 2 of this element.

As part of the boundary of the region 1, the line element then contributes the quantity $Nv_N'' + Tv_T''^{(1)}$, and as part of the boundary of 2 it contributes $-Nv_N'' - Tv_T''^{(2)}$. Thus the total

contribution made by this line element is $T(v_T'^{(1)} - v_T'^{(2)})ds'$. This is bounded by

$$-k \mid v_T'^{(1)} - v_T'^{(2)} \mid ds' \quad \text{and} \quad k \mid v_T'^{(1)} - v_T'^{(2)} \mid ds'$$

because the tangential stress T cannot exceed k in absolute value. Thus the Integral [42] which now equals

$$S\int (Xv_x' + Yv_y')ds + \int T(v_T'^{(1)} - v_T'^{(2)})ds' \quad \ldots [46]$$

cannot be smaller than

$$S\int (Xv_x' + Yv_y')ds - k\int \mid v_T'^{(1)} - v_T'^{(2)} \mid ds' \quad \ldots [47]$$

On the other hand, [40] shows that the Integral [42] cannot be larger than $k\int \gamma' \, dA$; thus

$$S\int (Xv_x' + Yv_y')ds \leq k[\int \gamma' dA + \int \mid v_T'^{(1)} - v_T'^{(2)} \mid ds'] \ldots\ldots [48]$$

Since the integral multiplying S on the left-hand side of this Relation has been stipulated to be positive by Relation [13], an upper bound for S is obtained by dividing the two sides of [48] by this integral. The minimum principle for the safety factor is thus extended to discontinuous velocity fields.

Plastic-Wave Propagation Effects in High-Speed Testing[1]

By E. H. LEE[2] and H. WOLF,[3] PROVIDENCE, R. I.

A material test carried out at high speed may be markedly influenced by plastic-wave propagation effects. In such a case, a variation of strain occurs along the test specimen, and the stress-strain relation cannot be determined from measurements made on the specimen as a whole. If average values are taken, it is shown that a spurious strain-rate influence will be deduced when propagation effects first begin to appear as the testing speed is increased. The effect is due not to a true material strain-rate dependence, but to the appearance of strain variations along the specimen, and its magnitude depends upon the dynamics of the whole test arrangement. The theoretical plastic-wave analysis of a particular test arrangement is also given. The range of speed is determined which permits satisfactory interpretation without the need for detailed analysis of plastic-wave propagation. Application to other test arrangements is discussed, and it is pointed out that a theoretical analysis can, in general, be made to predict the permissible speed range in planning a high-speed testing program.

Introduction

EXPERIMENTAL work has been carried out over a number of years to determine the influence of strain rate on the stress-strain relation of metals. Attempts to obtain the stress-strain relation for increasing values of the rate of strain have led to successive modification of testing-machine design in order to permit measurement with reasonable accuracy.

For so-called static tests, a beam type of testing machine is satisfactory, since a condition of equilibrium is obtained for each recorded point, and the balanced beam determines the corresponding stress. If tests at constant strain rates are required to determine the effect of rate of strain, a different design of testing machine is needed which permits measurement of the stress and strain while the strain continues to increase. In such a machine, for example (1),[4] the stress is measured continuously by the deflection of a stiff spring. For increasing values of the strain rate, this method of measuring stress becomes unsatisfactory, for the inertia forces, required to move parts of the machine, influence the spring deflection, which therefore gives a poor measurement of the force in the specimen itself, and so of the stress in the specimen. This difficulty can be overcome by suitable redesign of the machine to eliminate appreciable inertia between the specimen and the force-measuring element. For example, the force transmitted through the specimen could be measured by a resistance strain gage on an extension of the specimen which remains elastic.

For tests at higher strain rates the inertia of the specimen itself may become important, producing a nonuniform stress distribution along the specimen, which can be evaluated only by analyzing the propagation of plastic stress waves in the specimen. Taylor (2) has devised a dynamic compression test which utilizes the inertia forces of the specimen to generate the stress. However, most experimental work has been analyzed on the assumption that the stress and strain distributions in the specimen are uniform; in other words, that the influence of the inertia of the specimen itself is negligible. It will be shown that test results based on this assumption may introduce a spurious strain-rate effect if the inertia forces of the test specimen are not in fact negligible. In assessing the characteristics of a material, it is clearly important to eliminate this influence, for it represents a strain-rate effect which is a function of the detail design of the testing machine and the geometry of the test specimen.

The example considered in this paper will indicate how a comparatively simple calculation can be made to check the magnitude of this effect for any proposed test arrangement, and so to determine a corresponding strain-rate limit for the measurement of a true material speed effect without the need for detailed interpretation of the test results in terms of strain wave propagation.

A Method of High-Speed Compression Testing

The speed effect in copper has been investigated by Habib (3) who carried out high-speed compression tests on copper cylinders. The specimen, as shown in Fig. 1, was placed in contact with a heavy steel anvil, and was subjected to impact by a hardened steel piston. From the measurement of the impact and rebound velocities, and the known piston mass, the energy absorbed is determined. Assuming uniform strain in the specimen, the energy-deformation curves for a range of impact velocities and piston masses were used to determine stress-strain relations for a range of values of the average strain rate. In any single test, the average energy absorbed per unit volume is, with this assumption, equal to the area under the corresponding stress-strain curve up to the average strain occurring. Thus stress-strain curves for a fixed average strain rate are given by differentiating the corresponding energy-strain curves.

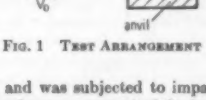

Fig. 1 Test Arrangement

---

[1] The conclusions presented in this paper were obtained in the course of research conducted under Contract N7onr-358 sponsored by the Office of Naval Research and the Bureau of Ships.

[2] Associate Professor of Applied Mathematics, Graduate Division of Applied Mathematics, Brown University. Mem. ASME.

[3] Assistant Professor of Mathematics, Hofstra College, Long Island, N. Y.

[4] Numbers in parentheses refer to the Bibliography at the end of the paper.

Contributed by the Applied Mechanics Division and presented at the Annual Meeting, New York, N. Y., November 26–December 1, 1950, of The American Society of Mechanical Engineers.

Discussion of this paper should be addressed to the Secretary, ASME, 29 West 39th Street, New York, N. Y., and will be accepted until January 10, 1952, for publication at a later date. Discussion received after the closing date will be returned.

Note: Statements and opinions advanced in papers are to be understood as individual expressions of their authors and not those of the Society. Manuscript received by ASME Applied Mechanics Division on May 15, 1950. Paper No. 50—A-35.

Let us consider the development of the plastic strain in such a test. On impact a compression-stress wave travels from the surface of impact, consisting of an elastic wave front, followed by a more slowly moving plastic wave front. The compressive stress behind the plastic wave front acts at the impact interface causing deceleration of the piston. The resulting reduction in velocity causes a diminution of the contact stress, and unloading waves travel into the specimen from the point of impact. Because metals behave elastically under decreasing stress after plastic flow, these unloading waves travel with the velocity of elastic waves and thus overtake and unload the plastic wave front, causing it to be propagated with continuously reduced maximum stress and strain. If the piston mass is small, the deceleration and associated unloading effect is marked, leading to a marked strain gradient in the specimen. For a very light piston, complete unloading and cessation of plastic flow could occur before the plastic wave reaches the anvil, causing localised compression at the impact end of the specimen.

With a heavy piston, the deceleration will be smaller and plastic flow may continue through many reflections of the plastic wave front at the anvil and impact surfaces. In the limit for an indefinitely large mass at low velocity, the kinetic energy of the piston would be absorbed in uniform compression along the gage length.

For a work-hardening material, such a variation in strain distribution itself causes an apparent variation in the stress-strain relation calculated on the assumption of uniform strain. This will be demonstrated by a simple example. Since the strain distribution varies with the variation in piston velocity which is used to determine the average strain rate, such a distribution effect will be interpreted erroneously as a true material strain-rate effect according to the type of analysis based on the assumption of uniform strain.

As a simple example, let us consider a material with a linear stress-strain relation as shown in Fig. 2. Consider this to be

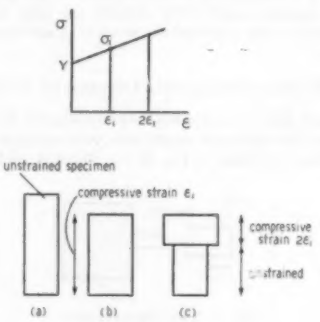

FIG. 2

independent of the strain rate. We are interested in strains large compared with elastic strains so that it will be permissible to neglect elastic strain, and so to consider elastic material to be rigid. Thus the stress-strain relation shows zero strain up to the yield stress Y, followed by plastic flow with a constant work-hardening coefficient.

The nominal compressive strain ϵ is defined as the reduction in length per unit initial length; σ is the nominal stress, defined as the compressive force per unit initial cross-sectional area. Nominal stress and strain values are used since they simplify the equations for plastic waves. Moreover, it is clear from the definitions that the work done during a strain increment $d\epsilon$ is $\sigma d\epsilon$ per unit initial volume of material.

Consider the unstrained cylindrical specimen shown at (a) in the lower part of Fig. 2; (b) shows this specimen subjected to the uniform strain ϵ_1. The energy absorbed per unit volume to produce this strain is equal to the area under the stress-strain curve up to the strain ϵ_1, which is the average stress $(Y + \sigma_1)/2$ multiplied by ϵ_1. Now consider the deformed specimen shown at (c), which is subjected to the same over-all reduction in length, but distributed so that one half of the specimen is subjected to strain of magnitude $2\epsilon_1$, the other half being unstrained. The average energy absorbed per unit volume of the whole specimen is in this case equal to one half the area under the stress-strain curve up to the strain $2\epsilon_1$, which is given by the average stress σ_1 multiplied by ϵ_1. This is greater than the absorption of energy required to produce the same reduction in length in uniform strain, since clearly $\sigma_1 > (\sigma_1 + Y)/2$. Thus a stress-strain relation based on energy absorption, combined with the assumption of uniform strain distribution, would produce an apparent rise in the stress-strain curve due to this nonuniform distribution of strain, even though the material stress-strain relation does not change. In general, it can be shown readily that, for a work-hardening material, any variation from uniform strain distribution causes an increase in energy absorption for a fixed reduction in length with a consequent apparent rise in the stress-strain curve.

This paper considers a method of analyzing a testing arrangement to determine conditions under which this influence is negligible, which will determine the region of testing in which a true average strain-rate effect can be determined, and beyond which a more refined analysis of the test results is necessary. Reference to published results shows that this limitation of each particular test arrangement has not always been adhered to, with the consequent deduction of a spurious material strain-rate effect.

Plastic-Wave Analysis of Impact Test

Let us consider the detailed analysis of the wave propagation in Habib's impact test (3), described in the previous section, to ascertain under what conditions a marked variation in strain results. The theory of plastic-wave propagation along a rod developed by von Kármán, Bohnenblust, and Hyers (4) can be applied directly. It is based on a fixed relationship between stress and strain in tension or compression for stresses increasing in absolute magnitude, which includes initial elastic deformation and subsequent plastic flow. If the absolute magnitude of the stress decreases, it is assumed that elastic strain increments only occur. Since we are interested in strains large in comparison with the elastic yield-point strain, we can effect a considerable simplification in the analysis by neglecting elastic strains, and so considering elastic material to be rigid.

High-speed tests are carried out to determine the change in the stress-strain relation due to variations of the average strain rate. Habib found little variation in the dynamic curves over the major part of the testing range, so that it will be permissible for us to use an average invariant stress-strain relation for our analysis. This will be generally possible in assessing a test arrangement, for the onset of marked strain variations can be expected to be given by the average stress-strain relation, and not to be influenced markedly by the secondary influence of strain rate.

A study of Habib's results shows that the dynamic relationship between nominal stress and nominal strain was linear to a high degree of approximation. This is indicated, according to the theory detailed in the Appendix, by his plot of plastic-wave velocity which shows only a small variation over a large range of strain. Therefore we shall assume a linear stress-strain relation, and adopt that shown in Fig. 2. In general, to determine the

range of satisfactory test speeds for a particular test arrangement, a linear approximation to the stress-strain curve will be satisfactory. Since this corresponds to constant plastic-wave velocity, the analysis of wave propagation is considerably simplified.

Since the report by von Kármán, Bohnenblust, and Hyers (4) is not readily accessible, and since for the linear stress-strain relation of Fig. 2 we require only a very special form of the theory, the basic relations needed are developed in the Appendix.

We consider compressive nominal stresses and strains to be positive, and displacements and velocities in the direction of x increasing also to be positive, where x is the initial-position coordinate of a particular cross section of the specimen. The co-ordinate x is used to distinguish this particular cross section throughout the motion; u is the displacement from the initial position, so that the position of a particular section at any time is given by the co-ordinate $x + u$. This use of Lagrange-type co-ordinates, in combination with nominal stress and nominal strain, simplifies the plastic-wave equation when large strains occur.

We consider the development of the impact by following the propagation of wave fronts in the x, t-plane, Fig. 3(a). The corresponding stress and strain magnitudes are determined by application of Equations [26], [27], [28], and [29] of the Appendix.

In Fig. 3(a) the specimen occupies the region OA of the x-co-ordinate. Impact occurs at the end O. A is in contact with the anvil, which determines the boundary condition $u = 0$ for $x = l$. Impact occurs at $t = 0$, causing an elastic wave of the magnitude of the yield stress Y to be propagated down the specimen, followed by a plastic wave of stress discontinuity, OB.

Our assumption of neglecting elastic strains implies an infinite velocity of propagation for elastic waves, so that the yield-point stress occurs throughout the specimen instantaneously. The linear stress-strain relation in the plastic range determines a constant wave velocity, and so a single plastic wave front of stress discontinuity. The deceleration of the piston due to the pressure between the impacting surfaces causes the plastic wave front to be propagated with continuously decreasing stress magnitude. The material behind the wave front, which has been previously subjected to higher stress, moves as a rigid body, so that its equation of motion can be considered with that of the piston until rebound occurs. Let σ and v be the stress and velocity behind the plastic wave front. Then the equation of motion for the piston of mass M, and the rigid part of the specimen of length ct, which moves with it, is

$$(M + \rho A c t)\frac{dv}{dt} = -\sigma A \quad \ldots\ldots\ldots\ldots [1]$$

using the nomenclature of the Appendix. Application of Equation [28] of the Appendix for the wave front gives

$$-Y = \rho c v - \sigma \quad \ldots\ldots\ldots\ldots [2]$$

Elimination of σ between Equations [1] and [2] gives

$$(M + \rho A c t)\frac{dv}{dt} = -A(Y + \rho c v) \quad \ldots\ldots\ldots [3]$$

which integrates directly to give

$$\left.\begin{aligned}(Y + \rho c v)(M + \rho A c t) &= \text{const}\\ &= (Y + \rho c v_0)M\end{aligned}\right\} \quad \ldots\ldots [4]$$

where v_0 is the piston velocity at impact.

Thus, writing $x = ct$, the stress behind the plastic wave front when it reaches the section x is given by Equations [2] and [4].

$$\sigma = \rho c v + Y = \frac{Y + \rho c v_0}{1 + \dfrac{\rho A x}{M}} \quad \ldots\ldots\ldots [5]$$

$\rho c v$, which can be used as a measure of the velocity of the piston, is given by Equation [2]. The stress and velocity can thus be simply represented by the rectangular hyperbola shown in Fig. 3(b). This solution applies unless the stress σ falls to the value Y, when v becomes zero by Equation [2], and plastic flow ceases. Neglecting elastic strains, the system remains at rest

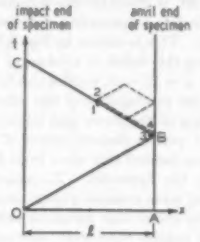

FIG. 3(a)

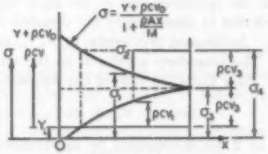

FIG. 3(b)

thereafter with the piston in contact with the specimen. In the complete analysis, the specimen is still subjected to elastic compression which will cause subsequent elastic vibration and rebound of the piston. However, the energy magnitudes involved will be negligible, compared with the energy absorbed in plastic flow, when plastic strains are large compared with elastic strain.

If the stress does not fall to Y for $x < l$, the solution applies until reflection of the plastic wave front occurs at B, and a reflected wave BC returns toward the impact end. In analyzing the behavior of the reflected wave BC, we must bear in mind that since the specimen has been subjected to varying values of maximum stress on the wave front OB, it will exhibit a varying yield stress for subsequent plastic flow. This is clarified in Fig. 4 which shows the stress-strain relation for repeated loading. Initial loading to the stress σ_2, corresponding to the point 2 in Fig. 4, gives zero strain up to the point 1, the yield point, followed by plastic flow along the work-hardening line 1-2. If the stress is then reduced to σ_3, the stress falls without change of strain, since the elastic recovery is neglected. On subsequent reloading to σ_3, there is no additional strain until the previous maximum stress σ_4 is reached; thereafter the continuation of the work-hardening line 4-5 applies. Thus, for reloading, the material behaves as if it has a yield stress equal to the maximum stress to which it has been previously subjected. After passage of the initial plastic wave through the specimen, the yield stress for subsequent plastic flow is given by the σ-curve in Fig. 3(b).

Reflection at the fixed anvil produces a wave of increased compressive stress, and the stress immediately ahead of this wave front, therefore, will be the new yield-stress value, since smaller

stress magnitudes are propagated with infinite velocity and can be analyzed on a rigid-body hypothesis. Since the part of the specimen ahead of the reflected wave decelerates with the piston as a rigid body, the stress falls off linearly with decreasing x, so that plastic flow is never initiated ahead of the wave front. The stress immediately ahead of the wave front BC is the same for each x as the stress immediately behind the wave front OB, and, in both cases, this stress produces deceleration of the piston and the rigid portion of the specimen between the piston and the wave front. This implies the same deceleration at corresponding positions of the wave front in both cases. Thus the velocity ahead of the wave front BC is given by the reflection of the ρcv-curve in Fig. 3(b), in the line representing the piston velocity at the time B in Fig. 3(a). This is shown in Fig. 3(b). (An alternative method of deducing this result is to observe that Equation [1], with ct replaced by $x = 2l - ct$, applies also to the deceleration of the piston during the propagation of the reflected wave BC.)

The known values of the stress and velocity ahead of the reflected wave front permit determination of the stress in the part of the specimen behind this wave front by use of the equations developed in the Appendix. We assume that the region behind the reflected wave remains plastic, and so the final result must be checked to insure that no stress reduction takes place there which would require rigid-body, and not plastic, analysis.

Consider the points 1, 2, 3, and 4 in Fig. 3(a), which are just ahead and just behind points on the reflected wave within the gage length of the specimen and at the anvil end. Stress and velocity magnitudes at these points are denoted by corresponding subscripts. As detailed previously, σ_1, σ_3, v_1, and v_3 are given in Fig. 3(b). The boundary condition at the anvil determines v_4 to be zero. Thus Equation [29] of the Appendix gives

$$\rho c v_3 + \sigma_3 = \sigma_4 \quad [6]$$

Conditions at 2 are determined by application of Equations [27] and [29] of the Appendix. These give in combination with Equation [6]

$$\rho c v_2 - \sigma_2 = -\sigma_4 = -(\rho c v_3 + \sigma_3) \quad [7a]$$

$$\rho c v_2 + \sigma_2 = \rho c v_1 + \sigma_1 \quad [7b]$$

But Fig. 3(b) shows that

$$\rho c v_1 + \sigma_1 = \rho c v_3 + \sigma_3$$

so that adding Equations [7a] and [7b] gives

$$\rho c v_2 = 0 \quad [8]$$

and

$$\sigma_2 = \sigma_4 \quad [9]$$

These relations apply for all positions 2 behind the wave front BC. The constant velocity and stress conditions for all points immediately behind the reflected wave BC, combined with Equations [26] and [27] of the Appendix and the boundary conditions at the anvil end, determine the region behind BC to have zero velocity, and to be subjected to constant stress until a further reflected wave is propagated from C. This is compatible both with the equations of plastic flow and the rigid-body unloading conditions, since it is a limiting case of both types of solution.

The stresses during reflection are shown in Fig. 3(b), and this solution applies unless and until the stress ordinate σ_4 intersects the σ-curve. At such an intersection the piston velocity is reduced to zero, and to our degree of approximation the system remains at rest thereafter.

If σ_4 is greater than the initial maximum stress at the impact end, the situation when the reflected wave reaches the impact end is a repetition of the initial impact with different values of impact velocity and yield stress of the specimen. The entire specimen has been subjected to the maximum stress σ_4, so that, for subsequent plastic flow, it has a yield stress of this magnitude; the specimen is at rest and the piston has the velocity v_3 shown in Fig. 3(b) when the point 1 is coincident with the end C. The subsequent motion thus can be analyzed by a repetition of the foregoing analysis.

Strain Distribution After an Impact Test

Fig. 4 shows that if plastic flow has occurred only in compression, the permanent strain produced at any section is a function

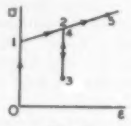

Fig. 4

of the maximum stress to which the section has been subjected. The relation is

$$\epsilon = \frac{1}{\rho c^2}(\sigma_{max} - Y) \quad [10]$$

since, according to the theory developed in the Appendix, the gradient of the work-hardening line is ρc^2. The maximum stress occurring during impact is shown in Fig. 3(b). In the particular case illustrated, plastic flow ceases during the second reflection, and the distribution of maximum stress is given by the σ-curve from the impact end until it intersects the ordinate σ_4. For larger x it has the constant value σ_4. Appropriate modification of Fig. 3(b) gives the maximum stress distribution for other impact conditions.

In order to study the influence of strain distribution on the high-speed test results discussed previously, it is convenient to consider impacts with pistons having a constant initial value of kinetic energy. With a stress-strain curve independent of the strain rate and uniform strain distribution, energy-absorption considerations determine constant strain magnitudes for these tests and, thus, constant over-all reduction in length. However, for impacts involving the same energy, but comprising high piston velocity and correspondingly small mass, nonuniform strain distribution will occur. According to the discussion in the section, A Method of High-Speed Compression Testing, the energy will be used less effectively to produce reduction in specimen length, which will fall short of the value based on uniform strain. A plot of the over-all compression against impact velocity for constant energy impacts therefore will indicate when distribution effects become important.

For the general analysis of this type of test it is convenient to use nondimensional variables. We use the following variables

$$\xi = \frac{\rho c v_0}{Y}, \text{ nondimensional velocity}$$

$$\eta = \frac{\rho l A}{M}, \text{ ratio of specimen mass to piston mass}$$

The condition for plastic flow to cease before reflection of the initial plastic wave at B is that ordinate σ_2 in Fig. 3(b), should be less than Y, which reduces to

$$\xi < \eta \quad [11]$$

The initial kinetic energy of the piston E, is given by

$$E = \frac{1}{2} M v_0^2 = \frac{YlA\epsilon_0}{2} \frac{\xi^2}{\eta} \quad [12]$$

where $\epsilon_0 = (Y_0)/(\rho c^2)$, so that $\Phi = \xi^2/\eta$ can be used to express the initial energy in nondimensional form. The shortening of the specimen is given by

$$\delta = \int_0^l \epsilon \, dx \quad [13]$$

which can be expressed in terms of the nondimensional compression $\Delta = \delta/(L\epsilon_0\Phi)$. This particular nondimensional combination is convenient since it gives a unique $\Delta - \xi$ relationship, independent of Φ, if plastic flow ceases during the first transition of the initial plastic wave.

The compression for uniform strain is given by the energy relation

$$\delta \left(Y + \frac{\delta \rho c^2}{2l} \right) A = E \quad [14]$$

which reduces to

$$\Delta = -\frac{1}{\Phi} + \sqrt{\frac{1}{\Phi^2} + \frac{1}{\Phi}} \quad [15]$$

If plastic flow ceases during the first traverse of the impact wave, the extent of the flow is given by $\hat{x}$, the value of x for which σ equals Y in Fig. 3(b). This determines

$$\frac{Y + \rho c v_0}{1 + \dfrac{\rho A \hat{x}}{M}} = Y$$

which reduces to

$$\hat{x} = l \frac{\xi}{\eta} \quad [16]$$

Thus the total compression is given by Equations [10] and [13]

$$\delta = \frac{Y}{\rho c^2} \int_0^{\hat{x}} \left(\frac{1 + \xi}{1 + \eta x/l} - 1 \right) dx$$

Algebraic reduction determines the nondimensional compression to be

$$\Delta = \frac{(1 + \xi) \log (1 + \xi) - \xi}{\xi^2} \quad [17]$$

which is seen to be independent of Φ. However, the range of velocity over which this formula is valid, $\xi < \eta$ (Equation [11]), or, in terms of Φ, $\xi > \Phi$, depends upon Φ.

If plastic flow ceases during the first reflection, the extent of the varying strain region is given by $\hat{x}$, for which $\sigma = \sigma_4$ in Fig. 3(b). To the right of this section the uniform strain corresponding to σ_4 exists. The integration of Equation [13] yields

$$\Delta = (1 + \xi) \left[\frac{2}{\Phi} \left(\frac{1}{1 + \dfrac{\xi^2}{\Phi}} - \frac{1}{1 + \xi} \right) - \frac{1}{\xi^2} \log \left(\frac{2}{1 + \dfrac{\xi^2}{\Phi}} - \frac{1}{1 + \xi} \right) + \frac{1}{\xi^2} \left(\frac{2}{1 + \dfrac{\xi^2}{\Phi}} - \frac{1}{1 + \xi} - 1 \right) \right] \quad [18]$$

The limit of this type of solution when the reflected wave just reaches the impact surface is $\hat{x} = 0$, which reduces to

$$\frac{\xi}{1 + \xi} = 2 \frac{\eta}{1 + \eta} \quad [19]$$

In this limiting case the specimen is strained uniformly corresponding to the maximum stress σ_4 in Fig. 3(b), and Equation [18] reduces to Equation [15].

As mentioned in the previous section, further reflections are treated by repetition of this type of analysis.

In Fig. 5 the regions in which the various types of solutions occur, and curves of constant impact energy, are shown as functions of the parameters ξ and η.

Equation [11] gives a straight line through the origin for the boundary between impacts which produce plastic flow due to the initial loading wave only, and those which involve reflection of the plastic wave at the anvil. The boundary between the

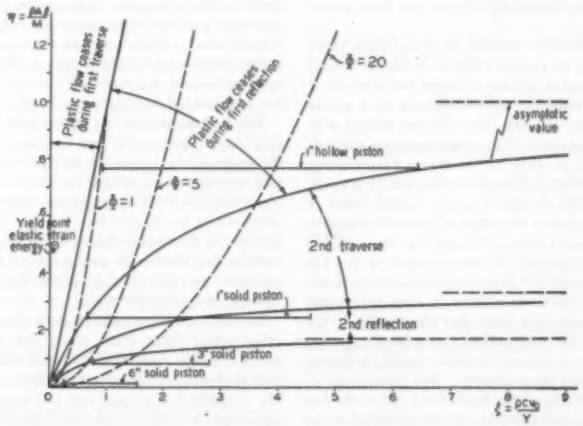

FIG. 5

single-reflection type of solution and the second traverse type, based on Equation [19], is shown. It is seen to be asymptotic to $\eta = 1$ for large ξ. The boundaries between subsequent types of solution also have horizontal asymptotes.

These boundary curves indicate that in general small ξ and large η (low impact velocity and small piston mass) produce few traverses and reflections of the plastic waves before plastic flow ceases. The horizontal asymptotes indicate that with sufficiently light pistons, only a limited number of traverses and reflections will occur, however high the impact velocity.

The broken curves in Fig. 5 show contours of constant impact energy Φ. These curves intersect the regions comprising different types of solution so that increase in impact velocity with constant energy corresponds to fewer traverses and reflections of the stress waves.

Fig. 6 shows the nondimensional over-all compression Δ plotted against ξ (the nondimensional impact velocity) for three energy values $\Phi = 1$, 5, and 20. The boundary points between the different types of solution are shown on these curves, and also the compression corresponding to uniform strain (Equation [15]). It has already been pointed out that if plastic flow ceases when the first reflected wave just reaches the impact surface, uniform strain results and the compression Δ is equal to the maximum permissible value. The curves in Fig. 6, which cover a wide range of energy, show that although a marked reduction in compression occurs at impact velocities above this value, the compression remains close to the limit for lower impact velocities. There is, of course, an infinity of values for small ξ when this limit is reached exactly, corresponding to all cases where reflected waves die out exactly at the impact surface. These results indicate that the strain-distribution effect is negligible as long as at least a single complete traverse and reflection occur, but that it may have an important influence on the final compression if plastic flow ceases during the first traverse or the first reflection of the plastic wave.

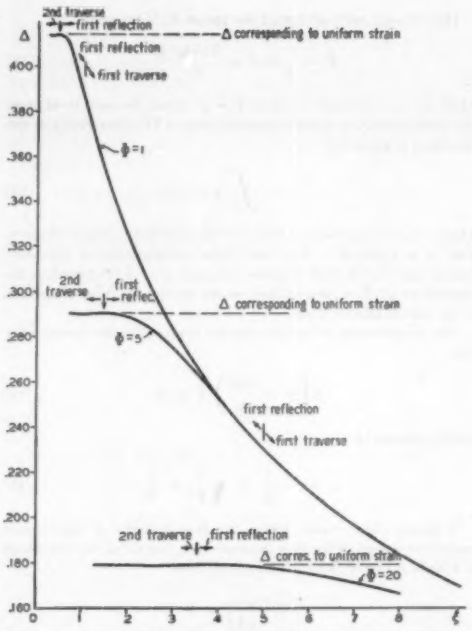

FIG. 6 TOTAL COMPRESSION Δ FOR IMPACTS WITH CONSTANT KINETIC ENERGY Φ

ANALYSIS OF TEST RESULTS

Let us consider the application of the results of the previous section to the analysis of Habib's test data (3).

An average dynamic stress-strain relation was obtained from the energy-deformation curve obtained with the 1-in. solid piston [Fig. 4 of (3)] which forms the basis of our analysis.

Let us first consider the approximations used in our idealized theory, to estimate where the theoretical analysis can be expected to give satisfactory results.

The actual stress-strain curve is rounded off at the yield point in place of the discontinuity in gradient shown in Fig. 2. Thus plastic flow is in fact initiated at a value of stress less than the Y previously given. Such a rounding off corresponds to a spread of plastic-wave propagation velocity, the velocity falling with increasing stress to the value used. This would produce a broadened dispersing wave front in place of the stress discontinuity of our theory which would tend to smooth out the resulting strain distribution somewhat. This influence occurs mainly below a strain of 2 per cent which is below the range of dynamic measurement and therefore will have a minor influence on the analysis.

A similar effect will be produced by the influence of the full equations of motion in place of the approximate one-dimensional theory adopted. The equation of motion in the x-direction only has been used, although it is clear that the inertia of the lateral motion associated with longitudinal strain does influence the motion, and would in fact prevent the discontinuity in section implied by a wave of stress discontinuity. For strains up to, say, 20 per cent, some smoothing of the wave front will occur due to this effect, but the strain distribution is not expected to be modified appreciably. Evidence for this statement is given by the comparison of a Taylor dynamic-compression-test specimen and the corresponding analysis based on waves of stress discontinuity (5). For the very large strains, lateral inertia will have an important influence, so that the regions of large ξ in Fig. 5 will be modified. It is, however, not in these regions where we make use of the analysis in this paper.

Finally, the influence of elastic deformation should be considered. This influence opposes the previous two considered, since we have assumed instantaneous spread of elastic effects, whereas the finite elastic-wave speed will produce some distribution effects. A single point on the energy contour corresponding to the elastic yield-point energy is shown in Fig. 5, and is seen to be well below our region of interest. Elastic effects, therefore, can be expected to play a minor role.

The test ranges used by Habib with the four pistons are shown by the four horizontal lines in Fig. 5. These indicate that, on the basis of the approximate theoretical analysis, the solid pistons correspond to reflections with at least a complete passage of a reflected wave through the specimen. The hollow piston corresponds to plastic flow ceasing during the first reflection. In view of the results shown in Fig. 6, this indicates that strain-distribution effects are negligible for the solid pistons, but will introduce an error of up to about 10 per cent of the strain in the case of the hollow piston.

In fact, the experimental data showed a small rate of strain effect which fitted static tests, and the results with the solid pistons, and a markedly increased rate of strain effect with the hollow piston. This anomalous behavior averaged out at about the equivalent of a 4 per cent increase in strain, which is in good agreement with the strain-distribution effect based on the plastic-wave analysis.

That the anomalous behavior was due to strain-propagation phenomena was suggested by Habib; however, he ascribed it to the proximity to a critical velocity at which the piston would move faster than the speed of propagation of plastic waves. It is clear from the present analysis, however, that the "critical" velocity in question is that at which wave effects become important and where one-dimensional plastic-wave theory is quite adequate to analyze the situation. The critical velocity associated with the influence of lateral inertia will occur at higher speeds of impact and thus will not have an important influence in the present range of tests.

The agreement between the theoretical analysis and the experimental results on the range of application of this apparatus, would not be modified appreciably by basing the theory upon the static stress-strain curve. Thus the satisfactory range of application of the apparatus for determining a true material average strain-rate effect could be predicted easily.

Application to Other Test Arrangements

The influence of wave-propagation effects in limiting the speed range for which simple analysis of test results is satisfactory, is a problem which arises generally in high-speed testing. The results obtained in the particular case considered in this paper give general indications for the consideration of other test arrangements, but, for more accurate analysis, a similar evaluation must be carried out in each case.

In general, if several traverses of the plastic wave up and down the specimen occur during straining, sensibly uniform conditions will occur, and the inertia of the specimens can be neglected in analyzing the results for the influence of average strain rate. This can be checked readily by evaluating an average value for the plastic wave velocity from the gradient of the stress-strain curve. However, Fig. 6 shows that the amount of smoothing of conditions along the specimen produced by a given number of traverses depends upon other factors, so that a more complete plastic-wave analysis is required to provide a close estimate of the satisfactory testing range.

Other examples in the literature of difficulties in the interpretation of test results due to propagation effects have occurred in the work of Warnock and Pope (6), and Warnock and Brennan (7). These papers are concerned with impact tests in which the specimen is loaded in tension. The specimen falls under gravity with its lower end attached to a massive tup, when the upper end is suddenly arrested by striking an anvil. Repeated tests of this type were carried out on the same specimen. It was found that in this type of loading the strain is concentrated at the anvil end, and spreads gradually down the gage length in repeated impacts. Before this was realized it was difficult to interpret static tests that were made on the specimens which had sustained a series of impact loads. Continued lower yield-point elongation was observed when the average extension was greater than the static yield-point elongation. This was finally found to be due to the unstrained material at the tup end of the specimen. The results of an approximate plastic-wave analysis of this test have been given (8).

From these examples, and the one discussed in detail in the paper, it is clear that wave-propagation phenomena should be anticipated in planning a high-speed testing program. The example given in detail shows how the influence of this phenomenon can be readily evaluated in a particular case.

BIBLIOGRAPHY

1 "Time Effect in Testing Metals," by H. Quinney, *The Engineer*, vol. 157, 1934, pp. 332–334.

2 "The Use of Flat-Ended Projectiles for Determining Dynamic Yield Stress. I. Theoretical Considerations," by G. I. Taylor, Proceedings of the Royal Society, series A, vol. 194, 1948, pp. 289–299.

3 "A Method of Making High-Speed Compression Tests on Small Copper Cylinders," by E. T. Habib, Journal of Applied Mechanics, Trans. ASME, vol. 70, 1948, pp. 248–255.

4 "The Propagation of Plastic Waves in Tension Specimens of Finite Length," by Th. von Kármán, H. F. Bohnenblust, and D. H. Hyers, NDRC Report A-103 (OSRD 946), 1942.

5 "The Analysis of the Plastic Deformation in a Cylinder of Shot Steel Striking a Rigid Target," by E. H. Lee and S. J. Tupper, British Official Report, ARD, TRS 4/44, 1944.

6 "The Change in Mechanical Properties of Mild Steel Under Repeated Impact," by F. V. Warnock and J. A. Pope, Proceedings of The Institution of Mechanical Engineers, London, England, vol. 157, 1947, pp. 33–43.

7 "The Tensile Yield Strength of Certain Steels Under Suddenly Applied Loads," by F. V. Warnock and J. B. Brennan, Proceedings of The Institution of Mechanical Engineers, London, England, vol. 159, 1948, pp. 1–14.

8 Discussion of (7), by E. H. Lee, p. 21.

Appendix

Theory of Plastic-Wave Propagation

The propagation of waves of compressive stress is considered for a material having the linear stress-strain relation shown in Fig. 2. Strains of the order of elastic strains are neglected. The analysis corresponds to the usual theory of elastic waves in rods in that it is one-dimensional, being based on the equation of motion in the direction of the rod axis only. This theory is a special case of that developed by von Kármán, Bohnenblust, and Hyers (4) for an arbitrary stress-strain relation.

The following nomenclature is used:

- x = Lagrange-type co-ordinate along initially unstrained rod
- u = displacement of a section, positive in direction of x increasing
- σ = nominal compressive stress, force per unit initial cross-sectional area
- $\epsilon = -\dfrac{\partial u}{\partial x}$, nominal compressive strain
- A = initial cross-sectional area of rod
- t = time
- ρ = density of material when unstrained

The equation of motion for an element initially of length dx is

$$A\rho dx \frac{\partial^2 u}{\partial t^2} = -A \frac{\partial \sigma}{\partial x} dx \quad \ldots\ldots\ldots\ldots [20]$$

This is valid for large strains. The relationship between σ and ϵ permits the substitution

$$\frac{\partial \sigma}{\partial x} = \frac{d\sigma}{d\epsilon}\frac{\partial \epsilon}{\partial x} = -\frac{d\sigma}{d\epsilon}\frac{\partial^2 u}{\partial x^2}$$

and Equation [20] becomes the wave equation

$$c^2 \frac{\partial^2 u}{\partial x^2} = \frac{\partial^2 u}{\partial t^2} \quad \ldots\ldots\ldots\ldots [21]$$

where

$$c^2 = \frac{1}{\rho}\frac{d\sigma}{d\epsilon} \quad \ldots\ldots\ldots\ldots [22]$$

c is the velocity of wave propagation, and is constant for plastic flow obeying the linear law of Fig. 2. In this case, we have the general solution

$$u = f(x + ct) + F(x - ct) \quad \ldots\ldots\ldots\ldots [23]$$

where f and F are arbitrary functions.

The particle velocity $v = \partial u/\partial t$, the strain $\epsilon = -\partial u/\partial x$, and

the stress $\sigma = Y + \rho c^2\epsilon$ can be expressed in terms of f and F, giving

$$\rho cv + \sigma = Y - 2\rho c^2 F'(x - ct) \quad [24]$$

$$\rho cv - \sigma = -Y + 2\rho c^2 f'(x + ct) \quad [25]$$

where F' and f' denote the first derivatives of F and f, respectively. Thus we have relationships on the characteristic lines, $(dx)/(dt) = \pm c$, in the x, t-plane

$$\rho cv + \sigma = \text{const}, \quad \frac{dx}{dt} = +c \quad [26]$$

$$\rho cv - \sigma = \text{const}, \quad \frac{dx}{dt} = -c \quad [27]$$

The foregoing analysis assumes continuous variation of stress and strain. If waves of stress discontinuity occur, the following similar relations are determined by the equations of continuity and momentum change

$$(\rho cv - \sigma)_1 = (\rho cv - \sigma)_2 \quad [28]$$

if points 1 and 2 are just behind, and just ahead of a stress wave traveling in the positive direction. This relationship is closely analogous to Equation [27].

For a wave traveling to the left

$$(\rho cv + \sigma)_1 = (\rho cv + \sigma)_2 \quad [29]$$

Application of Equations [26], [27], [28], and [29] enable stress and velocity distributions to be determined.

A New Method of Calculation of Reheat Factors for Turbines and Compressors

By JOSEPH KAYE[1] and K. R. WADLEIGH,[2] CAMBRIDGE, MASS.

A simple method is presented for rapid accurate calculation of reheat factors for adiabatic turbines and compressors with an infinite number of stages. The method is limited to fluids for which the following equation of state is adequate

$$pv = RT$$

and for which the specific heat is a function of temperature only. The method is based on the concept of the step efficiency—the efficiency of an infinitesimal stage based on the reversible adiabatic work—and on the concept of the relative pressure function. The method is used to produce charts of reheat factors for turbines and compressors for several gases. A theoretical justification is given for empirical rules of thumb which have been widely used to predict reheat factors for turbines and compressors with a finite number of stages.

Nomenclature

The following nomenclature is used in the paper:

- c_p = specific heat at constant pressure
- c_v = specific heat at constant volume
- h = enthalpy
- k = ratio of specific heats = $\frac{c_p}{c_v}$
- n = number of stages
- p = pressure
- p_r = relative pressure
- R = gas constant
- $\mathfrak{R}$ = reheat factor
- s = entropy
- T = temperature
- v = specific volume
- η = efficiency
- ρ = reheat gain (turbine) or loss (compressor)

Subscripts:

- c = compressor
- i = state i
- j = stage j
- n = state n or n stages
- s = at constant entropy or for a step (an infinitesimal stage)
- st = stage
- t = turbine
- ∞ = infinite stages or steps

Introduction

Multistage turbines and compressors handling many different working fluids over large ranges of pressure and temperature are being used today in increasing numbers. An important element in the design of these machines is the "reheat factor." Essentially, two methods for the calculation of reheat factors have been published. The more exact method of the two involves laborious step-by-step calculations such as those made by Thatcher[3] on steam. The work of Smith[4] is typical of the second method which is simpler but less exact in that it assumes that the working fluid is a perfect gas with a constant specific heat.

A simple and precise method for calculating turbine and compressor reheat factors is presented which may be used for any working fluid which obeys the equation of state

$$pv = RT$$

The restriction of constant specific heat is not required. The method depends on a simple means of determining the condition curve for an infinite number of stages, thus eliminating the need for a laborious trial-and-error solution. Upon introduction of simplifying assumptions, the method leads to a clearer understanding of approximate rules of thumb (which have been in use for many years) for prediction of reheat factors for a finite number of stages from those for an infinite number of stages.

Adiabatic Turbine Reheat Factors

The Condition Curve. The condition curve is defined as that curve which represents the locus of fluid states at the entrance and exit of each stage of a multistage turbine or compressor; it is usually presented on the enthalpy-entropy diagram. It is evident that the condition curve represents mathematically the path of states actually assumed by the fluid only if there are an infinite number of stages in the machines. If there are a finite number of stages, only certain points on the curve (at the stage entrance and exit conditions) correspond to the states actually assumed by the fluid, Figs. 1, 2, and 3.

Consider the process executed by a fluid in passing through a turbine stage as represented by Fig. 3. The heavy line is the actual path of states executed by the fluid and is identically the condition curve if an infinite number of steps is assumed. The step efficiency—the efficiency of the infinitesimal stage based on reversible adiabatic work—is defined as

$$\eta_{t\infty} \equiv \frac{dh}{dh_s} \quad \ldots\ldots [1]$$

If the working fluid is assumed to obey the equation of state

$$pv = RT \quad \ldots\ldots [2]$$

---

[1] Associate Professor, Mechanical Engineering, Massachusetts Institute of Technology. Jun ASME.

[2] Assistant Professor, Mechanical Engineering, Massachusetts Institute of Technology.

Contributed by the Applied Mechanics Division and presented at the Annual Meeting, Atlantic City, N. J., November 25–30, 1951, of The American Society of Mechanical Engineers.

Discussion of this paper should be addressed to the Secretary, ASME, 29 West 39th Street, New York, N. Y., and will be accepted until January 10, 1952, for publication at a later date. Discussion received after the closing date will be returned.

Note: Statements and opinions advanced in papers are to be understood as individual expressions of their authors and not those of the Society. Manuscript received by ASME Applied Mechanics Division, July 10, 1950. Paper No. 51—A-2.

[3] "Reheat Factors for Expansions of Superheated and Wet Steam," by C. G. Thatcher, Journal of Applied Mechanics, Trans. ASME, vol. 60, 1938, p. A-161.

[4] "The Calculation of Steam-Turbine Reheat Factors," by R. B. Smith, Journal of Applied Mechanics, Trans. ASME, vol. 60, 1938, p. A-156.

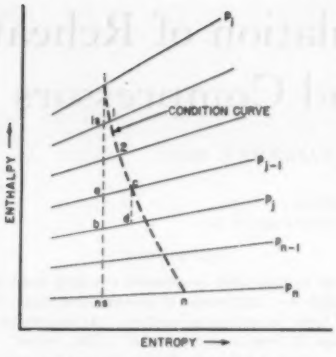

FIG. 1 CONDITION CURVE FOR TURBINE

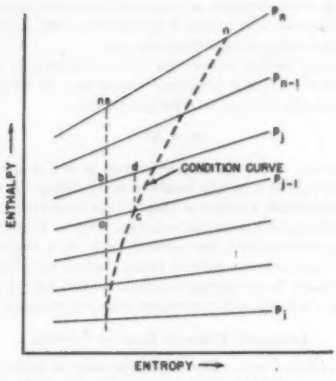

FIG. 2 CONDITION CURVE FOR COMPRESSOR

it can be shown[5] that the enthalpy and internal energy are functions only of temperature. If the specific heat at constant pressure is given by

$$c_p = f(T) \quad \ldots\ldots [3]$$

then

$$\left.\begin{aligned} dh &= c_p dT \\ dh_s &= c_p dT_s \end{aligned}\right\} \quad \ldots\ldots [4]$$

For a homogeneous system in the absence of electrical, magnetic, gravitational, capillarity, and chemical change, we may write

$$dh = Tds + vdp \quad \ldots\ldots [5]$$

and, for the reversible adiabatic process

$$dh_s = v_s dp \quad \ldots\ldots [6]$$

Combining Equations [1] through [6] yields

[5] "Thermodynamics," by J. H. Keenan, John Wiley & Sons, Inc., New York, N. Y., 1941.

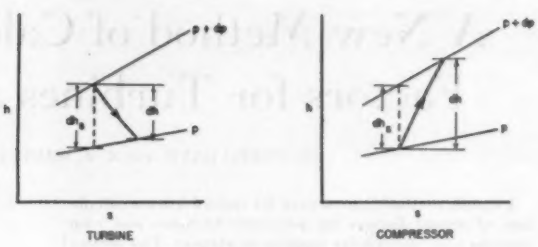

FIG. 3 INFINITESIMAL STAGE

$$c_p dT = \eta_{s\infty} RT_s \left(\frac{dp}{p}\right) \quad \ldots\ldots [7]$$

Noting that T and T_s differ only by an infinitesimal amount, Equation [7] may be written

$$\frac{c_p}{R}\frac{dT}{T} = \eta_{s\infty}\frac{dp}{p} \quad \ldots\ldots [8]$$

For a gas which obeys Equations [2] and [3], a simple relation between pressure and temperature along any isentropic, called the relative pressure p_r, has been developed and tabulated for many different gases;[6] thus

$$\frac{p_{rn}}{p_{ri}} = \left(\frac{p_n}{p_i}\right)_s \quad \ldots\ldots [9]$$

where

$$\ln p_r \equiv \frac{1}{R}\int_{T_0}^{T}\frac{c_p dT}{T} \quad \ldots\ldots [10]$$

Combining Equations [8] and [10] and integrating across a finite pressure change yields

$$\ln\left(\frac{p_{rn}}{p_{ri}}\right) = \int_{p_i}^{p_n}\eta_{s\infty}\frac{dp}{p} \quad \ldots\ldots [11]$$

or, for cases where $\eta_{s\infty}$ is constant,

$$\frac{p_{rn}}{p_{ri}} = \left(\frac{p_n}{p_i}\right)^{\eta_{s\infty,i-n}} \quad \ldots\ldots [12]$$

Through the use of the tabulated values of enthalpy and relative pressure as functions of temperature,[6] Equations [11] and [12] establish uniquely the condition curve for a finite expansion utilizing an infinite number of steps.

For an adiabatic multistage turbine with a finite number of stages n, Fig. 1, each stage may be imagined composed of an infinite number of steps. Associated with each stage is a unique value of step efficiency, $\eta_{s\infty}$, and a particular value of pressure ratio and enthalpy change. From Equation [12]

$$\left.\begin{aligned} \left(\frac{p_i}{p_1}\right)^{\eta_{s\infty,i-1}} &= \frac{p_{ri}}{p_{r1}} \\ \left(\frac{p_1}{p_2}\right)^{\eta_{s\infty,1-2}} &= \frac{p_{r1}}{p_{r2}}, \text{ etc.} \end{aligned}\right\} \quad \ldots\ldots [13]$$

Multiplying all n Equations [13] together, and defining $\eta_{s\infty,i-n}$ as the step efficiency for the entire turbine

[6] "Gas Tables," by J. H. Keenan and J. Kaye, John Wiley & Sons, Inc., New York, N. Y., 1948.

$$\left.\begin{aligned}\left(\frac{p_i}{p_1}\right)^{\eta_{sm},\,i-1} \times \left(\frac{p_1}{p_2}\right)^{\eta_{sm},\,1-1} \times \ldots \times \left(\frac{p_{n-1}}{p_n}\right)^{\eta_{sm},\,(n-1)-n} \\ = \frac{p_{ri}}{p_{rn}} = \left(\frac{p_i}{p_n}\right)^{\eta_{sm},\,i-n}\end{aligned}\right\} \quad [14]$$

For the particular case where the step efficiency is the same for all stages, $\eta_{sm,\,(j-1)-j}$ the step efficiency for the stages is identical to the step efficiency across the turbine

$$\eta_{sm,\,(j-1)-j} = \eta_{sm,\,i-n} \quad [15]$$

This result is independent of the mode of distribution of pressure ratios or of enthalpy drops throughout the turbine.

Reheat Factors for an Adiabatic Turbine With an Infinite Number of Stages

A typical condition curve for an adiabatic turbine with an infinite number of stages is represented by line $i - n$ in Fig. 1. Line $i - ns$ is the condition curve for reversible adiabatic expansion. Because, for all known vapors, the lines of constant pressure diverge with increasing entropy on the enthalpy-entropy diagram,[2] the isentropic drop in enthalpy across any pressure difference following an irreversible expansion ($h_i - h_d$) is larger than the isentropic drop in enthalpy between the same pressure limits following a reversible expansion ($h_s - h_b$). Consequently, because irreversibility exists in any real turbine, the ratio of the summation of isentropic drop in enthalpy over each individual stage to the isentropic drop in enthalpy across the entire turbine is greater than unity.

This ratio is called the reheat factor, which for the turbine with an infinite number of stages is

$$\mathfrak{R}_{i\infty,\,i-n} \equiv \frac{\int_{h_n}^{h_i} dh_s}{h_i - h_{ns}} \quad [16]$$

where the integral must be evaluated along the condition curve. The amount by which the reheat factor exceeds unity is called the reheat gain

$$\rho_{i\infty,\,i-n} \equiv \mathfrak{R}_{i\infty,\,i-n} - 1 \quad [17]$$

If the step efficiency may be assumed constant throughout the turbine, Equations [1] and [16] may be combined to give

$$\mathfrak{R}_{i\infty,\,i-n} = \frac{h_i - h_n}{(\eta_{sm,\,i-n})(h_i - h_{ns})} \quad [18]$$

The calculation of the reheat factor for an adiabatic turbine with an infinite number of stages and constant step efficiency is easily accomplished with the use of Equations [12] and [18] together with the tables of the properties, T, h, and p, for a gas conforming to Equations [2] and [3]. An illustrative example is given in the Appendix.

The stage efficiency based on reversible adiabatic work for the adiabatic single-stage turbine operating between states i and n in Fig. 1 is defined by

$$\eta_{st} \equiv \frac{h_i - h_n}{h_i - h_{ns}} \quad [19]$$

Combination of Equations [18] and [19] yields the following relationship between the stage efficiency and the step efficiency of the equivalent infinite-stage turbine operating between the same end states

$$\mathfrak{R}_{i\infty,\,i-n} = \frac{\eta_{st}}{\eta_{sm,\,i-n}} \quad [20]$$

Reheat Factors for an Adiabatic Turbine With a Finite Number of Stages

The reheat factor for a turbine with a finite number of stages operating with an inlet state i and an exit state n, as shown in Fig. 1, is defined by

$$\mathfrak{R}_{sm,\,i-n} \equiv \frac{\sum_{j=1}^{n} \Delta h_{sm,\,j}}{h_i - h_{ns}} \quad [21]$$

The corresponding reheat gain is defined by

$$\rho_{sm,\,i-n} \equiv \mathfrak{R}_{sm,\,i-n} - 1 \quad [22]$$

The calculation of reheat factors by means of Equation [21] is a step-by-step process for the general case where the step efficiency, pressure ratio, and enthalpy drop vary from one stage to the next. Two simplified cases are usually discussed in the literature. The first case corresponds to the design practice of assuming the same isentropic enthalpy drop and step efficiency in each of the n-stages; the second case assumes the same pressure ratio and step efficiency for each stage.

In the appendix it is shown that for the first case cited

$$\mathfrak{R}_{sm,\,i-n} = \frac{n\,\mathfrak{R}_{i\infty,\,i-n}}{\sum_{j=1}^{n} \mathfrak{R}_{i\infty,\,(j-1)-j}} \quad [23]$$

It is further shown that if the specific heat is assumed constant

$$c_p = \text{const}, \quad k \equiv \frac{c_p}{c_v} = \text{const}$$

the reheat gain for either of the cases cited may be calculated from

$$\frac{\rho_{sm,\,i-n}}{\rho_{i\infty,\,i-n}} \approx 1 - \frac{1}{n} - \frac{1}{n}\,\rho_{i\infty,\,i-n} + \frac{1}{n^2}\,\rho_{i\infty,\,i-n} \ldots \quad [24]$$

if terms of the order of $(\rho_{i\infty,\,i-n}/n)^2$ are neglected. Furthermore, if terms of the order of $\rho_{i\infty,\,i-n}/n$ are neglected, Equation [24] reduces to the well-known rule of thumb

$$\frac{\rho_{sm,\,i-n}}{\rho_{i\infty,\,i-n}} \approx 1 - \frac{1}{n} \quad [25]$$

Reheat Factors for an Adiabatic Compressor

In a turbine with more than one stage, the presence of irreversible processes results in an efficiency of the entire turbine which is greater than the average efficiency of the separate stages. The opposite is true in a compressor with more than one stage; the presence of irreversible processes reduces the over-all efficiency of the multistage compressor to less than the average efficiency of the separate stages.

Since the assumptions, analysis, and result for the compressor processes are analogous to those for the turbine, it will suffice to give merely the new quantities applicable to the compressor and the final results.

The following definitions apply to the compressor:

The step efficiency (Fig. 3), is

$$\eta_{sm\infty} \equiv \frac{dh_s}{dh}$$

The reheat factor for an infinite number of stages, Fig. 2, and with constant step efficiency is

$$\mathcal{R}_{\infty,i-n} \equiv \frac{\int_i^n dh_s}{h_{ns} - h_i} = \frac{\int_i^n \eta_{s\infty}\, dh}{h_{ns} - h_i}$$

$$\mathcal{R}_{\infty,i-n} = \frac{\eta_{s\infty}(h_n - h_i)}{h_{ns} - h_i}$$

The reheat factor for a finite number of stages is

$$\mathcal{R}_{n,i-n} \equiv \frac{\sum_{j=1}^{n} \Delta h_{s\,at\,j}}{h_{ns} - h_i}$$

The reheat loss for a finite number of stages is

$$\rho_{cn} \equiv \mathcal{R}_{cn} - 1$$

The following results apply to the compressor:

For states i and n along the condition curve, with constant step efficiency, we have

$$\frac{p_{ro}}{p_{ri}} = \left(\frac{p_n}{p_i}\right)^{\frac{1}{\eta_{s\infty}}}$$

For n-stages with the same isentropic rise of enthalpy and step efficiency in each stage, we get

$$\mathcal{R}_{cn,i-n} = \frac{n\mathcal{R}_{c\infty,i-n}}{\sum_{j=1}^{n} \mathcal{R}_{c\infty,(j-1)-j}},$$

and

$$\frac{\rho_{cn,i-n}}{\rho_{c\infty,i-n}} = \frac{1 - \frac{\sum_{j=1}^{n} \rho_{c\infty,(j-1)-j}}{n\rho_{c\infty,i-n}}}{1 + \frac{1}{n}\sum_{j=1}^{n} \rho_{c\infty,(j-1)-j}}$$

For constant specific heat, constant step efficiency, and either the same isentropic rise in enthalpy in each stage or the same pressure ratio across each stage, we get

$$\frac{\rho_{cn,i-n}}{\rho_{c\infty,i-n}} \approx 1 - \frac{1}{n} - \frac{1}{n}\rho_{c\infty,i-n} + \frac{1}{n^2}\rho_{c\infty,i-n}$$

neglecting terms of the order of $(\rho_{c\infty,i-n}/n)^2$, or

$$\frac{\rho_{cn,i-n}}{\rho_{c\infty,i-n}} \approx 1 - \frac{1}{n}$$

neglecting terms of the order of $\rho_{c\infty,i-n}/n$.

Calculated Results

The simple method of calculation of states along the condition curve for turbines and compressors has been used to calculate the reheat factors for these devices for several gases. The properties of these gases are tabulated in the "Gas Tables."[8]

The reheat factors for turbines with an infinite number of stages are plotted in Figs. 4, 5, and 6. In Fig. 4 the reheat factor is given for air entering the turbine at two different temperatures, and for the case where the specific heat of air is constant. The curves in Fig. 4 are very nearly straight lines from the origin up to a pressure ratio of about 50. There are three curves given for each value of the step efficiency.

In Fig. 5 the reheat factor is given for turbines with an infinite number of stages using products of combustion of hydrocarbons with 200 per cent of theoretical air.[7] This chart will be useful in problems involving design of many types of multistage turbines used in gas-turbine plants.

In Fig. 6 the reheat factors are given for a turbine with an infinite number of stages using several gases as turbine fluids. The curve labeled PG, $k = 1.667$, for a monatomic perfect gas such as argon, neon, mercury, and so forth, is independent of the turbine inlet temperature. There are two curves for air, one for the case where $k = 1.4$, and one where k is a function of temperature. Also shown on this chart are curves for products of com-

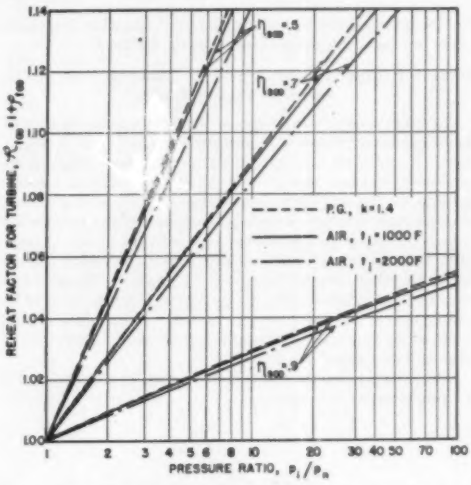
REHEAT FACTOR FOR TURBINE, $\mathcal{R}_{t\infty} = 1 + \rho_{t\infty}$
PRESSURE RATIO, p_i/p_n
$\eta_{s\infty}$ = .5
$\eta_{s\infty}$ = .7
$\eta_{s\infty}$ = .9
P.G., k = 1.4
AIR, t_i = 1000 F
AIR, t_i = 2000 F

Fig. 4 Effect of Turbine Inlet Temperature on Reheat Factors for Turbine Using Air

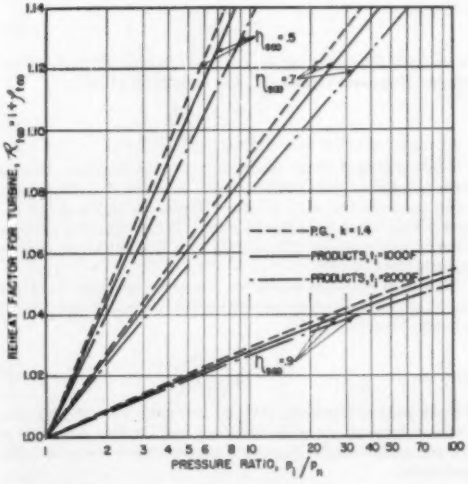
REHEAT FACTOR FOR TURBINE, $\mathcal{R}_{t\infty} = 1 + \rho_{t\infty}$
PRESSURE RATIO, p_i/p_n
$\eta_{s\infty}$ = .5
$\eta_{s\infty}$ = .7
$\eta_{s\infty}$ = .9
P.G., k = 1.4
PRODUCTS, t_i = 1000 F
PRODUCTS, t_i = 2000 F

Fig. 5 Effect of Turbine Inlet Temperature on Reheat Factors for Turbine Using Products of Combustion for 200 Per Cent Theoretical Air

[7] Reference 6, table 7.

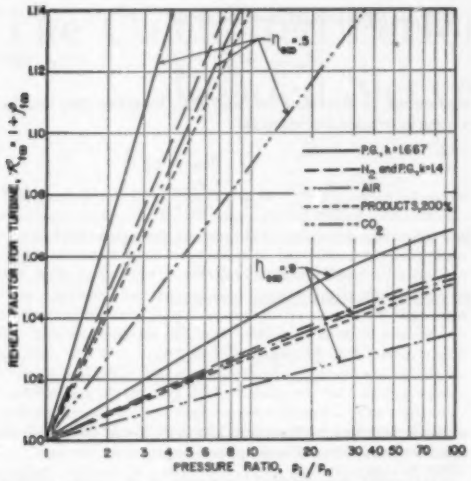

FIG. 6 TURBINE REHEAT FACTORS FOR DIFFERENT WORKING FLUIDS AND FOR A TURBINE-INLET TEMPERATURE OF 1500 F

bustion with 200 per cent theoretical air, for pure carbon dioxide, and for pure hydrogen.

Reheat factors for a compressor with an infinite number of stages and using air are given in Fig. 7. Again the curve labeled with a constant value of k is obtained on the basis of assuming a constant specific heat for air whereas the other two curves are for air with variable specific heat.

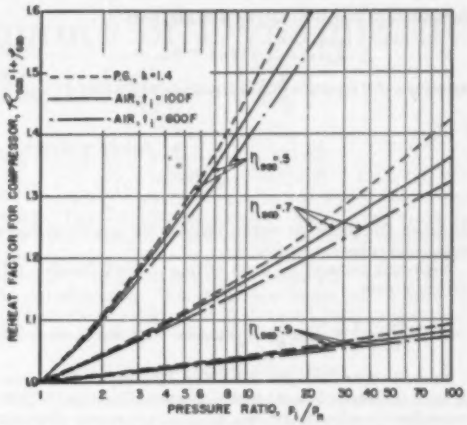

FIG. 7 EFFECT OF COMPRESSOR-INLET TEMPERATURE ON REHEAT FACTORS FOR COMPRESSOR USING AIR

Appendix

CALCULATION OF REHEAT FACTORS FOR AN ADIABATIC TURBINE USING AIR

The turbine with an infinite number of stages has an inlet temperature of 2000 F, and a pressure ratio of 8. What is the reheat factor for a step efficiency of 70 per cent?

Solution. Using data given in Table 1 of the "Gas Tables,"[3] we get

$$T_i = 2460 \text{ F abs}$$
$$h_i = 634.34 \text{ Btu/lb}$$
$$p_{ri} = 407.3$$
$$p_{rn} = p_{ri}\,(1/8) = 50.913$$
$$h_n = 359.77 \text{ Btu/lb}$$
$$h_i - h_n = 274.57 \text{ Btu/lb}$$
$$\left(\frac{p_1}{p_2}\right)^{\eta_{stm}} = (8)^{0.7} = 4.288$$
$$p_{rn} = p_{ri}\left(\frac{p_1}{p_1}\right)^{0.7} = \frac{}{} 407.3/4.288 = 94.99$$
$$h_n = 427.70 \text{ Btu/lb}$$
$$h_i - h_n = 206.64 \text{ Btu/lb}$$
$$\mathcal{R}_{tm} = \frac{h_i - h_n}{\eta_{stm}(h_i - h_{ni})} = \frac{206.64}{0.7(274.57)} = 1.0751$$
$$\rho_{tm} = 0.0751$$

CALCULATION OF REHEAT FACTORS FOR AN ADIABATIC TURBINE WITH A FINITE NUMBER OF STAGES FOR TWO SPECIAL CASES

Same Isentropic Drop in Enthalpy and Same Step Efficiency in Each Stage. The following identity may be written for the condition curve of Fig. 1

$$(h_i - h_n) = (h_i - h_1) + (h_1 - h_2) + \ldots + (h_{n-1} - h_n) \quad [26]$$

Expressions for the turbine and stage enthalpy drops obtained from Equation [18] when substituted in Equation [26] yield

$$\mathcal{R}_{tm,\,i-n}\,\eta_{stm,\,i-n}(h_i - h_{ni}) = \sum_{j=1}^{n}\left[\mathcal{R}_{tm,\,(j-1)-j}\,\eta_{stm,\,(j-1)-j}\,\Delta h_{st\,j}\right] \quad [27]$$

Since $\Delta h_{st\,j}$ and η_{stm} are assumed constant, Equation [27] may be combined with Equation [21] to give

$$\mathcal{R}_{tm,\,i-n} = \frac{n\mathcal{R}_{tm,\,i-n}}{\sum_{j=1}^{n}\mathcal{R}_{tm,\,(j-1)-j}} \quad [28]$$

Making use of Equations [17] and [22], Equation [28] may be rewritten in terms of reheat gains

$$\frac{\rho_{tm,\,i-n}}{\rho_{tm,\,i-n}} = \frac{1 - \dfrac{\sum_{j=1}^{n}\rho_{tm,\,(j-1)-j}}{n\rho_{tm,\,i-n}}}{1 + \dfrac{1}{n}\sum_{j=1}^{n}\rho_{tm,\,(j-1)-j}} \quad [29]$$

An approximation to Equation [29] which is useful in design procedures results if the specific heats are assumed constant, i.e., c_p = const, $k \equiv c_p/c_v$ = const. It is well known that the reheat factor can then be expressed as

$$\mathcal{R}_{tm,\,(j-1)-j} = \frac{1}{\eta_{stm}}\left[\frac{1 - \left(\dfrac{p_j}{p_{j-1}}\right)^{\frac{k-1}{\eta_{stm}k}}}{1 - \left(\dfrac{p_j}{p_{j-1}}\right)^{\frac{k-1}{k}}}\right] \quad [30]$$

For small values of the pressure ratio, Equation [30] has been approximated[4] by

$$\rho_{tm,\,(j-1)-j} \approx \frac{k-1}{2k}(1 - \eta_{stm})\ln\frac{p_{j-1}}{p_j} \quad [31]$$

Summation of Equations [31] for n-stages yields

$$\sum_{j=1}^{n} \rho_{t\infty,\,(j-1)-j} \approx \rho_{t\infty,\,i-a} \quad \ldots\ldots [32]$$

Substitution of Equation [32] in Equation [29] yields

$$\frac{\rho_{ta,\,i-a}}{\rho_{t\infty,\,i-a}} \approx \frac{1-\frac{1}{n}}{1+\frac{\rho_{t\infty,\,i-a}}{n}} \quad \ldots\ldots [33]$$

Equation [33] yields the correct limits as the number of stages approaches either 1 or infinity.

Neglecting terms of the order of $(\rho_{t\infty,\,i-a}/n)^2$, Equation [33] may be written

$$\frac{\rho_{ta,\,i-a}}{\rho_{t\infty,\,i-a}} \approx 1-\frac{1}{n}-\frac{1}{n}\rho_{t\infty,\,i-a}+\frac{1}{n^2}\rho_{t\infty,\,i-a} \quad \ldots [34]$$

Same Pressure Ratio and Same Step Efficiency in Each Stage. If again the specific heat is assumed constant, Equation [30] indicates that the reheat factor, $\mathfrak{R}_{t\infty,\,(j-1)-j}$, is constant. Equation [27] therefore becomes

$$\mathfrak{R}_{t\infty,\,i-a}\,(h_i - h_{ss}) \approx \mathfrak{R}_{t\infty,\,(j-1)-j} \sum_{j=1}^{n} \Delta h_{s\,at\,j} \quad \ldots [35]$$

Combining Equations [21] and [35] yields

$$\mathfrak{R}_{ta,\,i-a} \approx \frac{\mathfrak{R}_{t\infty,\,i-a}}{\mathfrak{R}_{t\infty,\,(j-1)-j}} \quad \ldots\ldots [36]$$

Making use of Equations [17] and [22], Equation [36] may be written in terms of the reheat gain

$$\frac{\rho_{ta,\,i-a}}{\rho_{t\infty,\,i-a}} \approx \frac{1-\frac{\rho_{t\infty,\,(j-1)-j}}{\rho_{t\infty,\,i-a}}}{1+\rho_{t\infty\,(j-1)-j}} \quad \ldots\ldots [37]$$

Since the stage reheat factor is constant, Equation [32] becomes

$$n\rho_{t\infty,\,(j-1)-j} \approx \rho_{t\infty,\,i-a} \quad \ldots\ldots [38]$$

Combining Equations [37] and [38] yields

$$\frac{\rho_{ta,\,i-a}}{\rho_{t\infty,\,i-a}} \approx \frac{1-\frac{1}{n}}{1+\frac{\rho_{t\infty,\,i-a}}{n}} \quad \ldots\ldots [39]$$

which is identical to Equation [33] which was developed for equal isentropic drops of enthalpy per stage.

* This result was obtained previously in a slightly different manner by Prof. C. R. Soderberg.

The Calculated Performance of Dynamically Loaded Sleeve Bearings—III

By J. T. BURWELL,[1] CAMBRIDGE, MASS.

In parts I and II of this series (6, 7),[2] the performance of dynamically loaded sleeve bearings was calculated neglecting the transverse flow in the oil film, i.e., the bearing was assumed to be wide compared to its diameter, and then side-leakage factors based upon constant-load calculations were applied. In the present paper the performance is calculated for bearings assumed to be so narrow that film flow due to pressure in the direction of motion can be neglected. In this case the dependence upon bearing width appears explicitly and no side-leakage factors are required. Conclusions about the performance of the bearing under various simple types of loading are drawn. The two solutions for the limiting cases of very wide and very narrow bearings are compared and found to be qualitatively similar. From this it is concluded that bearings of arbitrary width should show the same qualitative behavior. Finally, the present solution is compared with exact calculations for certain narrow bearings, and the error involved in the present approximation is thereby determined.

Introduction

THE solution of the Reynolds equation in the hydrodynamic theory of lubrication as applied to dynamically loaded sleeve bearings developed by Harrison (1), and by Swift (2), assumed no transverse flow of the oil in the bearing. As such, it is accurate only for bearings which have a large axial width compared to their diameter and in this respect is analogous to the familiar Sommerfeld solution for the constantly loaded bearing.

On the other hand, the solution of Reynolds equation, including side leakage, has been worked out exactly in certain ranges for full and partial bearings subjected to a constant load by Muskat and Morgan (3), by Cameron and Wood (4), and by Waters (5). The complete case including side leakage in bearings subjected to dynamic loads has not been solved, and it appears to be so complicated that it is doubtful whether it ever will be. Burwell (6, 7), solved the problem approximately by applying the side-leakage factors obtained by either Waters or Cameron and Wood to the solution for the dynamically loaded bearing obtained by Swift. This procedure, however, implies that the side-leakage factor for the two types of loading will be the same at the same eccentricity. This is a distinct assumption but the best that could be done under the circumstances.

There is one case, however, in which an analytical solution for the dynamically loaded bearing with side leakage can be obtained. This is the situation where the bearing is very narrow in axial width compared to its diameter. Under the condition of constant loading this case was first treated by Michell (8) for the plane slider[3] and by Cardullo (9), and recently by Ocvirk (12), for the journal bearing. It is the purpose of the present paper to solve this case for a dynamically loaded bearing and to see whether the range of application is broad enough to be of practical value.

The Differential Equation

The nomenclature to be used in the following development is essentially the same as that used in reference (6) and is as follows:

r = radius of journal or bearing
d = diameter of journal or bearing
l = axial width of bearing
c = radial clearance or difference in radii of bearing and journal
h = oil-film thickness at position θ
h_0 = minimum oil-film thickness at position $\theta = \pi$
e = distance between center of journal and bearing, called eccentricity $= c - h_0$
$\eta = e/c$, called eccentricity ratio
η max = maximum value of η during a cycle
η_0 = value of η given by the equation for constant load
η_m = value of η at cusps of certain orbits
$\xi = \dfrac{\eta}{(1-\eta^2)^{1/4}}$, called eccentricity function
$\xi = \dfrac{\eta}{(1-\eta^2)^{3/4}}$, another eccentricity function
θ = angular position of any point in oil film measured from maximum-film-thickness end of line of centers
α = angular rotational displacement of journal relative to bearing
β = angle between direction of load and fixed point on bearing, measured in direction of rotation
φ = angle between direction of load and minimum-film-thickness end of line of centers measured in direction of rotation
t = time
$\tau = 2\pi N t$, dimensionless time or crank angle
U = relative tangential velocity of surfaces
V = relative normal velocity of surfaces
$\dfrac{d\alpha}{dt}$ = instantaneous angular velocity of journal
N_t = average angular velocity of journal in revolutions per unit time, a constant
N_p = average frequency of rotation or oscillation of load in revolutions or cycles per unit time
μ = absolute viscosity of lubricant
p = pressure at any point [4], in oil film
p_0 = pressure in oil film at the sides of bearing
W = total radial load applied by shaft to oil film

---

[1] Associate Professor, Department of Mechanical Engineering, Massachusetts Institute of Technology.

[2] Numbers in parentheses refer to the Bibliography at the end of the paper.

Contributed by the Applied Mechanics Division and presented at the Annual Meeting, Atlantic City, N. J., November 25–30, 1951, of The American Society of Mechanical Engineers.

Discussion of this paper should be addressed to the Secretary, ASME, 29 West 39th Street, New York, N. Y., and will be accepted until January 10, 1952, for publication at a later date. Discussion received after the closing date will be returned.

Note: Statements and opinions advanced in papers are to be understood as individual expressions of their authors, and not those of the Society. Manuscript received by ASME Applied Mechanics Division, October 25, 1950. Paper No. 51—A-7.

[3] Michell also treated the problem of the plane slider of any width in the same paper.

$P = \dfrac{W}{2rl}$ = load per unit projected area of bearing

P_0 = maximum amplitude of P for periodic load

$S = \left(\dfrac{r}{c}\right)^2 \dfrac{\mu N_j}{P}$, often called Sommerfeld variable

$S' = \left(\dfrac{r}{c}\right)^2 \dfrac{\mu N_p}{P}$

S_0, S_0' = values of S and S' corresponding to $P = P_0$

f_j = friction coefficient on journal

f_b = friction coefficient on bearing

x, y, z = set of Cartesian co-ordinates

x' = dimensionless quantity defined by Equation [34]

The generalized Reynolds equation for the pressure at any point in an oil film which is quite thin compared to its other two dimensions is as follows

$$\frac{\partial}{\partial x}\left(\frac{h^3}{\mu}\frac{\partial p}{\partial x}\right) + \frac{\partial}{\partial z}\left(\frac{h^3}{\mu}\frac{\partial p}{\partial z}\right) - 6\frac{\partial}{\partial x}(hU) - 12V = 0 \ldots [1]$$

where the y-direction is taken normal to the film, the x and z-directions lie in the film, and the origin is fixed relative to one of the two surfaces (10). The relative tangential motion of the two bounding solid surfaces is taken as being in the x-direction, which results in no loss in generality, and is designated by U while the relative motion of the surfaces toward or away from each other in the y-direction is designated by V. Term h is the film thickness at any point in the film x, z, and p and μ are the pressure and oil viscosity at that point.

If every term in Equation [1] is multiplied by $dx\,dz$, then each term represents the net oil flow in or out of an infinitesimal volume of height h, and cross section $dx\,dz$ due to such factors as a pressure gradient, viscous drag by the moving surface, or squeezing by the surfaces approaching each other. The equation expresses the fact that since the oil is incompressible, the net sum of all of these flows into the volume must be zero.

The assumption made by Michell and by Cardullo is that if the bearing is sufficiently narrow axially compared to its diameter, then the flow of the oil due to a pressure gradient in the direction of motion will be so much less than that due to a pressure gradient in the transverse direction that the former can be neglected. In this case Equation [1] becomes

$$\frac{\partial}{\partial z}\left(\frac{h^3}{\mu}\frac{\partial p}{\partial z}\right) - 6\frac{\partial}{\partial x}(hU) - 12\,V = 0 \ldots\ldots [2]$$

In a sense this is the reverse of the assumption made in deriving the Sommerfeld equation where the pressure flow in the z-direction is the term that is neglected.

The Pressure Equation

The expression for the pressure in the oil film can be obtained at once by integrating Equation [2] without regard to the particular type of bearing so long as neither h, U, nor V depends on z. In this case double-integration of Equation [2] with respect to z whose origin is placed on the center line of the bearing and evaluation of the two integration constants by the boundary conditions (a), $(dp)/(dz) = 0$ at $z = 0$, owing to the transverse symmetry of most bearings, and (b), $p = p_0$ at $z = l/2$, the sides of the bearing, leads to the following equation

$$p - p_0 = \frac{3\mu}{h^3}\left[\frac{\partial}{\partial x}(hU) + 2V\right]\left(z^2 - \frac{l^2}{4}\right) \ldots\ldots [3]$$

on the usual assumption that the viscosity is constant throughout the oil film.

Equation [3] applies to various types of bearings, plane slider or journal, and either constant or variable loading. These particular conditions will determine the values of h, U, and V. For the case of a journal bearing

$$x = r\theta \ldots\ldots [4]$$

and

$$h = c(1 + \eta\cos\theta) \ldots\ldots [5]$$

These quantities have already been defined at the beginning of the section and are shown in Fig. 1.

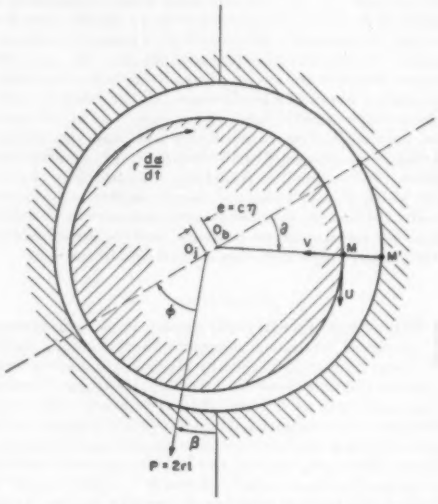

Fig. 1 Cross Section of Sleeve Bearing Under Dynamic Loading

If the load applied to the bearing varies, then the center of the shaft, in general, will move in the clearance space relative to the center of the bearing. If the origin is taken at the center of the bearing, and the bearing is considered fixed, then the shaft center will have instantaneous radial and tangential velocities equal to $c(d\eta)/(dt)$ and $c[d/(dt)(\beta + \varphi)]$. Any point M on the surface of the shaft at angular position θ (see Fig. 1) will have tangential and normal velocities relative to an opposite point M' on the surface of the bearing made up of the resolved components of the velocity of the shaft center relative to the bearing center plus the velocity of the surface of the shaft $r(d\alpha)/(dt)$ about its own center. These are (10)

$$\left.\begin{aligned} U &= r\frac{d\alpha}{dt} + c\frac{d\eta}{dt}\sin\theta - c\eta\frac{d}{dt}(\beta + \varphi)\cos\theta \\ V &= c\frac{d\eta}{dt}\cos\theta + c\eta\frac{d}{dt}(\beta + \varphi)\sin\theta \end{aligned}\right\} \ldots [6]$$

Substitution of Expressions [4], [5], and [6] into Equation [3] and neglecting higher powers in the ratio C/R which is usually of the order 1/1000th lead to

$$p - p_0 = 6\left(\frac{r}{c}\right)^2 \mu \left[\left(\frac{l}{d}\right)^2 - \left(\frac{z}{r}\right)^2\right] \frac{1}{(1 + \eta \cos\theta)^3} \left\{\eta \frac{d}{dt}\left[\alpha - 2(\beta + \varphi)\right]\right\} \sin\theta - \frac{d\eta}{dt}\cos\theta \Big\} \quad \ldots [7]^4$$

This equation is analogous to Equation [1] in reference (6) or Equation [4] of reference (7)[5] for the pressure distribution in the infinitely wide bearing except that it contains the dependence on z directly, i.e., the effect of side leakage. This dependence is seen to be parabolic. The component of the pressure due to the tangential velocity, called the "wedge-film" term, is seen to be 90 deg out of phase with the component due to the radial motion of the shaft, called the "squeeze film." The physical significance of these two terms is discussed more fully in references (6) and (10).

An interesting comparison can be drawn between Equation [7] and the equation for the pressure distribution in the infinitely wide bearing. The latter equation originally given in the form of Equation [1] in reference (6) was later corrected to the form of Equation [4] in reference (7), in order to conform with the somewhat arbitrary definition of the reference pressure p_0 as the pressure in the oil film at the angular position $\theta = 0$. If, however, the reference pressure is defined as the mean of the pressure distribution all around the film in the infinitely wide bearing, then the expression takes the form of Equation [1] in reference (6), which is a more suitable one for the present comparison. This definition for p_0 assumes of course that it is sufficiently high so that the pressure nowhere in the film becomes negative. In an infinitely wide bearing this could be done only by introducing oil into the bearing at a supply pressure p_s, but this would disturb the pressure distribution in the vicinity of the oil inlet, forcing it to become p_s at that point no matter what the equation predicted. However, an infinitely wide bearing is not a physical reality and possibly the best way to relate p_0, as defined here, to any externally imposed pressure is to consider that it is equal either (a) to the ambient pressure at the sides of a very wide but finite bearing, or (b) to the oil-supply pressure p_s at points in the bearing far removed axially from the oil inlet. This could apply to oil-holes if spaced sufficiently far apart axially, or to a circumferential oil groove. It would not apply to an axial groove since the latter will always determine the value of the pressure at its angular position in the film.

With this definition of p_0 then Equation [1] in reference (6) is applicable, and it may be written in slightly different form as follows

$$p - p_0 = 6\left(\frac{r}{c}\right)^2 \mu \left[\frac{1}{(1 + \eta\cos\varphi)} + \frac{1}{(1 + \eta\cos\varphi)^3}\right] \left\{\frac{\eta}{2 + \eta^2}\frac{d}{dt}\left[\alpha - 2(\beta + \varphi)\right]\sin\theta - \frac{d\eta}{dt}\cos\varphi\right\} \quad \ldots [8]$$

Comparison of this equation with Equation [7] shows the two to be very similar in form. The dependence upon the two components of the relative velocity of the journal is seen to be almost the same in the two cases, the only difference being a factor of $(2 + \eta^2)$ as opposed to a factor of 2 in one of the two terms.

The dependence on θ is interesting. In both cases it is a function of powers of the quantity $1/(1 + \eta\cos\theta)$.

[4] Strictly speaking, the coefficient of $d\eta/dt$ is $\left(\cos\theta - \frac{c}{r}\frac{\eta}{2}\right)$ rather than simply $\cos\theta$. The term $\frac{c}{r}\frac{\eta}{2}$ is not negligible compared to $\cos\theta$ in the immediate vicinity of $\theta = \pm\pi/2$ but its contribution to the total pressure, and therefore to the load capacity, will be negligible.

[5] The latter equation has a factor of 6 η missing from the first term on the right-hand side.

Load and Friction Equations

The total instantaneous load that such a bearing can support is obtained by integrating the pressure components normal to and parallel with the line of centers. In other words

$$W\sin\varphi = \int_{\theta_1}^{\theta_2}\int_{-l/2}^{+l/2}(p - p_0)\sin\theta\, r\,d\theta\,dz \quad \ldots [9a]$$

$$W\cos\varphi = \int_{\theta_1}^{\theta_2}\int_{-l/2}^{+l/2}(p - p_0)\cos\theta\, r\,d\theta\,dz \quad \ldots [9b]$$

Integration over z is simply carried out. Integration over θ raises the question of the angular extent of the load-carrying region of the oil film, i.e., the value of the limits of integration θ_1 and θ_2. Equation [7] shows that it is perfectly possible for the pressure p to be considerably less at certain points in the oil film than the ambient pressure p_0 at the sides of the bearing. If the latter is only atmospheric, then it is mathematically possible for the oil-film pressure to be negative in certain regions of the film, at which points it will suck air in from the sides of the bearing, since the latter is so narrow.

The correct boundary conditions for such an incomplete oil film are that both the pressure difference and the pressure gradient are zero at the trailing edge of the film (4, 5), which are based on considerations of continuity of flow in the θ-direction. However, in the present derivation, pressure flow in the θ-direction is neglected, so that discontinuity in the pressure gradient at the trailing edge is now mathematically allowable. Hence the boundary conditions for the oil film are simply that the pressure difference (from the sides of the bearing) be zero at the two ends of the film θ_1 and θ_2. From Equation [7] this means that θ_1 and θ_2 are solutions of the equation

$$\tan\varphi = \frac{2\frac{d\eta}{dt}}{\eta\frac{d}{dt}\left[\alpha - 2(\beta + \varphi)\right]} \quad \ldots [10]$$

Since these solutions differ by π this means that θ_2 always equals $\theta_1 + \pi$ and that the film is always 180 deg in extent. In particular, for a stationary journal center where $(d\eta)/(dt) = 0$, such as occurs under a constant load, the limits of the load-carrying film will be 0 and +180 deg from Equation [10].

However, the general solution of Equations [9] with the limits of integration determined by Equation [10] are so complicated, except in certain special cases, that they will not be written down here, although they can be obtained in a straightforward manner if desired.[6] Instead it will be assumed that the bearing is always immersed in an external pressure p_0 sufficient so that the absolute pressure in the film nowhere becomes negative. The exact magnitude of p_0 does not matter since it does not appear in the load capacity, being equal on the loaded and unloaded sides of the bearing. In this case, therefore, the oil film is complete around the bearing, and the limits of integration become 0 and 2π.

Substitution of Equation [7] into Equations [9], and integration[7] lead to the following expressions for the two components of the load

[6] Ott (17) has given such solutions for the infinitely wide bearing using these limits for the film extent. However, as pointed out in the foregoing, these are not the correct boundary conditions to use in such a bearing where the pressure flow is considered.

[7] Evaluation of most of the resulting integrals is most easily effected by making use of the ingenious transformation suggested by Sommerfeld (11),

$$1 + \eta\cos\theta = \frac{1 - \eta^2}{1 - \eta\cos\gamma}$$

$$\frac{1}{S}\sin\varphi = 4\pi^2\left(\frac{l}{d}\right)^2\frac{\eta}{2(1-\eta^2)^{3/2}}\frac{1}{2\pi N_f}\frac{d}{dt}\left[\alpha-2(\beta+\varphi)\right] \quad \ldots\ldots [11a]$$

$$\frac{1}{S}\cos\varphi = 4\pi^2\left(\frac{l}{d}\right)^2\frac{1+2\eta^2}{(1-\eta^2)^{5/2}}\frac{1}{2\pi N_f}\frac{d}{dt}\eta \ldots [11b]$$

where $1/S$ is the dimensionless load

$$\frac{P}{\left(\frac{r}{c}\right)^2\mu N_f}$$

These equations are analogous to Equations [2] of reference (6) for the infinitely wide bearing. The first equation gives the component of the load carried by the wedge-film component of the pressure which is entirely perpendicular to the line of centers, and the second equation gives that carried by the squeeze-film component which is parallel to the line of centers.

Like the corresponding equations for the infinitely wide bearing, the operating variables, with the exception of N_f which is combined with t to form a dimensionless time or phase angle, appear only as combined in the Sommerfeld variable S. The combining of the operating variables into the single Sommerfeld variable means that not only problems of variable load but also of variable viscosity and variable speed (through α) can also be handled. However, the variable-load problem is the most important practical one, particularly periodic loading such as occurs on the bearings of reciprocating machinery. In this problem the quantity of practical interest is the maximum value which the eccentricity η attains at any time during the load cycle η_{max} since this corresponds to the minimum value which the minimum oil-film thickness h_0 reaches during the cycle, which in turn determines the limit of safe operation of the bearing.

The present equations differ from those for the infinitely wide bearing in containing the explicit dependence on bearing width l so that side-leakage factors for bearings of finite width do not have to be applied afterward, as was done in references (6) and (7). This dependence is seen to be simply on the square of the width-to-diameter ratio.

A further point about the dependence on the l/d ratio is that it appears only in the combination $(1/S)(d/l)^2$. These two factors are kept separate in these and all the subsequent equations because the dimensionless load $1/S$ occurs so commonly in the field of hydrodynamic journal-bearing lubrication that it facilitates comparison with other results. However, the product $(1/S)(d/l)^2$ may be combined to form the single dimensionless combination

$$\frac{P}{(l/c)^2\mu N}$$

of all the operating variables and dimensions in the equations. This is also a dimensionless load which may turn out to be of as practical value as the Sommerfeld variable S has been. In terms of it Equations [11] may be written

$$\frac{P}{(l/c)^2\mu N_f}\sin\varphi = \pi^2\frac{\eta}{2(1-\eta^2)^{3/2}}\frac{1}{2\pi N_f}\frac{d}{dt}\left[\alpha-2(\beta+\varphi)\right] \quad \ldots\ldots [12a]$$

$$\frac{P}{(l/c)^2\mu N_f}\cos\varphi = \pi^2\frac{1+\eta^2}{(1-\eta^2)^{3/2}}\frac{1}{2\pi N_f}\frac{d}{dt}\eta \ldots\ldots [12b]$$

These equations are independent of bearing diameter just as the equations for the infinitely wide bearings are independent of bearing width.

Equations [11] can be simplified somewhat by means of the following substitution

$$\xi = \frac{\eta}{(1-\eta^2)^{3/2}}$$

leading to

$$\frac{1}{S}\sin\varphi = 4\pi^2\left(\frac{l}{d}\right)^2\frac{\xi}{2}\frac{1}{2\pi N_f}\frac{d}{dt}\left[\alpha-2(\beta+\varphi)\right]. \quad [13a]$$

$$\frac{1}{S}\cos\varphi = 4\pi^2\left(\frac{l}{d}\right)^2\frac{1}{2\pi N_f}\frac{d}{dt}\xi \ldots\ldots [13b]$$

The quantity ξ is similar in nature to the eccentricity function ξ defined in reference (6) in that it spreads out the scale determining journal position near $\eta = 1$. It would appear to be the appropriate variable for this problem since for constant loading, as will be seen in the following, ξ varies directly with the load, and its time derivative varies directly with the squeeze-film component of the load support.

The friction is given by the following equations, due to Muskat and Morgan (3)

$$\frac{r}{c}f_j = \frac{\eta}{2}\sin\varphi + \frac{2\pi^2 S}{(1-\eta^2)^{1/2}} \ldots\ldots [14a]$$

$$\frac{r}{c}f_b = -\frac{\eta}{2}\sin\varphi + \frac{2\pi^2 S}{(1-\eta^2)^{1/2}} \ldots\ldots [14b]$$

where the values of η and φ for a given value of S are determined by Equations [11].

Equations [11] relate the co-ordinates η and φ of the shaft center to the magnitude $1/S$ and direction β of the load which the bearing can support, all quantities, in general, being functions of time. If the position of the shaft is known as a function of time, then the load that can be carried can be found immediately from the equations. This, however, is not usually the situation in practice. It is rather the converse problem of determining the shaft position for a given dynamic loading so that the factor of safety of bearing operation can be determined. This problem is not easy to solve because in Equations [11] not only do the unknown co-ordinates η and φ appear but also their time derivatives so that, while in theory η and φ are completely determined, integration of the equations to obtain analytical solutions does not seem to be generally possible. Numerical integration must be resorted to which is laborious and must be repeated for each different value of any of the parameters. This was also true of the corresponding equations for the infinitely wide bearing. Hence, as in that case, solutions for the special cases of various simple types of loading will be given first, after which the procedure for solving more general types will be indicated. Since it turns out that these special cases are very similar in nature to those for the infinitely wide bearing, only the analytical expressions themselves differing slightly, the latter will only be tabulated and discussed briefly here. For further details including their physical significance the reader is referred to the corresponding cases in reference (6).

Constant Load in Fixed Direction

In the simplest case of a constant load in a fixed direction with a constant shaft speed, S is a constant, $(d\beta)/(dt) = 0$ and $(d\alpha)/(dt) = 2\pi N_f$. Equations [11], therefore, become

$$\frac{1}{S}\sin\varphi = 4\pi^2\left(\frac{l}{d}\right)^2\frac{\eta}{2(1-\eta^2)^{3/2}}\left[1-2\left(\frac{1}{2\pi N_f}\frac{d}{dt}\varphi\right)\right] \quad \ldots\ldots [15a]$$

$$\frac{1}{S}\cos\varphi = 4\pi^2\left(\frac{l}{d}\right)^2\frac{1+2\eta^2}{(1-\eta^2)^{5/2}}\frac{1}{2\pi N_j}\frac{d\eta}{dt} \quad \ldots\ldots [15b]$$

This pair of equations can be solved by eliminating dt between them and integrating the resulting equation. This gives

$$\frac{1}{S}\sin\varphi = \pi^2\left(\frac{l}{d}\right)^2\frac{\eta}{(1-\eta^2)^{3/2}} - k^2\frac{(1-\eta^2)^{3/2}}{\eta} \quad \ldots [16]$$

where k^2 is the integration constant which depends upon the initial conditions, i.e., the position of the journal at some particular time. For each value of k^2, this is the equation for a closed path or orbit in which the shaft center moves continously even under a constant load. The explanation for this is given in reference (6). A family of such curves for a value of $S = 1.68$ is shown in Fig. 2, each path corresponding to a different value of k.

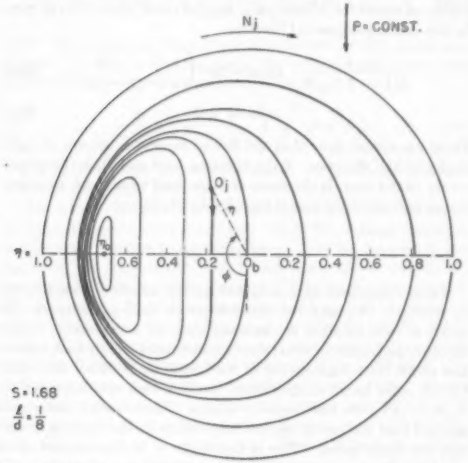

FIG. 2 PATHS OF JOURNAL CENTER UNDER A CONSTANT LOAD ($S = 1.68$, $\eta_0 = 0.7$, $l/d = 1/8$.)

The motion of the shaft center in any of these orbits can be obtained by eliminating φ between Equations [16] and [15b] and integrating the resulting equation.[3] This gives

$$2\pi^4 S^2\left(\frac{l}{d}\right)^4\frac{\eta^2}{(1-\eta^2)^3} = \left[1 + 4\pi^2 k^2 S^2\left(\frac{l}{d}\right)^2\right]^{1/2}$$
$$\sin\pi N_j(t-t_0) + \left[1 + 2\pi^2 k^2 S^2\left(\frac{l}{d}\right)^2\right] \quad \ldots\ldots [17]$$

where k^2 and t_0 are the constants of integration. The corresponding one for φ may be obtained by eliminating η or

$$\frac{\eta}{(1-\eta^2)^{3/2}}$$

between Equations [16] and [17].

It can be seen from Equation [17] that the frequency of the motion of the shaft center around its orbit is exactly one half the period of revolution of the shaft regardless of the eccentricity. In other words $(1/2)N_j$ appears to be the natural frequency of the system. In the case of the infinitely wide bearing it was not possible to integrate the equation of motion analytically. However, Swift (2) found by graphical and approximate methods that the frequency was generally somewhat less than half the frequency of shaft rotation, although it approached this value in certain special cases. It depended on the size of the orbit which is not true in the present case.

The pole of the family of orbits given by Equation [16] corresponds to a stationary position of the shaft for this value of $1/S$. In this case both $(d\varphi)/(dt)$ and $(d\eta)/(dt)$ are equal to zero, and Equations [15] reduce to

$$\frac{1}{S} = 2\pi^2\left(\frac{l}{d}\right)^2\frac{\eta}{(1-\eta^2)^{3/2}} = 2\pi^2\left(\frac{l}{d}\right)^2\xi \quad \ldots [18a]$$

$$\varphi = +\frac{\pi}{2} \quad \ldots\ldots [18b]$$

This is generally taken to be the position of the shaft under a constant load. (This value of η will be designated η_0 in the subsequent discussion.) It may be compared with the well-known Sommerfeld solution for the infinitely wide bearing, namely

$$\frac{1}{S} = 12\pi^2\frac{\eta}{(2+\eta^2)(1-\eta^2)^{1/2}} \quad \ldots\ldots [19a]$$

$$\varphi = +\frac{\pi}{2} \quad \ldots\ldots [19b]$$

For a given value of η these two sets of equations will yield equal values of $1/S$ when l/d has the value

$$\left(6\frac{1-\eta^2}{2+\eta^2}\right)^{1/2}$$

a curve of $1/S$ versus l/d composed of the appropriate sections of the two Equations [18a] and [19a] joined at this value of l/d must form the upper limit of the actual load capacity for bearings of intermediate width which have a continuous oil film. This is because neglect of the pressure flow in the θ-direction in deriving Equation [18a] leads to too high a value of $1/S$, while neglect of side leakage in Equation [19a] also leads to too high a value. However, this envelope curve may be helpful in fixing limits for approximate solutions for bearings of intermediate width.

As remarked in an earlier section, if the oil film is discontinuous, owing to the development of negative pressures, then, for the particular case of a constantly loaded bearing, the angular limits θ_1 and θ_2 of the film are simply 0 and π. With these limits Equations [9] can be integrated to give

$$\frac{1}{S}\sin\varphi = 4\pi\left(\frac{l}{d}\right)^2\frac{\pi}{4}\frac{\eta}{(1-\eta^2)^{3/2}} \quad \ldots\ldots [20a]$$

$$\frac{1}{S}\cos\varphi = 4\pi\left(\frac{l}{d}\right)^2\frac{\eta^2}{(1-\eta^2)^2} \quad \ldots\ldots [20b]$$

whence

$$\frac{1}{S} = 4\pi\left(\frac{l}{d}\right)^2\frac{\eta}{(1-\eta^2)^2}\left[\eta^2 + \frac{\pi^2}{16}(1-\eta^2)\right]^{1/2} \quad [21a]$$

$$\tan\varphi = \frac{\pi}{4}\frac{(1-\eta^2)^{1/2}}{\eta} \quad \ldots\ldots [21b]$$

These equations have recently been obtained by Ocvirk (12). It is interesting that Equation [21b] is very close to the empirical relation

$$\eta = \cos\varphi$$

[3] This is most easily done in terms of the function ξ.

which has been found to fit experimental observations, such as those of Nücker (13), on journal attitude.

Comparison of Equations [18a] and [21a] for the load capacity of the complete and broken films, respectively, shows that while the complete film will carry a greater load at small eccentricities, the incomplete film will carry a greater one at high eccentricities, as is shown in Fig. 3. This is fortunate since a complete film can seldom exist at the potentially high negative pressures associated with high eccentricities. The same situation has been found for

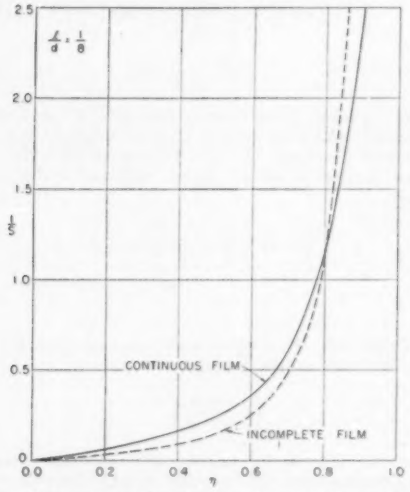

FIG. 3 COMPARISON OF DIMENSIONLESS LOAD $1/S$ UNDER ASSUMPTION OF A CONTINUOUS AND OF AN INCOMPLETE FILM $(l/d = 1/8.)$

the infinitely wide bearing (14), and the explanation is the same, namely, that at the low eccentricities the reduced pressures on the unloaded side of the complete film contribute to the load support, while at the high eccentricities the line of centers for the incomplete film is free to rotate to bring the high-pressure region of the film directly under the load, thus utilizing it more efficiently.

Another point of interest about Equation [18a] or [21a] is the relation between the dimensionless load $1/S$ and the minimum oil-film thickness h_0. Since

$$1 - \eta = h_0/c \qquad [22]$$

it follows that for large eccentricities (values of η near unity) Equation [18a] predicts that $1/S$ should vary inversely as $h_0^{3/2}$, and Equation [21a] predicts that it should vary inversely as h_0^3. Hence the conclusion of Blok (15) that the load capacity should vary inversely as h_0 is not generally valid, although an analysis by Cameron and Wood (4) shows that it does hold for very wide bearings.

CONSTANT ROTATING LOAD

The next special case to be considered is that of a load of constant magnitude rotating at a constant speed. In this case $1/S$ is constant and $(d\beta)/(dt) = 2\pi N_p$. If the shaft speed is taken as constant then $(d\alpha)/(dt) = 2\pi N_j$. Introduction of these values, elimination of dt between Equations [11a] and [11b] and integration lead to

$$\frac{1}{S(1 - 2\,N_p/N_j)} \sin\varphi = \pi^2 \left(\frac{l}{d}\right)^2 \frac{\eta}{(1-\eta^2)^{1/2}} - k^2 \frac{(1-\eta^2)^{1/2}}{\eta} \qquad [23]$$

This is the equation for a family of closed orbits exactly like those for the constant fixed load, Equation [16], except that the dimensionless load $1/S$ is modified by the factor

$$\frac{1}{(1 - 2\,N_p/N_j)}$$

The positions of these orbits is fixed relative to the load line and, therefore, they rotate around the bearing. Similar families of orbits were found for the infinitely wide bearing (6).

The shaft position of most practical interest is the pole of this family of orbits for which both $(d\eta)/(dt)$ and $(d\varphi)/(dt)$ are zero. In this case Equations [11] become

$$\frac{1}{S(1 - 2\,N_p/N_j)} \sin\varphi = 2\pi^2 \left(\frac{l}{d}\right)^2 \frac{\eta}{(1-\eta^2)^{1/2}} \qquad [24a]$$

$$\varphi = \pm\,\pi/2 \qquad [24b]$$

These equations show that the line of centers is always at right angles to the direction of the rotating load and that the eccentricity of the shaft is the same as if the load were fixed, provided the magnitude of the load is modified by the factor

$$\frac{1}{(1 - 2\,N_p/N_j)}$$

Similar equations were obtained for the infinitely wide bearing in reference (6), and the dependence of load capacity on the speed of load rotation is discussed there in considerable detail. In brief, as Equation [24a] shows immediately, high load capacities result from high speeds of load rotation in either direction. On the other hand, at the critical speed of load rotation given by $N_p = (1/2)N_j$, the load capacity is zero. Conversely, under zero applied load the line of centers may rotate in the bearing at one half the shaft speed. This is the origin of oil-film-excited shaft whirl.

For a rotating load on a nonrotating shaft $N_j = 0$ and Equations [24] become

$$\frac{1}{S'} = \frac{P}{(r/c)^2 \mu N_p} = 4\pi^2 \left(\frac{l}{d}\right)^2 \frac{\eta}{(1-\eta^2)^{1/2}} \qquad [25a]$$

$$\varphi = -\pi/2 \qquad [25b]$$

or twice the load capacity of a nonrotating load on a shaft rotating at the same speed.

STATIONARY-SHAFT AND FIXED-LOAD DIRECTION

Under these conditions both $(d\alpha)/(dt)$ (as well as N_j) and $(d\beta)/(dt)$ are zero so that Equations [11] or [12] becomes

$$\frac{P}{(l/c)^2 \mu} \sin\varphi = -\frac{\pi}{2} \frac{\eta}{(1-\eta^2)^{1/2}} \frac{d\varphi}{dt} \qquad [26a]$$

$$\frac{P}{(l/c)^2 \mu} \cos\varphi = \frac{\pi}{2} \frac{1 + 2\eta^2}{(1-\eta^2)^{1/2}} \frac{d\eta}{dt} \qquad [26b]$$

In these equations P can assume negative values in order to take account of oscillating loads. Dividing one of these equations by the other and integrating leads to

$$\sin\varphi = k \frac{(1-\eta^2)^{1/2}}{\eta} \qquad [27]$$

as the equation for the path which the nonrotating shaft center will follow under any load having a fixed direction. This path is seen to be independent of the load or how it varies with time, but the motion of the shaft center in this path will depend on these factors. The value of the integration constant k determines the particular path followed, and this in turn is determined by the initial position of the shaft. These paths are plotted in Fig. 4, and are independent both of $1/S$ and of l/d.

The motion of the shaft center in these paths can be obtained by eliminating either η or φ between Equation [27] and either of Equations [26]. The result is

$$\left(\frac{\eta^2}{(1-\eta^2)^3} - k^2\right)^{1/2} = \frac{2}{\pi\mu}\left(\frac{c}{l}\right)^2 \int Pdt + k' \quad [28a]$$

$$k \cot \varphi = \frac{2}{\pi\mu}\left(\frac{c}{l}\right)^2 \int Pdt + k' \quad [28b]$$

where the constants k and k' are determined by the initial conditions. For the particular case of the central straight-line path in Fig. 3, $k = 0$ and these equations reduce to

$$\frac{\eta}{(1-\eta^2)^{3/2}} = \frac{2}{\pi\mu}\left(\frac{c}{l}\right)^2 \int Pdt + k' \quad [29]$$

The integral is easily evaluated when the dependence of the oscillating load on time is known.

This type of operation occurs in practice most commonly in piston pins in reciprocating machinery where the angular rocking is usually small enough to be negligible. The load support is due mainly to the squeeze film, i.e., to Equation [26b],[9] and the action is similar to a hydraulic damper. If the load is symmetrical, then Equation [28] or [29] shows that the motion of the shaft will be oscillatory, and its maximum eccentricity can be calculated. If, however, the load has a net component in one direction, then its contribution to the integral on the right-hand side of the equations will increase indefinitely with time. Hence the mean value of η during a cycle will increase indefinitely with time and the shaft will drift toward contact with the bearing wall (at points A or A' in Fig. 3). While the equations show that theoretically it will take an infinite time (or an infinite load) to reach actual contact, yet in practice the safe minimum film thickness may be transgressed in a relatively short time. The same characteristics were found in reference (6), and a suggestion is given there as to why piston pins which are often nonsymmetrically loaded still work so well in practice.

General Case of a Periodic Load

For the case of a load that varies periodically in magnitude and direction, such as in the connecting-rod bearings of reciprocating machinery we can write

$$P = P_0 p(2\pi N_p t) \quad [30]$$

where P_0 is the maximum amplitude of P during the cycle, $p(2\pi N_p t)$ is any periodic function of the time normalized to a maximum amplitude of unity, and N_p is the frequency of the applied load. Likewise $\beta(2\pi N_p t)$ will also be a periodic function of the time. For simplicity we introduce the dimensionless time

$$\tau = 2\pi N_p t \quad [31]$$

so that $p(\tau)$ and $\beta(\tau)$ each has a period of 2π or some submultiple thereof. In most cases where $(d\alpha)/(dt)$ varies with the time, as in a connecting-rod bearing, its period will also be integrally related to that of τ. If Equations [13], which are the most suitable form for the present purposes, are expressed in terms of these quantities they then become

$$\frac{p(\tau)}{S_0}\sin\varphi = 4\pi^3\left(\frac{l}{d}\right)^3 \frac{\xi}{2}\frac{N_p}{N_i}\frac{d}{d\tau}\left[\alpha(\tau) - 2\beta(\tau) - 2\varphi\right] \quad [32a]$$

$$\frac{p(\tau)}{S_0}\cos\varphi = 4\pi^3\left(\frac{l}{d}\right)^3 \frac{N_p}{N_i}\frac{d}{dt}\,\xi \quad [32b]$$

where

$$S_0 = \left(\frac{r}{c}\right)^2 \frac{\mu N_i}{P_0} \quad [33]$$

These equations can be simplified somewhat more by introducing the variable

$$x' = 2\pi^3 S_0 \left(\frac{l}{d}\right)^3 \frac{N_p}{N_i}\xi \quad [34]$$

in terms of which they become

$$p(\tau)\sin\varphi = x'\frac{d}{d\tau}(\alpha - 2\beta - 2\varphi) \quad [35a]$$

$$p(\tau)\cos\varphi = 2\frac{dx'}{d\tau} \quad [35b]$$

Solutions of these equations are obviously independent of the particular value of S_0 and depend only on the wave form of the load, $p(\tau)$ and $\beta(\tau)$, and on the speed $(d\alpha)/(d\tau)$ which includes the frequency ratio N_p/N_i.

These equations are practically identical in form with the corresponding ones for the infinitely wide bearing (see Equations [21] in reference 6) with the only difference being that the constant $1/a$ now equals 2 instead of approximately 3. Since this difference is not expected to have any effect on the qualitative behavior of the solutions and very little effect quantitatively on their magnitudes, the conclusions drawn about the solutions of the former equations should apply quite well to the present equations. Briefly, the principal conclusions were as follows:

(*a*) Even for the simplest analytical forms of periodic loading such as a sinusoidal reciprocating load, Equations [35] cannot be solved analytically and resort must be had to numerical methods.

(*b*) The higher the frequency of load oscillation the greater is the load capacity.

(*c*) There is some evidence that when $N_p = N_i/2$ the load capacity is zero, just as was the case with a constant rotating load. This is borne out by the fact that Equation [17] showed this to be a natural frequency of the system.

However, the present equations have the advantage over the corresponding equations for the infinitely wide bearing in that the latter involved an approximation so that they were valid only for large values of η (greater than about 0.55) while the present equations are exact for all values of η.

Simple Analytical Forms of Reciprocating Loads

For reciprocating loads the direction of the line of action of the load does not change. Hence $(d\beta)/(d\tau) = 0$ in Equations [35] but $p(\tau)$ must be allowed to assume negative values in order to take account of the reversal in direction of the load. Also, $(d\alpha)/(d\tau) = N_i/N_p$.

While for most types of reciprocating load Equations [35] must then be integrated numerically there is one simple type for which they can be solved analytically. This is a square-wave alternating load. This is possible because of the existence of the

[9] Equation [29] is entirely squeeze film since $\sin\theta$ is zero so that Equation [26a] vanishes.

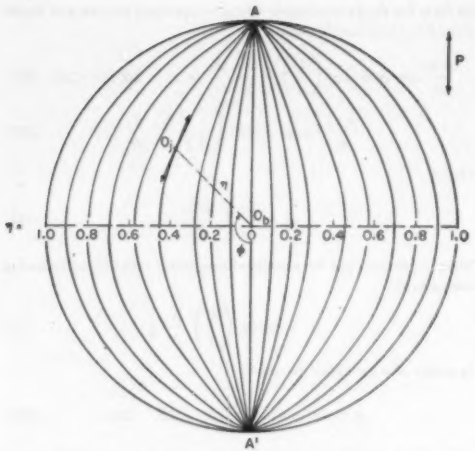

FIG. 4 PATHS OF NONROTATING JOURNAL CENTER UNDER ANY TYPE OF LOADING HAVING A FIXED DIRECTION

analytical expression, Equation [17], for the motion of the shaft center under a fixed load which can be applied to each half cycle of the square-wave alternating load. Hence Equations [16] and [17] rather than Equations [35] will be used in the following derivation.

The square-wave load is described analytically by $p(\tau) = +1$ for $0 < \tau < \pi$ and $p(\tau) = -1$ for $\pi < \tau < 2\pi$. During each half cycle between $\varphi = 0$ and π $\varphi = \pi$ and 2π, the path should follow a section of one of orbits described by Equation [16], and illustrated in Fig. 2. At the end of that particular half cycle, the shaft center switches to the corresponding orbit for a fixed load in the opposite direction which is the mirror image of the first orbit reflected across the line $\varphi = 0$. This is illustrated in the curves in Fig. 5 where orbits constructed in the manner to be described later are shown for $S_0 = 1.68$, $l/d = 1/8$, and load-frequency ratios N_p/N_j of 1/4, 3/8, and 1. That for $N_p/N_j = 1/3$ is simply a circle of radius $\eta = 1$, corresponding to the shaft touching the bearing throughout its orbit. The values of η at the junction points of the two branches of the path, called η_m, are given by Equation [16] when $\varphi = 0$ or π. This yields

$$\pi \frac{l}{d} \frac{\eta_m}{(1 - \eta_m)^{3/2}} = k \quad \ldots\ldots\ldots\ldots\ldots\ldots [36]$$

This value of k substituted in Equation [17] gives the times at which the shaft center is at these two points, namely, the two solutions of the following resulting equation

$$t - t_0 = \frac{1}{\pi N_j} \sin^{-1}\left[\frac{-1}{1 + 4\pi^4 S_0^2 \left(\frac{l}{d}\right)^4 \frac{\eta_m^2}{(1 - \eta_m)^3}}\right] \ldots [37]$$

The difference between these two solutions is the time taken for the shaft center to travel from one point to the other and must from symmetry equal half the period of the shaft center motion, which in turn is equal to half the period of the load cycle $1/N_p$. This gives the following relation between the value of η_m and N_p

$$\tan \frac{\pi}{4} \frac{N_j}{N_p} = 2\pi^3 S_0 \left(\frac{l}{d}\right)^3 \frac{\eta_m}{(1 - \eta_m)^{3/2}} \ldots\ldots [38]$$

Now η_m is not necessarily the maximum value η_{max} of η in its orbit, as may be seen for instance in Fig. 5(*b*). In cases where it is not, as in Figs. 5(*a*) and (*b*), η_{max} will fall at positions at right angles to η_m, i.e., at $\varphi = \pm\pi/2$. This turns out to be the case when $N_p < 1/3\, N_j$. Its relation to η_m can be found by use of Equation [16] with $\sin\varphi = \pm 1$, and k given by Equation [36]. This relation is as follows

$$\frac{\eta_m^2}{(1 - \eta_m)^3} = \frac{\eta_{max}^2}{(1 - \eta_{max})^3} - \frac{1}{\pi^2 S_0 \left(\frac{l}{d}\right)^2} \frac{\eta_{max}}{(1 - \eta_{max})^{3/2}} \ldots [39]$$

Finally, combining Equations [38] and [39], we arrive at the desired relation, namely

$$2\pi^2 S_0 \left(\frac{l}{d}\right)^2 \frac{\eta_{max}}{(1 - \eta_{max})^{3/2}} = 1 - \sec \frac{\pi}{4} \frac{N_j}{N_p}, \quad \frac{1}{4} < \frac{N_p}{N_j} < \frac{1}{2} \quad \ldots\ldots [40a]$$

$$2\pi^2 S_0 \left(\frac{l}{d}\right)^2 \frac{\eta_{max}}{(1 - \eta_{max})^{3/2}} = \tan \frac{\pi}{4} \frac{N_j}{N_p}, \quad \frac{N_p}{N_j} > \frac{1}{2} \quad [40b]$$

These equations show the dependence of the maximum eccentricity of the shaft under this type of loading on the frequency of load application.

Since from Equation [18*a*] the quantity

$$\frac{1}{2\pi^2 S_0 \left(\frac{l}{d}\right)^2 \frac{\eta_{max}}{(1 - \eta_{max})^{3/2}}}$$

equals unity for a constant load, this quantity can be considered as a relative load capacity, i.e., it is the ratio of the load that can be carried for any load-frequency ratio N_p/N_j to that for a constant load at the same eccentricity, and its value is the same for all eccentricities. This relative load capacity is shown graphically in Fig. 6 where it is plotted against the ratio N_p/N_j using Equations [40]. The principal conclusions from the equations and the figure are as follows:

(*a*) The relative load capacity is zero at the critical frequency where $N_p = N_j/2$.

(*b*) Above this frequency it increases indefinitely with increasing frequency. At high frequencies it asymptotically approaches the value $(4/\pi)(N_p/N_j)$.

(*c*) Below the frequency $N_p = N_j/4$ the journal center paths become more complicated, and the derivation given in the foregoing will not be applicable. However, the trend of the curve suggests that it probably approaches the constant-load value of unity at $N_p/N_j = 0$.

Similar conclusions were arrived at in the case of the infinitely wide bearing, and Fig. 6 is generally similar in shape to Fig. 9 of reference (6).[10] However, whereas in that case these conclusions had to be inferred from numerical integrations for particular values of the parameters and therefore lacked generality, they can be proved quite generally in the present case because of the existence of the analytical solution [40].

The square-wave loading is the only type for which an analytical solution so far has been found. For other types of loading, numerical integration seems to be necessary. As an example, Fig. 7 shows the journal center path under a sinusoidal alternating load having an amplitude $S_0 = 1.68$ (for which $\eta_0 = 0.7$) and a frequency $N_p = N_j$ for a bearing of $l/d = 1/8$. It is seen to be

[10] The present curve is somewhat lower. For instance, at $N_p/N_j = 1$, the relative load capacity is 1.0 instead of 1.25. See Table 1 of reference (6).

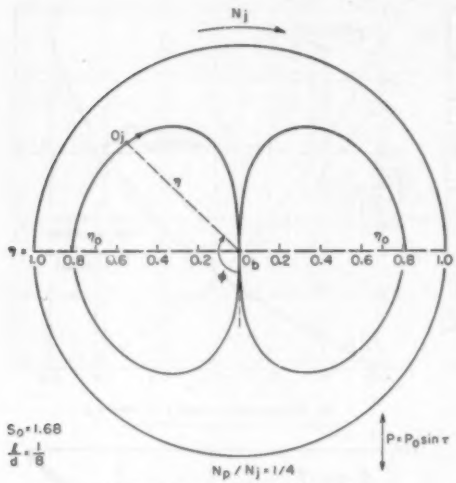

(a) For frequency ratio $N_p/N_j = 1/4$

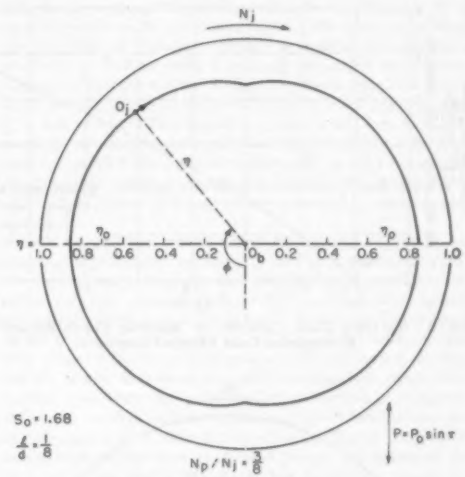

(b) For frequency ratio $N_p/N_j = 3/8$

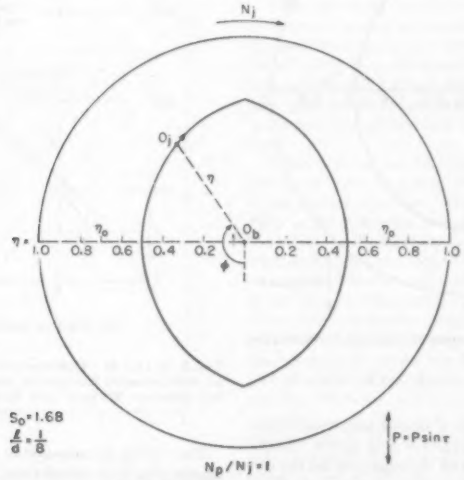

(c) For frequency ratio $N_p/N_j = 1$

FIG. 5 PATHS OF JOURNAL CENTER UNDER SQUARE-WAVE ALTERNATING LOAD

($S_0 = 1.68$, $\eta_0 = 0.7$, $l/d = 1/8$.)

generally similar in shape to that shown in Fig. 6(b) of reference (6)—the maximum eccentricity in this case being 0.68. Such orbits have been observed recently by Simons (16) in a bearing having $l/d = 1/2$.

DISCUSSION AND CONCLUSIONS

The question that naturally arises is in regard to the theoretical validity of the equations derived here, notably the load Equations [11], in view of the approximation that was made of neglecting the pressure flow in the direction of motion. As was pointed out at the beginning, no exact solution for the general case of a bearing of arbitrary width under dynamic loading now exists. Furthermore, there is every indication that its derivation would be so complicated and laborious that it is doubtful whether such a solution will be obtained in the near future. However, exact solutions for bearings of finite width have been obtained for the particular case of a constant fixed load. Such solutions have been obtained by Muskat and Morgan (3) for the case of an incomplete

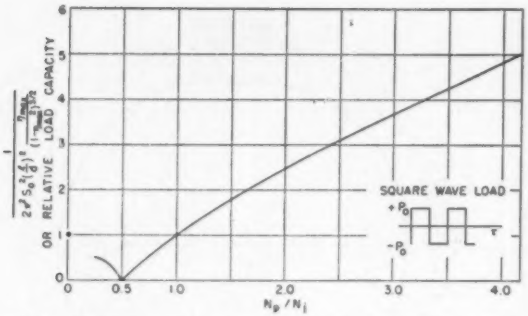

FIG. 6 RELATIVE LOAD CAPACITY OF BEARING UNDER SQUARE-WAVE ALTERNATING LOAD VERSUS FREQUENCY

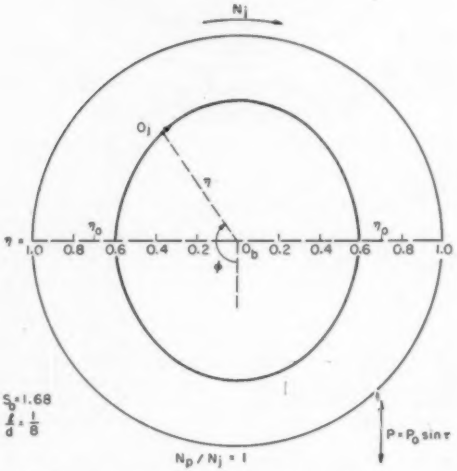

FIG. 7 PATH OF JOURNAL CENTER UNDER SINUSOIDAL ALTERNATING LOAD

($S_0 = 1.68$, $\eta_o = 0.7$, $l/d = 1/8$, $N_p/N_j = 1.$)

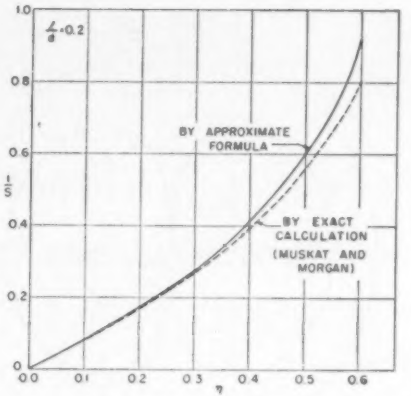

(a) Dimensionless load $1/S$ versus η

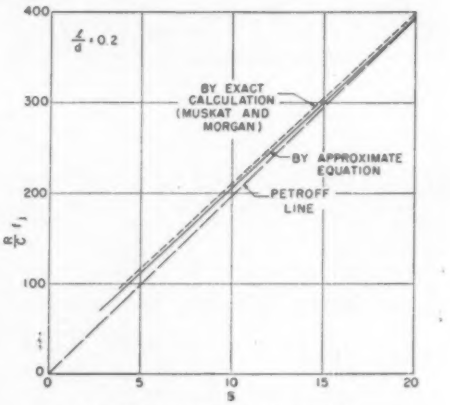

(b) Friction coefficient $(r/c)f_j$ versus S

FIG. 8 (a AND b) COMPARISON OF PERFORMANCE AS CALCULATED BY APPROXIMATE EQUATIONS FOR NARROW BEARING AND BY EXACT SOLUTION OF MUSKAT AND MORGAN ON ASSUMPTION OF A CONTINUOUS FILM

film for values of η up to 0.6, and by Cameron and Wood (4) for the case of an incomplete film for values of η up to 0.8. Therefore these do permit a comparison with the equations for the corresponding cases in the present work.

In Fig. 8(*a*), $1/S$ versus η from Equation [18*a*] is plotted for $l/d = 0.2$ for comparison with the exact results of Muskat and Morgan for the same case. The latter calculations stop at $\eta = 0.6$, but it is doubtful whether a continuous film would exist at higher eccentricities anyway. The two are seen to differ by about 10 per cent at $\eta = 0.6$, and only 2 per cent at $\eta = 0.3$, the Equation [18*a*] giving too high a value. This is probably because the pressure flow in the θ-direction which it neglects will relieve somewhat the pressure which would otherwise exist in the high-pressure region. Muskat and Morgan also calculated for this case that $\varphi = +\pi/2$ for all eccentricities, in agreement with Equation [18*b*].

The friction is compared in Fig. 8(*b*), where $(r/c)f_j$ is plotted against S for both calculations. This is obtained by substituting the required values of η and φ from Equations [18] into Equation [14*a*]. Muskat and Morgan used the same friction equation in the same way employing their own η versus S data. It is seen that the two agree more closely than do the values of $1/S$.

In Fig. 9(*a*) the same comparison is made between Equation [21*a*] and the exact results of Cameron and Wood for $l/d = 1/4$. (In this case it is more convenient to use as the abscissa the function $1/[1 - \eta] = c/h_0$ in order to spread out the scale at the higher eccentricities.) The approximate Equation [21*a*] is seen to predict a value of $1/S$ which is about 20 per cent too high at $\eta = 0.8$, but only 8 per cent too high at $\eta = 0.6$ and correspondingly less percentage error at smaller values of η.

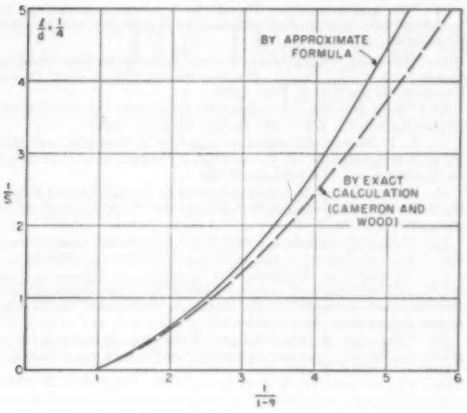

(a) Dimensionless load $1/S$ versus $\frac{1}{1-\eta}$

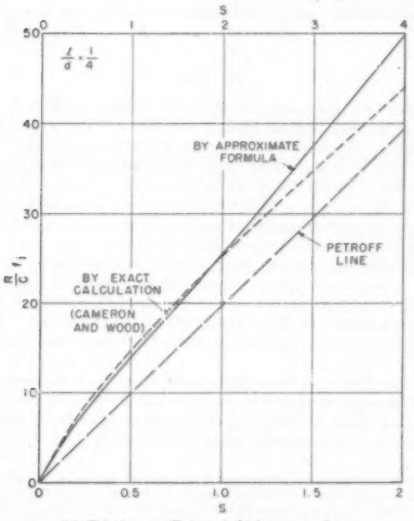

(b) Friction coefficient $(r/c)f_1$ versus S

FIG. 9 COMPARISON OF PERFORMANCE AS CALCULATED BY APPROXIMATE EQUATIONS FOR NARROW BEARING AND BY EXACT SOLUTION OF CAMERON AND WOOD ON ASSUMPTION OF AN INCOMPLETE FILM

The friction coefficients are compared in Fig. 9(*b*).[11] In contrast the error is seen to be less for larger values of $1/S$.

In both the foregoing cases the agreement should be better with narrower bearings because the approximation becomes increasingly more accurate as the bearing width decreases to zero. Therefore it appears that for bearings having widths $l = d/4$ or less, the present equations will predict the load capacity to an accuracy of about 20 per cent or better. For bearings in which the lubricant is supplied through a central circumferential groove, their load capacity is equal to the sum of two separate bearings of half the width. Hence the present equations should apply equally well to circumferentially grooved bearings with $l = d/2$ or less. This includes a great many connecting-rod bearings, especially in automobile and Diesel engines. Hence the present equations should be of considerable practical value in the design of such bearings through not requiring the application of side-leakage factors afterward as was necessary in references (6) and (7).

Even beyond the widths where the present equations are quantitatively accurate we may still infer from these results that the same qualitative features such as orbital motions of the shaft center, zero load capacity at $N_p = N_f/2$ and high load capacity at high load frequencies will still hold. This conclusion is based on the great similarity in the general form of the equations and their behavior for the present analysis of very narrow bearings and the former analysis of very wide bearings (6). When both extreme cases show the same qualitative features, it seems unlikely that bearings of intermediate width will behave very differently, and this is borne out by some of Simons' (16) experimental observations such as those of the orbital motion of the shaft center like that in Fig. 6. In fact, it might be possible by perturbation or other methods to calculate solutions for the intermediate case in terms of these two limiting solutions.

Where the results for the two limiting cases do differ, those for the narrow bearing are simpler and more exact. Examples are the load Equations [13] in terms of the function ξ which are exact for all values of η, the equations of motion, Equations [17] and [28], which could not be expressed analytically for the wide bearings, and the analytical relation, Equation [40], between the maximum eccentricity and load frequency for a square-wave load.

A final point of interest in the present equations lies in the fact that in the form, Equation [12], the performance is independent of the bearing diameter. This means that narrow bearings can carry as much average pressure as wider bearings provided that the clearance is reduced proportionately. Since, in large bearings particularly, the factors which practically limit the smallest clearance achievable are such things as elastic shaft deflection under load, misalignment, geometrical accuracy, and so forth, all of which are usually proportional to the bearing span[12] it follows that the maximum value of the ratio achievable should not depend markedly on the bearing width. Hence the average support pressure will be independent of bearing width and the load capacity, therefore, will vary with the width for a given shaft diameter. Actually, since the equations predict a somewhat higher pressure than an exact theory would because of the neglected pressure flow, it follows that the load capacity will not decrease as fast as the bearing width. These conclusions have an influence on the problem of designing sleeve bearings for very flexible shafts, such as in gas turbines, which may be subjected to high transient loads.

Falz (18) has discussed the practical considerations and methods of lubrication in substituting for ball or roller bearings, sleeve bearings which are equally narrow.

BIBLIOGRAPHY

1 "The Hydrodynamical Theory of the Lubrication of a Cylindrical Bearing Under Variable Load, and of a Pivot Bearing," by W. J. Harrison, Cambridge Philosophical Society, vol. 22, 1920, p. 373.

2 "Fluctuating Loads in Sleeve Bearings," by H. W. Swift,

[11] The friction Equation [14a] assumes a complete film for the viscous shear term, but it was used in these calculations because of the uncertainty as to the actual viscosity of the oil-air mixture in the broken film region. Cameron and Wood employ the same equation so that the two results should be comparable.

[12] This will not be true of surface finish but this factor is not usually critical in large bearings.

Journal of The Institution of Civil Engineers, vol. 5, 1937, pp. 161–195.

3 "Studies in Lubrication," by M. Muskat and F. Morgan, *Journal of Applied Physics*, vol. 9, 1938, pp. 393–409; vol. 10, 1939, pp. 46–61; vol. 10, 1939, pp. 398–407.

4 "The Full Journal Bearing," by A. Cameron and Mrs. W. L. Wood, Proceedings of The Institution of Mechanical Engineers, vol. 161, 1949, pp. 59–64.

5 "Characteristics of Centrally Supported Journal Bearings," by E. O. Waters, Trans. ASME, vol. 64, 1942, pp. 711–719.

6 "The Calculated Performance of Dynamically Loaded Sleeve Bearings," by J. T. Burwell, JOURNAL OF APPLIED MECHANICS, Trans. ASME, vol. 69, 1947, pp. A-231–245.

7 "The Calculated Performance of Dynamically Loaded Sleeve Bearings—II," by J. T. Burwell, JOURNAL OF APPLIED MECHANICS, Trans. ASME, vol. 71, 1949, pp. 358–360.

8 "Die Schmierung ebener Flächen," by A. G. M. Michell, *Zeitschrift für Mathematik und Physik*, vol. 52, 1905, pp. 123–138.

9 "Some Practical Deductions From the Theory of Lubrication of Short Cylindrical Bearings," by S. E. Cardullo, Trans. ASME, vol. 52, Paper No. MSP-52-12, 1930, pp. 143–153.

10 "Hydrodynamic Lubrication of Sleeve Bearings Subject to Varying Loads," by J. T. Burwell, *Lubrication Engineering*, vol. 4, 1948, pp. 67–71 and 74.

11 "Zur hydronamischen Theorie der Schmiermittelreibung," by A. Sommerfeld, *Zeitschrift für Mathematik und Physik*, vol. 50, 1904, pp. 97–153.

12 "Effect of Misalignment on Plain Bearings at High Rotative Speeds," by F. W. Ocvirk, Progress Report No. 6 from Cornell University to the NACA, June, 1950.

13 "Über den Schmiervorgang im Gleitlager," by W. Nücker, Forschungsheft No. 352 (VDI), Berlin, Germany, 1932.

14 J. T. Burwell discussion of paper by A. Cameron and Mrs. W. L. Wood, reference (4), Proceedings of The Institution of Mechanical Engineers, vol. 161, 1949, pp. 67–68.

15 "Fundamental Mechanical Aspects of Thin Film Lubrication," by H. Blok: Symposium on Lubrication, New York Academy of Sciences, March, 1950.

16 "The Hydrodynamic Lubrication of Cyclically Loaded Bearings," by E. M. Simons, Trans. ASME, vol. 72, 1950, pp. 805–816.

17 "Zylindrische Gleitlager bei instationarer Belastung," by H. H. Ott, *Mitteilungen aus dem Institut für Thermodynamik und Verbrennungsmotorenbau an der Eidgenös.* Technische Hochschule, Zurich, Switzerland, No. 7, 1948.

18 "Gleitlager als Austausch für Wälzlager," by E. Fals, *Zeitschrift des Vereines deutscher Ingenieure*, vol. 88, 1944, pp. 573–579.

The Theory of Plasticity Applied to a Problem of Machining[1]

By E. H. LEE[2] and B. W. SHAFFER[3]

The recently developed methods of analyzing stress and strain distributions in the plane plastic flow of an ideally plastic material are applied to the problem of machining. It is shown that the idealized stress-strain relationship involves justifiable assumptions for this application. Analytical expressions are obtained for orthogonal machining which give the machining force, the chip thickness, and the chip deformation in terms of the tool geometry, the relevant coefficients of friction, and the appropriate yield stress of the work. With increasing friction at the tool face or decreasing rake angle the development of a built-up nose arises naturally as a consequence of the analysis. The theory includes this phenomenon. The results of this theory are compared with published experimental results, and with other theoretical analyses. Satisfactory agreement with experiment is obtained.

Introduction

We shall consider the case of orthogonal machining in which the tool has a single straight cutting edge perpendicular to the direction of motion. A new surface is generated parallel with the original surface.

The usual case is considered, in which the depth of cut is small compared with the length of the cutting edge. Deformation is then predominantly in plane strain, apart from an edge effect where some sideways spread occurs. We can therefore apply the theory of plastic flow in plane strain which has been extensively developed in recent years.

Only machining with continuous chip formation will be considered. Such a chip is normally obtained in the machining of ductile materials, and is the type of chip most commonly encountered in practice.

The theory to be used assumes an ideally plastic material which does not work-harden. This is known to be a good approximation for iron and steels at high strain rates such as occur in machining (1, 2, 3).[4] However, this theory has been found to give satisfactory agreement with experiment even using lead (4), which has a rounded stress-strain curve, so that the theory which will be developed in the paper also can be expected to provide a useful approximation for materials other than steel.

In machining under normal conditions, strains of the order of magnitude unity occur. The elastic yield-point strain of most materials is of the order 10^{-3}, and, therefore, can be safely neglected in analyzing the large plastic deformation. Thus we can adopt the rigid-plastic type of theory in which material subjected to strains of elastic order only is considered rigid. The basic equations for this type of analysis have appeared in recent papers (4, 6) and will not be repeated here. The stresses must satisfy the equilibrium equations, for inertia forces are negligible, and the yield condition in the region of plastic flow. The velocity field of flow must determine strain rates which satisfy the Mises flow condition. A complete solution satisfies the stress and velocity equations, the boundary conditions in stress and velocities, including the boundary velocities determined by the motion of the rigid regions, and the condition that stresses transmitted from the plastic regions must be capable of being withstood by the rigid regions without producing large plastic flow. The latter condition can often be checked without calculating the stress distribution in the elastic regions, by considering an extension of the plastic stress field into the rigid regions to ascertain that a stress field with stress less than or equal to the yield stress is possible. It is found following Hencky (9) most convenient to consider the solution in terms of the orthogonal net of slip lines or trajectories of maximum shear stress which satisfy simple geometrical relations and permit the stress and velocity equations to be written in a simple form.

Machining Without a Built-Up Nose

Let us consider the application of the theory discussed in the previous section to the problem of machining.

A point in the material to be removed is initially unstressed when it is some distance ahead of the tool. As the tool approaches it the stress builds up until it reaches the yield limit. The particle then enters a region of high strain rate where plastic deformation occurs, deforming the material of the work into the form of a chip. In this process the work material has been set in motion and is now moving up the face of the tool. As it leaves the nose of the tool the chip is free apart from its continuity with the work material, through the elements behind it, and the stress falls off to zero. A stress field which performs this operation, and which will be shown to satisfy the equations of plastic flow is shown in Fig. 1.

Both sets of slip lines are straight, the two systems being parallel with AC and DB, respectively. The configuration of the field is determined by the tool rake angle γ, and by $\measuredangle DBC = \eta$, which will be shown to be associated with friction conditions at the tool face. The scale of the figure is determined by the depth of cut t_1.

It will be shown that in this solution plastic flow occurs entirely across the shear line AC, the triangle ABC being a fictitious plastic field which is the limit of a rigid region. The reason for the consideration of the slip-line field in ABC is associated with the need to examine the transmission of the ma-

---

[1] The results presented in this paper were obtained in the course of research conducted at Brown University under Contract N7onr-358 sponsored jointly by the Office of Naval Research and the Bureau of Ships. This paper is a condensation of a report (5)[4] in which a fuller discussion is given of the type of solution adopted, and its justification for this problem.

[2] Associate Professor of Applied Mathematics, Graduate Division of Applied Mathematics, Brown University, Providence, R. I. Mem. ASME.

[3] Assistant Professor of Mechanical Engineering, New York University, New York, N. Y. Jun. ASME.

[4] Numbers in parentheses refer to the Bibliography at the end of the paper.

Contributed by the Applied Mechanics Division and presented at the Annual Meeting, Atlantic City, N. J., November 25–30, 1951, of The American Society of Mechanical Engineers.

Discussion of this paper should be addressed to the Secretary, ASME, 29 West 39th Street, New York, N. Y., and will be accepted until January 10, 1952, for publication at a later date. Discussion received after the closing date will be returned.

Note: Statements and opinions advanced in papers are to be understood as individual expressions of their authors and not those of the Society. Manuscript received by ASME Applied Mechanics Division, October 24, 1949. Paper No. 51—A-5.

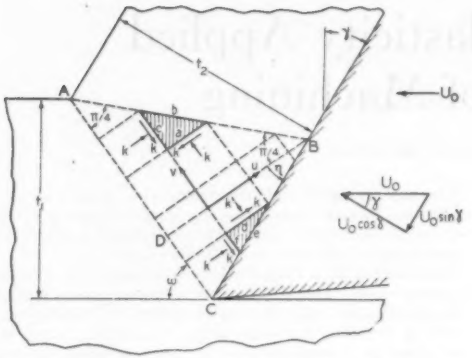

FIG. 1 SLIP-LINE FIELD CONFIGURATION WITH NO BUILT-UP NOSE

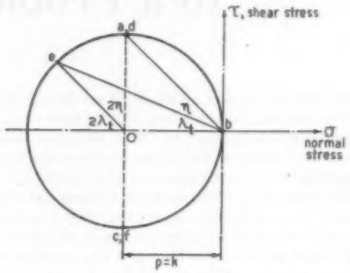

FIG. 2 CORRESPONDING MOHR'S CIRCLE DIAGRAM

chining force between the tool face and the shearing surface AC. An extension of the plastic field below AC is not considered, since it is apparent from the configuration of the boundaries of the material that the spread of the machining force into the work material below AC presents no difficulties. In certain circumstances the transmission of the machining force through the chip does not lead to critical stress conditions either. In these cases, only the line of shear AC need be considered, its direction being chosen to give the minimum machining force. This type of solution has been developed by Ernst and Merchant (10) and its range of application will be considered in a later section.

The form of Fig. 1 is associated with the simple velocity boundary conditions: (*a*) The material ahead of the tool is rigid and at rest; (*b*) The tool is moving with uniform velocity; and (*c*) the chip must leave the plastic region as a rigid body.

Let us consider the stress distribution. Since the slip lines are straight, the stress distribution is uniform in ABC.

According to the present theory, which considers elastic material to be rigid, the chip above AB is subjected to no forces, and so no stress is transmitted across AB. The zero shear across AB determines that the slip lines are inclined at $\pi/4$ radians with this line.

The uniform stress field, ABC, can perhaps best be studied by means of Mohr's circle diagram[5] which is shown in Fig. 2. The maximum shear-stress condition determines the radius of the Mohr's circle to be k, and the zero traction on AB determines that it should pass through the origin. There are two possible circles satisfying these conditions, one in which all normal stress components are tensile and the other in which all are compressive, but it is obvious in this case that the stresses ahead of the tool are compressive, so that Fig. 2 shows the appropriate choice.

The points marked in Fig. 2 represent the stresses on the corresponding elements in Fig. 1. The normal stress on the slip lines is determined by the abscissa of the center of the circle to be equal to k, for the slip-line directions lie on the vertical diameter of the Mohr's circle, as shown. The traction at the tool face BC is given by the point e. According to the construction of the Mohr's circle diagram, $\angle doe$ is equal to 2η, where η is the angle DBC in Fig. 1.

From Fig. 2 the friction conditions at the tool face can be determined. The traction on BC is given by the point e, the ordinate of which gives the shear stress, and the abscissa the normal stress. The ratio of these stresses gives the coefficient of friction at the tool face, $\mu_t = \tan \lambda_t$, so that λ_t, the angle of friction, is given by $\angle ebo$. But $\angle ebd$ is equal to η, since the angle subtended by a chord at the circumference is one half the angle subtended at the center. Also $\angle obd = \pi/4$, so that

$$\eta = \frac{\pi}{4} - \lambda_t \qquad [1]$$

Let us now consider the magnitude of the angle ω at which AC is inclined to the horizontal. This angle is called the shear angle and its magnitude has received considerable attention in the study of machining. BD is inclined at the angle $(\eta + \gamma)$ with the vertical, and this is equal to ω, since AC is perpendicular to BD. Thus we have, using Equation [1]

$$\omega = \eta + \gamma = \frac{\pi}{4} - \lambda_t + \gamma \qquad [2]$$

Thus the shear angle ω increases with the rake angle γ, and decreases with increasing friction at the tool face.

Let us now consider the velocity distribution. The velocity components u and v along the slip lines are shown in Fig. 1. The tool is moving to the left with velocity U_0 and the work below AC is at rest.

Continuity of the material across AC requires the normal component of the velocity of the particles to be equal on either side of this line. Since this is zero for the material at rest below AC, u, the velocity normal to AC, is zero along AC. For straight slip lines, Equation [5] of (6) then determines u to be zero throughout the field ABC.

Consider now contact conditions between the tool and the work along BC. Since the tool exerts a pressure against the chip along this line, they are in contact, and the components of the velocity of each, normal to BC, must be the same. Since u is zero, this requires

$$v \cos \eta = U_0 \cos \gamma \qquad [3]$$

Since u and v are both constant in ABC, it moves as a rigid body, and no plastic strain is taking place in it. Across AC there is a discontinuity of magnitude v in the tangential component of velocity. It is this discontinuity of velocity, corresponding to a line of infinite strain rate, which produces the plastic deformation in the chip.

Continuity of velocity across AB determines the motion of the chip to be that of ABC, so that it slides up the tool face CB extended. The curling away from the tool, which is observed in practice, is associated with residual stress and thermal strain

[5] This construction is presented in (8) pp. 15–20.

conditions which are not considered in the present rigid-plastic analysis.

Thus the configuration shown in Fig. 1, with plastic deformation occurring at AC, and a region of limiting stress in ABC, satisfies the stress and velocity conditions of the problem. Let us consider what this implies in terms of quantities which can be checked by experiment—the force on the tool and the chip thickness.

The horizontal component of the force on the tool is the most significant force variable, for it determines the power expended in machining. The total force on the tool can best be obtained by using the fact that ABC is in equilibrium, and so writing the tool force equal to the force transmitted across AC. According to Fig. 2, the shearing and normal stresses on AC are both equal to k. Since the depth of cut $t_1 = AC \sin \omega$, the components of the total force along and normal to AC are both $(kt_1)/(\sin \omega)$. By making use of Equation [2], the horizontal component of this force may be written

$$F_t = kt_1 [1 + \cot \omega] = kt_1 \left[1 + \cot \left(\frac{\pi}{4} - \lambda_t + \gamma\right)\right] \quad \ldots [4]$$

In Fig. 3 $(F_t)/(kt_1)$ is plotted against the angle of friction λ_t for tools with different rake angles γ. The form of Equation [4] indicates that these are all identical curves displaced from each other along the λ_t axis by the amount γ. For convenience an auxiliary scale of μ_t, the coefficient of friction, is shown.

It is seen that, according to this solution, the machining force

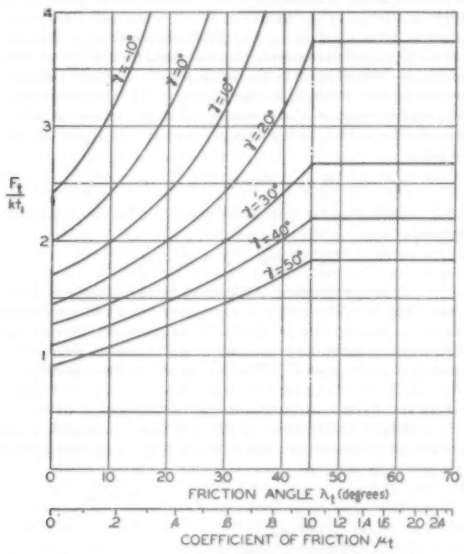

FIG. 3 MACHINING FORCE AS A FUNCTION OF FRICTION FOR VARIOUS TOOLS WITHOUT A BUILT-UP NOSE

F_t increases with increasing friction, and decreases with increasing rake angle γ.

It will be observed that in Fig. 3 force curves of constant magnitude have been drawn for $\lambda_t > \pi/4$. When $\lambda_t = \pi/4$, it is clear from Fig. 2 that the frictional shear at the tool-chip interface is equal to k, the maximum which the chip material can transmit. For larger values of λ_t, shear flow of the chip material occurs where it is in contact with the tool face, rather than frictional slip between the chip and the tool.

The component of the machining force F_n, normal to the surface of the work, is given by the corresponding component of the traction on AC

$$F_n = kt_1 [\cot \omega - 1] \quad \ldots [5]$$

The chip thickness t_2, shown in Fig. 1, is equal to $AC \cos \eta$, since AC is perpendicular to BD. Thus by making use of Equations [1] and [2] we have

$$t_2 = t_1 \frac{\cos \eta}{\sin \omega} = t_1 \frac{\cos \left(\frac{\pi}{4} - \lambda_t\right)}{\sin \left(\frac{\pi}{4} - \lambda_t + \gamma\right)} \quad \ldots [6]$$

In Fig. 4 the chip-thickness ratio $r = t_2/t_1$, is plotted against the angle of friction λ_t for tools with various rake angles. As

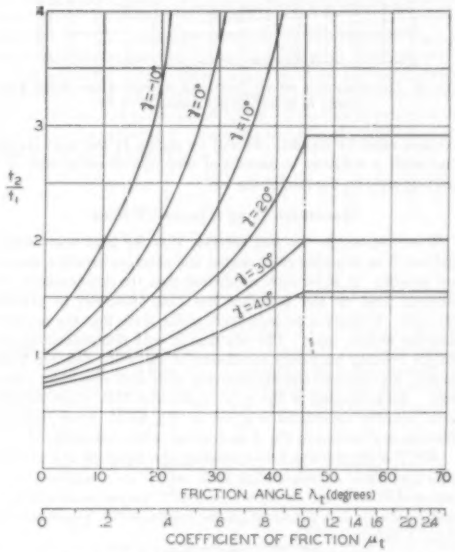

FIG. 4 CHIP-THICKNESS RATIO AS A FUNCTION OF FRICTION FOR VARIOUS TOOLS WITHOUT A BUILT-UP NOSE

for F_t, r is seen to increase with increasing friction below $\lambda_t = \pi/4$, and to decrease with increasing rake angle. It also takes on a modified form for $\lambda_t > \pi/4$.

Since the solution gives particle velocities at all points in the field, the deformation of an initially square network embedded in the work material can be obtained, and an example is shown in Fig. 5. It can be seen that simple shear occurs across the shear line, and that lines initially parallel to the surface lie longitudinally in the chip.

A study of this solution shows at once that it cannot apply for all possible values of λ_t and γ, for $\sin (\pi/4 - \lambda_t + \gamma)$, which in effect appears in the denominators of the expressions for both F_t and r (Equations [4] and [6]), can be zero for reasonable values of γ and λ_t. The solution then determines F_t and r both to be infinite. The reason for this difficulty, associated with zero and

negative values of the argument $(\pi/4 - \lambda_t + \gamma)$, can be appreciated from Fig. 1, since this argument is equal to the shear angle ω. It is thus clear that for certain conditions, namely, small or negative rake angles and high friction, another

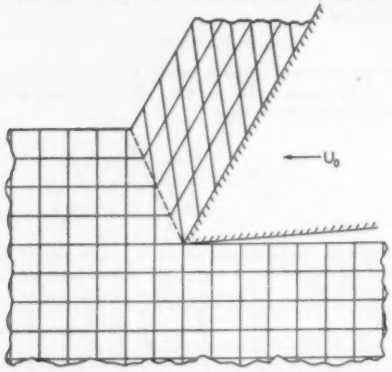

FIG. 5 DEFORMATION OF AN INITIALLY SQUARE GRID WITH FRICTION; $\lambda_t = 35°$, RAKE ANGLE $\gamma = 30°$

solution must be sought. It will be shown in the next section that such a solution is associated with the development of a built-up nose on the face of the tool.

MACHINING WITH A BUILT-UP NOSE

It was shown in the last section, that for high tool friction and small or negative rake angles, the solution detailed there is not tenable. It is for such conditions that the development of a built-up nose on the tool face has been observed in practice (11, 12). This gives an indication of the form that the modified solution should take. The solution is still determined by the simple velocity boundary conditions of the work material being at rest, and the tool and chip moving with their respective velocities. An indication of the type of slip-line field which satisfies such velocity conditions is given in (6), which determines the slip-line field shown in Fig. 6 as detailed in the following:

$ABCF$ is the slip-line field consisting of a region ACF of circular arcs and their corresponding radii added to a uniform stress region ABC. It will be shown that ABC moves as a rigid body, and so that it is a fictitious plastic region which represents the

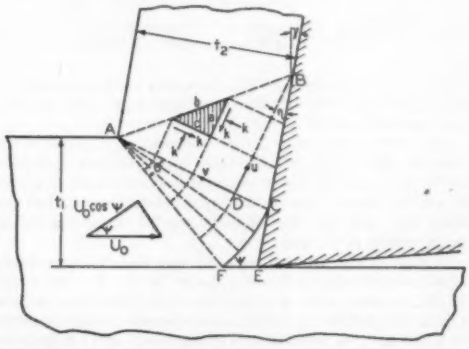

FIG. 6 SLIP-LINE FIELD CONFIGURATION WITH A BUILT-UP NOSE

limit of a rigid region. The rigid region CFE takes the form of a built-up nose on the face of the tool, and it is considered to be in a limiting state of stress near the apex F under the shear stress along FC and the friction on FE. This is assumed since a reduction in ψ, the apex angle at F, would reduce the machining force but increase the stress intensity in the nose. The balance, therefore, can be expected to produce minimum ψ consistent with a permissible stress distribution in the nose. The development of such a nose in practice is shown by Herbert (11), and is thought to occur in the early transient stages of a cut. Initial deposits on the tool will produce smaller friction forces at first, and as friction builds up, material will be accumulated both from the chip and from the work surface which passes under the tool. The analysis of the configuration of Fig. 6 shows that the presence of a built-up nose, even though its dimensions are small compared with the depth of cut, can have a large influence on the machining force and chip thickness.

For the case of a built-up nose, there is no solution corresponding to that of Ernst and Merchant (10), in which the stress in ACB is not critical, for a study of the stress distribution shows the nose material close to C also to be in a limiting state of stress, which does not permit the angle ACB to be increased without exceeding the limiting shear stress there.

Let us consider the stress distribution corresponding to Fig. 6. As in the case of the solution without a built-up nose, the boundary AB merely supports the free chip without having any surface tractions applied across it. As in Fig. 2, this determines the uniform stress distribution in ABC, and leads to the expression given in Equation [1] for the angle η in terms of the angle of friction at the tool face, λ_t. The normal stress on the slip line AC is equal to k. The equilibrium equation, Equation [2] of (6), then determines the normal stress over AF to be equal to $k(1 + 2\theta)$, where θ is the angle FAC. Now AC, which is perpendicular to BD, is inclined at $(\eta + \gamma)$ to the horizontal. The configuration at F determines AF to be inclined at $\pi/2 - \psi$ to the horizontal, so that θ is given by the difference of these angles

$$\theta = \pi/2 - \psi - \eta - \gamma \quad \ldots\ldots\ldots\ldots [7a]$$

By substituting for η from Equation [1], this expression becomes

$$\theta = \pi/4 - \psi + \lambda_t - \gamma \quad \ldots\ldots\ldots\ldots [7b]$$

The stress system along AF is given by the Mohr's circle diagram, Fig. 7. The point G represents the stress components acting on the slip line FC at F. It was shown previously that this limiting stress also applies to the region of the built-up nose close to the apex F. Thus the stress components acting at F on the base of the nose FE are given by the point H in Fig. 7, where the Mohr's circle construction determines $\angle GPH$ to be equal to 2ψ. The traction on FE at F must be consistent with friction conditions there. Let λ_n be the angle of friction between

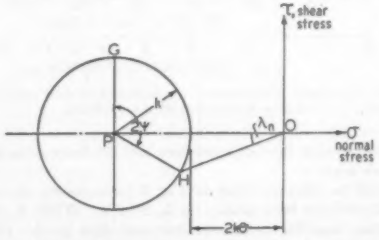

FIG. 7 CORRESPONDING MOHR'S CIRCLE DIAGRAM FOR AF

the two regions of the work material in contact along FE. Since the tool is moving to the left, the friction force on the nose must be directed from F to E. According to the sign convention used in Mohr's circle diagram, this requires H to have a negative ordinate, which implies that $\psi \geq \pi/4$, where the equality sign corresponds to no friction. Since the normal and shear-stress components across FE at F are given by the abscissa and ordinate of H, $\angle HOP$ must be equal to the angle of friction λ_s. It is of interest to observe that since the shear angle at which AF is inclined to the horizontal must be positive as shown in Fig. 6, ψ must be less than $\pi/2$.

Thus, given the rake angle γ, and the angles of friction λ_t and λ_n, the stress field, Fig. 6, is determined, for η is given by Equation [1] in terms of λ_t, and the friction condition on FE determines ψ according to Fig. 7. Figs. 2 and 7 can be combined to give the graphical means of solution shown in Fig. 8. Here,

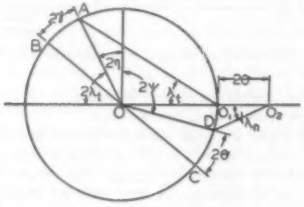

FIG. 8 COMBINED MOHR'S CIRCLE DIAGRAMS

unit radius is used for the Mohr's circle since the magnitude of k does not influence this aspect of the solution. A single circle is used to represent both Figs. 2 and 7, the corresponding origins of stress co-ordinates being O_1 and O_2, respectively. Point A, which determines the tractions at the tool chip interface, is determined by the angle of friction $\lambda_t = \angle AO_1O$. The stress components on a vertical plane in this uniform stress region are given by B, where $\angle AOB = 2\gamma$, for the tool face is inclined at the rake angle γ to the vertical. Using the origin O_2, the tractions on the horizontal base are given by OD which is rotated $(\pi + 2\theta)$ from OB to change from the vertical plane to the horizontal, and to compensate for the rotation of the stress system at the nose apex by θ relative to that in the uniform-stress region. For a particular problem, the origin O_2 as well as the point D is found by drawing a set of parallel lines inclined at the friction angle λ_n with the normal stress axis, and then picking out the particular line for which the arc length CD is equal to the distance from O_1 to O_2. Thus the angle θ is determined, and so is the solution.

When θ has been obtained, the configuration of the slip-line field is determined, its scale being given by the depth of cut t_1.

In considering the velocity solution, it is advantageous to superpose on the entire system the velocity U_0, equal and opposite to the tool velocity. This brings the tool to rest, with the undeformed work material approaching it with velocity U_0. Application of Equation [5] of (6), in combination with the boundary conditions, then determines the slip-line velocity components u and v shown in Fig. 6. Thus v is zero throughout AFC.

$$u = U_0 \cos \psi \qquad [8]$$

throughout the plastic field, and

$$v = U_0 \cos \psi \tan \eta \qquad [9]$$

in ABC. Continuity of velocity across AB determines maintenance of contact between the chip and the tool along the tool face above B.

Thus all conditions of the problem are satisfied by the solution depicted in Fig. 6. Let us now consider the machining force and chip thickness corresponding to this solution. Since the region $ABCF$ is in equilibrium, and there are no forces transmitted along AB, the force applied at the tool face FCB is equal to the force along AF. By obtaining the tool force in this way, integration along the arc FC is avoided and the calculations are simplified. The horizontal component of the force on AF, F_t', is then determined as in the case without a built-up nose, and is given by the relationship

$$F_t' = kt_1 (1 + 2\theta + \tan \psi) \qquad [10]$$

where θ is given by Equations [7].

To obtain the total machining force applied to the tool, we must add to F_t', the frictional force F_t'', acting on the base of the built-up nose FE. The magnitude of the shear stress close to the apex F is given by the ordinate of H in Fig. 7, but along the line FE there will be some variation due to the distribution of stress in the nose. This would be difficult to calculate, since the nose is expected to be stressed only elastically in the region where it is supported by the tool face along CE. However, traction on CE is responsible for only a minor part of the total machining force, so that it will be sufficiently accurate to assume the known traction on FE at F to apply all along FE. Thus the shearing stress on FE has the magnitude $-k \cos 2\psi$, according to Fig. 7, and the corresponding horizontal force is

$$F_t'' = -\frac{kt_1 \cos 2\psi}{\cos \psi \cos \gamma} \left[\cos \left(\frac{\pi}{4} - \lambda_t \right) - \sin (\psi + \gamma) \right] \qquad [11]$$

The total machining force F_t is given by

$$F_t = F_t' + F_t'' \qquad [12]$$

where the individual terms are given by Equations [10] and [11].

The component of the machining force F_n, normal to the surface of the work, is given by the corresponding component of the traction across AF in Fig. 6, combined with the pressure on the base of the built-up nose. As in the case of the shear stress, we assume the pressure on FE to be constant and equal to that at F, giving

$$F_n = kt_1 \left[(1 + 2\theta) \tan \psi - 1 + \frac{\sin \left(\frac{\pi}{4} + \lambda_t \right) - \sin (\psi + \gamma)}{\cos \psi \cos \gamma} (1 + 2\theta - \sin 2\psi) \right] \qquad [13]$$

The chip thickness ratio, $r = t_2/t_1$, can be obtained from the geometry of Fig. 6, for $AF = AC = t_1/\cos \psi$, and, since AC is perpendicular to BD, $t_2 = AC \cos \eta$. We thus have

$$t_2 = \frac{t_1 \cos (\pi/4 - \lambda_t)}{\cos \psi} \qquad [14]$$

On the basis of the velocity solution, the deformation of an initially square grid scribed on the work material can be calculated. Fig. 9 shows a particular case with $\gamma = 10$ deg, $\lambda_t = 30$ deg, and $\mu_n = 0$. Finite shear occurs across AF in Fig. 6, and also across AC unless $\lambda_t \geq \pi/4$. Shearing also takes place in the region AFC. However, the simple form which the velocity solution takes of constant u and zero v in AFC, produces uniform shear in the chip above AC.

The stress and velocity solution for machining with a built-up nose, which has been detailed in this section, provides a satisfactory solution for certain ranges of the variables. The manner

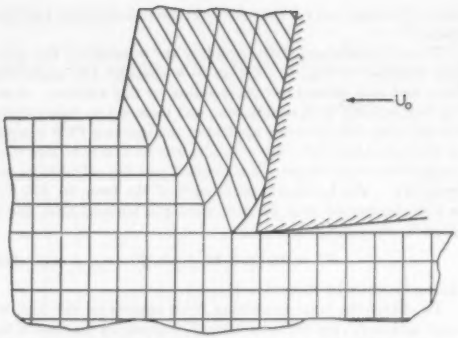

FIG. 9 DEFORMATION OF AN INITIALLY SQUARE GRID WITH BUILT-UP NOSE; $\lambda_t = 30$ DEG, $\mu_m = 0$, $\gamma = 10$ DEG

in which it can be integrated with the solution for no built-up nose, to cover the entire range of possible variables, is dealt with in the next section.

THE COMPOSITE SOLUTION

In the previous sections two complete solutions of the stress and velocity distributions in machining have been given. For certain ranges of the variables the nonbuilt-up-nose solution was shown to involve machining forces and chip-thickness ratios which increased without limit. The built-up-nose solution applies only for certain ranges of the variables. In this section we shall show that use of both types, in combination with the solution due to Ernst and Merchant (10), determines a satisfactory set of solutions for all possible ranges of the variables.

Let us first compare the solution due to Ernst and Merchant (10) with our nonbuilt-up-nose solution, for they are both based on simple shear across a single plane. Ernst and Merchant assume that the maximum shear stress k occurs on a single plane, and choose its direction so that the machining force F_t is a minimum. The direction is given by φ', the shear angle at which the slip plane is inclined to the horizontal. This corresponds to ω in Fig. 1. The minimum condition is shown in (10) to give

$$\varphi' = \frac{\pi}{4} - \frac{\lambda_t}{2} + \frac{\gamma}{2} \quad \ldots\ldots [15]$$

With the corresponding machining force

$$F_t = 2kt_1 \cot \varphi' \quad \ldots\ldots [16]$$

From the solution in an earlier section, ω is given by Equation [2]

$$\omega = \frac{\pi}{4} - \lambda_t + \gamma$$

Thus

$$\varphi' - \omega = \tfrac{1}{2}(\lambda_t - \gamma) \quad \ldots\ldots [17]$$

But ω determines a limiting stress field in the chip, such that the transmission of the machining force produces the maximum permissible shearing stress k. Thus φ' determines an acceptable solution only when $\varphi' < \omega$, or $\lambda_t < \gamma$, according to Equation [17], for otherwise the chip material cannot transmit the force corresponding to this solution. This consideration can perhaps be most easily visualized by considering the special case of a frictionless tool. In Fig. 1, AC then makes an angle of $\pi/4$ with BC. The full shear stress k has to be supported on AC with only normal stress on BC.

Consider the situation in the region of C, as illustrated in the Mohr's circle diagram, Fig. 10. The stress point AC has the ordinate k, equal to the shear stress across AC in Fig. 1. The stress point CB, corresponding to CB in Fig. 1, must lie on the σ-axis since there is no tool frictional stress. It is only possible to join such points with a Mohr's circle of radius not greater than k, by choosing the radius to be k, and the radii to the two stress points to be inclined at $\pi/2$. This corresponds to an angle

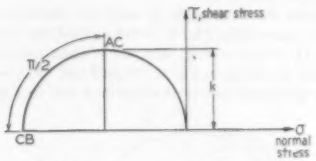

FIG. 10 MOHR'S CIRCLE FOR THE LIMITING CHIP STRESS

of $\pi/4$ between the planes AC and BC in Fig. 1. If $\angle ABC$ is less, then no stress configuration can be found.

For larger angles the shear stress can be transmitted as normal pressure on a plane at $\pi/4$ to AC, and the additional wedge of material could be considered to carry this pressure while subjected only to hydrostatic pressure with no shearing stresses. In practice, of course, such distributions would interact to produce an elastic solution throughout. Thus, in this case, $\pi/4$ is the smallest possible value for $\angle ACB$, and this corresponds to the largest possible shear angle ω. The same argument applies in the case of tool friction, when again ω is the largest possible shear angle, and φ' is only admissible if $\varphi' < \omega$. This consideration shows that while Ernst and Merchant were correct in seeking a minimum for the machining force, the minimum must be sought under the subsidiary condition that it is associated with a satisfactory stress distribution in the chip. According to the present theory, the subsidiary condition takes control when $\gamma < \lambda_t$, or, according to Equations [15] and [16], when $F_t/kt_1 > 2$.

If we use the expressions developed in this paper to consider the variation of the machining force for a tool of given rake angle γ, and given nose base angle of friction λ_t, for increasing values of λ_t, a continuous curve is obtained as indicated schematically in Fig. 11. In the range AB no built-up nose occurs because the

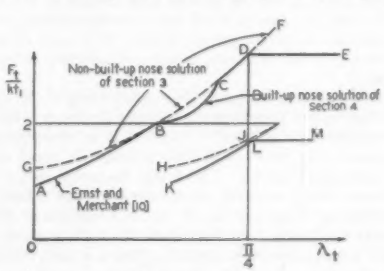

FIG. 11 VARIATION OF MACHINING FORCE WITH TOOL FRICTION (Given rake angle γ, and given nose base friction coefficient μ_m.)

tool-face friction is too small. BC corresponds to the existence of a built-up nose, and, in this range, calls for a machining force smaller than the appropriate nonbuilt-up-nose solution indicated by the broken line. A built-up nose, therefore, would occur in

this range. At C the nose-base friction inhibits the development of a built-up nose, and the simple shear solution applies in the range CD. For values of $\lambda_i > \pi/4$, shear failure rather than friction occurs at the tool-chip interface, and the rigid-plastic solution remains identical with that corresponding to $\lambda_i = \pi/4$.

The point B is the limiting point at which the Ernst and Merchant solution was shown herein to be valid. Thus AB in Fig. 11 is given by Equation [16]. The limiting chip-stress nonbuilt-up-nose solution is given by the broken line GB, which does not apply in this region. For tool friction higher than that corresponding to B, the limiting chip-stress solutions apply.

For particular values of γ and λ_i, two or only one of the types of solution AB, BC, or CD may occur. Solutions corresponding to DE always arise for $\lambda_i > \pi/4$.

A comparison of this theory of machining with other theories, and with published experimental measurements is given in the next section. Before turning to these, we attempt to assess the influence of elasticity.

It was pointed out in the foregoing that since plastic strains of the order of magnitude unity occur in machining, it would be permissible, in making a study of the plastic deformation, to consider elastic material to be rigid. The extent of the rigid regions, however, does influence the plastic region, and the validity of the rigid regions is studied by considering the extension of the plastic stress field into them. For example, in Fig. 6, ABC is subjected to uniform compression which determines pressure on the tool along CB, but not above B. In fact, the effect of the elastic resilience of the chip material will be to smooth out the discontinuity in pressure at B, extending the region of pressure further up the tool face. However, this will not have an appreciable influence in the neighborhood of C, and so will have only a minor effect on the over-all solution. With the usual friction condition at the tool face this spreading of the pressure will not change the ratio of over-all normal to tangential force.

For the case $\lambda_i > \pi/4$, that is, when failure occurs in the chip material at the tool face in place of frictional slip, spreading of the pressure region will increase the over-all frictional force, causing an increase in the machining force over that given by the rigid-plastic type of solution. Thus in Fig. 4 the effect of elasticity is expected to be negligible for $\lambda_i < \pi/4$. However, in the region where $\lambda_i > \pi/4$, some increase of force is expected with increase of λ_i.

Comparison With Experiment and With Other Theories

In making a comparison between a theory of machining and experimental observations, sensitivity of the limiting shear stress k to variations of rate of strain and temperature must be considered. In mild steel, high strain rate can increase the yield stress threefold (3), and marked increases occur for other metals. High temperatures result in large reductions in the yield stress, and since about 90 per cent of the work expended in plastic flow appears in the form of heat [see Farren and Taylor (13)], this can have an important effect on machining forces. The distribution of temperature resulting from this heat generation depends upon the depth of cut and the cutting speed; an increase in either inhibits the conduction of heat to the tool and work. The temperature conditions will also influence the coefficients of friction at the tool face and the nose base. It has also been suggested that size effect may have an appreciable influence (14) on k. In view of these complications, it would seem that a check of the theory which does not involve the magnitude of k would be most satisfactory. To achieve this we will use the variables adopted by Merchant (17, 18) to check his theory, since they are independent of the magnitude of k. His ordinate φ', the shear angle for shear over a single plane, is given by the expression

$$\tan \varphi' = \frac{\cos \gamma}{r - \sin \gamma} \quad [18]$$

where the chip-thickness ratio r was measured for given conditions. The expression for this ratio has already been developed, and is given by Equation [6] for no built-up nose, and by Equation [14] for the built-up-nose solution. His abscissa $(\lambda - \gamma)$, which is equal to $(\lambda_i - \gamma)$ for shear over a single plane, is calculated by means of the expression

$$\tan \lambda = \frac{F_n + F_t \tan \gamma}{F_t - F_n \tan \gamma} \quad [19]$$

where the force components normal and tangential to the surface of the work were measured experimentally. The analytical expressions for these quantities are given by Equations [4], [5], [12], [13]. It should be noted that Equation [19] is independent of k, which is a common factor in the numerator and denominator.

For a solution with simple shear over a single shear plane, φ' gives the inclination of the shear plane to the horizontal, and λ the angle of friction λ_i. When values corresponding to a built-up nose solution are substituted, φ' and λ no longer have this simple significance, but represent a mean value of these magnitudes over the more complicated deformation process. However, although the simple significance of the plot is lost, comparison with experimental values in this way does provide a check of the theory.

Fig. 12 shows experimental results of φ' plotted against $(\lambda - \gamma)$, and also curves corresponding to the present theory for $\gamma = 10$ deg and a range of λ_i and μ_i. Point A is the transition point between the built-up nose solution and the Ernst-Merchant solution, the results of the latter applying to the left of this point. AF is the limiting chip-stress nonbuilt-up-nose solution (Equation 2) which applies for sufficiently high λ_i and μ_i, as detailed in the previous section. The curves above this line represent built-up-nose solutions. The curve BD, corresponding to $\lambda_i = \pi/4$, represents the conditions at which frictional slip along the tool changes to shear breakdown in the chip material. According to the rigid-plastic theory, this line applies for all higher values of λ_i. It was pointed out in the previous section, however, that consideration of elastic effects would extend the diagram to the right of this line.

The range of the experimental points in Fig. 12 indicates that the present theory modified by the influence of elasticity would reproduce the experimental data for a range of coefficients of friction at the tool face and under the built-up nose in the region of unity. This is a satisfactory check of the theory, for such friction coefficients are reasonable. The spread in coefficients of friction is to be associated with the temperature conditions. For example, increasing the depth of cut will produce more localised heat due to friction and shear at the chip face which is in contact with the built-up nose and the tool. This will produce a reduction in the yield stress there. For coefficients of friction close to unity, reduction of the limiting shear stress there will produce an apparent decrease in the coefficient of friction. Such an effect is demonstrated by the experimental data. It also explains the disappearance of a built-up nose at high speeds[4] and may contribute to the increased efficiency of metal cutting with thick chips (20).

In (18) Merchant also presented experimental data for machining celluloid with a tool having a large rake angle. In this

[4] See Boston's discussion of (10), p. 339.

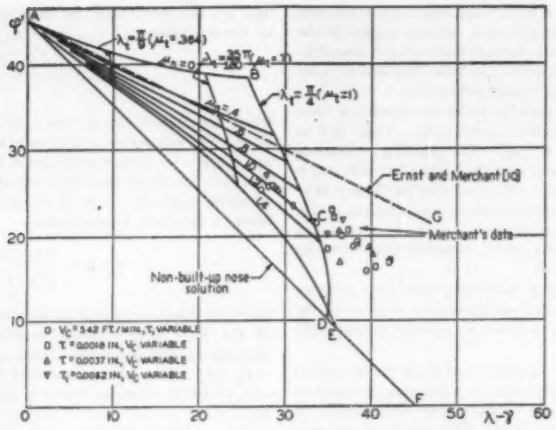
Ernst and Merchant [10]
Merchant's data
Non-built-up nose solution
O V_c = 542 FT./MIN., T_1 VARIABLE
D T_1 = 0.0018 IN., V_c VARIABLE
Δ T_1 = 0.0037 IN., V_c VARIABLE
▽ T_1 = 0.0082 IN., V_c VARIABLE
$\lambda - \gamma$

FIG. 12 COMPARISON OF THEORETICAL PREDICTION AND EXPERIMENTAL RESULTS DUE TO MERCHANT (18)

experiment $\lambda_i - \gamma$ was shown to be negative, and the results were found to agree with the Ernst-Merchant theory. This also agrees with the theory developed in this paper, since, as has been shown in the previous section, their solution is valid for negative values of $\lambda_i - \gamma$.

Boston[7] gives experimental evidence concerning the transition to a built-up nose corresponding to the point A in Fig. 12. It was observed when machining aluminum with a 45-deg rake-angled tool, that a narrow built-up nose occurred in the form of a thin film of aluminum adhering to the tool face immediately above the cutting edge. This condition determines a coefficient of friction of unity or greater at the tool face, and the theory predicts the limiting rake angle $\gamma = 45$ deg for the initiation of a built-up nose, thus giving agreement with the experimental observation.

Having obtained the values of λ_i and λ_n from the comparison of theoretical and experimental data in Fig. 12, let us consider the corresponding slip-line field and strain distribution. Fig. 13 shows this for $\lambda_i = \lambda_n = \pi/4$, which corresponds to a mean of the experimental observations. We see that the dimensions of the nose are small, although the angle through which the nose turns the slip lines has a profound effect on the solution. The corresponding nonbuilt-up-nose solution would give a shear plane parallel to AC, which would determine a much thicker chip and much higher machining force. Although this configuration closely resembles shear over a single plane, it differs considerably from the Ernst-Merchant solution in that the shear angle is about 7 deg less.

The coefficient of friction of unity at the tool face determines no shear across AC, since the face of the built-up nose approaches the tool face tangentially. This, combined with the small shear in the region AFC, gives a deformation field which closely resembles simple shear over the single line AF. We suggest that such a configuration could be attributed to simple shear without a built-up nose on the basis of micrographs of the metal structure. In taking such photomicrographs, the tool has in the past been stopped, and the conditions at the nose disturbed. Moreover, while machining is in progress, it is difficult to examine in detail conditions at the nose of the tool, and there will be a chip-edge effect which will influence the conditions observed. The thickness of the built-up nose for this case is only 2 per cent of the chip width EA.

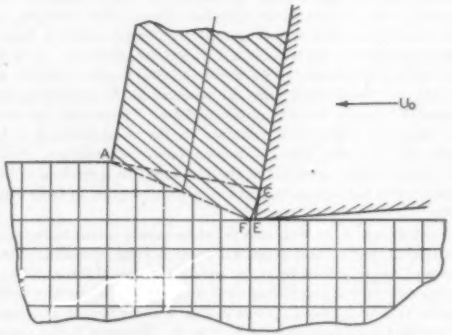

FIG. 13 DEFORMATION OF AN INITIALLY SQUARE GRID FOR $\mu_i = 1$, $\mu_n = 1$, $\gamma = 10°$

Thus, according to the theory presented, the entire range of experimental data shown in Fig. 12 corresponds to the existence of a built-up nose, even though these results have been classified as a Type 2 chip with no built-up nose. It seems that the type of nose predicted, which is small and stable, is an embryonic counterpart of the intermittent built-up nose which is classed as a Type 3 chip. Such a large built-up nose is apparently unstable for normal machine rigidities, and parts of the nose are shed intermittently from a chattering tool. It is not necessary to associate such a phenomenon with the development of a built-up nose, and the suggestion of the existence of a built-up nose, corresponding with the data in Fig. 12, does not imply the consideration of a Type 3 chip as normally understood.

In the previous section it was shown that the Ernst and Merchant solution [10] is not valid for $\lambda_i > \gamma$, for then the stress distribution in the chip dominates the solution. This solution would not, therefore, be expected to agree with experiment for positive values of $(\lambda_i - \gamma)$. That this discrepancy exists was shown by Merchant (18) using the experimental data reproduced in Fig. 12. Their theoretical prediction determines the

[7] Bibliography (12), p. 126.

line AG which lies above the experimental points. It is this high value of φ' to which no satisfactory chip-stress distribution corresponds, which calls for the modification of the theory given in this paper.

Merchant (18) considered a different modification in seeking to rectify his theoretical prediction. He considered the disparity to be due to the influence of hydrostatic pressure on the maximum shear stress k. It is known that the yield stress of a material increases under the influence of hydrostatic pressure, and, using Bridgman's data (19), Merchant adopted a linear relation between the yield stress in shear and the normal pressure across the shear plane. We will call the proportionality constant c. Using this relationship, in combination with the method of choosing the shear angle φ' to give minimum machining force, agreement with experiment is obtained for an appropriate choice of c. The results reproduced in Fig. 12 were reproduced by his theory for $c = 0.23$. This corresponds to a ratio of compression to tensile yield stress of 1.73, whereas this ratio is known to be close to 1. It would seem, therefore, that the influence of hydrostatic pressure on the yield stress is much less than that required to play a significant role in the theory of machining.

The theory presented in this paper shows that experimental results are predicted on the basis of the usual theory of plasticity. The only apparent discrepancy with observation is that a built-up nose is predicted for conditions which are normally associated with a Type 2 chip. However, the configuration determined by the theory shows that the built-up nose is of such proportions that it would be difficult to observe in practice. This suggestion is put forward, for checking in future experimental work.

BIBLIOGRAPHY

1 "Some Factors Affecting the Plastic Deformation of Sheet and Strip Steel and Their Relation to the Deep Drawing Properties," by J. Winlock and R. W. Leiter, Trans. ASM, vol. 25, 1937, pp. 163–205.

2 "High Speed Testing of Mild Steel," by J. H. Holloman and C. Zener, Trans. ASM, vol. 32, 1944, pp. 111–122.

3 "The Testing of Materials at High Rates of Loading," by G. I. Taylor, *Journal of The Institution of Civil Engineers*, vol. 26, 1946, pp. 486–518.

4 "The Theory of Wedge Indentation of Ductile Materials," by R. Hill, E. H. Lee, and S. J. Tupper, Proceedings of the Royal Society of London, series A, vol. 188, 1947, pp. 273–289.

5 "The Theory of Plasticity Applied to a Problem of Machining," by E. H. Lee and B. W. Shaffer, ONR Report A11-43/57, Brown University, Providence, R. I., 1949.

6 "A Method of Numerical Analysis of Plastic Flow in Plane Strain and Its Application to the Compression of a Ductile Material Between Rough Plates," by R. Hill, E. H. Lee, and S. J. Tupper, JOURNAL OF APPLIED MECHANICS, Trans. ASME, vol. 73, 1951, pp. 46–52.

7 "The Theory of Combined Plastic and Elastic Deformation With Particular Reference to a Thick Tube Under Internal Pressure," by R. Hill, E. H. Lee, and S. J. Tupper, Proceedings of the Royal Society of London, series A, vol. 191, 1947, pp. 278–303.

8 "Theory of Elasticity," by S. P. Timoshenko, McGraw-Hill Book Company, Inc., New York, N. Y., 1934.

9 "Über einige statisch bestimmte Fälle des Gleichgewichts in plastischen Körpern," by H. Hencky, *Zeitschrift für angewandte Mathematik und Mechanik*, vol. 3, 1923, pp. 241–251.

10 "Chip Formation, Friction, and High Quality Machined Surfaces, by H. Ernst and M. E. Merchant, from "Surface Treatment of Metals," Trans. ASM, vol. 29, 1941, pp. 299–378.

11 "Work-Hardening Properties of Metals: Their Relation to Metal-Cutting Operations and Cutting Temperatures," by E. G. Herbert, Trans. ASME, vol. 48, 1926, pp. 705–748.

12 "What Happens When Metal Is Cut," by O. W. Boston, Trans. ASME, vol. 52, 1930, Paper No. MSP-52-11.

13 "The Heat Developed During Plastic Extension of Metals," by M. A. Farren and G. I. Taylor, Proceedings of the Royal Society of London, series A, vol. 107, 1925, pp. 422–451.

14 "An Analysis of the Mechanics of Metal Cutting," by D. C. Drucker, *Journal of Applied Physics*, vol. 20, 1949, pp. 1013–1021.

15 "Progress Report No. 1 on Tool-Chip Interface Temperature," by K. J. Trigger, Trans. ASME, vol. 70, 1948, pp. 91–98.

16 "Progress Report No. 2 on Tool-Chip Interface Temperatures," by K. J. Trigger, Trans. ASME, vol. 71, 1949, pp. 163–174.

17 "Mechanics of the Metal Cutting Process. I. Orthogonal Cutting and a Type 2 Chip," by M. E. Merchant, *Journal of Applied Physics*, vol. 16, 1945, pp. 267–275.

18 "Mechanics of the Metal Cutting Process. II. Plasticity Conditions in Orthogonal Cutting," by M. E. Merchant, *Journal of Applied Physics*, vol. 16, 1945, pp. 318–324.

19 "On Torsion Combined With Compression," by P. W. Bridgman, *Journal of Applied Physics*, vol. 14, 1943, pp. 273–283.

20 "A Research in the Elements of Metal Cutting," by O. W. Boston, Trans. ASME, vol. 48, 1926, pp. 749–848.

Design Data and Methods

It is important that the data contained in technical papers be made readily available to designing engineers. In order to satisfy these needs of industry, this section of the Journal includes a concise presentation of data and information drawn chiefly from papers previously published by the Applied Mechanics Division of The American Society of Mechanical Engineers.

Critical Loads on Variable-Section Columns in the Elastic Range

By GORDON SILVER,[1] MINEOLA, N. Y.

This paper concerns the calculation of that loading (single or compound) on a variable-section column which causes elastic instability failure. The columns have the following end conditions: One end fixed with the opposite end free, both ends pinned, both ends fixed, one end fixed with the opposite end pinned.

Nomenclature

The following nomenclature is used in the paper:

x = distance along length of column
y = distance normal to column
δ = maximum virtual deflection y, when $P = P_{cr}$
P = axial load on column
P_{cr} = load causing elastic primary instability failure of column
Q = virtual lateral load at ends of columns with one or both ends fixed to maintain equilibrium of virtual loading when column section varies unsymmetrically, or has unsymmetrical end conditions
M = virtual end moments on columns described for Q
A = area of any cross section of column
$\sigma = \dfrac{P_{cr}}{A}$ = stress on cross section of area A, when $P = P_{cr}$

Introduction

A practical method for calculating critical loads on columns of these types is presented using numerical integration.[2] Four examples are worked, each for different end conditions. These end conditions are the ones most commonly encountered in practice. They include the following:

1 One end fixed; opposite end free.
2 Both ends pinned.
3 Both ends fixed.
4 One end fixed; opposite end pinned.

Analytical bases for the numerical procedures are also presented but it is not essential that these be studied in order to work any problem given. The procedure is to use Equation [4] for condition 1, Equation [7] for condition 2, Equation [9] for condition 3, or Equation [10] for condition 4, and to follow the tabular form of the applicable illustrated problem and integrate numerically.

The solutions are approximations, but the errors are not significant as reference to the numerical solution of Case I shows when compared to an analytically exact solution of the same column. If it is desired to reduce the error, the answer of the first approximation[3] is substituted back in the original equation; the tabular process is then repeated, producing an answer with a much smaller error than the first. This is also illustrated. For most practical cases the first approximation should be close enough, since the error should not exceed 5 per cent compared with an analytical solution.[4]

The method illustrated here will handle a large number of section changes with litth more work than that required for few section changes, as a study of some of the illustrated problems will reveal. The method follows the familiar critical-load derivations expounded in textbooks, using Euler's double integration method wherein constants of integration are determined by the boundary conditions of the problem, technique usually familiar to engineers.

As an additional guide to using this method to solve this type of problem, note that the derived approximate curves conform more closely to the theoretically exact curves as boundary conditions increase. Thus the curve for the cantilever column is least exact, and the curve for both ends fixed is most exact.

As a final step in any problem, the derived critical load should be divided by the minimum section area for a maximum axial stress. This stress must not exceed the proportional limit of the material, or the answer is invalid. The theory gives incorrectly high answers where the proportional limit is exceeded. An extension of the theory into the plastic range is being studied.

Basis of Assumed Solution of Differential Equation

The differential equation of the virtual elastic curve of the column is written

$$EI\frac{d^2y}{dx^2} = f_1(y) + f_2(x) \quad \ldots\ldots\ldots\ldots\ldots\ldots [1]$$

The solution to this equation can be written in the general form

[1] Structural Engineer.

[2] See also, solution by a graphical method, "Theory of Elastic Stability," by S. Timoshenko, McGraw-Hill Book Company, Inc., New York, N. Y., 1936, pp. 131–133.

Note: Statements and opinions advanced in papers are to be understood as individual expressions of their authors and not those of the Society. Manuscript received by ASME Applied Mechanics Division, March 5, 1951.

[3] Footnote 2, p. 86.

[4] For method of calculating the upper and lower limits for P_{cr}, see Ibid., p. 86.

$$y = \phi(x)$$

which can be approximated in polynomial form

$$y = a_0x^n + a_1x^{n-1} + \ldots a_kx^{n-k} + \ldots + a_n \ldots\ldots [2]$$

The constant coefficients are determined by the boundary conditions of a particular case. The value of n for a given case is determined by the number of changes the sign of the curvature undergoes. The expression for curvature being

$$k = \frac{d^2y}{dx^2} \ldots\ldots [3]$$

it is required that n equal the number of changes of sign in curvature plus 2. For a cantilever column, for example, Fig. 1(*b*)

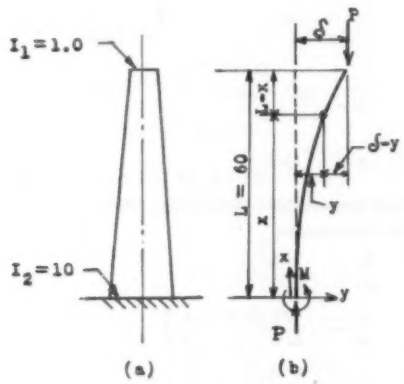

FIG. 1

shows the curvature to be of constant sign, therefore

$$\frac{d^2y}{dx^2} = \text{const}$$

from which it follows that n need not exceed 2. Two represents the minimum number of conditions required to solve this case. Solutions also may be obtained by introducing additional arbitrarily imposed conditions so chosen as to increase the accuracy of the solution. The solutions here presented show, however, that accuracy greater than that obtained with the curve satisfying the minimum number of conditions is not necessary.

COLUMNS WITH VARYING SECTION

Case I. Column with one end fixed and opposite end free, refer to Fig. 1(*b*). Determination of constants in Equation [2]

$$y = Ax^2 + Bx + C$$

$$y = 0 \text{ at } x = 0;\ C = 0$$

$$\frac{dy}{dx} = 2Ax + B$$

$$\frac{dy}{dx} = 0 \text{ at } x = 0;\ B = 0$$

$$y = Ax^2$$

$$y = \delta \text{ at } x = L$$

$$\delta = AL^2$$

$$A = \frac{\delta}{L^2}$$

$$y = \frac{\delta x^2}{L^2} \ldots\ldots [4]$$

Check of assumed curve against exact solution follows:

First Approximation

$$EI\frac{d^2y}{dx^2} = P(\delta - y)$$

$$\frac{d^2y}{dx^2} = \frac{P\delta}{EI}\left(1 - \frac{x^2}{L^2}\right)$$

$$\frac{dy}{dx} = \frac{P\delta}{EI}\left(x - \frac{x^3}{3L^2}\right) + C_1;\ C_1 = 0$$

$$y = \frac{P\delta}{EI}\left(\frac{x^2}{2} - \frac{x^4}{12L^2}\right) + C_2;\ C_2 = 0 \ldots\ldots [5]$$

$$\delta = \frac{5P\delta L^3}{12EI}$$

$$P_{cr} = \frac{12}{5}\frac{EI}{L^2} = 2.40\frac{EI}{L^2} \text{ (error = 3 per cent)}$$

Exact solution

$$P_{cr} = \frac{\pi^2 EI}{4L^2} = \frac{2.469\,EI}{L^2}$$

Second Approximation

Substituting P_{cr} for P in Equation [5]

$$y = \frac{12}{5}\frac{EI}{L^2}\frac{\delta}{EI}\left(\frac{x^2}{2} - \frac{x^4}{12L^2}\right)$$

$$\frac{d^2y}{dx^2} = \frac{P}{EI}(\delta - y) = \frac{P}{EI}\left[\delta - \frac{12}{5}\frac{\delta}{L^2}\left(\frac{x^2}{2} - \frac{x^4}{12L^2}\right)\right]$$

$$\frac{d^2y}{dx^2} = \frac{P\delta}{EI}\left[1 - \frac{12}{5L^2}\left(\frac{x^2}{2} - \frac{x^4}{12L^2}\right)\right]$$

$$y = \frac{P\delta}{EI}\left[\frac{x^2}{2} - \frac{12}{5L^2}\left(\frac{x^4}{24} - \frac{x^6}{360L^2}\right)\right]$$

$$= \frac{P\delta}{EI}\left[\frac{x^2}{2} - \frac{1}{150L^2}(15x^4 - x^6)\right] \ldots\ldots [6]$$

$$\delta = \frac{P\delta L^3}{EI}\left[\frac{1}{2} - \frac{14}{150}\right] = \frac{61}{150}\frac{P\delta L^3}{EI}$$

$$P_{cr} = \frac{2.46\,EI}{L^2} \text{ (error = 0.5 per cent)}$$

By substituting this value in Equation [6], a third approximation would be obtained, more accurate than the second. For most practical cases, however, the first approximation is accurate enough.

A numerical example of Case I is given herewith. Although a second approximation is not usually necessary it is given in this case to illustrate the numerical technique.

Case I. Cantilever Column in Form of a Truncated Cone refer to Figs. 1(*a* and *b*).

To compare with example by Timoshenko (reference 2, p. 136) for $\frac{I_1}{I_2} = 0.10$ and $n = 4$.

$$y = \delta \frac{x^2}{L^2}; \quad EI \frac{d^2y}{dx^2} = M = P(\delta - y) = P\delta\left(1 - \frac{x^2}{L^2}\right)$$

TABLE 1 FIRST APPROXIMATION

1	2	3	4	5	6	7	8	9
x	$\frac{M}{P\delta}$	I	$\frac{M}{P\delta I}$	$\frac{dx}{2}$	$\frac{E\Delta\theta}{P\delta}$	$\frac{E\theta}{P\delta}$	$\frac{E\Delta y}{P\delta}$	$\frac{Ey}{P\delta}$
0	1.00	10	0.100			0		0
				5	1.16		5.80	
10	0.973	7.28	0.133			1.16		5.80
				5	1.52		19.20	
20	0.888	5.22	0.170			2.68		25.00
				5	1.86		36.10	
30	0.750	3.68	0.203			4.54		61.10
				5	2.13		56.05	
40	0.556	2.50	0.222			6.67		117.20
				5	2.15		77.50	
50	0.305	1.47	0.208			8.82		194.70
				5	1.04		93.40	
60	0	1.00	0			9.86		288.10

NOTES:
At $x = 60$, $y = \delta$; $(E\delta)/(P\delta) = 288.1$. $P_{cr} = 10^7/288.1 = 34{,}700$ lb. Exact solution $P_{cr} = 33{,}300$ lb (error = 4 per cent).
For the second approximation, the values of $(Ey)/(P\delta)$ of the first approximation are used:
$M = P(\delta - y) = P[(288.1/E)P_{cr}\delta - y]$, where y equals values listed in column 9, $P = P_{cr} = E/288.1$, and $y = \delta$ at $x = 60$.
At $x = 30$, for example

$$M = P\left[\left(\frac{288.1}{E}\right)\left(\frac{E}{288.1}\right)\delta - \left(\frac{61.10}{E}\right)\left(\frac{E}{288.1}\right)\delta\right] = P\delta\left(\frac{227.0}{288.1}\right) = 0.785P\delta$$

This value appears in column 11 with other similarly derived values.

$$M = P\delta\left(1 - \frac{Ey}{P_{cr}\delta}/288.1\right) \text{ refer to Figs. 1(}a \text{ and } b\text{).}$$

TABLE 2 SECOND APPROXIMATION

10	11	12	13	14	15	16	17	18
x	$\frac{M}{P\delta}$	I	$\frac{M}{PI\delta}$	$\frac{dx}{2}$	$\frac{E\Delta\theta}{P\delta}$	$\frac{E\theta}{P\delta}$	$\frac{E\Delta y}{P\delta}$	$\frac{Ey}{P\delta}$
0	1.00	10	0.100			0		0
				5	1.17		5.85	
10	0.986	7.28	0.134			1.17		5.85
				5	1.55		19.45	
20	0.913	5.22	0.175			2.72		25.30
				5	1.95		36.95	
30	0.788	3.68	0.214			4.67		62.25
				5	2.24		57.00	
40	0.593	2.50	0.234			6.93		119.25
				5	2.27		80.75	
50	0.325	1.47	0.220			9.22		200.00
				5	1.10		97.80	
60	0	1.00	0			10.33		297.80

NOTES:
At $x = 60$, $y = \delta$; $E\delta/P_{cr}\delta = 297.8$; $P_{cr} = E/297.8 = 33{,}550$ lb (error = 0.75 per cent).

Case II. Columns with both ends pinned. Determination of constants of Equation [2], refer to Fig. 2(*b*).

$$y = Ax^3 + Bx + C$$

$$y = 0 \text{ at } x = 0; \quad C = 0$$

$$\frac{dy}{dx} = 2Ax + B$$

$$0 = AL + B, \quad \frac{dy}{dx} = 0 \text{ at } x = \frac{L}{2}$$

$$B = -AL$$

$$y = Ax^3 - ALx = Ax(x - L)$$

$$\delta = \frac{AL}{2}\left(\frac{L}{2} - L\right) = \frac{-AL^3}{4} \quad y = \delta \text{ at } x = \frac{L}{2}$$

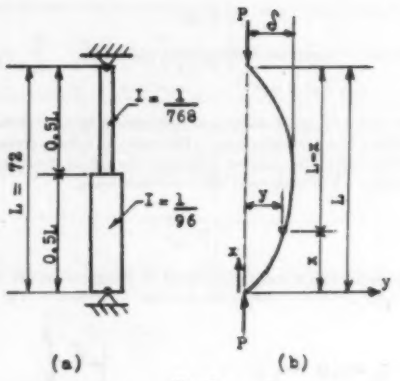

FIG. 2

$$A = \frac{-4\delta}{L^2}$$

$$y = \frac{4\delta x}{L^2}(L - x) \quad [7]$$

Check of assumed curve against exact solution.

First Approximation

$$\frac{d^2y}{dx^2} = -\frac{4P\delta}{EIL^2}(Lx - x^2)$$

$$\frac{dy}{dx} = -\frac{4P\delta}{EIL^2}\left(\frac{Lx^2}{2} - \frac{x^3}{3}\right) + C_1$$

$$0 = -\frac{4P\delta L}{EI}\left(\frac{1}{8} - \frac{1}{24}\right) + C_1$$

$$C_1 = \frac{P\delta L}{3EI}$$

$$y = -\frac{4P\delta}{EIL^2}\left(\frac{Lx^3}{6} - \frac{x^4}{12}\right) + \frac{P\delta Lx}{3EI} + C_2; \; C_2 = 0 \quad [8]$$

$$\delta = -\frac{4P\delta L^3}{EI}\left(\frac{1}{48} - \frac{1}{192}\right) + \frac{P\delta L^3}{6EI}$$

$$\delta = -\frac{P\delta L^3}{16EI} + \frac{P\delta L^3}{6EI} = \frac{5}{48}\frac{P\delta L^3}{EI}$$

$$P_{cr} = \frac{9.6EI}{L^2} \text{ (error = 3 per cent)}$$

Exact solution

$$P_{cr} = \frac{\pi^2 EI}{L^2} = \frac{9.87\,EI}{L^2}$$

Second Approximation

By substituting the first approximation for P_{cr} in Equation [8]

$$y = +\frac{16}{5}\frac{EI}{L^2}\frac{\delta Lx}{EI} - \frac{192EI\delta}{5EIL^4}\left(\frac{Lx^3}{6} - \frac{x^4}{12}\right)$$

$$= \frac{16}{5}\frac{\delta x}{L} - \frac{16}{5}\frac{\delta}{L^3}\left(2x^3 - \frac{x^4}{L}\right)$$

$$= \frac{16}{5}\frac{\delta}{L}\left(x - \frac{2x^3}{L^2} + \frac{x^4}{L^3}\right)$$

$$\frac{d^2y}{dx^2} = -\frac{16P\delta}{5EIL}\left(x - \frac{2x^3}{L^3} + \frac{x^4}{L^3}\right)$$

$$\frac{dy}{dx} = -\frac{16}{5}\frac{P\delta}{EIL}\left(\frac{x^2}{2} - \frac{x^4}{2L^3} + \frac{x^5}{5L^3}\right) + C_1$$

$$C_1 = +\frac{8}{25}\frac{P\delta L}{EI}$$

$$y = -\frac{16}{5}\frac{P\delta}{EIL}\left(\frac{x^3}{6} - \frac{x^5}{10L^2} + \frac{x^6}{30L^3}\right) + \frac{8}{25}\frac{P\delta Lx}{EI}$$

$$y = -\frac{8}{75}\frac{P\delta}{EIL}\left(5x^3 - \frac{3x^5}{L^2} + \frac{x^6}{L^3}\right) + \frac{8}{25}\frac{P\delta Lx}{EI}$$

$$\delta = -\frac{8}{75}\frac{P\delta L^3}{EI}\left(\frac{5}{8} - \frac{3}{32} + \frac{1}{64}\right) + \frac{4}{25}\frac{P\delta L^3}{EI}$$

$$\delta = -\frac{P\delta L^3}{600EI}(40 - 6 + 1) + \frac{4}{25}\frac{P\delta L^3}{EI}$$

$$\delta = -\frac{P\delta L^3}{600EI}(35 - 96) = \frac{61P\delta L^3}{600EI}$$

$$P_{cr} = \frac{9.83EI}{L^2} \text{ (error = 0.50 per cent)}$$

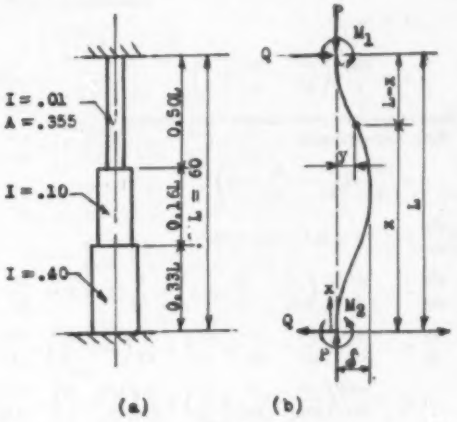

FIG. 3

A numerical example of Case II is given herewith.

Case II. Column with pin-ends. To compare with a test column,[a] refer to Figs. 2(*a* and *b*).

$$y = \frac{4\delta x}{L^2}(L - x);\ M = Py = \frac{4P\delta x}{L^2}(L - x);\ EI\frac{d^2y}{dx^2} = -M$$

TABLE 3

2	3	4	5	6	7	8	9	10	11
$-\frac{M}{P\delta}$	I	$-\frac{M}{P\delta I}$	$\frac{\Delta x}{2}$	$-\frac{E\,\Delta\theta}{P\delta}$	$-\frac{E\theta}{P\delta}$	$-\frac{E\,\Delta y}{P\delta}$	$-\frac{Ey}{P\delta}$	$-C_1x$	$\frac{Ey}{P\delta} + C_1x$
z, in.	in.^{4}	1/in.^{4}	in.	rad/in.	rad/in.	in.$^{-2} \times 10^{-4}$	in.$^{-2} \times 10^{-4}$	in.$^{-2} \times 10^{-4}$	in.$^{-2} \times 10^{-4}$
0	0.0013	0			0		0	0	0
0.438		336	4.5	1510	1510	6.8	6.8	−119	112.2
0.750		575	4.5	4100	5610	32.1	38.9	−238	199.1
0.938		720	4.5	5830	11440	76.9	115.8	−357	241.2
1.000	0.0013	768	4.5	6700	18140	133.0	248.8	−477	228.2
1.000	0.0104	96	0	0	18140	0	248.8	−477	228.2
0.938		90	4.5	837	18977	167.0	415.8	−596	180.2
0.750		72	4.5	730	19707	173.5	590.8	−715	124.7
0.438		42	4.5	514	20221	178.5	769.8	−834	64.2
0	0.0104	0	4.5	189	20410	182.0	952.8	−952.8	0

[a] Column 3, Table 1, "Critical Load of Columns of Varying Cross Section," by W. T. Thomson, Trans. ASME, vol. 72, 1950, pp. 132–134.

NOTES:

$P_{cr} = \frac{2{,}750{,}000}{244{,}300} = 11.23$ lb (see Appendix)

P_{cr} (test) = 10.5 lb (error = 7 per cent)

Case III. Column fixed at both ends, refer to Fig. 3(*b*). Determination of constants in Equation [2]

$$y = Ax^4 + Bx^3 + Cx^2 + Dx + E$$

$E = 0$ since $y = 0$ at $x = 0$

$$\frac{dy}{dx} = 4Ax^3 + 3Bx^2 + 2Cx + D$$

$D = 0$, since $\frac{dy}{dx} = 0$ at $x = 0$

$0 = 4AL^3 + 3BL^2 + 2CL$, since $\frac{dy}{dx} = 0$ at $x = L$

$$0 = \frac{1}{2}AL^3 + \frac{3}{4}BL^2 + CL, \text{ since } \frac{dy}{dx} = 0 \text{ at } x = \frac{L}{2}$$

$$0 = 3AL^2 + \frac{3}{2}BL^2$$

$B = -2AL$

$0 = 2AL^3 - 2CL$

$C = AL^2$

$y = Ax^4 - 2ALx^3 + AL^2x^2$

$$\delta = AL^4\left(\frac{1}{16} - \frac{1}{4} + \frac{1}{4}\right), \text{ since } y = \delta \text{ at } x = \frac{L}{2}$$

$$A = 16\frac{\delta}{L^4}$$

$$\eta = \frac{16\delta x^2}{L^2}\left(\frac{x^2}{L^2} - \frac{2x}{L} + 1\right) \quad \text{.....[9]}$$

Check of assumed curve against exact solution.

First Approximation

$$y = \frac{16\delta x^2}{L^2}\left(\frac{x^2}{L^2} - \frac{2x}{L} + 1\right)$$

$$EI\frac{d^2y}{dx^2} = -Py + Q(L-x) + M_1$$

$$\frac{d^2y}{dx^2} = -\frac{16P\delta x^2}{EIL^2}\left(\frac{x^2}{L^2} - \frac{2x}{L} + 1\right) + \frac{Q}{EI}(L-x) + \frac{M_1}{EI}$$

$$\frac{dy}{dx} = -\frac{16P\delta}{EIL^2}\left(\frac{x^5}{5L^2} - \frac{x^4}{2L} + \frac{x^3}{3}\right) + \frac{Q}{EI}\left(Lx - \frac{x^2}{2}\right) + \frac{M_1 x}{EI}$$

$$y = -\frac{16P\delta}{EIL^2}\left(\frac{x^6}{30L^2} - \frac{x^5}{10L} + \frac{x^4}{12}\right) + \frac{Q}{EI}\left(\frac{Lx^2}{2} - \frac{x^3}{6}\right) + \frac{M_1 x^2}{2EI}$$

$$0 = -\frac{16P\delta L^3}{60EI}(2 - 6 + 5) + \frac{QL^3}{3EI} + \frac{M_1 L^2}{2EI},$$

$$(y = 0 \text{ at } x = L)$$

$$0 = -\frac{4P\delta L^3}{15EI} + \frac{QL^3}{3EI} + \frac{M_1 L^2}{2EI}$$

$$0 = -\frac{8P\delta L}{30EI} + \frac{3QL^2}{8EI} + \frac{M_1 L}{2EI}, \left(\frac{dy}{dx} = 0 \text{ at } x = \frac{L}{2}\right)$$

$Q = 0$ (in actual problems with unsymmetrical variations of I, Q will not equal zero)

$$M_1 = \frac{8}{15}P\delta$$

$$y = -\frac{16P\delta}{EIL^2}\left(\frac{x^6}{30L^2} - \frac{x^5}{10L} + \frac{x^4}{12}\right) + \frac{8P\delta x^2}{30EI}$$

$$\delta = -\frac{16P\delta L^3}{60EI}\left(\frac{2}{64} - \frac{6}{32} + \frac{5}{16}\right) + \frac{1}{15}\frac{P\delta L^3}{EI}$$

$$\delta = \frac{P\delta L^3}{40EI}$$

$$P_{cr} = \frac{40EI}{L^2}$$

Exact solution $= \frac{4\pi^2 EI}{L^2} = \frac{39.48EI}{L^2}$ (error = 1.01 per cent).

A numerical example of Case III is given herewith.

Case III. Column with fixed ends (75S-T aluminum alloy; $E = 10^7$ psi); refer to Fig. 3(*a*).

$$y = \frac{16\delta x^2}{L^2}\left(\frac{x^2}{L^2} - \frac{2x}{L} + 1\right); EI\frac{d^2y}{dx^2} = -M = -\frac{16P\delta x^2}{L^2}\left(\frac{x^2}{L^2} - \frac{2x}{L} + 1\right) + Q(L-x) + M_1$$

TABLE 4

1	2		3	4			5	6			7			8		
x	M		I	M/I			$\Delta x/2$	$E\Delta\theta$			$E\theta$			$E\Delta y$		
	Q	$P\delta$		M_1	Q	$P\delta$		M_1	Q	$P\delta$	M_1	Q	$P\delta$	M_1	Q	$P\delta$
0	$M_1 + 60$		0.40	2.5 +	150							0				
10	$M_1 + 50$	-0.309	0.40	2.5 +	125 —	0.773	5	25 +	1375 —	3.86	25 +	1375 —	3.86	125 +	6880 —	19
20	$M_1 + 40$	-0.791	0.40	2.5 +	100 —	1.98	5	25 +	1125 —	13.75	50 +	2500 —	17.6	375 +	19380 —	107
20	$M_1 + 40$	-0.791	0.10	10.0 +	400 —	7.91	0		0		50 +	2500 —	17.6		0	
30	$M_1 + 30$	-1.00	0.10	10.0 +	300 —	10.0	5	100 +	3500 —	89.55	150 +	6000 —	107	1000 +	42500 —	624
30	$M_1 + 30$	-1.00	0.01	100	+ 3000 —	100.0	0		0		150 +	6000 —	107		0	
40	$M_1 + 20$	-0.791	0.01	100	+ 2000 —	79.1	5	1000 +	25000 —	805	1150 +	31000 —	1000	6500 +	185000 —	5550
50	$M_1 + 10$	-0.309	0.01	100	+ 1000 —	30.9	5	1000 +	15000 —	550	2150 +	46000 —	1550	16500 +	385000 —	12780
60	$M_1 + 0$		0.01	100			5	1000 +	5000 —	154.5	3150 +	51000 —	1710	31500 +	485000 —	16300

NOTES:

$P_{cr} = 9270$ lb (see Appendix); minimum area $= 0.355$ in.^{2} [see Fig. 3(*a*)].

$\sigma = 9270/0.355 = 26{,}100$ psi

Since this is below the proportional limit for 75S-T aluminum alloy the value of P_{cr} is valid.

Case IV. Column fixed at one end, pinned at opposite end, refer to Fig. 4(*b*). Determination of constants in Equation [2].

$$y = Ax^3 + Bx^2 + Cx + D$$

$D = 0$, since $y = 0$ at $x = 0$

$$\frac{dy}{dx} = 3Ax^2 + 2Bx + C$$

$C = 0$, since $\frac{dy}{dx} = 0$ at $x = 0$

$0 = AL^3 + BL^2$, since $y = 0$ at $x = L$

$B = -AL$

$$y = Ax^3 - ALx^2 = A(x^3 - Lx^2)$$

$$\frac{dy}{dx} = A(3x^2 - 2Lx)$$

Since $\frac{dy}{dx} = 0$ at $x = 0$, $A \neq 0$

Since $\frac{dy}{dx} = 0$ at $0 < x < L$, and $A \neq 0$, $3x^2 - 2Lx = 0$

$$x = \frac{2}{3}L$$

$$\delta = AL^3\left(\frac{8}{27} - \frac{4}{9}\right) = -\frac{4}{27}AL^3 \quad y = \delta \text{ at } x = \frac{2}{3}L$$

$$A = -\frac{27}{4}\frac{\delta}{L^3}$$

$$y = \frac{27}{4}\frac{\delta}{L^3}(Lx^2 - x^3) = \frac{27\delta x^2}{4L^3}\left(1 - \frac{x}{L}\right) \quad \ldots\ldots[10]$$

Check of assumed curve against exact solution.

Case IV. Column with one end fixed and opposite end pinned. (75S-T Aluminum alloy; $E = 10^7$ psi, refer to Figs. 4(*a* and *b*).

$$y = \frac{27}{4}\frac{\delta x^2}{L^3}\left(1 - \frac{x}{L}\right); \quad EI\frac{d^2y}{dx^2} = -M = -\frac{27P\delta x^2}{4L^3}\left(1 - \frac{x}{L}\right) + Q(L - x)$$

First Approximation

$$y = \frac{27\delta x^2}{4L^3}\left(1 - \frac{x}{L}\right)$$

$$EI\frac{d^2y}{dx^2} = -Py + Q(L - x)$$

$$\frac{d^2y}{dx^2} = -\frac{27P\delta x^2}{4EIL^3}\left(1 - \frac{x}{L}\right) + \frac{Q}{EI}(L - x)$$

$$\frac{dy}{dx} = -\frac{27P\delta}{4EIL^3}\left(\frac{x^3}{3} - \frac{x^4}{4L}\right) + \frac{Q}{EI}\left(Lx - \frac{x^2}{2}\right) + C_1, \; C_1 = 0$$

$$y = -\frac{27P\delta}{4EIL^3}\left(\frac{x^4}{12} - \frac{x^5}{20L}\right) + \frac{Q}{EI}\left(\frac{Lx^3}{2} - \frac{x^3}{6}\right) + C_2, \; C_2 = 0$$

$$0 = -\frac{27P\delta L^3}{4EI}\left(\frac{1}{30}\right) + \frac{QL^3}{3EI} \qquad y = 0 \text{ at } x = L$$

$$Q = \frac{27P\delta}{40L}$$

$$y = -\frac{27P\delta}{4EIL^3}\left(\frac{x^4}{12} - \frac{x^5}{20L}\right) + \frac{27}{40}\frac{P\delta}{EIL}\left(\frac{Lx^3}{2} - \frac{x^3}{6}\right)$$

$$y = -\frac{27P\delta}{40EIL^3}\left(\frac{5x^4}{6} - \frac{x^5}{2L} - \frac{L^2x^3}{2} + \frac{Lx^3}{6}\right)$$

$$\delta = +\frac{27}{40}\frac{P\delta L^3}{EI}\left(\frac{18}{243}\right) = \frac{1}{20}\frac{P\delta L^3}{EI} \qquad y = \delta \text{ at } x = \frac{2}{3}L$$

$$P_{cr} = \frac{20EI}{L^2} \text{ (error = < 1 per cent)}$$

For this case, as in Case III, the curve first assumed closely approximates the curve representing the exact solution of the differential equation owing to the number of conditions which the assumed curve must satisfy. The error, as indicated, is less than 1 per cent, which is within the accuracy usually demanded of an engineering solution, so that no additional approximations are necessary.

TABLE 5

1 x	2 M	3 I	4 M/I	5 $\Delta x/2$	6 $E\,\Delta\theta$	7 $E\theta$	8 $E\,\Delta y$
0	$30\,Q$	0.40	$75\,Q$			0	
				2.5	$345\,Q - 0.98\,P\delta$		$861\,Q - 2.45\,P\delta$
5	$25\,Q - 0.156\,P\delta$	0.40	$63\,Q - 0.39\,P\delta$			$345\,Q - 0.98\,P\delta$	
				2.5	$280\,Q - 4.10\,P\delta$		$2400\,Q - 15.11\,P\delta$
10	$20\,Q - 0.500\,P\delta$	0.40	$50\,Q - 1.25\,P\delta$			$625\,Q - 5.08\,P\delta$	
				0	0		0
10	$20\,Q - 0.500\,P\delta$	0.10	$200\,Q - 5.00\,P\delta$			$625\,Q - 5.08\,P\delta$	
				2.5	$875\,Q - 33.63\,P\delta$		$5310\,Q - 109.5\,P\delta$
15	$15\,Q - 0.845\,P\delta$	0.10	$150\,Q - 8.45\,P\delta$			$1500\,Q - 38.71\,P\delta$	
				2.5	$625\,Q - 46.13\,P\delta$		$9061\,Q - 308.9\,P\delta$
20	$10\,Q - 1.000\,P\delta$	0.10	$100\,Q - 10.00\,P\delta$			$2125\,Q - 84.84\,P\delta$	
				0	0		0
20	$10\,Q - 1.000\,P\delta$	0.03	$333\,Q - 33.33\,P\delta$			$2125\,Q - 84.84\,P\delta$	
				2.5	$1250\,Q - 148.6\,P\delta$		$13750\,Q - 795.7\,P\delta$
25	$5\,Q - 0.782\,P\delta$	0.03	$167\,Q - 26.10\,P\delta$			$3375\,Q - 233.4\,P\delta$	
				2.5	$420\,Q - 65.25\,P\delta$	$3795\,Q - 298.6\,P\delta$	$17930\,Q - 1330\,P\delta$
30	0	0.03	0				

Notes:
$P_{cr} = 20{,}400$ lb (see Appendix); minimum area = 0.61 in.^{2}, see Fig. 4(*a*).

$$\sigma = \frac{20{,}400}{0.61} = 33{,}500 \text{ psi}$$

Since this is below the proportional limit for 75S-T aluminum alloy, the value of P_{cr} is valid.

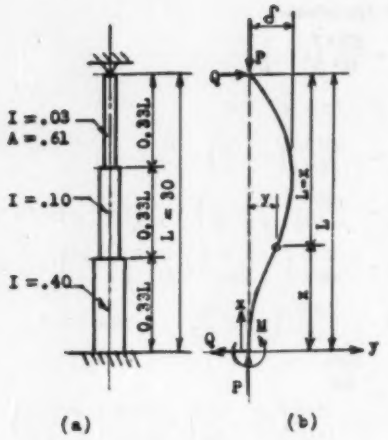

FIG. 4

Appendix

This Appendix is presented to explain the calculations required for interpolating in the tables for Cases II, III, and IV.

Interpolation is required because the condition $y = \delta$ when $P = P_{cr}$ must be satisfied. For columns of constant I and for cantilever columns, the value of x where $y = \delta$ is known, but for columns of varying I, excluding the cantilever, this value of x is a function of the variation of I and must be determined for each particular problem. This can best be done by interpolating from data derived in the tables.

Case II (See Table 3).

To satisfy $y = 0$ at $x = 72$

$$C_1 = +\frac{952{,}800}{72} = +13{,}220 \text{ (see column 10)}$$

$$y = \delta \text{ at } \theta = 0$$

To find x for $\theta = 0$

Applying C_1 to column 7 we find $\theta = 0$ at $27 < x < 36$. Setting $x - 27 = \Delta x$, we have, from columns 7 and 8

$$(11{,}440 + 13{,}220)\frac{\Delta x}{2} + (13{,}220 + 18{,}140)\left(\frac{9 - \Delta x}{2}\right) = 133{,}000$$

from which $\Delta x/2 = 1.21$, $x = 29.42$.

The integration for the interpolation is necessary only from column 9 to column 11. The interpolated value thus derived in column 11 = 244,300

$$P_{cr} = \frac{E}{244{,}300}$$

E is determined from the test data (see footnote to Table 3)

$$P_{cr} \text{ (uncut column)} = 54.5 \text{ lb} = \frac{\pi^2 EI}{L^2}$$

$$I \text{ (uncut column)} = \frac{1}{96}$$

$$L = 72$$

$$E = \frac{(54.5)(96)L^2}{\pi^2} = 2.75 \times 10^3 \text{ psi}$$

$$P_{cr} = \frac{2{,}750{,}000}{244{,}300} = 11.23 \text{ lb}$$

P_{cr}(test) = 10.50 lb (error = 7 per cent)

This error could be reduced by computing a second approximation but for most practical cases 7 per cent error is not considered significant.

Case III. To determine x for $\theta = 0$ set $x_1 = x$ at $\theta = 0$

Σ column 8 = 56,000 M_1 + 1,123,760 Q — 35,360 $P\delta$ = 0, since at $x = L = 60$, $y = 0$.

From column 7, 3150 M_1 + 51,000 Q — 1710 $P\delta$ = 0 since at $x = L = 60$, $\theta = 0$.

Solving for M_1 and Q gives

$$M_1 = 0.166P\delta$$

$$Q = 0.023P\delta$$

Applying these values to column 7 it is seen that $\theta = 0$ at $30 < x < 40$

$$\text{At } x = 30,\ E\theta = +57.4\ P\delta,\ \frac{M}{I} = -13.5\ P\delta$$

$$\text{At } x = 40,\ E\theta = -87.0\ P\delta,\ \frac{M}{I} = -15.9\ P\delta$$

Letting $x_1 = x$ at $\theta = 0$

$$\Delta x_1 = x_1 - 30$$

$$k = \frac{M}{I} \text{ at } x = x_1$$

Then, from Table 4

$$(-13.5\ P\delta + k)\left(\frac{\Delta x_1}{2}\right) + 57.4\ P\delta = 0$$

$$(-15.9\ P\delta + k)\left(5 - \frac{\Delta x_1}{2}\right) + 87.0\ P\delta = 0$$

This yields $\Delta x_1 = 4.16$ in., and $x_1 = 34.16$ in. Column 8 is summed up to $x = 34.16$, giving

$$\delta = \frac{1079\ P\delta}{E}$$

for which $P_{cr} = 9270$ lb.

Case IV. To determine x for $\theta = 0$, set $x_1 = x$ at $\theta = 0$

Σ column 8 = 49312 Q — 2562 $P\delta$ = 0, since at $x = L = 30$, $y = 0$. This gives $Q = 0.052\ P\delta$. Applying this value to column 7 shows $E\theta = 0$ at $20 < x < 25$.

$$\text{At } x = 20,\ E\theta = +26.8\ P\delta;\ \frac{M}{I} = -16\ P\delta$$

$$\text{At } x = 25,\ E\theta = -58.0\ P\delta;\ \frac{M}{I} = -17.4\ P\delta$$

Using notation similar to Case III, and data from Table 5

$$(-16\ P\delta + k)\left(\frac{\Delta x_1}{2}\right) + 26.8\ P\delta = 0$$

$$(-17.4\ P + k)\left(2.5 - \frac{\Delta x_1}{2}\right) + 58\ P\delta = 0$$

This yields $\Delta x_1 = 1.65$ and $x_1 = 21.65$. Column 8 is summed up to $x = 21.65$, giving $\delta = \frac{489\ P\delta}{E}$ from which $P_{cr} = 20{,}400$ lb.

Discussion

Evaluation of Stress Distribution in the Symmetrical Neck of Flat Tensile Bars[1]

E. H. Lee.[2] Presumably the type of strain distribution considered by the author applies only for a range of width-to-thickness ratios, for with flat wide specimens the constraint of the width prevents contraction, and necking occurs through the thickness of the specimen. Thickness gradients then become large, and the system no longer can be considered as in plane stress. It seems that there is a range of width-thickness ratios sufficiently large to permit the assumption of plane stress, and sufficiently small to avoid sharp necks producing local reduction in the thickness. Perhaps the author would comment on the range of validity of this type of behavior.

Author's Closure

The comments made by Professor Lee are appreciated. The author agrees, as was stated in the text, that the type of strain distribution considered can be applied only for a relatively narrow-range width-to-thickness ratio.

Presumably the type of sharp necks in the thickness direction that Professor Lee described for larger width-to-thickness ratios is the same type of necking described in the literature by Koerber, Siebel, Bijlaard, and Hill.

A separate investigation was carried out by the author to study what effect the width-to-thickness ratio and strain-hardening has on the mode of necking. These results were presented at the First U. S. National Congress of Applied Mechanics, June, 1951, at Chicago, Ill. The later results indicate that the mode of necking will undergo a transition from the symmetrical-type neck to the oblique neck as the width-to-thickness ratio is increased. However, there are not sufficient data available to make a general statement.

Free Vibrations of a Pin-Ended Column With Constant Distance Between Pin Ends[1]

N. J. Hoff.[2] The most important result obtained in the paper is an explanation of the failure of attempts to establish a nondestructive method of testing the elastic stability of structures. It often has been proposed that such structures should be loaded up to as high values of the loads as can be reached without danger of permanent deformation. At different load levels the lowest natural mode of vibration of the structure should be excited. The curve representing the natural frequencies plotted against the load can be extrapolated, and the buckling load of the structure is the load at which the natural frequency is zero.

The author has shown that in an ordinary column test the natural frequency depends greatly upon the amplitude of the vibration, and the frequency is considerably higher than zero at the instability load. As an example, it might be mentioned that when the amplitude is one half the radius of gyration of the cross section, the frequency at the buckling load is equal to 20 per cent of the natural frequency of a column upon which no end load is acting. This is true, naturally, only if the load is applied by means of controlled end displacements, as is done in an ordinary testing machine, and not through the application of dead weights. Consequently, extrapolation of the curve to zero frequency results in a load differing substantially from the critical load of the classical theory of stability. Moreover, variations in the amplitude of the vibrations at different stages of the loading cause a great deal of scatter in the results and add to the difficulties of obtaining the buckling load by means of vibration tests.

It appears, therefore, that attempts at determining the buckling load by such nondestructive tests either have to be given up or else will have to be modified in the light of the author's results.

E. H. Lee.[3] With reference to the author's comments on the restriction on the initial shape of the strut, it may be worth mentioning that this type of analysis will go through for an initial eccentricity comprising a sine curve with any integral number of half waves. While this provides an infinite number of initial configurations, they cannot be superimposed to cover any initial shape since the problem is nonlinear.

Vibration of Rectangular and Skew Cantilever Plates[1]

M. Z. v. Krzywoblocki.[2] As mentioned in the paper, the Rayleigh-Ritz method gives an upper bound, but it is possible to find a lower bound. The combination: The Rayleigh-Ritz and the Weinstein methods proved to be a successful mathematical tool, giving upper and lower bounds. It may be of interest to apply this combination in the case considered by the author.

Analysis of Deep Beams[1]

A. J. Durelli.[2] The problem dealt with here by the authors is very important in many industrial applications, and the contribution made by them will certainly be welcome since the study is far from exhausted.

It may be worth mentioning that a series of papers was pub-

[1] By Julius Aronofsky, published in the March, 1951, issue of the Journal of Applied Mechanics, Trans. ASME, vol. 13, pp. 75–84.

[2] Professor of Applied Mathematics, Brown University, Providence, R. I.

[1] By David Burgreen, published in the June, 1951, issue of the Journal of Applied Mechanics, Trans. ASME, vol. 73, pp. 135–139.

[2] Head, Department of Aeronautical Engineering and Applied Mechanics, Polytechnic Institute of Brooklyn, Brooklyn, N. Y. Mem. ASME.

[3] Professor of Applied Mathematics, Brown University, Providence, R. I. Mem. ASME.

[1] By M. V. Barton, published in the June, 1951, issue of the Journal of Applied Mechanics, Trans. ASME, vol. 73, pp. 129–134.

[2] Professor of Gasdynamics and Theoretical Aerodynamics; Secretary, Panel on Fluid and Solid Mechanics, University of Illinois, Urbana, Ill.

[1] By H. D. Conway, L. Chow, and G. W. Morgan, published in the June, 1951, issue of Journal of Applied Mechanics, Trans. ASME, vol. 73, pp. 163–172.

[2] Supervisor, Armour Research Foundation of Illinois Institute of Technology, Chicago, Ill. Jun. ASME.

lished a short time ago along lines similar to those followed by the authors (1 to 6).[3] A comparison is made in these papers between the finite-difference method and the method of superimposing two stress functions in very much the same way as the authors did (2, 4). A photoelasticity test (5) was also conducted to check results. In other papers published shortly after (3, 6), the Galerkin method was used to approach the solution of the same problem, comparisons again were made, and tables were given for several loading conditions and widths of supports. Several of the numerical applications were made for beams loaded on the lower boundary, but the photoelastic test considers a beam loaded on the upper boundary. An interesting point brought out by this test is that the maximum stress is not on the axis of symmetry but on the lower boundary near the support.

A photoelastic test to check the authors' results does not seem too difficult to realize in the case of loading on the upper boundary. Uniform loading can be obtained either by using several sheets of cardboard (7), or by means of air pressure applied to a thin rubber hose placed inside a metal channel, with one side of the hose resting on the photoelastic specimen. The separation of the principal stresses should be easily obtained by iteration methods since all boundary conditions will be known and the shape is rectangular.

The related problem of the high beam on three supports, loaded on the lower boundary, has recently been approached using Fourier's series (8).

BIBLIOGRAPHY

1 "Vigas de Gran Altura Sometidas a Cargas Uniformes," by M. M. Guttero, *Ciencia y Tecnica*, vol. 107, July, 1946, pp. 1–55; August, 1946, pp. 81–134, and September, 1946, pp. 204–240.

2 "Sobre la Viga Simplemente Apoyada con Seccion Rectangular de Gran Altura," by E. Butty, *Ciencia y Tecnica*, vol. 109, October, 1947, p. 195.

3 "Solucion Variacional del Problema de la Viga Rectangular Simplemente Apoyada de Gran Altura," by A. Guzman and C. Luisoni, *Ciencia y Tecnica*, vol. 3, September, 1948, p. 119.

4 "Comentarios Sobre Vigas de Gran Altura Simplemente Apoyadas," by F. Garcia Olano and E. Fliess, *Ciencia y Tecnica*, vol. 3, November, 1948, p. 288.

5 "Ensayo Fotoelastico de una Viga de Gran Altura," by E. Scimmarella and M. Palacio, *Ciencia y Tecnica*, vol. 113, November, 1949, p. 249.

6 "Sobre la Viga Simplemente Apoyada de Gran Altura," by A. Guzman and C. Luisoni, *Ciencia y Tecnica*, vol. 114, 1950, p. 285.

7 "Distribution of Stresses in Partial Compression," by A. J. Durelli, Proceedings of the 13th Semi-Annual Eastern Photoelasticity Conference, June, 1941, p. 25.

8 "The Wall-Like Beam on Three Supports," by H. Parkus, *Oesterreichisches Ingenieur Archiv*, vol. 2, 1948, p. 185.

M. Z. v. Krzywoblocki.[4] The authors apply to the case of continuously distributed stresses the strain-energy method and a numerical method of finite difference and compare the results. But there does not exist any strain-energy method in the case considered by the authors. The sentence in the paper, "This solution by strain-energy methods would be exact only if an infinite number of parameters were used," cannot be accepted from a mathematical standpoint. Similarly, the conditions for a minimum V used by the authors are not, under any circumstances, sufficient conditions for a minimum of a function of n-variables. In the defense of the authors it should be mentioned that there exists a confusion in the literature on the subject, increased, perhaps, by the fact that one of the writers cited by the authors invented and published in one of his textbooks a proof of that method, which proof violates all the principles of elementary differential calculus and is no proof at all. It assumes as the base that the condition for a minimum of a function of n-variables is sufficient in the same form as accepted by the authors. But the conditions for a minimum of a function of n-variables are much more complicated. Moreover, we are seeking the absolute minimum of the function of n-variables and not a minimum. From the nature of the problem so defined, it is obvious which analysis must be used—calculus of variations. This question was pointed out in 1936 by Th. Pöschl in his brief and excellent but evidently unnoticed or forgotten paper in "Der Bauingenieur." Here are Pöschl's points:

1 The so-called strain-energy method is mathematically rigorous only in the case of concentrated loads.

2 From a mathematical standpoint it cannot be used under any circumstances in the case of continuously distributed stresses.

3 In the last case the methods of the calculus of variation should be used.

The writer published in 1947, two short papers on this subject in the *Journal of The Franklin Institute* and two letters in the *Journal of the Aeronautical Sciences* (under the titles, "On the So-called Principle of Least Work Method"). Recently, his paper with all details and with a proposition of the generalized Castigliano's principle appeared in *Oesterreichisches Ingenieur Archiv* (1951). In one of the examples it was shown clearly how large errors and completely wrong results may be obtained using the procedure called strain-energy method in the case of continuously distributed stresses.

The writer askes the authors of the paper to accept these remarks not as a criticism but as a certain contribution to the explanation of their results. The wrong conception of Castigliano's theorem should have been corrected earlier, since, in the case of continuously distributed stresses, the procedure used is a purely random-choice engineering process which in certain instances gave fair results. But it is impossible to foresee in which cases it will succeed and in which cases it will not. Hence it always should be verified by reliable methods (tests, etc.) and applied only to similar cases.

In case there are some fundamental changes in the system, the procedure again should be verified. Previous authors often supported their results based upon that procedure by experimental tests; but it does not mean that one may claim that the process always gives a solution (what is more, an exact solution). It is quite possible that tests will approve the results of the procedure in the present case justifying the authors' considerations.

The writer wishes that this would be the case. Even that fact should not be used as a justification for not presenting the truth to readers, which is that no item in this procedure has a mathematical justification, and one cannot talk about a minimum or exact solution, and that the cited author who developed the method simply misinterpreted the mathematical conception of the minimum of the strain-energy.

Closure by H. D. Conway

The comments of the discussers are appreciated.

The list of recent publications given by Dr. Durelli indicates the very considerable interest taken in the subject. Since the publication of the paper, further photoelastic tests have been made applying the load through various media (including cardboard) and quite good agreement with the theoretical results has been obtained.

In the first method of analysis used in the paper, the writing of the approximate stress function in the form of a series of polynomials leads, after equating the partial derivatives of the strain energy to zero, to a set of algebraic equations which yield

[3] Numbers in parentheses refer to the Bibliography at the end of this discussion.

[4] Professor of Gasdynamics and Theoretical Aerodynamics; Secretary, Panel on Fluid and Solid Mechanics, University of Illinois, Urbana, Ill.

the parameters. An infinite number of parameters do not necessarily lead to an exact solution and this statement in the paper is retracted.

As the author understands it, Professor Krzywoblocki's criticism of the method is that the foregoing procedure does not necessarily lead to a minimum value of the expression for the strain energy. The writer believes that the following (suggested by Prof. J. N. Goodier) shows that it does.

The strain energy V may be written as the integral of

$$V_0 = \frac{1}{2E}\left\{\sigma_x^2 + \sigma_y^2 - 2\mu\sigma_x\sigma_y + 2(1+\mu)\tau_{xy}^2\right\}$$

where the stresses are such that V is stationary ($\partial V/\partial a = 0$) for the set of variations we admit. Assuming that the stresses are varied to $\sigma_x + \delta\sigma_x$, $\sigma_y + \delta\sigma_y$ and $\tau_{xy} + \delta\tau_{xy}$, respectively, and that equilibrium and the original boundary conditions are maintained, the corresponding strain energy is the integral of

$$\frac{1}{2E}\left\{\sigma_x^2 + \sigma_y^2 - 2\mu\sigma_x\sigma_y + 2(1+\mu)\tau_{xy}^2 + 2\sigma_x\delta\sigma_x + 2\sigma_y\delta\sigma_y - 2\mu(\sigma_x\delta\sigma_y + \sigma_y\delta\sigma_x) + 4(1+\mu)\tau_{xy}\delta\tau_{xy} + (\delta\sigma_x)^2 + (\delta\sigma_y)^2 - 2\mu\delta\sigma_x\delta\sigma_y + 2(1+\mu)(\delta\tau_{xy})^2\right\}$$
$$= V_0 + \delta V_0 + \text{value of } V_0 \text{ for } \delta\sigma_x, \delta\sigma_y, \delta\tau_{xy}$$

Since δV_0 (integrated) is zero and the third term is always positive, we have the conditions for a minimum.

Further comment seems unnecessary. Suffice it to say, that despite the dire consequences predicted by Professor Krzywoblocki, the writer still believes the foregoing to be a very valuable method.

Large-Deflection Theory for Plates With Small Initial Curvature Loaded in Edge Compression[1]

SAMUEL LEVY.[2] The analysis of plates with mixed boundary conditions, that is, displacement conditions on one pair of edges and stress conditions on the other, is often necessary in structural design but is generally difficult to make. The author has managed to obtain such solutions with the additional complications of initial curvature and large deflections. Although his primary object was to evaluate various methods of deducing buckling loads from measured center deflections and strains, the methods he has developed for taking account of mixed boundary conditions are quite general and will be useful in analyzing other plate problems.

The author develops an "exact" solution for several examples of buckling of a square plate, and from the resulting plots of deflection and strain versus load, draws interesting conclusions regarding five widely used approximate methods of estimating buckling loads from test data. The comparison of experimental results with the computed curves confirms the theoretical derivations and shows the important effects both of initial deviations from flatness and of restraint of the supported edges from transverse displacements.

The writer believes that it will be necessary to use large-deflection theories to explain satisfactorily a large proportion of the secondary effects associated with the bending of plates. The importance of even small deviations from flatness, as evidenced by the author's Fig. 4, was first brought to light by Hu, Lundquist, and Batdorf. The additional importance of the absence of restraint (in plane warping) along the supported edges has never been so clearly shown as in the comparison of Figs. 2 and 3 in the paper. The stress distribution in the plate at loads of about 1.7 times the buckling value is markedly different in the two cases.

S. B. BATDORF[3] AND G. J. HEIMERL.[3] Experimental buckling stresses are obtained mainly for three purposes, as follows:

1 To check theory.
2 To indicate the behavior of actual structures.
3 To provide a basis for calculating postbuckling behavior.

The paper is concerned with an evaluation of current procedures for predicting experimental buckling loads for the purpose of checking theories, which are usually concerned with the behavior of perfectly constructed and perfectly loaded specimens. Accordingly, the paper deals with the determination of the buckling loads of flat plates from measured behavior of imperfect plates. The analysis is based upon boundary conditions of uniform displacement of the loaded edges and stress-free supported edges. In these respects, it differs from NACA Technical Note 1124 which was concerned with a comparison of the behavior of imperfect plates with that of perfect plates when all edges were kept straight. It would appear that the author's boundary conditions are appropriate for a single plate and for a variety of more complex test specimens, such as rectangular tubes, for example, whereas the boundary conditions of the Technical Note mentioned are more appropriate for structures such as stiffened panels in which the continuity of the sheet helps to hold the edges of each constituent plate straight.

With regard to methods for predicting flat-plate buckling loads experimentally, the author showed that the point of inflection of the curve of load versus deflection gives the true buckling load more accurately than other methods which have been used. Reference to the curves of TN 1124 indicates that this is true also when the side edges of the plate are kept straight. It is generally recognized, however, that slopes cannot be reliably determined when test data exhibit appreciable scatter. It would seem that this remark should apply a fortiori to the determination of the point of inflection, which in effect represents a determination of the second derivative of the curve, whereas the slope constitutes only the first derivative. Moreover, if one is concerned with either plastic buckling or with buckling with a stress close to the elastic limit of the material, there actually may be no point of inflection. For these two reasons it might be expected that the vertical tangent of the plot of load against axial median strain at the center of the plate would generally be preferable to the inflection-point method. However, it should be noted that this method is of limited applicability; whereas the load versus median axial-strain curve exhibits a vertical tangent when the sides of the plate are stress-free, no vertical tangent occurs when the sides are kept straight.

As the author has indicated, the top-of-the-knee method will give somewhat lower buckling loads. It may be in order to point out here that the top-of-the-knee method has been used extensively by the NACA for checking flat-plate theory, but it has been applied only to cases in which there was negligible initial curvature, for example, extruded H-, Z-, and channel sections, and drawn square tubes. Consequently, the knee of the curve is so sharp that little latitude actually exists for choice of buckling stress, and the experimental buckling loads can be considered to be a close indication of the flat-plate buckling load.

According to both the author's results and those of TN 1124, initial eccentricity influences plate behavior markedly in the vi-

[1] By J. M. Coan, published in the June, 1951, issue of the JOURNAL OF APPLIED MECHANICS, Trans. ASME, vol. 73, pp. 143–151.

[2] Aircraft Structures Group, U. S. Department of Commerce, National Bureau of Standards, Washington, D. C. Mem. ASME.

[3] Structures Research Division, NACA, Langley Airforce Base, Va.

cinity of the flat-plate buckling load, while well above this load the load-deflection curves tend to merge. This means that the flat-plate buckling load is a useful parameter for determination of the postbuckling behavior of the plate, for example, maximum strength. However, it would not constitute a good index to the behavior of real plates in the vicinity of the buckling stress, and for the second type of experiment it therefore may be desirable to measure something other than the flat-plate buckling load.

For some purposes the most significant feature of buckling is the deviation from flatness, and for such purposes some parameter, which reflects the behavior in this respect of practical structures with their initial imperfections, should be chosen. In this connection it may be of interest that in NACA tests of stiffened panels the vertical tangent to the curve of load versus axial strain, measured on the convex side of the buckle crest, has often been taken to indicate buckling.

Author's Closure

The author appreciates the comments made. He feels that it is extremely important for internal stress distributions to carefully estimate the boundary conditions along the supported edges as Levy points out. He further agrees with Batdorf and Heimerl that for many structures composed of imperfect (i.e., non-flat) elements the most practical criterion of buckling may be the maximum compressive strain on the convex side of the element. However, he was mainly interested in determining critical loads for imperfect plates with various edge conditions and did not feel that this criterion was pertinent except in the limiting case of the flat plate.

It might be of interest to note that theoretical solutions for the 3 orthotropic cases mentioned by the author have been made by Syed Yusuff and that they agree satisfactorily with the author's test data for orthotropic plates (1). To the best of the author's knowledge, Yusuff's work has not been published; however, a copy of his thesis is available in the library of the Polytechnic Institute of Brooklyn, Brooklyn, N. Y.

Buckling of a Sandwich Cylinder Under Uniform Axial Compressive Load[1]

George Gerard.[2] The author treats small wave-length instability or wrinkling of a circular sandwich cylinder by making the fundamental assumption that the system possesses rotational symmetry. As the result of an investigation conducted for the Office of Naval Research under Contract N6-onr-279, TOV, certain experimental data are available and are offered in discussion of this paper.

Fig. 1, herewith, shows a 12-in-radius sandwich cylinder with a $^1/_8$-in. end-grain balsa core of approximately 5.5-pcf density and 0.01-in. 24S-T4 aluminum-alloy faces. Since the theoretical data for critical stresses contained in the paper are for a considerably different core material, this discussion is limited to the buckle patterns obtained in the tests. Accordingly, Fig. 1 is evidence in support of the assumption of rotationally symmetric deformations for small wave-length instability.

Fig. 2 shows a cross section of a buckled sandwich cylinder of the same construction as that shown in Fig. 1, and also the buckle pattern of the inner face. It is evident that the inner pattern consists of a series of small circumferential buckles and, therefore,

Fig. 1 Sandwich Cylinder Where Wrinkling Occurred

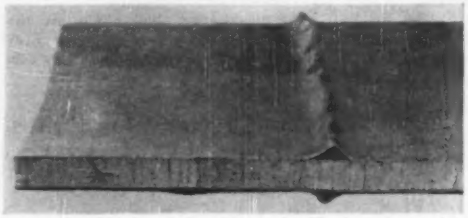

Fig. 2 Cross Section of Buckled Sandwich Cylinder of Same Construction as in Fig. 1

lacks rotational symmetry. The number of circumferential buckles is very large and confined to one band so that the assumption of rotational symmetry appears to be reasonable for theoretical purposes. It should be noted that these conclusions are based on observations of buckle patterns made after failure of the cylinders rather than at the instant of instability.

For the type of instability where the sandwich element buckles as a unit, Fig. 3 is characteristic of the buckle patterns obtained. Rotational symmetry clearly was not obtained for the cylinder shown, which had a 10-in. radius, $^1/_8$-in. cellular cellulose-acetate core of approximately 5-pcf density, and 0.01-in. 24S-T4 aluminum-alloy faces. This mode of instability is not treated in the author's paper but is contained elsewhere.[3] It may be of some interest that in the latter paper buckling loads were obtained for both rotationally symmetric and circumferential buckling modes. As is the case for the linear theory of a homogeneous cylinder, buckling loads of both theories were essentially the same.

There is one significant aspect of the analysis presented by the author which bears amplification. The solution for the wrinkling stress was obtained by considering a limiting form of instability in which essentially the wave length relative to the sandwich thickness becomes vanishingly small. In the other limit, when the

[1] By A. C. Eringen, published in the June, 1951, issue of the Journal of Applied Mechanics, Trans. ASME, vol. 73, pp. 195–202.

[2] Assistant Professor of Aeronautical Engineering, College of Engineering, New York University, New York, N. Y. Jun. ASME.

[3] "Buckling of Sandwich Cylinders Under Axial Compression," by F. K. Teichmann, C. T. Wang, and G. Gerard, *Journal of the Aeronautical Sciences*, vol. 18, no. 6, June, 1951, pp. 398–406.

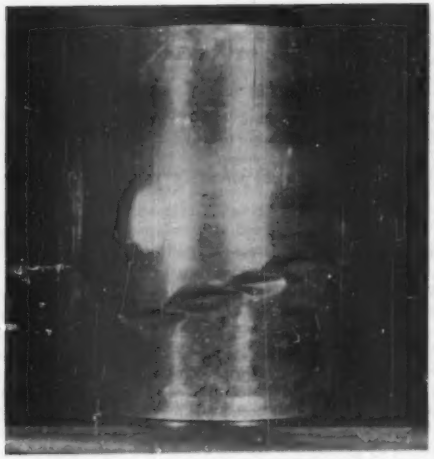

FIG. 3 SANDWICH CYLINDER WHERE BUCKLING OCCURRED AS A UNIT

wave length-thickness ratio becomes very large, it can be shown that buckling of the sandwich as a unit is obtained. Actually, these assumptions concerning the wave lengths form the basis of two different systems of equilibrium equations which have been commonly used in sandwich-plate problems. For the complete spectrum, the more general system such as Equation [39] of the paper should be considered.

AUTHOR'S CLOSURE

Professor Gerard's discussion is very enlightening. It offers a sound support for the basic assumption of the present paper by experimental evidence, namely, rotationally symmetric buckling takes place for thick sandwich cylinders. It is perhaps necessary further to find a criterion in terms of nondimensional thickness parameter τ, to determine when rotationally symmetric buckling ceases to exist.

It is, however, further pointed out that the buckling load is essentially the same for both types of instability, namely, rotationally symmetric and unsymmetric buckling.

The present paper endeavors to explain the ripple type of instability which, in practice, is common to thick sandwich structure. Thus the buckling load obtained is essentially for a small wave-length instability. However, eigenvalues of Equations [32] (rather than [39]) are complete and contain the other cases.

Thermal Effects in Calendering Viscous Fluids[1]

J. T. BERGEN.[2] This paper represents a distinct contribution to the understanding of the rolling process since the question of thermal effects in this process has been largely ignored until the present. The phenomenon of blisterlike formations immediately below the surface of a calendered plastic material is more or less familiar to those who deal with calenders, and it is of interest to note that the author's conclusions impose a definite limit upon the speed, for a given set of conditions, at which a viscous (plastic) material may be calendered.

It should be pointed out that not all types of blister defects appearing in a calendered plastic material are believed by the writers to be caused by thermal effects. Another type of blister even more commonly observed is associated with another relation between the cohesion of the mass and its adhesion to the surface of the calender roll. Such blisters have been attributed to entrained air pockets which are carried through the pressure zone of the calender. However, these questions will be discussed in greater detail at a later date.

One assumption taken at the outset of the author's discussion involves the maintenance of an isothermal at the surface of the roll. Considering one-dimensional heat flow in the unsteady state, the differential equation for the change in temperature within the body as a function of time may be shown to be[3]

$$\frac{\partial u}{\partial t} = \alpha^2 \frac{\partial^2 u}{\partial x^2} \qquad [1]$$

where u is the temperature at distance x from the origin and at time t; α^2 is the thermal diffusivity of a material with thermal conductivity k, specific heat c, and density ρ

$$\alpha^2 = k/\rho c$$

As these authors show,[4] Equation [1] of this discussion is a linear homogeneous differential equation, the solution of which may be expressed as the product of separate functions of the two independent variables, namely, $X(x)$ and $T(t)$. Thus Equation [1] becomes, after separating variables

$$\frac{T'(t)}{\alpha^2 T(t)} = \frac{X''(x)}{X(x)} = q$$

where q is a constant, and the primes denote differentiation with respect to the appropriate variable. Rewriting this equation we find, for x = const

$$T'(t) = \alpha^2 q T(t) \qquad [2]$$

Equation [2], herewith, states that, at a given co-ordinate point x, the rate of change of the temperature in the transient case is proportional to the thermal diffusivity of the material. The appropriate parameters for linoleum color mix given by the author and those for cast iron given by Marks[5] yield a ratio of thermal diffusivity for cast iron compared with linoleum color mix of about 130. Hence, near the interface, the rate of heat flow into the cast iron is sufficiently greater than the rate of heat flow out of the linoleum mass that the assumption of an isothermal roll surface seems justifiable.

Finally, the assumption of viscous behavior on the part of such a material as linoleum color mix has been shown to be at least qualitatively correct[6] to the extent that the picture presented by the author for a viscous liquid may be taken to represent the actual case quite closely.

---

[1] By M. Finston, published in the March, 1951, issue of the JOURNAL OF APPLIED MECHANICS, Trans. ASME, vol. 73, pp. 12-18.

[2] Research Laboratories, Armstrong Cork Company, Lancaster, Pa.

[3] "Advanced Mathematics for Engineers," by H. W. Reddick and F. H. Miller, John Wiley & Sons, Inc., New York, N. Y., 1947.

[4] Ibid., p. 264.

[5] "Mechanical Engineers, Handbook," by L. S. Marks, McGraw-Hill Book Company, Inc., New York, N. Y., 1941.

[6] "Pressure Distribution in the Calendering of Plastic Materials," by J. T. Bergen and G. W. Scott, Jr., JOURNAL OF APPLIED MECHANICS, Trans. ASME, vol. 73, March, 1951, pp. 101-106.

Fluid Flow Through Porous Metals[1]

P. Grootenhuis.[2] A knowledge of the fluid flow through porous materials made by powder-metallurgy methods is becoming of importance with the advent of sweat cooling. The authors have made a valuable contribution, and the method of correlating the experimental data is most interesting. It must be remembered, however, that such a correlation depends upon the determination of the two empirical constants α and β as defined in Equation [4] or [11] of the paper. An experimental determination of the pressure drop-flow characteristic must be made to evaluate these constants for each different type of porous compact. Such an experiment might even be necessary for compacts made of powders of substantially the same particle shape but of varying particle size.

One of the most important objects of a correlation of experimental data as presented in the paper, Fig. 4, should be that no further experiments are necessary to determine similar data for new specimens. It seems that the correlation falls short of this requirement.

The results of similar experiments on some porous metallic compacts were published by the present writer in 1949.[3] The pressure-drop versus flow characteristics were determined for a number of porous-bronze disks, of various thicknesses, and made from powders substantially spherical in shape but varying in size. The results were correlated in a manner analogous to that suggested by Rose[4] for fluid flow through beds of granular materials. The correlation of some of the results is given in Fig. 1, herewith. The resistance coefficient ψ for the isothermal flow of gases is defined as

$$\psi = \frac{(\rho_1^2 - \rho_2^2)\, g\, d}{2\, C\, T\, G^2\, L\, F(f)}$$

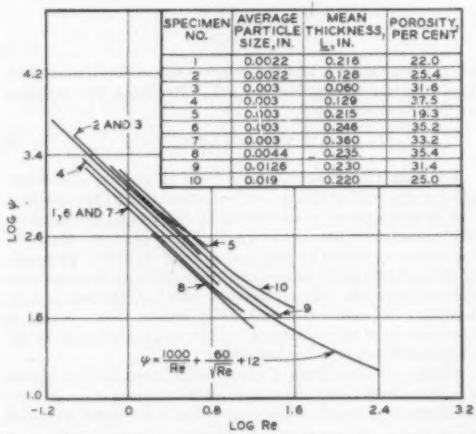

Fig. 1 Correlation of Results for Fluid Flow Through Beds of Granular Materials

where

ρ_1 = upstream pressure
ρ_2 = downstream pressure
d = average particle size
C = gas constant
T = absolute temperature
G = weight rate of flow per unit area
L = thickness of the specimen

and $F(f)$ is a function of the porosity, f

$$= \frac{2.4\,(1-f)^{2.5}}{f}$$

The second characteristic used is the Reynolds number $Re = Gd/\mu$, where μ is the absolute viscosity of the gas.

This correlation depends upon only one empirical relationship, namely, the porosity function $F(f)$. The numerical constants of this function have been derived from the numerous experiments on beds of granular materials of widely varying properties. The graph shows that the correlation between the flow data for the porous disks and the generalized curve by Rose is reasonably good. No allowance has been made for the inevitable distortion of the particles during manufacture. The greatest divergence is shown by specimens 8 and 10, which were made from powders having a poor particle-size distribution.

This correlation shows that as a first approximation, these porous metal disks have flow characteristics similar to those of beds of packed granulars and that, by making use of the well-accepted correlation formulas for such granular materials, the flow properties of new porous metals can be estimated without having to resort to experiments. It is only necessary to measure the average particle size of the powder used in the manufacture. This usually has to be known in any case, to determine the pressing and sintering conditions needed to make the required compact.

It would be of interest if the authors could estimate the average particle size of the powders used and recalculate their experimental data as suggested in these notes. For nonspherical particles the porosity function and shape factors as given by Rose and Rizk[5] or by Coulson[6] should be used.

Authors' Closure

The authors wish to thank Mr. Grootenhuis for his interesting discussion. His suggestion that the porous-metal flow data presented by the authors be correlated in terms of the particle size of the powder forming the compact, however, indicates that the authors have not sufficiently emphasized the raison d'être of their paper. This fact is that the loss of identity suffered by the individual particles in the method of compact manufacture employed by the authors is so complete that no analytical correlation between the original particle size and the flow resistance of the compact has been found to exist. Such a situation required the use of two empirically determined characteristic-length parameters, such as the coefficients α and β defined by the authors.

The authors were careful to point out that in the ideal case of a bed of spherical particles, flow data could be correlated with the use of a single length parameter, the particle diameter. Such a correlation is of course possible with porous metals prepared by the conventional method presumably used by Mr. Grootenhuis, in which closely sized spherical particles, compacted lightly if at all, are sintered under closely controlled conditions of time

[1] By L. Green, Jr., and P. Duwez, published in the March, 1951, issue of the Journal of Applied Mechanics, Trans. ASME, vol. 73, p. 39.

[2] Mechanical Engineering Department, Imperial College of Science and Technology, City and Guilds College, London, England.

[3] "The Flow of Gases Through Porous Metal Compacts," by P. Grootenhuis, *Engineering*, vol. 167, April 1, 1949, p. 291.

[4] "An Investigation Into the Laws of Flow of Fluids Through Beds of Granular Materials," by H. E. Rose, Proceedings of The Institution of Mechanical Engineers, vol. 153, 1945, p. 141.

[5] "Further Researches in Fluid Flow Through Beds of Granular Material," by H. E. Rose and A.M.A. Rizk, Proceedings of The Institution of Mechanical Engineers, vol. 160, 1949, p. 493.

[6] "The Flow of Fluids Through Granular Beds," by J. M. Coulson, Institution of Chemical Engineers, vol. 27, December, 1949.

and temperature. Such a metal, which must retain some of the original void volume of the sphere bed to remain permeable, is typified by the commercial porous-bronze specimen shown in the authors' Fig. 1. It may be seen from this figure that the identity of the individual grains is largely preserved, and in this case knowledge of the grain diameter (and possibly of a suitable shape factor) may permit a prediction of the flow resistance of the compact by the standard methods of fluid mechanics.

In the method of manufacture used by the authors, on the other hand, the metal powder is mixed with a powdered solid which undergoes a phase change into a gaseous state at a temperature slightly below the sintering temperature of the metal. This intimate mixture is then pressed in a die under pressures ranging up to 100,000 psi, and the resulting compact sintered at high temperature. The permeability of the metal is thus due to the pores formed by the escape of the gases generated by the decomposition of the porosity-forming agent. A metal prepared by this technique is typified by the stainless-steel specimen shown in the authors' Fig. 1, from which the loss of particle identity may be seen. This loss of identity, although it complicates the flow picture, is rewarded by a mechanical strength in the compact greater than that obtained by the conventional technique.

In closing, the authors would like to express their preference for the granular bed correlation of Ergun and Orning[7] over that of Rose,[8] since they believe that the two-term quadratic expression of Ergun and Orning gives a clearer picture of the resistance mechanism. In addition, the dimensionless coefficient of the quadratic term (see the authors' Equation [16]) provides a measure of the effect of particle orientation (the mode of sphere packing) upon the flow resistance. This effect has been neglected by Rose, who considers the resistance of a sphere bed (in the absence of wall effects) to be completely described by the particle diameter and bed porosity, but recent work by Martin, McCabe, and Monrad[9] has shown it to be important in certain cases of systematic sphere packing.

The Solution of Elastic Plate Problems by Electrical Analogies[1]

M. V. Barton.[2] The use of an analog computer for the solution of plate problems is valuable for the study of complicated plates having difficult boundary conditions, or in which the plate is variable in thickness, or has unusual plan form. Since, however, the differential equations to be solved for the plate have been approximated in terms of finite differences, the function of the computer is to solve sets of simultaneous algebraic equations representing particular boundary value or characteristic-value problems. Therefore it may be of interest to compare the results obtained by the analog computer with results obtained by brute-force calculations.

It has been the experience of the writer that the type of characteristic-value problem such as the vibration of the rectangular plate discussed in the paper is very laborious to solve by usual numerical procedures. For example, using an iteration procedure on a set of 12 finite-difference equations (same number as used by the author), the characteristic value continues to oscillate between plus and minus values after 24 iterations. An alternative method is to expand the determinant of the equations to obtain the characteristic equation, which in this case is a twelve-degree polynominal, and extract the roots of interest. This has been done to determine the lowest characteristic value for the vibrating cantilever plate. The frequency is found to be $0.503\ 1/a^2\sqrt{D/m}$, as compared with the author's value of $0.501\ 1/a^2\sqrt{D/m}$. The close correlation of these values is an indication of the accuracy of the computer. As the author points out, these values are much lower than the test frequency because of the approximation inherent in the finite-difference method so that comparisons with experimental results are not a good basis for judging the computer's effectiveness.

It is interesting to note that the values of frequency obtained for the vibrating cantilever plate using the twelve equations are lower bounds. The value of the fundamental frequency obtained by the Rits method using a 9-term series of orthogonal beam functions to represent the deflection gives an upper bound of $0.556\ 1/a^2\sqrt{D/m}$ which is less than 2 per cent higher than the experimental value. Therefore it may be desirable to use the analog computer to solve the set of equations resulting from the application of the Rits method rather than using the finite-difference method since for some problems greater accuracy can be obtained with fewer cells.

P. G. Hodge, Jr.[3] The author's solution of the elastic plate problem was particularly interesting to the writer because it can be applied immediately to the elastic plane-strain problem. As is well known, if a stress function ψ is defined by

$$\sigma_x = \partial^2\psi/\partial_y^2,\ \sigma_y = \partial^2\psi/\partial_x^2,\ \tau_{xy} = -\partial^2\psi/\partial_x\partial_y$$

then ψ must satisfy the author's Equation [10] with the right-hand side equal to zero

$$\frac{\partial^4\psi}{\partial_x^4} + 2\frac{\partial^4\psi}{\partial_x^2\partial_y^2} + \frac{\partial^4\psi}{\partial_y^4} = 0 \quad \ldots\ldots\ldots\ldots [1]$$

If the region under consideration is simply connected, the boundary conditions for ψ can be expressed in terms of the stress vector $\mathbf{T}$ applied to the boundary of the region in plane strain. If $\mathbf{n}$ and $\mathbf{t}$ are unit vectors, respectively, normal and tangential to the boundary

$$\psi = \int_0^s\int_0^s \mathbf{T}\cdot\mathbf{n}\,ds\,ds,\ \frac{\partial\psi}{\partial n} = -\int_0^s \mathbf{T}\cdot\mathbf{t}\,ds \quad \ldots\ldots [2]$$

where the integrations are to be taken around the boundary. Thus the boundary conditions can always be computed in the form of Equations [a] and [c] of the author's paper. It follows, then, that exactly the same network can be used to solve a problem in plane elastic strain.

The writer would now like to pose the much more difficult problem of elastic-plastic plane strain. Here the stress function ψ must be continuous with continuous first and second derivatives throughout the region, must satisfy the boundary conditions, Equation [2] of this discussion, and the yield inequality

$$\left[\frac{\partial^2\psi}{\partial_x^2} - \frac{\partial^2\psi}{\partial_y^2}\right]^2 + 4\left[\frac{\partial^2\psi}{\partial_x\partial_y}\right]^2 - 4k^2 \leq 0 \quad \ldots\ldots [3]$$

---

[7] "Fluid Flow Through Randomly Packed Columns and Fluidised Beds," by S. Ergun and A. A. Orning, *Industrial and Engineering Chemistry*, vol. 41, 1949, p. 1179.

[8] "Pressure Drop Through Stacked Spheres: Effect of Orientation," by J. J. Martin, W. L. McCabe, and C. C. Monrad, *Chemical Engineering Progress*, vol. 47, 1951, p. 91.

[1] By R. H. MacNeal, published in the March, 1951, issue of the Journal of Applied Mechanics, Trans. ASME, vol. 73, pp. 59–67.

[2] Research Engineer, Defense Research Laboratory, The University of Texas, Austin, Tex. Mem. ASME.

[3] Assistant Professor of Mathematics, University of California, Los Angeles, Calif. Jun. ASME.

Wherever the inequality in Equation [3] herewith is valid, it must satisfy Equation [1]. This problem is an exceedingly difficult one analytically, and only a very few special cases have been solved.[4] Therefore, if it were possible to construct an electrical analog for this case, it would be a valuable contribution to elastic-plastic theory. This would involve a nonlinear element, which would, in effect, put a "ceiling" on the current that could be carried by any element. Current which would violate this ceiling must then be "rerouted" via other elements in such a way as to preserve the continuity conditions.

Author's Closure

The author wishes to thank Dr. Barton for the numerical verification of the analog-computer results. In the author's opinion, the reason for the lack of agreement between the experimental value for the lowest mode frequencies and the values calculated by finite differences lies in a crude and fortunately avoidable approximation in the distribution of inertias. In the author's paper and presumably in Dr. Barton's calculations, unit masses are connected to interior points; $^1/_2$ unit masses are connected to edge points and $^1/_4$ unit masses are connected to corner points. If instead a distribution is adopted that is statically equivalent to the distributed mass load, better results will be obtained. The square cantilever plate problem has recently been repeated using a finer-mesh (5 cells on a side). The computed frequency is $0.542\,\frac{1}{a^2}\sqrt{D/m}$ which compares well with Dr. Barton's experimental result which is $0.546\,\frac{1}{a^2}\sqrt{D/m}$.

It is probably not practical to use the analog computer to solve the set of equations resulting from an application of the Ritz method. In any event the Ritz method does not produce good values for stresses while in the finite difference method the calculated stresses satisfy statics exactly.

The author wishes to point out to Professor Hodge that the problem of constructing an electric analogy for the elastic plane-strain problem was investigated by G. Kron[5] a few years ago. His plane-strain network was derived as a special case of a network representing a three-dimensional elastic field. Network analyzer solutions were presented in a companion paper.[6]

One form of the plane-strain circuit is similar to the network shown in the author's paper with the W-circuit removed.

The construction of an analog for the elastic-plastic plane-strain problem would be difficult. If the yield inequality were imposed directly on the stress components

$$|\sigma_x| < K_1 \qquad |\sigma_y| < K_2 \qquad |\tau_{xy}| < K_3$$

these conditions could be handled by means of current limiters employing crystal diodes. Unfortunately the condition is imposed on the principal stress as shown in the foregoing Equation [3], which condition cannot easily be imposed on an electric circuit.

[4] "Plane Elastic-Plastic Problem: Plastic Regions Around Circular Holes in Plates and Beams (Russian)," by L. A. Galin, *Prikladnaia Matematika i Mekhanika*, vol. 10, 1946, pp. 365–386; "An Elastic-Plastic Problem With a Nonbiharmonic Plastic State (Russian)," by O. S. Parasyuk, ibid., vol. 13, 1948, pp. 367–370.

[5] "Equivalent Circuits of the Elastic Field," by G. Kron, JOURNAL OF APPLIED MECHANICS, Trans. ASME, vol. 66, 1944, pp. A-149–161.

[6] "Numerical and Network Analyzer Solution of the Equivalent Circuits for the Elastic Field" by G. Carter, JOURNAL OF APPLIED MECHANICS, Trans. ASME, vol. 66, 1944, pp. A-162–167.

The Propagation of Longitudinal Waves of Plastic Deformation in a Bar of Material Exhibiting a Strain-Rate Effect[1]

D. S. Wood.[2] The author has assumed a certain flow law in which the stress depends upon strain rate as well as strain, in an attempt to obtain a better agreement between the theory of plastic strain waves and experimental observations of these waves. This is a good example of the type of procedure which must be followed in order to determine the mechanical properties of materials at the very high strain rates reached in impact tests. The particular flow law assumed by the author leads to improved agreement between theory and experiment in one respect, but, unfortunately, one of the most prominent features of the experimental results is lost, namely, the region of constant plastic strain near the impact end. The writer has the feeling that this disagreement is associated with the fact that the assumed flow law requires purely elastic response of the material to instantaneous finite changes of stress. This implies that the correct flow law must be such that instantaneous finite changes of stress are, in general, accompanied by instantaneous finite changes of plastic strain. A flow law of this type is

$$\sigma = h(\epsilon) - R(\dot{\epsilon})[h(\epsilon) - f(\epsilon)]$$

where

$f(\epsilon)$ represents the static stress-strain relation
$h(\epsilon)$ represents a stress-strain relation for instantaneously applied stresses
$R(\dot{\epsilon})$ is a function of the strain rate such that
$R(0) = 1$, and $R(\infty) = 0$

With regard to the results of compressive impact tests on lead (20), referred to by the author, it should be noted that those specimens which did not show a region of constant plastic strain near the impact end exhibited mushrooming at the impact end; that is, marked lateral flow occurred at the impact surface. For this reason, it appears that any theory properly describing these particular experimental results must be a two-dimensional rather than a one-dimensional theory. Hence, it is difficult to see how a theory of the type presented by the author can describe these results properly.

E. H. Lee.[3] The numerical integration, the results of which are given in this paper, illustrates the length and complication of a wave analysis for a stress-strain relation involving a strain-rate dependence. Although the assumed, seemingly reasonable, relationship does not reproduce all the experimental results, it is valuable in emphasizing features of the stress, strain, strain-rate relation required.

The remarkable requirements called for by the experimental results cited in references (18) and (19) of the paper, have not, it is believed, been generally appreciated. After impact a region of uniform permanent strain is obtained, which comprises material which has been subjected to the maximum stress throughout the duration of impact, and material which has only instantane-

[1] By L. E. Malvern, published in the June, 1951, issue of the JOURNAL OF APPLIED MECHANICS, Trans. ASME, vol. 73, pp. 203–208.

[2] Assistant Professor of Mechanical Engineering, California Institute of Technology, Pasadena, Calif. Jun. ASME.

[3] Professor of Applied Mathematics, Brown University, Providence, R. I. Mem. ASME.

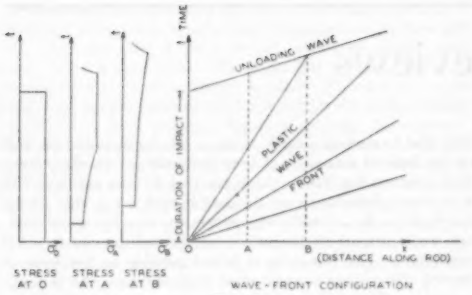

FIG. 1

ously been subjected to this stress. This condition is shown in Fig. 1, herewith, which illustrates approximate loading cycles at different sections of the rod. To a high degree of accuracy, uniform strain is obtained throughout the extent *OB* of the travel of the wave of maximum stress, and a stress, strain, strain-rate relation must be found which gives the same plastic strain for this widely different range of loading histories.

AUTHOR'S CLOSURE

The author wishes to thank Professors Wood and Lee for their pertinent discussion of the paper.

Perhaps the flow law should permit some instantaneous plastic response to applied stress, as suggested by Professor Wood; but the author doubts that a law of the particular form suggested would predict the region of constant strain near the impact end, since the factor $R(\dot{\epsilon})$ would not affect the maximum strain attained at different cross sections in the same degree because the strain-rate history varies greatly from one section to another near the impact end, as was pointed out by Professor Lee. It almost seems that the multiplier R should be a function of the velocity with which the impact end is struck instead of the strain rate in order to predict the constant-strain region, but such a dependence on velocity does not seem reasonable.

The author agrees with Professor Wood that a two-dimensional theory would be needed to describe properly the deformation in lead bars under compressive impact, when mushrooming occurs at the impact end. A law of the type used by the author, which predicts continued flow, could at best only account for the beginning of mushrooming.

Shakedown in Continuous Media[1]

P. G. HODGE, JR.[2] Professor Symonds is certainly to be congratulated on having extended the concept of shakedown to the important case of continuous media. It is perhaps of some interest to notice that the inequality Equation [25] of the paper, obtained as a necessary condition for shakedown in a particular example, can, in fact, be generalized. To this end, let s_{ij}° and $s_{ij}^{\circ\circ}$ be any two admissible elastic-stress states. Then, a necessary condition for shakedown is

$$\left(\frac{s_{ij}^{\circ\circ} - s_{ij}^{\circ}}{2}\right)\left(\frac{s_{ij}^{\circ\circ} - s_{ij}^{\circ}}{2}\right) \leq 2k^2 \quad \ldots\ldots [1]$$

[1] By P. S. Symonds, published in the March, 1951, issue of the JOURNAL OF APPLIED MECHANICS, Trans. ASME, vol. 73, pp. 85–89.

[2] Assistant Professor of Mathematics, University of California, Los Angeles, Cal. Jun. ASME.

For assume that the Inequality [1] is false, then

$$s_{ij}^{\circ} s_{ij}^{\circ} > 8k^2 \quad \ldots\ldots [2]$$

where the notation $s_{ij}^{\circ} = s_{ij}^{\circ\circ} - s_{ij}^{\circ}$ has been introduced. In addition, if there exists a shakedown state, it follows from the author's Equation [6] that

$$(\bar{r}_{ij} + s_{ij}^{\circ})(\bar{r}_{ij} + s_{ij}^{\circ}) \leq 2k^2 \quad \ldots\ldots [3]$$

$$(\bar{r}_{ij} + s_{ij}^{\circ} + s_{ij}^{\circ})(\bar{r}_{ij} + s_{ij}^{\circ} + s_{ij}^{\circ}) \leq 2k^2 \quad \ldots\ldots [4]$$

However, it will now be shown that the Inequalities [2], [3], and [4], herewith, are inconsistent.

The Inequality [4] can be continued in the form

$$2k^2 \geq (\bar{r}_{ij} + s_{ij}^{\circ})(\bar{r}_{ij} + s_{ij}^{\circ}) + 2\,s_{ij}^{\circ}(\bar{r}_{ij} + s_{ij}^{\circ}) + s_{ij}^{\circ} s_{ij}^{\circ} = (\bar{r}_{ij} + s_{ij}^{\circ})(\bar{r}_{ij} + s_{ij}^{\circ}) - 2|s_{ij}^{\circ}(\bar{r}_{ij} + s_{ij}^{\circ})| + s_{ij}^{\circ} s_{ij}^{\circ} \quad \ldots\ldots [5]$$

The second step is valid, since in view of Inequality [2] of this discussion and the fact that the first term in the middle member of Equation [5] is nonnegative, the second term is less than zero. In view of Cauchy's inequality (following author's Equation [16]), Equation [5] leads to

$$2k^2 \geq (\bar{r}_{ij} + s_{ij}^{\circ})(\bar{r}_{ij} + s_{ij}^{\circ}) - 2[(\bar{r}_{ij} + s_{ij}^{\circ})(\bar{r}_{ij} + s_{ij}^{\circ}) \times s_{mn}^{\circ} s_{mn}^{\circ}]^{1/2} + s_{mn}^{\circ} s_{mn}^{\circ} = [\sqrt{s_{mn}^{\circ} s_{mn}^{\circ}} - \sqrt{(\bar{r}_{ij} + s_{ij}^{\circ})(\bar{r}_{ij} + s_{ij}^{\circ})}]^2 \quad \ldots\ldots [6]$$

Finally, it follows from Expressions [6], [2], and [3], herewith, that

$$2k^2 > [\sqrt{8k^2} - \sqrt{2k^2}]^2 = 2k^2 \quad \ldots\ldots [7]$$

which is an obvious contradiction. Thus the Inequality [1] is a necessary (although, in general, not a sufficient) condition for shakedown.

AUTHOR'S CLOSURE

Professor Hodge's contribution is appreciated. Unfortunately, as he states, the theorem he proves gives a necessary but not sufficient condition for shakedown. An interesting subject for future study is the relation between the theorems concerning the load limits for which shakedown just occurs, and those which recently have been proved concerning the loads at which unrestricted plastic flow occurs under steady proportional loading of an elastic perfectly plastic body.[3,4] In the case of continuous frame structures close analogies exist between the analytical methods for proportional loading and for variable, repeated loads.[5,6] It would be of great interest to find whether similar analogies can be utilized also in the case of continuous media.

[3] "The Safety Factor of an Elastic-Plastic Body in Plane Strain," by D. C. Drucker, H. J. Greenberg, and W. Prager, Paper No. 51—A-3, to be presented at the Annual Meeting, Atlantic City, N. J., Nov. 25–30, 1951, of THE AMERICAN SOCIETY OF MECHANICAL ENGINEERS.

[4] "Extended Limit Theorems for Structures and Continuous Media," by D. C. Drucker, W. Prager, and H. J. Greenberg, technical report, No. 59, Brown University to Office of Naval Research, March, 1951.

[5] "A Method for Calculating the Failure Load for a Framed Structure Subjected to Fluctuating Loads," by B. G. Neal and P. S. Symonds, *Journal of the Institution of Civil Engineers* (London), vol. 35, 1950–1951, pp. 186–198.

[6] "New Techniques for Computing Plastic Failure Loads of Continuous Frame Structures," by P. S. Symonds and B. G. Neal, paper presented at First U. S. National Congress of Applied Mechanics, Chicago, Ill., June 11–16, 1951, technical report No. 62, Brown University to Office of Naval Research, August, 1951.

Book Reviews

Statistical Decision Function

STATISTICAL DECISION FUNCTION.[1] By Abraham Wald. John Wiley and Sons, Inc., New York, N. Y., 1950. Cloth, 6 × 9 in., bibliography, index, ix and 179 pp., $5.

REVIEWED BY B. EPSTEIN[2]

IN THIS book Professor Wald has brought together virtually all that is known concerning the theory of statistical decision. Results which up to now were available only in journal articles are related one to the other and made part of a coherent theory. In addition, Professor Wald, the originator of this beautiful body of results, presents some new material which had not been published previously. In this book Wald has laid down the general framework of a decision theory, has proved a number of key theorems, and has indicated that a vast unexplored territory lies before us. With his untimely passing[3] those workers who remain will return time and again to this book for inspiration and guidance.

Perhaps Wald's greatest contribution during his lifetime and particularly in this book is that he focused attention on the really central aim of the statistician and statistical theory. It is the central aim of statistics to make the best possible decisions on the basis of information furnished by observations made on a random process. In this statement we mean to encompass the efficient design of experiments where one's object is to run experiments in such a way as to get the maximum amount of information per observation. It includes the problem of making the "best" estimate of some unknown parameter(s) from a set of observations. It includes the problem of minimizing in some sense the chances of making a wrong choice between two or more hypotheses when all we have to go on are a number of observations following some probability law. In its all-inclusiveness this theory becomes of central importance to physical, biological, and social scientists, to engineers, and to all those who are continually grappling with the problem of how to design experiments better, of how to get the most out of their data, and of how to take an action on the basis of the observations which is best in some reasonable sense.

To R. A. Fisher, the eminent British statistician, and his school do we owe the great strides which have been made in the scientific design of experiments. His classic work "Design of Experiments" should be required reading for all who are experimenters, whether their purpose be to wrest another secret from nature, or finding a cure for any one of the terrible diseases which afflict man and other living things, or finding a better way of making a screw. To Jerzy Neyman and Egon Pearson, and indeed to many statisticians both here and abroad, do we owe the beautiful theory of testing hypotheses and estimation. In this theory Neyman and Pearson made explicit the ideas of "best" estimates and "best" tests, introduced various criteria for "bestness," developed methods for finding "best" tests when they existed. They introduced the ideas of errors of first and second kind, acceptance (or rejection) regions, power curves, and made people aware that they should choose tests which as frequently as possible lead to making a right decision. If, for instance, we wish on the basis of a number of tests to decide (*a*) whether to say that a patient has TB, or (*b*) to say that he does not have TB, it is clearly desirable to use the data in such a way that on the one hand we do not send a sick person out into the world without treatment, or on the other, commit well persons to a TB sanitarium. Unfortunately, it is not possible on the basis of limited observations to avoid these kinds of errors. In fact, one cannot simultaneously make both of these errors small without paying for this assurance by increasing the number of observations. In the Neyman-Pearson theory a method is developed for handling these kinds of problems. These ideas are perhaps best known to engineers by their application (an independent and to some extent prior development) by Harold Dodge and H. G. Romig of the Bell Telephone Laboratories. In this context errors of the first and second kind become, on the one hand, rejection of good lots (producers' risk) and on the other, acceptance of bad lots (consumers' risk).

In the light of the earlier work by Fisher, Neyman, Pearson, and many others, Wald's great contribution is that he introduced a new element into the design of experiments and testing of hypotheses. Wald recognized that while it is important that we make the probability of a wrong decision and hence wrong action as small as possible, it is essential that we further consider the possible loss due to taking the wrong action on the basis of the evidence. If one defines with Wald the idea that the risk of a procedure is the expected cost of taking observations plus the expected loss, it is clear that it is desirable in some sense to choose that decision procedure which minimizes the risk. Wald proposes a procedure known as minimax, which is to choose that decision rule which has the smallest maximum risk; others (including Wald) have suggested other possible methods for choosing a "best" decision procedure, e.g., to choose that procedure for which the average risk is as small as possible. While arguments may be presented pro and con for various definitions of "best" decision procedures, it is clear that such problems should be of basic concern to experimenters, and to those charged with making possibly high-policy decisions on the basis of collected information.

Perhaps the greatest difficulty in applying this theory (and hence an area in which much work should be done) is that Wald assumes that cost of experimentation, losses, and hence risks, can all be measured in terms of money. While this is a useful assumption to make in building up a purely mathematical theory it is perfectly apparent that there are many practical problems where the cost of a wrong decision could not possibly be assessed in purely monetary terms. It may be a cliché, but it is still to the point to ask how much is a human life worth, if our decision happens to be the erroneous one of letting a dangerously contaminated consignment of drugs go out on the market. Similarly, how does one measure in monetary terms the wrong decision not to manufacture a drug which it turns out some years later is really an effective cure for some disease? Clearly, these problems become most critical in the area of the social and biological sciences, although they are surely present in all problems, and consequently some general theory of value will have to be brought in. Value judgments involving at least a ranking of the objectives of an experiment will have to be made if one wishes to apply Wald's ideas in the real world.

[1] Reprinted from *Applied Mechanics Reviews*, vol. 4, September, 1951, pp. 492–493.

[2] Department of Mathematics, Wayne University, Detroit, Mich.

[3] Professor Wald and his wife were killed in an airplane accident in India on Dec. 13, 1950.

It is always unpleasant for a reviewer to have to point to a blemish in the work he is reviewing. It is particularly so in this case, since this book is going to be a classic no matter what minor faults it may have. The point this reviewer wishes to make is that the book is difficult to read. This is true for the professional statistician and is a hundredfold true for the natural scientist, the social scientist, the medical man, the engineer. The results are given so abstractly and the treatment is so complicated that the reviewer thinks that many readers will simply give up in despair. There should have been more motivation and more could have been accomplished by not trying to be so general as to obscure essential ideas. This criticism is directed not only at this book, but also at all those who feel that it is not necessary to motivate their results and to, so to speak, take the reader into their confidence.

In closing we should like to bring to the attention of the reader a number of articles which explain in a simple way some of the basic motions in Wald's theory of decision functions. These are: "The Utility of Analysis of Choices Involving Risk," by M. Friedman and L. J. Savage, *Journal of Political Economy*, vol. 56, 1948, pp. 279–304; "Statistical Decision by the Method of Minimum Risks: An Application," by R. Clay Sprowls, *Journal of the American Statistical Association*, vol. 45, 1950, pp. 238–248; "The Theory of Statistical Decision," by L. J. Savage, *Journal of the American Statistical Association*, vol. 46, 1951, pp. 55–67. It is also recommended that the interested reader study carefully the ideas contained in chapters 1 and 5 of Prof. J. Neyman's recent book "First Course in Probability and Statistics," Henry Holt and Company, New York, N. Y., 1950.

Dimensional Analysis

DIMENSIONAL ANALYSIS AND THEORY OF MODELS. By Henry L. Langhaar. John Wiley & Sons, Inc., New York, N. Y.; Chapman & Hall, Ltd., London, England, 1951. Cloth, 6 × 9 in., 15 figs., 3 tables, problems, index, xi and 166 pp., $4.

REVIEWED BY PAUL A. LIBBY[4]

FOR engineers and students unfamiliar with dimensional analysis or familiar with its applications in only a limited field, this book will be interesting and illuminating. Professor Langhaar has achieved an attractive balance between theory and application. Thus one finds the statement and proof of the basic Buckingham theorem, an illustration of the Rayleigh method, and the application of matrix algebra to the systematic determination of dimensionless products. Furthermore, one finds many practical applications of dimensional analysis chosen from the fields of marine engineering, underwater explosions, elasticity, structural design, vibrations, fluid mechanics, heat conduction, heat transfer, and electromagnetism.

Professor Langhaar has been careful to avoid a danger inherent in a book on such a specialized topic, namely, not providing the reader with a proper perspective. Thus he has pointed out the limitations of dimensional analysis and the need for a physical and theoretical understanding of the problem before dimensional analysis can be profitably brought to bear. In particular, it has been pointed out that the engineer in deciding what variables should be introduced into the analysis "must understand why and how . . . . (each) variable influences the phenomenon."

An aerodynamicist will notice several minor errors. It is stated that the aerodynamic forces on a body moving at flight Mach numbers greater than 0.80 are little affected by Reynolds number changes. The recent work on shock-wave boundary-layer interaction and on base pressures have indicated strong Reynolds number effects. Further, it is stated that fluid density does not affect the incompressible laminar boundary-layer velocity distribution because "the inertia forces are slight." The inertia forces in the boundary layer are of the same order of magnitude as the viscous forces and the density does appear implicitly through the kinematic viscosity. Although other reviewers may find minor errors in the text on their fields of specialization, these will not detract from a useful and stimulating book.

[4] Assistant Professor of Aeronautical Engineering, Polytechnic Institute of Brooklyn, Brooklyn, N. Y.

The Behavior of Engineering Metals

THE BEHAVIOR OF ENGINEERING METALS. By H. W. Gillett. John Wiley and Sons, Inc., New York, N. Y.; Chapman and Hall, Ltd., London, England, 1951. Cloth, 5½ × 9 in., 58 figs., 17 tables, appendix, subject and author indexes, xvi and 395 pp., $6.50.

REVIEWED BY JOSEPH MARIN[5]

THIS book deals with metallurgy and was prepared for engineers who have not specialized in this field. Its objective is to aid those who are not metallurgists in the selection of metals in engineering design. In order to meet the objective the author has not discussed various theories on behavior of metals, and the use of technical terms has been reduced to a minimum.

The first part of the book deals with basic concepts of metallurgy, including mechanical tests, specifications, notches and surface stresses, stress concentration, chemical and physical properties, and quality control.

A second section of this book considers the behavior of each of the main commercial metals and alloys.

In the remaining chapters the factors which influence the selection of metals and alloys are considered. These factors include machinability, various fabrication methods, corrosion, wear, high temperature, cost, and availability.

The author has brought together in one book the many considerations involved in the selection of materials for engineering purposes. His important contributions to metallurgy made him an outstanding metallurgist of his day and a reflection of this background is found in the method of presentation and content of this book.

Servomechanisms and Regulating System Design

SERVOMECHANISMS AND REGULATING SYSTEM DESIGN. Volume 1. By Harold Chestnut and Robert W. Mayer. John Wiley & Sons, Inc., New York, N. Y., 1951. Cloth, 6 × 9 in., illus., tables, bibliography, problems, index, xiii and 505 pp., $7.75.

REVIEWED BY JOHN A. HRONES[6]

THIS book of 500 pages is written as an introductory text in automatic-control theory, the title being somewhat misleading as little space is devoted to design considerations and no discussion of actual components is included although transfer functions for a number of commonly used systems are developed. The chapter headings given below indicate the ground covered. (1) the automatic-control problem, (2) manipulation of complex numbers, (3) solution of linear differential equations, (4) Laplace transforms for the solution of linear differential equations, (5) steady-state operation with sinusoidal driving functions, (6) methods of determining system stability, (7) typical control elements and their transfer functions, (8) types of servomechanisms and con-

[5] Professor of Engineering Mechanics and Research Professor of Engineering Materials, The Pennsylvania State College, State College, Pa. Mem. ASME.

[6] Professor of Mechanical Engineering, Massachusetts Institute of Technology, Cambridge, Mass. Mem. ASME.

trol systems, (9) complex plane representation of feedback control-system performance, (10) design use of complex plane plot to improve system performance, (11) attention concepts for use in feedback control-system design, (12) application of attenuation—phase diagrams to feedback control design problems, (13) multiple loop and multiple-input feedback control systems, (14) comparison of steady-state and transient performance of servomechanisms.

The authors have done a thorough and detailed job of handling the mathematics and theory of automatic control. The applications mentioned are largely in the servomechanism field although reference to process control is made in the problems at the end of the book.

This book should prove to be a good standard reference book gathering together a great deal of necessary information in essentially conventional fashion as it is presented in a number of schools. The emphasis is largely on mathematics with little attention paid to the more difficult problem of the actual design characteristics and limitations of real physical systems. The indication is that such material will be touched upon in volume 2.

Marks's Mechanical Engineers' Handbook

MECHANICAL ENGINEERS' HANDBOOK. Edited by Lionel S. Marks. McGraw-Hill Book Company, Inc., New York, N. Y.; Toronto, Ont., Can.; London, England. Fifth edition, 1951. Fabrikoid, 6 × 9 in., thumb-indexed, illus., index, xvii and 2236 pp., $15.

REVIEWED BY C. O. DOHRENWEND[7]

THE general layout and contents of this fifth edition is similar to that of the fourth edition. It contains, like the fourth edition, sixteen major sections dealing with the various aspects of mechanical engineering.

Many details of the various sections have been revised and improved; thus the handbook has been brought up to date and its utility enhanced. One major improvement is the enlarged format; this not only makes the text of the book more legible, but also makes the tables and charts easier to use.

Since Marks's Handbook is so well known and widely used, it is only necessary for this review to point out that the major alterations and additions have been to cover more adequately the newer developments in the field of mechanical engineering.

Kent's Mechanical Engineers' Handbook

KENT'S MECHANICAL ENGINEERS' HANDBOOK. (Wiley Engineering Handbook Series.) Vol. 1. Design and Production Volume, edited by C. Carmichael. Vol. 2. Power Volume, edited by J. K. Salisbury. John Wiley & Sons, Inc., New York, N. Y.; Chapman and Hall, Ltd., London, England. Twelfth edition paged in sections, 1950. Leather, 5½ × 8½ in., illus., diagrams, charts, tables, bibliographies, $8.50 each volume.

REVIEWED BY C. O. DOHRENWEND[7]

THE twelfth edition of this handbook is in two volumes of the Wiley Handbook Series.

The first on power is edited by J. Kenneth Salisbury and replaces the eleventh edition by R. T. Kent and the second on Design and Production is edited by Colin Carmichael and replaces the eleventh-edition volume on design and shop practice edited also by R. T. Kent.

The volume on power has been reorganized and widely rewritten. The basic reorganization is in groups of sections as follows: sections 1 to 4 treat the basic factors common to any power process; sections 5 and 6 treat the service functions of pumping and piping; sections 7 to 10 treat power-producing equipment; sections 11 and 12 are devoted to refrigeration, heating, ventilating, and air conditioning; sections 13 to 15 cover the subject of transportation power; section 16 treats electric power; section 17 discusses atomic energy; and sections 18 to 20 deal with instrumentation, power testing, and mathematical tables.

The new treatment of the various topics all point to the modern trends toward the more active subjects such as, combustion-gas turbines, jet-propulsion aircraft, heat pumps, axial-flow compressors, atomic energy, and instrumentation.

The volume on design and production has shifted the emphasis to underscore the fact that design and production are in reality but two phases of a single activity. Like its sister volume it has been reorganized into groups of sections as follows: sections 1 to 6 treat the problems of selection of material; sections 7 to 9 are devoted to design principles; sections 10 to 18 cover the selection and design of machine components, sections 19 to 25 treat production processes; sections 26 and 27 cover production-plant equipment; and section 28 is devoted to mathematical tables.

With minor exceptions the two volumes have been nearly completely rewritten with considerable additions as to data and illustrations collected from a wide variety of sources. This procedure has brought the volumes up to date and greatly increased their value to the practicing engineer.

Ordinary Nonlinear Differential Equations

ORDINARY NON-LINEAR DIFFERENTIAL EQUATIONS; in Engineering and Physical Sciences. By N. W. McLachlan. Oxford University Press, New York, N. Y., 1950. Cloth, 9¼ × 6 in., 89 figs., bibliography, index, vi and 201 pp., $4.25.

REVIEWED BY K. KLOTTER[8]

THE fertile pen of the author, who in recent years has presented the scientific public with several textbooks on various subjects in applied mathematics and applied physics, has turned here to a theme which has something of the luster of the latest fashion: the nonlinear differential equations.

As the nonlinear field comprises everything but the linear "exclave" it is, of course, a wide one and the necessity for any author to make a selection of specific topics and methods which he is going to treat is obvious. This naturally leaves much to his tastes and predilections.

How the author of the book under review has selected and organized his material may be seen from the contents. The first chapter gives a general introduction listing a wide variety of phenomena which can be described by nonlinear differential equations. However, practically every physical phenomenon is intrinsically a nonlinear one and becomes treatable by linear equations only after simplifications, often quite bold ones; therefore, the list may be considered somewhat arbitrary or even perfunctory.

The second and third chapters deal with the equations which are readily integrable either with or without elliptic integrals and elliptic function. Chapter four considers equations "having periodic solutions" and embraces the two very distinct and different phenomena of self-sustained oscillations and of forced vibrations.

[7] Head, Department of Mechanics, Rensselaer Polytechnic Institute, Troy, N. Y. Mem. ASME.

[8] Associate Professor of Engineering Mechanics, Stanford University, Stanford, Calif.

The fifth chapter is entitled "Method of Slowly Varying Amplitude and Phase," and presents the method which is customarily linked to the names of Kryloff and Bogoliuboff. The next chapter discusses a special aspect of the results of the foregoing one and is entitled "The Equivalent Linear Equation," which is just another expression for determining the "average frequency." In chapter seven, equations with periodic coefficients are treated. The related phenomena are usually referred to as having "parametric excitation." As an example, cubic (or similar) terms have been added to the (linear) Mathieu equation. The eighth, and last, chapter deals with "Graphical and Numerical Solutions."

Because the book contains hardly any essential, original contribution on the part of the author and because of the nature of the contents, it assumedly is intended to serve as a textbook. It, therefore, must be judged by textbook standards. One expects a textbook to present the basic concepts and ideas which govern the methods discussed, their assumptions, their scope of application, and their limitations. Unfortunately, little of this nature is found in this work. The reviewer wishes to point out two striking examples to support this statement.

First, on page 42, van der Pol's equation is established

$$\ddot{y} - b(1 - y^2)\dot{y} + ay = 0 \quad \ldots\ldots\ldots\ldots\ldots\ldots [5]$$

For solving this equation, the author suggests: "..... Let $y = A \sin \omega_0 t$, then substituting into Equation [5] multiplying by $\cos \omega_0 t$ and integrating from $t = 0$ to $2\pi/\omega_0$ ..... we get $A = 2$ and repeating the above procedure, but multiplying by $\sin \omega_0 t$, we obtain..... $\omega_0^2 = a$..... Hence we obtain the approximate periodic solution

$$y = 2 \sin a^{1/2} t \ldots\ldots" \quad \ldots\ldots\ldots\ldots [14]$$

No indication is given as to why this procedure is adopted or as to the assumptions involved, or as to the general nature of the result (limit cycle). Nor is any indication given that this procedure is equivalent to the Ritz-Galerkin method; it appears wholly as a trick, serving only an immediate purpose. Hardly any student, the reviewer feels sure, will be able to grasp anything of the significance of what is accomplished by this procedure and to what other problems this method (seemingly no method at all) may be applied.

Second, the powerful tool of the phase-plane, which on one hand, allows a representation of complete classes of motions and on the other hand, offers abundant opportunities for integrating practically any differential equation of the second order, appears in chapter eight again as merely a trick for effecting a graphical integration. Nothing is said about the generality of the method in the two directions indicated above; its name is not even mentioned.

The author's informal manner of writing, which was quite charming in some of his earlier books, amounts to a severe deficiency in this one.

Data Book on Hydrocarbons

DATA BOOK ON HYDROCARBONS—Application to Process Engineering. By J. H. Maxwell. D. Van Nostrand Company, Inc., New York, N. Y., 1951. Cloth, 7 × 10 in., viii and 259 pp., tables, references, index, charts, $5.

REVIEWED BY JOSEPH KAYE[9]

THE collection of basic properties of hydrocarbons and petroleum fractions given in this reference book is useful for the solution of many engineering problems. In the short space of 260 pages, a large variety of different properties of many types of hydrocarbons is presented in either tabular or graphical form.

The first six chapters of the book present data on the melting point, boiling point, density, critical constants, molecular weight, vapor pressure, and fugacity of pure hydrocarbons, of some organic compounds, and of various petroleum fractions. Most of these properties are presented on charts which are well done. In addition, the use of the charts and data in the solution of problems is illustrated by several detailed examples.

The seventh chapter presents data on specific heat, latent heat of vaporization, as well as diagrams of enthalpy – pressure, enthalpy – temperature, and enthalpy – entropy. Most of these charts are for pure hydrocarbons but some are for petroleum fractions. There are, for example, individual Mollier diagrams for eight simple hydrocarbons. Chapter 8 presents density data for hydrocarbons and mixtures as well as a series of charts of the p-v-T relations for hydrocarbon vapors. Chapter 9 has a series of charts and nomographs on the viscosities of different hydrocarbons, oils, and vapors. Chapter 10 presents data on the heat of combustion of hydrocarbons and mixtures and some data on the properties of flue gases.

The last four chapters of the book present charts for solution of problems dealing with flow of fluids in pipes and other channels, with flow of heat, with equilibrium flash vaporization, and with fractionating towers. Tables of conversion factors and an adequate index comprise the rest of the volume.

Engineers who have had occasion to work with properties of hydrocarbons will find this volume a valuable reference book.

Advances in Applied Mechanics

ADVANCES IN APPLIED MECHANICS, Vol. II, Edited by R. von Mises and Th. von Kármán. Academic Press, Inc., New York, N. Y., 1951. Cloth, 5¾ × 9 in., tables, figs., references, author and subject indexes, x and 233 pp., $6.50

REVIEWED BY HUGH L. DRYDEN[10]

THIS book is a collection of five papers, each of which gives a survey of the present state of research in a selected, usually narrow, field of applied mechanics. Three of the five deal with topics in fluid mechanics, one with the bending of curved tubes, and one with the application of inverse and semi-inverse methods of investigating the mathematical equations applicable to problems in fluid mechanics and elasticity.

The first paper is a 19-page review of recent applications of statistical theory to the spectrum and decay of isotropic turbulence by Th. von Kármán and C. C. Lin.

The second paper is a guide to the literature on the theory of steady compressible flow in a laminar boundary layer by G. Kuerti.

R. A. Clark and E. Reissner present the results of their own analysis of the problem of the bending of curved tubes, in which the bending of the tube is considered as a problem of the theory of thin shells. The theory is developed for a tube with uniform circular cross section.

P. F. Neményi in a stimulating paper describes representative examples of inverse and semi-inverse methods of investigating the solutions of partial differential equations to illustrate the nature, value, and potentialities of this approach. Such methods often lead to the discovery of unsuspected properties of the solutions.

The final paper by P. Ya. Polubarinova-Kochina and S. B. Falkovich on the theory of filtration of liquids in porous media is a translation of a paper which originally appeared in a Russian technical magazine. All but a dozen of the 197 references are to Russian papers and the paper aims to "present the development

[9] Associate Professor of Mechanical Engineering, Massachusetts Institute of Technology, Cambridge, Mass. Mem. ASME.

[10] Director, National Advisory Committee for Aeronautics, Washington, D. C. Fellow ASME.

and current state in the Soviet Union of the theory of filtration of liquids, mainly of the part of it which deals with exact solutions." The quality of the translation of the original by D. R. Mazkevich is outstanding.

The present volume maintains the high standard of the first volume of the series and it is to be hoped that other volumes will cover more topics and appear more frequently.

Steam Turbines

STEAM TURBINES. By Edwin F. Church, Jr. McGraw-Hill Book Company, New York, N. Y. Third edition, 1951. Cloth, 6 × 9 in., xvi and 531 pp., illus., $6.

REVIEWED BY JOSEPH H. KEENAN[11]

THIS book has become an American classic. The present third edition establishes it more firmly than ever as a reference work for the turbine designer as well as "an intermediate text" as claimed on the dust cover.

The author has undertaken with skill and painstaking care the task of reporting on American practice in the design of steam turbines. To this end he has searched the literature and interviewed the designers. In his Preface to the Third Edition he lists the new material as follows: "descriptions of improved experimental methods used, and results obtained in tests of nozzles and blades; more general treatment of blading theory and performance with various degrees of reaction; variations of fluid flow through nozzles and blades at different radii; twisted blades; elementary aerodynamic theory and its application to the design of turbine parts; effects of sonic or near-sonic velocities on the flow in turbines; vibration of shafts, wheels, and blades, their effects and control; forms taken by turbines due to differences in steam and exhaust conditions, magnitude of output and use applications; forms taken by turbine structural elements, and materials used in them to meet the special requirements presented by high steam pressure and temperature; high speed of rotation, and large capacity; forms of governors suitable for turbines of various types and sizes; and performance data selected to cover a wide range of sizes and types of turbines."

The deficiencies of this book arise, perhaps, from the ascendancy in the author of the reporter over the analyst. The file cabinets of the turbine designer hold a mass of empirical and analytical material that has been only in small measure correlated and integrated into a technical structure. It is an appalling miscellany the index to which resides in the minds of the turbine designers. The author has brought some of this material into a kind of order, but the evidence of disorder is still present.

It would, in fact, take a strong and, perhaps, ruthless analytical hand to bring this material into order. But it is not in analysis that this book is at its best. Sound analysis requires first and foremost a carefully selected vocabulary with rigorous definitions. In this book the terms energy, available energy, heat available, and so on, are used loosely. The quantity "internal thermal efficiency," defined as turbine work over heat input, has almost as little reason for existence in a study of modern steam plants as it would have in a gas-turbine plant. The internal engine efficiency is defined as the ratio of turbine work to Rankine work, though Rankine's name in this connection refers to a cycle and not to a turbine process. The "degree of reaction" is defined on page 230 in two ways which are not identical, neither of which is satisfactory for the compressible case, and one of which is unintelligible except for a subsequent equation which seems to mean something else. On page 284 an equation is invalid because pdv has been substituted for vdp. On page 208 it is stated, in contravention of dimensional requirements, that work is equal to change of tangential momentum.

The statement on page 195 that the velocity coefficient of an impulse blade decreases with increase in density of the steam runs counter to most observations of turbulent flow. For example, on page 294 it is stated that Dollin's measurements on reaction blades indicate an increase in velocity coefficient with increase in Reynolds number.

The general analytical approach is seldom employed. For example, the justification of reheat, regeneration, and other modifications of the Rankine cycle is not satisfying. Nowhere is there a general analytical approach to the multistage turbine as a problem in fluid mechanics, for example, the effect of scale on specific weight or efficiency is not discussed. The first reference to the summation of "wheel speeds squared" seems to be on page 418. Generalization is usually left to the inductive skill of the reader.

Despite these criticisms, the book contains good material which is often skillfully explained. The discussions of the state of the art of measuring performance of nozzles and blades are interesting and complete. Chapter 9 on aerodynamic considerations and chapter 10 on elements of supersonic flow are good examples of elementary exposition of difficult subjects. The chapters on vibrations, structural elements, and governing are good descriptive material. The chapters on losses and turbine performance are made up of material skillfully gleaned from more or less recent literature. The book closes with a chapter devoted to design calculations for three different turbines—none of which, unfortunately, is of the reaction type.

The illustrations are generous in number and excellent in quality. Many are selected from the recent literature on steam turbines. All told, they constitute a notable collection of graphic material and one of the strongest features of the book.

This new edition will be welcome to the teacher of turbine design and to the designer himself. It is in many ways a major improvement over the previous one. It will doubtless exceed in popularity its popular predecessors.

Basic Thermodynamics

BASIC THERMODYNAMICS. By Charles L. Brown. McGraw-Hill Book Company, Inc., New York, N. Y., 1951. Cloth, 6 × 9 in., figs., references, problems, tables, appendix, charts, index, x and 266 pp., $4.50.

REVIEWED BY JOHN A. GOFF[12]

A GOOD basic course in thermodynamics for engineering students should nowadays, especially in view of recent rapid advances in this and related fields, start with a logical and reasonably complete exposition of thermodynamic theory calculated to give the student a sound comprehension of fundamental concepts including the following: statistical equilibrium and macroscopic properties, quasi-static (reversible) and irreversible changes, internal energy, convected energy, adiabatic inaccessibility, empirical temperature, absolute temperature and entropy, the identical relations of thermodynamics. Enough should be said about the practical realization of internal energy, absolute temperature, and entropy to convince the student that entropy has every bit as good a claim to physical reality as does internal energy or any other thermodynamic property. The course should then proceed to show how these concepts, suitably extended where necessary, are to be used in the analysis of practical engineering problems.

[11] Professor of Mechanical Engineering, Massachusetts Institute of Technology, Cambridge, Mass. Mem. ASME.

[12] Professor of Mechanical Engineering, Towne Scientific School, The University of Pennsylvania, Philadelphia, Pa. Fellow ASME.

Admittedly there is not enough time in one semester to give all of the good course outlined, and the instructor is thereby forced to adopt some sort of compromise. The author of the book under review has chosen to compromise the theory and in so doing has, at any rate in the opinion of the reviewer, reduced his treatment of it to pure rigmarole. Thus in his discussion of nonflow irreversible processes he admits that "in the usual real process" the integral $\int pdv$ "has no meaning," but he goes on to say that even so "the integral can be determined approximately and this approximation can be very useful since some error is usually permissible." It is, of course, absurd to say that a thing that simply does not exist can nevertheless be approximated, but the author bases much of his discussion of the first and second laws on this very absurdity. In bold-faced type on page 26 he asserts that "For a given process the heat absorbed. . .is independent of whether the system is closed or open and steady-flow" in order to be able to conclude that the work done in steady flow is less than that done in the absence of flow by the amount of the increase in the product pv. In the absence of a clear explanation of what is to be meant by *a given process* both the assertion and the conclusion are strictly meaningless.

The only discussion the author offers of absolute temperature is contained in three sentences on page 4 which say that absolute temperature "is based not on properties of matter but upon the conversion of heat into work," that it "is difficult to evaluate and the commonly used International Scale is believed to approximate it very closely," and that it "is taken to be proportional to the pressure (with some correction) of a quantity of gas such as nitrogen maintained at a constant volume." Entropy, according to the author, is an arbitrary (*sic*) function so chosen as to validate the equation, $_1q_2 = \int_1^2 Tds$, obtained by analogy from $_1w_2 = \int_1^2 pdv$ on the specious argument that since "heat is the transfer of energy caused by a temperature difference," absolute temperature is "the driving force in heat transfer" just as "the driving force in work is pressure." In his discussion of perfect-gas mixtures he explains in a footnote that "the entire difficulty" in taking proper account of the entropy of mixing "is due to the use of an arbitrary base for entropy calculations and is illustrative of the care which must be taken with such expedients."

Nowhere does the author even mention the identical relations of thermodynamics and the important use that can be and is made of them in compiling thermodynamic properties. Indeed he would lead the student to believe that an appeal to experiment is necessary in order to conclude that $pv = RT$ implies $u = u(T)$ and $c_p - c_v = R$. The fact that $Tds = du + pdv$ is an identical relation is obscured by the manner in which he writes the nonflow energy equation.

To the reviewer the author's compromise seems shortsighted especially for a terminal course in engineering thermodynamics; he is convinced by experience that engineering students who have performed satisfactorily in their mathematics courses through the integral calculus are ready for and eminently entitled to more mature instruction in such a fundamental and far-reaching subject as thermodynamics; he feels that if something must for want of time be omitted from or slighted in the course outlined in the first paragraph of this review, it should be the practical applications, not the theory.

The practical problems treated sketchily by the author include: heating and cooling devices; compressors, pumps, and expanders; vapor-power cycles; gas-power cycles; refrigeration; nozzles; cooling towers; and air conditioning. A short chapter on heat transmission is appended. The chapters dealing with nozzles and air conditioning are especially weak. In the former appears the curious statement that "Since gases behave differently above the speed of sound, this helps to account for the necessary variations in area" of the convergent-divergent nozzle. The book contains numerous strictly meaningless statements of this kind.

Four-Bar Linkage

ANALYSIS OF THE FOUR-BAR LINKAGE—Its Application to the Synthesis of Mechanisms. By John A. Hrones and George L. Nelson. Published jointly by The Technology Press of the Massachusetts Institute of Technology and John Wiley & Sons, Inc., New York, N. Y., 1951. Cloth, 11 × 17 in., xx and 730 pp., $15.

REVIEWED BY G. J. TALBOURDET[12]

HERE is a book which should be of special interest to every machine designer and student of mechanical motions. Thanks to the ingenuity and efforts of the authors, valuable and practical information of the characteristics of a network of points on the connecting link of a four-bar linkage is available through charts and in such readily usable form that much of the present "cut-and-try" method of approach can be eliminated.

Time and again, full advantage of the possibilities of the common four-bar linkage in mechanisms is overlooked by the designer through lack of knowledge of its characteristics or through lack of ability to analyze it. This treatise is therefore filling an important gap by presenting not only the geometry of this basic linkage, its classification, mathematical relationships together with illustrative examples, but also by including over 7000 displacements of 50 points on the connecting link of 146 four-bar linkages of various link-length ratios. This voluminous aggregation of 730 charts should enable the designer to determine, in a few minutes, the basic dimensions of the four-bar linkage and the position of the point on the connecting link which are most likely to meet his requirements.

The simplicity of presentation and the organization of the material are such that anyone should be able, in a relatively short time, to understand fully the characteristics of this basic mechanism and the variety of motions which can be derived from it.

For example, every chart contains a title block in which are given the three basic link-length ratios and the position of 50 points on the connecting link. The displacement trajectories of these points are on sets of five charts each, ten trajectories for each chart, with the displacement of the driven crank included on one chart. Sets of various link-length ratios are also formed into groups where in each group two of the basic link ratios are held constant, while the third is progressively varied. Furthermore, as the charts are reproduced with a constant drive crank length, a change in the actual link length does not alter the motion characteristics of the linkage as long as the link-length ratios are held constant. It merely introduces a scale change. Thus through the combinations of these link-length ratios with their respective charts, the designer can rapidly thumb through the pages and note the page numbers on which the motion characteristics approach most closely his requirements. For his final analysis, the designer may need a cardboard model to check the behavior of the linkage, but meanwhile, time and effort will have been saved in determining the approximate dimensions of the links.

An extremely interesting feature of the charts is that besides the displacement trajectories, the average velocity of the points during every 5-deg angular displacement of a uniformly rotating crank can be readily computed from the length of each of the 72 dashes forming the trajectory and the time for the drive crank to rotate 5 deg. An approximate value of the acceleration can also be rapidly obtained by subtracting vectorially one dash length from an adjacent one and dividing by the square of the time.

---

[12] Mechanical Engineer, Research Division, United Shoe Machinery Corporation, Beverly, Mass. Mem. ASME.

According to the authors the trajectory at any point is accurate to 0.010 in. and the errors in dash-space length rarely exceed 5 per cent and are usually smaller. This accuracy was made possible by designing and building an apparatus in which the length of the links were held to within ±0.005 in. and the reproductions were one half the scale of the originals. The length of the drive crank of the apparatus was 5 in. and the tolerances indicated above are referred to this basic size. Under such conditions the resulting accuracy is appreciably greater than could be expected from the usual hand-plotting methods.

Although the trajectory charts of the motion characteristics of points on the connecting link form the bulk of this imposing book, many pages are also devoted to a general discussion of the four-bar linkage, where its classifications as crank and rocker, drag-link and double-rocker mechanisms are included, together with a chart to determine the class of operation from the link ratios. To anyone interested in the mathematics of this basic mechanism, relationships are given for the motion of the driven link, and a reference is made for the motion of a point on the connecting link.

Several excellent examples with their respective charts are included to show how dwell periods, simple and logarithmic computers, double-oscillating cranks, and symmetrical motion paths can be obtained from the combination of four-bar linkages with other links and sliders. However, a few more examples of four-bar linkages combined with cams and planetary gearing would have been a useful addition in indicating the wide applications of this basic mechanism.

The book is, indeed, a valuable contribution to our knowledge of mechanisms and to the realization of the importance of the common four-bar linkage in mechanical motions.

Methods of Operations Research

METHODS OF OPERATIONS RESEARCH. By Phillip M. Morse and George E. Kimball. The Technology Press, Massachusetts Institute of Technology, Cambridge, Mass., and John Wiley & Sons, Inc., New York, N. Y., 1951. Cloth, 8 × 11 in., vii and 158 pp., figs., tables, bibliography, subject index, $4.

REVIEWED BY DAVID BENDEL HERTZ[14]

ACCORDING to the authors, this book is a description of an applied science, "a scientific method of providing executive departments with a quantitative basis for decisions regarding the operations under their control." The book describes methodology used in specific instances during World War II to determine measures of effectiveness, strategical kinematics, tactical problems involving measure and countermeasure effectiveness of gunnery and bombardment, and operational experiments with equipment and tactics. Included also is a description of methods of selecting personnel, establishing, and operating an operations research group. This latter section is brief and is derived almost entirely from military experience.

The authors indicate that the methods described are applicable to many problems of industry and government. Some simple examples are given with respect to industry problems, but these are treated only briefly in passing. Operations research is, without question, an important tool which is due to be applied with increasing intensity to complex industrial problems as the power and utility of its methods become more widely known. Its emphasis upon defining the objectives of, and measuring and analyzing results of field operations (as distinct from exploring the unknown in a laboratory) makes it closely akin to the modern concepts of industrial engineering. Indeed, there are operations research workers in England, where applications to industry have been vigorously pressed since the war, who feel that the methods have their genesis in the "scientific management" movement. The industrial engineer for some time has been "working out the aspects of problems which are amenable to quantitative analysis and reporting his findings to an executive."

An early chapter in the book covers some fundamental probability and statistical theory. Some excellent tables applying to the problems described are included at the end of the book. The concepts of stability, control limits, and confidence intervals which are probably of primary importance in the application of operations research methods to industrial and other problems of "organized complexity" are not covered. On the other hand, the military operations described are of considerable interest. The discussion of the generalized Lanchester equations is particularly noteworthy, as an application of differential equations from biology and chemical kinematics to probability series with a time parameter.

It would have been useful had the authors more clearly differentiated between the two important aspects of modern operations research: (1) the significance of methods used to obtain results, and (2) the significance of the results themselves. It should be recognized that the first is determinative of the second. It is emphasis on the first which distinguishes operations research from other forms of gathering and manipulating data. It is this requirement which makes for the utility of interdisciplinary teams in undertaking operations research, and increases the likelihood of solving difficult and complex problems by using the methodologies of diverse sciences.

The book is worthy of the scrutiny of all scientific workers, in and out of industry. It is hoped that it will encourage the publication of further works in which problems of method and the applications of operations research thinking to nonmilitary operations are more fully explored.

[14] Assistant Professor of Industrial Engineering, Columbia University, New York, N. Y. Mem. ASME.

JOURNAL OF APPLIED MECHANICS

VOL. 19
NOS. 1-4

1952

PUB. 575

UNIVERSITY MICROFILMS
ANN ARBOR, MICHIGAN. 1953

RESOLUTION CHART

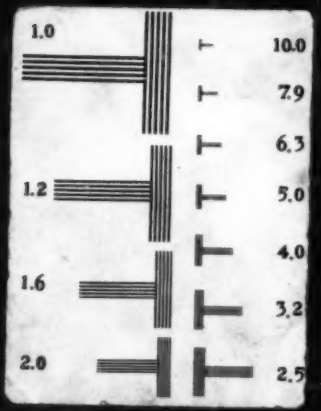

100 MILLIMETERS

INSTRUCTIONS Resolution is expressed in terms of the lines per millimeter recorded by a particular film under specified conditions. Numerals in chart indicate the number of lines per millimeter in adjacent "T-shaped" groupings.

In microfilming, it is necessary to determine the reduction ratio and multiply the number of lines in the chart by this value to find the number of lines recorded by the film. As an aid in determining the reduction ratio, the line above is 100 millimeters in length. Measuring this line in the film image and dividing the length into 100 gives the reduction ratio. Example: the line is 20 mm. long in the film image, and 100/20 = 5.

Examine "T-shaped" line groupings in the film with microscope, and note the number adjacent to finest lines recorded sharply and distinctly. Multiply this number by the reduction factor to obtain resolving power in lines per millimeter. Example: 7.9 group of lines is clearly recorded while lines in the 10.0 group are not distinctly separated. Reduction ratio is 5, and 7.9 x 5 = 39.5 lines per millimeter recorded satisfactorily. 10.0 x 5 = 50 lines per millimeter which are not recorded satisfactorily. Under the particular conditions, maximum resolution is between 39.5 and 50 lines per millimeter.

Resolution, as measured on the film, is a test of the entire photographic system, including lens, exposure, processing, and other factors. These rarely utilize maximum resolution of the film. Vibrations during exposure, lack of critical focus, and exposures yielding very dense negatives are to be avoided.